C-MAPExp
Final Report

ESA Study

"Scientific and Technical Assistance for the Deployment of a flexible airborne spectrometer system during C-MAPExp"

ESTEC Contract No. 4000106993/12/NL/FF/lf

Lead author:

Heinrich.Bovensmann@iup.physik.uni-bremen.de

Institute of Environmental Physics (IUP) / Institute of Remote Sensing (IFE), University of Bremen (UB), Bremen, Germany

Co-Author:

T. Krings, K. Gerilowski, Institute of Environmental Physics (IUP), University of Bremen (UB), Bremen, Germany

Bruno Neininger, METAIR AG, Switzerland

Thomas Ruhtz, Carsten Lindemann, Free University of Berlin, Germany

Change log

Version	**Date**	**Status**	**Authors**	**Reason for change**
Draft 0.3	20.01.2014	To Team	H. Bovensmann	Initial internal version
Draft 0.9	02.05.2014	To Team	T. Krings, B. Neininger, H. Bovensmann	Internal full draft final for final internal revision
Final 1.0	04.05.2014	To ESA	See cover	Delivery to ESA
Final 1.1	30.07.2014	To ESA	See Cover	Addition of table 13 and chapter on relation to CarbonSat spatial scale (chapter 10)

Table of Contents

Applicable Documents

Id.	Title	Reference
AD-1	Technical Assistance for the Deployment of a flexible airborne spectrometer system during C-MAPExp, Request for Quotation	RFQ-3-13609/12/NL/FF/lf
AD-2	Technical Assistance for the Deployment of a flexible airborne spectrometer system during C-MAPExp, Statement of Work	EOP-SM/2363/DS-ds
AD-3	Technical Assistance for the Deployment of a flexible airborne spectrometer system during C-MAPExp, Proposal dated 1.8.2012	

References

Id.	Title	Reference
RD-1	Gerilowski et al. 2011	Gerilowski, K., A. Tretner, T. Krings, M. Buchwitz, P. P. Bertagnolio, F. Belemezov, J. Erzinger, J. P. Burrows, and H. Bovensmann, MAMAP – a new spectrometer system for column-averaged methane and carbon dioxide observations from aircraft: instrument description and performance analysis, Atmos. Meas. Tech., 4, 215-243, 2011.
RD-2	Krings et al 2011	Krings, T., Gerilowski, K., Buchwitz, M., Reuter, M., Tretner, A., Erzinger, J., Heinze, D., Pflüger, U., Burrows, J. P., and Bovensmann, H.: MAMAP – a new spectrometer system for column-averaged methane and carbon dioxide observations from aircraft: retrieval algorithm and first inversions for point source emission rates, Atmos. Meas. Tech., 4, 1735-1758, doi:10.5194/amt-4-1735-2011, 2011.
RD-3	MRD 2012	CarbonSat Mission Requirement Document v1.1
RD-4	Bovensmann et al. 2010	Bovensmann, H., Buchwitz, M., Burrows, J. P., Reuter, M., Krings, T., Gerilowski, K., Schneising, O., Heymann, J., Tretner, A., and Erzinger, J.: A remote sensing technique for global monitoring of power plant CO_2 emissions from space and related applications, Atmos. Meas. Tech., 3, 781-811, 2010.
RD-5	CIP 2012	C-MAPExp Campaign Implementation Plan, University of Bremen, October 2012
RD-6	Krings et al 2013	Krings, T., K. Gerilowski, M. Buchwitz, J. Hartmann, T. Sachs, J. Erzinger, J. P. Burrows, H. Bovensmann, Quantification of methane emission rates from coal mine ventilation shafts using airborne remote sensing data, Atmos. Meas. Tech., 6, 151–166, 2013.
RD-7	DAR 2013	C-MAPExp Data Acquisition Report (DAR), Version 1.0, University of Bremen, July 2013.

1. Purpose of Document

This final report describes the C-MAPExp campaign executed in August 2012, its data processing and quality, a description of the generated data set, preliminary results for selected targets and its overall achievements.

The document is structured as follows: Chapter 2 summarises the main campaign objectives and overall campaign set-up. Chapter 3 gives a summary of the instrumentation as used in the campaign. In chapter 4 it is summarised how the campaign was performed, which targets where flown, which data set was collected and examples of the collected data are given.

Chapter 5 contains background information about how the campaign data is processed and chapter 6 gives a summary on the campaign data format and data archive.

An initial analysis of the in-situ measurements to derive emission was performed by METAIR and is summarised in Chapter 7.

Chapter 8 contains the initial analysis of the remote sensing data set to derive emissions, first using external meteorological parameters and second using meteorological parameters from the in-situ campaign data set.

The data analysis part of the report is closed with chapter 9, where inversion results from both in-situ and remotes sensing are compared and discussed.

The report closes with a summary (Chapter 10) and some recommendation and lessons learned (Chapter 11).

2. The C-MAPExp campaign objectives and campaign set-up

The C-MAPExp campaign was planned and executed to support the demonstration of CarbonSat capabilities in:

- Quantification of "gradients" in atmospheric CO_2 and CH_4 from strong local greenhouse gas sources e.g. from coal-fired power plants, localized industrial complexes, landfills, etc.
- Derivation of CO_2 and CH_4 emissions from atmospheric gradient measurements.

This is addressed through the collection, processing and preliminary analysis of airborne remote sensing and airborne in-situ data from CH_4 and CO_2 emitting targets of different but mostly known emission strength. Within this project, an airborne campaign combining remote sensing (RS) measurement (similar to CarbonSat) of XCO_2 and XCH_4 with in-situ measurements of atmospheric CO_2 and CH_4 concentration as well as wind speed and direction in the boundary layer was performed in August 2012 [RD-5].

For the remote sensing of the greenhouse gases CO_2 and CH_4, the Methane Airborne MAPper (MAMAP) was flown on a Cessna T207A above the boundary layer. MAMAP [Gerilwoski et al. 2011] is an airborne 2 channel NIR-SWIR grating spectrometer system for accurate measurements of gradients on column-averaged methane and carbon dioxide concentrations. It was jointly developed by the Institute of Environmental Physics / Remote Sensing (IUP/IFE), University of Bremen (Germany) and the Helmholtz Centre Potsdam, German Research Centre for Geosciences (GFZ). It has to be noted that MAMAP has – in comparison to CarbonSat EE8 no 2 µm CO_2 channel, which is limiting MAMAP's capability to detect very small gradients for example from biosphere fluxes.

For the in-situ airborne measurements, the small research aircraft (METAIR-DIMO) was flown in the boundary layer to perform in-situ measurements in the plume emitted from the target, to perform background concentration measurements and to perform wind measurements needed for the interpretation of the total column measurements of MAMAP. The aircraft is equipped with underwing-pods, carrying up to 50 kg scientific payload each. The standard equipment measures the meteorological parameters wind (three-dimensional components in turbulent resolution), fast temperature and fast, redundant humidity. A two-channel aerosol counter (MetOne for >0.3 and >0.5 µm) can characterise the structure of the boundary layer. The chemical measurements are for CO_2 (redundant), CO, O_3, NO_2, NOx, NOy, Ox, and – in the focus here – CH_4. The methane monitor is a "Los Gatos DLT-100 Fast Methane Analyser" which was bought by ETH Zurich, modified in a joint project, and was flown during three years for about 40 measuring days. The data turned out to be very reliable and accurate (comparison with flask-samples, analysed at MPI Jena). More details about the instrumentation can be found in [RD-5] and references therein.

With both aircrafts, dedicated and coordinated flights were performed in an area with strong localised emission sources of CO_2 and CH_4. The main campaign area encloses targets in the Rhine-Ruhr, but also some targets in southern Lower Saxony were flown.

3. Description of main campaign instrumentation

3.1. Methane Airborne MAPper (MAMAP) on Cessna

For the remote sensing of the greenhouse gases CO_2 and CH_4 the Methane Airborne MAPper (MAMAP) will be flown on a Cessna T207A above the boundary layer. MAMAP is an airborne 2-channel NIR-SWIR grating spectrometer system for accurate measurements of gradients on column-averaged methane and carbon dioxide concentrations (for details, see Gerilowski et al. 2011, Krings et al. 2011 and [RD-5]).

CH_4/CO_2-SWIR-spectrometer	O_2-NIR-spectrometer
F = 300 mm temperature stabilized grating spectrometer system (f/3.9)	F = 300 mm temperature stabilized grating spectrometer system (f/3.9)
Grating: 600 grooves/mm	**Grating:** 1200 grooves/mm
Detector: LN cooled 1024 pixel InGaAs FPA	**Detector:** 512 x 512 pixel CCD Sensor, TE cooled, 6 pixel binned in imaging direction
Spectral range: 1.590 - 1.690 nm	**Spectral range:** 755 - 785 nm
Spectral resolution: ~0.82 nm FWHM	**Spectral resolution:** ~0.46 nm FWHM
Spectral sampling: ~8 pix/FWHM	**Spectral sampling:** ~ 6 pix/FWHM
Detector-SNR: ~ 1000 at ~ 0.6 - 1.0 sec. integration/co-adding time	**Detector-SNR:** ~ 4000 (1D-binned) at ~ 0.6 - 1.0 sec integration/co-adding time
Detector-Cooling: Liquid Nitrogen (LN) (~ 1.5 l LN / 10h operation)	**Detector-Cooling:** Peltier
IFOV: ~ 1.14° across track(CT) x ~ 1.14° along track	**IFOV: :** ~ 1.14° across track(CT) x ~ 1.14° along track
Spatial resolution: at 3 km flight altitude, ground speed 200 km/h, the co-added ground pixel size is in the order of 55 m along track x 60 m across track (non-imaging)	**Spatial resolution:** at 3 km flight altitude, ground speed 200 km/h, the co-added ground pixel size is in the order of 55 m along track x 60 m across track (non-imaging)
Precision: ~ 0.3 % $XCH_4(CO_2)$ & $XCO_2(CH_4)$ (1 σ) for 0.6-1 sec co-adding/integration time (precision is defined as the random error of the retrieved XCH_4 and XCO_2 columns due to instrument noise). Slightly degraded precision expected for $XCH_4(O_2)$ & $XCO_2(O_2)$. **Relative Accuracy:** < 0.5 % $XCH_4(CO_2)$ & $XCO_2(CH_4)$ on spatial scales in the range of 20-30 km at clear sky, < 1 % $XCH_4(CO_2)$ & $XCO_2(CH_4)$ on spatial scales in the range of ~ 100 km at clear sky. **Measurement modes**: nadir- (terrestrial targets) or glint- radiance (marine targets) on demand, zenith sky irradiance (optional as reference).	
Size: 2 standard racks, 556 x 650 x 968 mm each. **Weight:** 2 x ~120 kg. **Power consumption:** ~ 600 Watt at nominal operation, < 1000 Watts at warm-up	
Flight record: Cessna Caravan (RWE), Cessna 207 (FU-Berlin), DC3T-BT67 (AWI Polar-5, Transport Canada certification)	

MAMAP was jointly developed by the Institute of Environmental Physics / Remote Sensing (IUP/IFE), University of Bremen (Germany) and the Helmholtz Centre Potsdam, German Research Centre for Geosciences (GFZ). MAMAP is fully certified for the Cessna T207A and was already flown successfully in 2008 and 2011 on that aircraft. Data analysis methods for MAMAP data are well developed to derive from the gradient measurement the emission strength of strong point sources [Krings et al. 2011, 2013].

For MAMAP, it was demonstrated that the instrument is able to detect and retrieve the total dry column of the greenhouse gases CH_4 and CO_2 with a precision of ~ 0.3% (1-sigma) at local scales (several 10s of km), and that MAMAP is an appropriate tool for detection and inversion of localized GHG emissions from aircraft (Gerilowski et al. 2011, Krings et al. 2011, 2013, Annex 1).

Assuming a wind speed of ~ 2-3 m/s (min. for Gauss plume inversion), a 0.3% precision translates to a (flight path and pointing accuracy dependent) detection limit of this airborne non-imaging instrument of approx. to 1-2kt CH_4/yr (1-2Mt CO_2/yr) and a minimum quantifiable (error 50%) source strength of approx. 5 kt CH_4/yr (5 Mt CO_2/yr), assuming that on the scale of a plume extension, the precision is dominating the relative accuracy.

For extended sources, the relative accuracy might be dominated by systematic biases due to albedo and scattering effects. Assuming a 1 % relative accuracy over scales of 100 km would allow quantifying upper limit constraints for extended area fluxes in the order of several 100 mg CH_4 m^{-2} day^{-1} (4 m/s wind speed, 100x100 km^2). To detect wetland emissions, this value needs to be decreased significantly, for example, by decreasing the relative accuracy for the given scale by algorithm improvements and/or hardware modifications (i.e. adding an additional channel to the instrument in analogy to CarbonSat's SWIR-2 channel or increasing the instrument spectral resolution).

Therefore, MAMAP, with its current proven instrument and algorithm performance, is well suited for the detection of strong point sources of CH_4 and CO_2. Different optimizations and instrument redevelopments to further decrease the detection limit and/or improve the relative accuracy are planned.

In comparison to CarbonSat, there are some differences to be mentioned:

- Due to the measurement geometry MAMAP has compared to CarbonSat an enhanced sensitivity to the column below the aircraft.
- MAMAP in comparison to CarbonSat does not allow for "absorber free" solar reference measurements, with the consequence that MAMAP delivers no absolute single total column data, but accurate gradients in columns below aircraft.
- As MAMAP on a Cessna can only probe gradients on small scales up to 100 km, quantification of larger scale biospheric fluxes is not feasible with MAMAP on a Cessna (but with CS).
- MAMAP has no 2 µm channel

During the campaign the instrument worked as expected with the performance known from previous campaigns and without any problems.

3.2. In-situ GHG sensor on METAIR-DIMO

For the in-situ airborne measurements, the small research aircraft METAIR-DIMO was flown in the boundary layer to catch the plumes emitted from the target and to perform background measurements. The aircraft was equipped with underwing-pods, carrying up to 50 kg scientific payload each. The standard equipment measures the meteorological parameters wind (three-dimensional components in turbulent resolution), fast temperature and fast, redundant humidity. A two-channel aerosol counter (MetOne for >0.3 and >0.5 μm) can characterise the structure of the boundary layer. The chemical measurements are for CO_2 (redundant), CO, O_3, NO_2, NO_x, NO_y, O_x (= O_3+NO_2), and – in the focus here – CH_4. The methane monitor is a "Los Gatos DLT-100 Fast Methane Analyser" which was bought by ETH Zurich, modified in a joint project, and was flown during three years for about 40 measuring days. The data turned out to be very reliable and accurate (comparison with flask-samples, analysed at MPI Jena). METAIR prepared the standard instrumentation as described above, with the focus on CH_4 and CO_2. All other parameters can be very useful, as well (e.g. the ratio of CH_4 to CO, CO_2 and NO_x can characterise sources).

During the campaign the instrument worked as expected with the performance known from previous campaigns and without any problems. Also some in-situ probes by flasks were performed which will be analysed by MPI Jena.

All in-situ parameters listed could be measured at the specified quality (see table below), however, the focus was on CH_4, CO_2, 3-d-wind, and the temperature profiles. Other parameters like H_2O (humidity) and aerosols were useful for checking the boundary layer height in cases where this was not obvious just based on virtual potential temperature (an important input for the inversion of the remote-sensing results). CO and NOx are available as well. However, since this was not within the scope of this project, they were not systematically analysed.

The table below is summarizing the in-situ measurements system performance.

prio	parameter	instrument/method	inss	mod	rem	range; resolution	temporal resolution	precision; accuracy	calibration & checks
1	position (x,y,z)	GPS TANS Vector and second GPS for moving map	1996	0	1, 2	global; 1 m	10 Hz	0.1 m; 10 m	fix points
1	ground speed (GS, vx, vy, vz)	GPS TANS Vector and second GPS for moving map	1996	0	1, 2	0..100; 0.1 m/s	10 Hz	0.01; 0.1 m/s	zero & wind calculation
1	attitude angles (azi, pitch, roll)	GPS TANS Vector	1996	0	1	0..360°/±90°; 0.1°	5 Hz	0.05; 0.2°	fix & wind calculation
2	acceleration (ax, ay, az)	Kistler/DLR	1996	1	2	±30; 0.001 m/s^2	10 Hz	0.001; 0.01 m/s^2	integration to vx, vy, vz
2	air temperature (T)	Meteolabor TP-3 thermocouple	1990	1		-50..+50 °C; 0.01 K	5 Hz	0.01; 0.5 K	mercury thermometer & integration of zInt
2	dew point	Meteolabor TP-3 dew point mirror	1990	1		T-40 K..T; 0.01 K	1 Hz	0.01; 0.5 K	psychrometer & infrared
1	flow angles and TAS	five hole probe using Keller capacitive sensors	1996	3	3	±30°; 0.1°	10 Hz	0.1; 0.5°	wind calculation
1	wind (u, v, w)	post-processing from above parameters	1996	3	3	±30; 0.1 m/s	10 Hz	0.1; 0.5 m/s	consistency of wind calculation (min TKE)
2	aerosol number (>0.3 and >0.5 µm)	MetOne R4903 optical particle counter (2-channel OPC)	1996	1		0..300 n/ml; 1 n/ml	3 Hz	1 n/ml	none (last factory cal)
1	CH_4	Fast Methane Analyzer Los Gatos LGR DLT-100	2009	2	4	1800..5000; 0.1 ppb	5 Hz	0.1; 2 ppb	lab and flasks, very stable
2	CO	Aerolaser AL-5003 (fast Vacuum UV-fluorescence)	2001	2		0..2000; 0.5 ppb	5 Hz	0.5; 5 ppb	in-flight zero and calgas
1	CO_2	closed and open path IRGA LI-6262 and LI-7500 (combined use)	2001	2	5	320..800; 0.01 ppm	10 Hz	0.01; 0.5 ppm	cal gas and/or flasks
2	H_2O	open path IRGA LI-7500 (combined with dew point mirror)	2001	2	5	0..30; 0.01 g/kg	10 Hz	0.01; 0.2 g/kg	dew point
3	O_3	single cell UV photometer built at PSI, based on a Monitorlabs instrument	1990	1	6	0..500; 0.5 ppb	10 s	0.5; 2 ppb	O_3-generator & rem 4
3	NO_2, NOx, NOy, HNO_3, PAN, Ox	NOxTOy: 6-channel instrument using Luminol chemoluminescence and chemical converters (developed and built by PSI and Metair)	1998	3	6	0.5..200; 0.1 ppb	1 Hz	0.1 ppb; 0.5 ppb + 20% sig	complex procedure; not applied here; focus on NO_2 and NOx
3	vertical digital photography	Canon PowerShot S100, remote control from cockpit	2009	0		up to 12 Mpix	3 s	n.a.	n.a.
3	CO_2, CO, CH_4, N_2O, H_2, SF_6, ^{18}O, ^{13}C	grab samples in glass flasks, analyzed at MPI-Jena	2005	0	7	upon request MPI	6/flight	upon reqest MPI	specialized lab at MPI-Jena

prio: Priority for C-MAPExp: 1: core-parameter; 2: important parameter; 3: nice to have – as long as it is running without problems
inss: In service since (year) including integration in the post-processing
mod: Degree of modification: 0: original instrument; 1: minor modifications; 2: major modifications; 3: built by metair
rem: remarks:

1: A more advanced IMU/GPS (OXTS RT3102) is available but does not fit in the configuration with the CH4-Monitor in the LH-pod (backup)

2: With the 3-axis high-sensitivity, low noise accelerometers, the movement of the boom, and hence, the precision and resolution of the position, and the wind is improved

3: Both the flow angles and the winds are a result of complex calibrations and post-processing (know-how built into the post-processing software)

4: Corrected for H2O interference (dilution and spectroscopic; details see Hiller et al. 2014)

5: These IRGAs are modified for airborne use by Metair (e.g. reference gas, N2-flushing instead of scrubbers, etc.)

6: The consistency of NO2+O3 = Ox can be used for the checking and adjustment of the calibration

7: flask samples were performed during C-MAPExp.

range and resolution: The measured range and useful resolution of the parameter (based on experience when not identical with data sheets)

temporal resolution: The useful temporal resolution of the parameter (sometimes less than the recorded resolution)

precision is the repeatability of signals for recognizing some pattern, whereas accuracy is the absolute accuracy of the values after post processing

calibration or checks: Keywords on how the quality of the parameter is checked and validated

4. Overview of campaign as performed

4.1. Summary of campaign and flown targets

In this section an overview is given about the campaign as performed. The campaign was successfully performed based on the priorities and guidelines summarised in the Campaign Implementation Plan [RD05]. The table below summarises the campaign activities as performed. Reference to the target numbers can be found in Annex 1.

Date	Day of Week	Activity	Comment
10.8.2012	Fri	Integration MAMAP into Cessna	
11.8.2012	Sat	1st Test Flight Berlin	Minor issues with O2 band channel, fixed on-site
12.8.2012	So	2nd Test Flight MAMAP Berlin and Transfer to Dinslaken, Arrival METAIR at Dinslaken	
13.8.2012	Mo	Aircrafts ready at Dinslaken, Test flight T1.7, T2.2, T2.4, 2.9	**Start Data Acquisition Phase**
14.8.2012	Tue	T2.3, 2.4, DIMO pre-screening T2.11-2.15	
15.8.2012	Wed	Targets: 1.1, 1.4, 1.5, 1.7, 2.2, 2.9	
16.8.2012	Thu	Targets: 1.1, 1.4, 1.5, 2.3	
17.8.2012	Fri	Targets: 1.1, 1.2, 1.4, 1.5, 2.2, 2.3, 2.5	
18.8.2012	Sat	Targets: 1.1 - 1.5, 2.2, 2.5, 2.10	
19.8.2012	Sun	Targets: 2.1, 2.2	
20.8.2012	Mo	No Flights	
21.8.2012	Tue	No Flights	
22.8.2012	Wed	No Flights	
23.8.2012	Thu	T1.4, FLEX Selhausen/Altendorf	
24.8.2012	Fri	End of Acquisition Phase, dis-integration	
25.8.2012	Sat		

Table 1: Campaign schedule as executed. Details of the targets flown by METAIR-DIMO and MAMAP/Cessna are listed in tables Table 2 and Table 3.

During the period between 14.08.2012 and 23.08.2012 the weather was systematically better than the forecasted conditions. Even when some clouds limited the remote-sensing during some days, the conditions for the in-situ measurements were good to ideal. The criteria for ideal or less ideal measurements are discussed with the inversion method in Chapter 7.

In [RD-05] it was planned also to fly with the MetAir Dimona cylinders around sources. This was not necessary, as the point sources under study emitted plumes that were clearly detectable above the background within single cross sections (see the detailed description in Chapter 7). Flying cylinders on different altitudes would have multiplied the flying time by a factor of at least four, or – vice versa – much less targets could have been measured, with a poorer vertical resolution.

It was therefore decided that it is more important to probe the plumes with the best possible resolution (as many levels as possible, within a quasi-stationary duration) instead of flying around in low background concentrations for >80% of the time. In some cases, "curtains" in two distances could be flown. However, also this was not a clear advantage (see the discussion in Chapter 7). Single curtains flown in high resolution during suitable weather conditions are regarded as the optimum now.

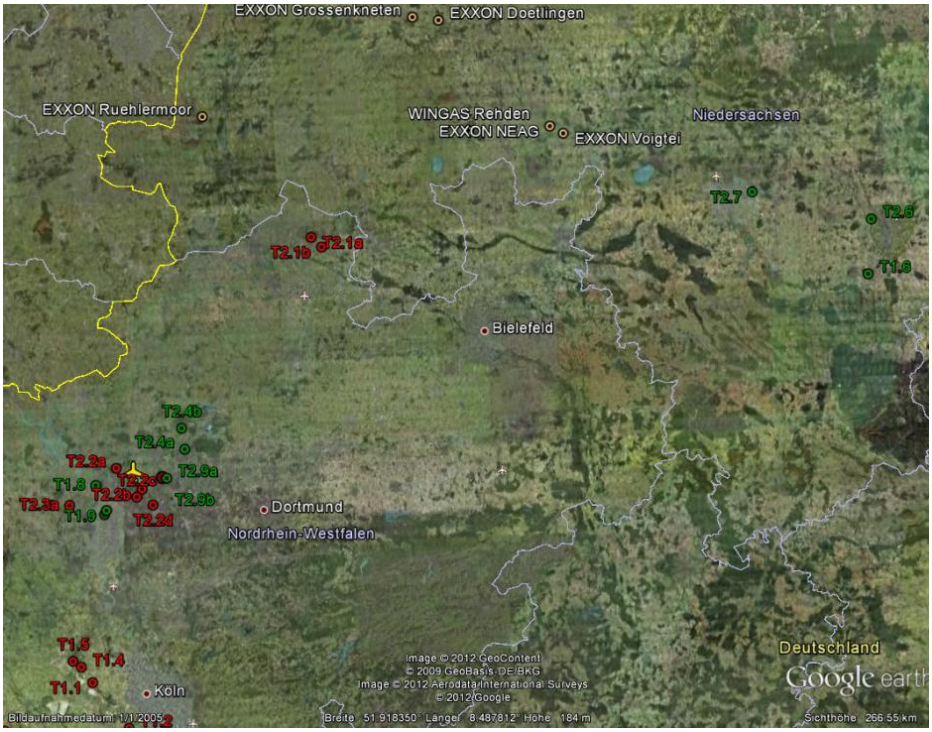

Figure 1: Overview map of campaign area. The yellow airplane marks the airfield Dinslaken Schwarze Heide. Red: high priority targets; Green: medium priority targets. Target summary see tables 1-3. Target details see Annex.

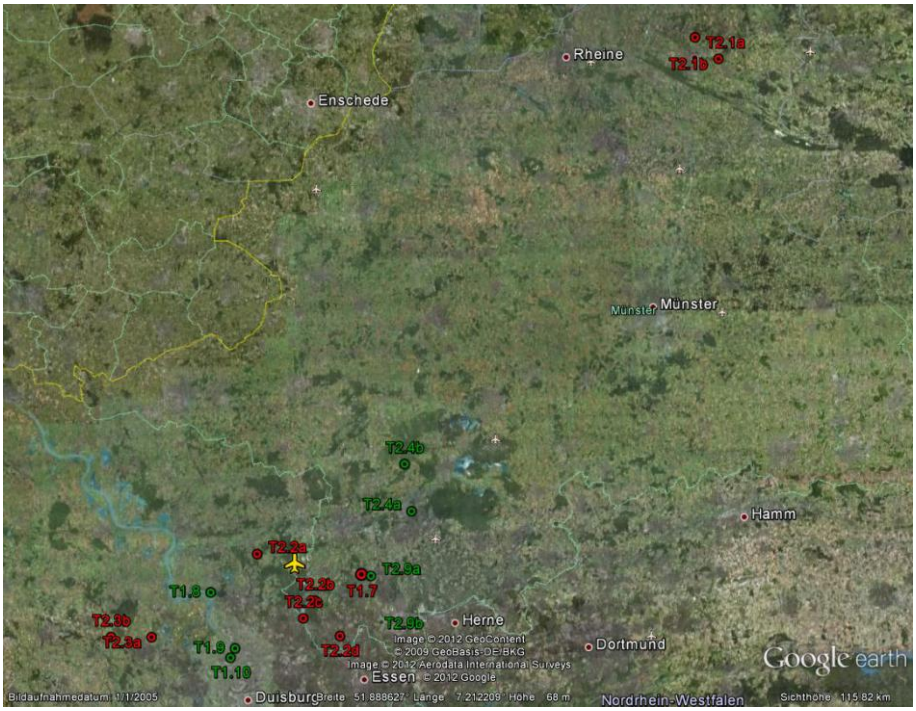

Figure 2: Overview map of mid to northern NRW targets. The yellow airplane marks the airfield Dinslaken Schwarze Heide. Red: high priority targets; Green: medium priority targets. Target summary see tables 1-3. Target details see Annex.

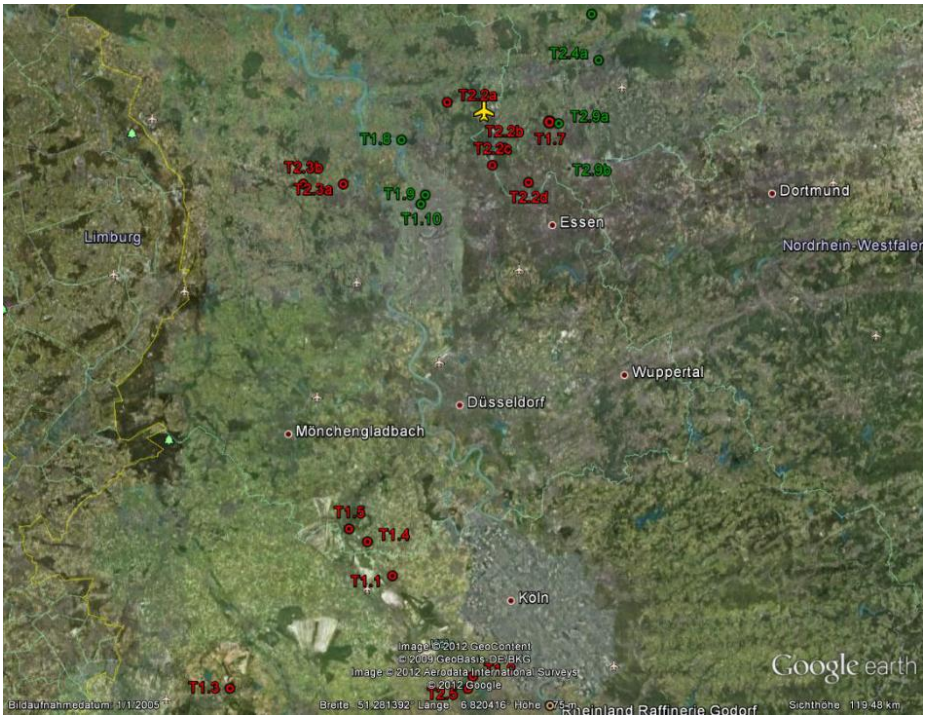

Figure 3: Overview map of mid to southern NRW targets. The yellow airplane marks the airfield Dinslaken Schwarze Heide. Red: high priority targets; Green: medium priority targets. Target summary see tables 1-3. Target details see Annex 1.

In the following tables the campaign activities per airplane are given together with a first assessment about the quality of the data and its suitability for further analysis.

C-MAPExp	Flight Days in August 2012	13	14	15	16	17	18	19	23
METAIR									
	Lee von Koeln						X		
	RWE neu			X	X	X	X		
T1.1	RWE Kraftwerk Niederaussem			X	X	X	X		
T1.2	RWE Kraftwerk Goldenberg					X	X		
T1.3	RWE Kraftwerk Eschweiler						X		X
T1.4	RWE Kraftwerk Neurath			X	X	X	X		
T1.5	RWE Kraftwerk Frimmersdorf			X	X	X	X		
T1.6	Salzgitter Flachstahl GmbH								
T1.7	Kraftwerk Scholven	X		X					
T2.1	RAG Anthrazit Ibbenbüren							X	
T2.1	Bockradener Schacht							X	
T2.1	Theodorschacht							X	
T2.2	RAG Bergwerk Prosper-Haniel	X		X		X		X	
T2.2	Schacht Hünxe	X		X				X	
T2.2	Schacht Prosper - 9	X		X		X	X	X	
T2.2	Haniel Schacht 1	X		X		X		X	
T2.2	Förderberg	X				X		X	
T2.3	RAG Bergwerk West		X		X	X			
T2.3	Rossenray / Schacht 1		X		X	X			
T2.3	Schacht Friedrich Heinrich - 4		X		X	X			
T2.4	RAG Bergwerk Auguste Victoria	X							
T2.4	Schacht AV 7	X							
T2.4	Schacht AV 8	X	X						
T2.5	AVG Zentraldeponie Vereinigte Ville					X	X		
T2.6	Deponie Watenbüttel BS								
T2.7	ABZ Hannover/Lahe								
T2.8	Deponie Schöneicher Plan								
T2.9	Ruhr Öl Gelsenkirchen	X		X					
T2.10	Rheinland Raffinerie Godorf						X		
T2.11	EXXON Grossenkneten		X						
T2.12	EXXON NEAG		X						
T2.13	EXXON Voigtei		X						
T2.14	EXXON Dötlingen		X						
T2.15	WINGAS Rehden		X						
T2.16	EXXON Rühlermoor								
	FLEX Selhausen								X
	FLEX Altendorf								X
	high concentrations detected								
	enhanced concentrations detected								
	no or low enhancement detected								

Table 2: Flights performed by METAIR Dimo and initial indication about signals detected.

During the eight observation days, the in-situ airplane (MetAir) documented 52 plumes, from which 18 were very clear, 28 detectable as well, but less pronounced or less densely flown, and 6 targets observed turned out not to emit detectable amounts of CO_2 or CH_4 during the time of observations.

C-MAPExp	Flight Days in August 2012	12	13	14	15	16	17	18	19	23
MAMAP										
T1.1	RWE Kraftwerk Niederaussem				+		++	+		
T1.2	RWE Kraftwerk Goldenberg							o		
T1.3	RWE Kraftwerk Eschweiler							+++		+
T1.4	RWE Kraftwerk Neurath (incl. neue Blöcke)				+		+	o		
T1.5	RWE Kraftwerk Frimmersdorf				+		o	o		
T1.6	Salzgitter Flachstahl GmbH									
T1.7	Kraftwerk Scholven				o				o	
T2.1.a	RAG Anthrazit Ibbenbüren									
T2.1.b	Bockradener Schacht								++	
T2.1.c	Theodorschacht								++	
T2.2.a	RAG Bergwerk Prosper-Haniel									
T2.2.b	Schacht Hünxe		+						o	
T2.2.c	Schacht Prosper - 9		++		+				o	
T2.2.d	Haniel Schacht 1		o		o				o	
T2.2.e	Förderberg		o						o	
T2.3.a	RAG Bergwerk West									
T2.3.b	Rossenray / Schacht 1			o			o			
T2.3.c	Schacht Friedrich Heinrich - 4			++		++	++			
T2.4.a	RAG Bergwerk Auguste Victoria									
T2.4.b	Schacht AV 7 (incl EVONIK/INEOS)		o						o	
T2.4.c	Schacht AV 8		o							
T2.5	AVG Zentraldeponie Vereinigte Ville							o, o		
T2.6	Deponie Watenbüttel BS									
T2.7	ABZ Hannover/Lahe									
T2.8	Deponie Schöneicher Plan	o								
T2.9	Ruhr Öl Gelsenkirchen		o						o	
T2.10	Rheinland Raffinerie Godorf (Werk Nord + Süd)							o, o		
T2.11	EXXON Grossenkneten									
T2.12	EXXON NEAG									
T2.13	EXXON Voigtei									
T2.14	EXXON Dötlingen									
T2.15	WINGAS Rehden									
T2.16	EXXON Rühlermoor									
	FLEX Selhausen									X
	FLEX Altendorf									X

Suitable for Inversion (preliminary, based on visual inspection of quick looks):	
++	probably very well suited for inversion with Gaussian model approach
+	probably invertable with Gaussian model approach
o	not well suited for inversion, either no increase in column detected or very patchy pattern and/or bad met. conditions

Table 3: Flights performed by MAMAP/Cessna and initial indication about plume signals detected and suitability for further data analysis. Targets marked with thick line box are proposed to be analysed further with high priority.

During the eight observation days, the remote sensing airplane (Cessna FUB with MAMAP) documented 39 plumes, from which 16 were clear and of good quality for flux inversion, and 23 were not well suited for flux inversion either due to a plume at or below the detection limit or due to non-optimum meteorological conditions (partly cloudy, strong boundary layer disturbances etc.).

4.2. Examples of collected data

In the following, to give an impression on the data quality based on quick look data analysis, initial results are presented for one selected campaign day. The selected day is the 19.8.2012 with fair weather conditions in the morning. Coordinated flights with both airplanes were performed in the morning (8:30-10:50 UTC) over the Ibbenbüren active coal mine area (T2.1), which includes two coal mine exhaust shafts and a small power plant.

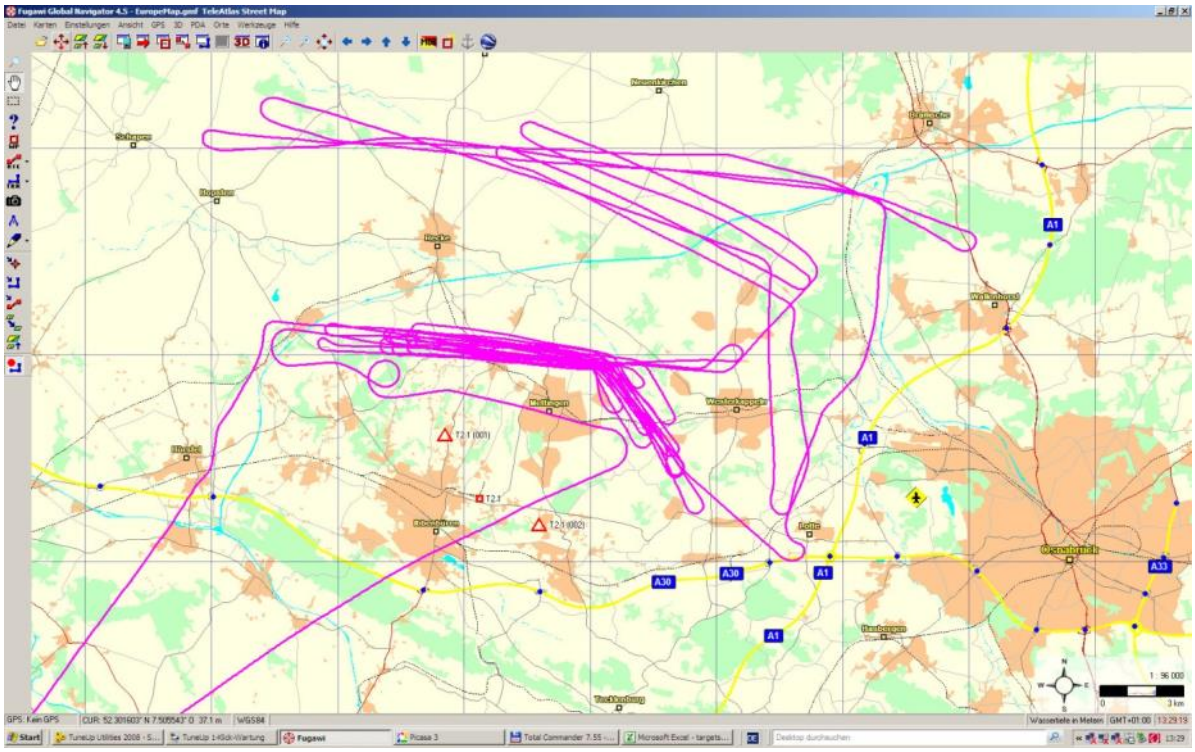

Figure 4: Flight pattern of METAIR DIMO over Ibbenbüren 19.8.2012. The red triangles are marking the two coal mine exhaust shafts and the red square is marking the small power plant.

In the early morning the campaign area was dominated by clear sky conditions. At the End of the flight, medium height clouds started to contaminate clear sky, in some areas with visible shadows. This is documented by photographs taken during the flight; see Figure 5 and Figure 6. A photographic documentation of all campaign days can be found in Annex 2.

For all data quick-look analysis were performed. Examples can be found in the next chapter.

Figure 5: Left: Cloud situation over Ibbenbüren 19.8.2012 in the morning. Right: Power plant Ibbenbüren.

Figure 6: Situation at the End of the flight, march through of medium height clouds in some areas with visible shadows.

4.3. Quick look processing

After each flight, the team performed a quality check on the raw data, normally on the same day, to determine data quality sufficiency. A quick look data analysis up to concentration maps was performed for selected targets within a few days to verify data quality. To decide if the flight can be declared as successful quick-look processing was done at the end of the campaign.

Data saving and quick looks MAMAP

During measurements, MAMAP data are saved on different solid state disks of the instrument (separate for O_2, CH_4/CO_2, and camera/gyro). Correct functioning of the instrument is ensured in-flight by the operator checking the recorded spectra. However, no trace gas information is available immediately in-flight.

Raw data are downloaded post flight and stored on at least two different hard drives at different locations. Quick looks in form of geo-referenced qualitative total column information using a generic radiative transfer model simulation are typically available within a few days at latest, depending on maintenance and calibration work to be conducted at the instrument.

Figure 8 shows an example quick look of XCH_4 data from the coal mine ventilation shafts of the RAG Anthrazit Ibbenbüren. An example for XCO_2 released from the coal fired power plant in Eschweiler is shown in Figure 7.

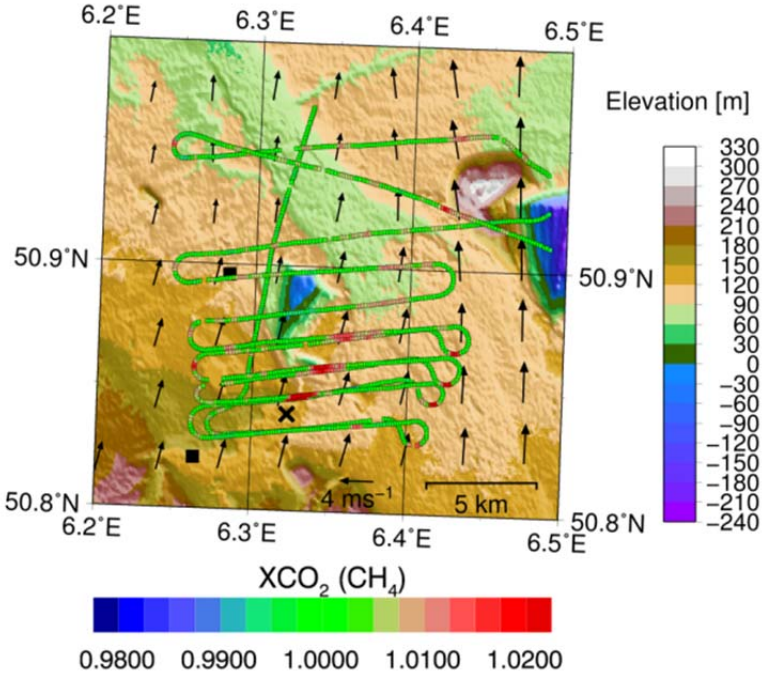

Figure 7: MAMAP flight pattern and quick-look analysis of the coal fired power plant Eschweiler (center location denoted by black cross) on 18.8.2012.The CO_2 plume is visible as an enhancement in the XCO_2 dry column ratio. Wind field is indicated by black arrows. Topography map underneath.

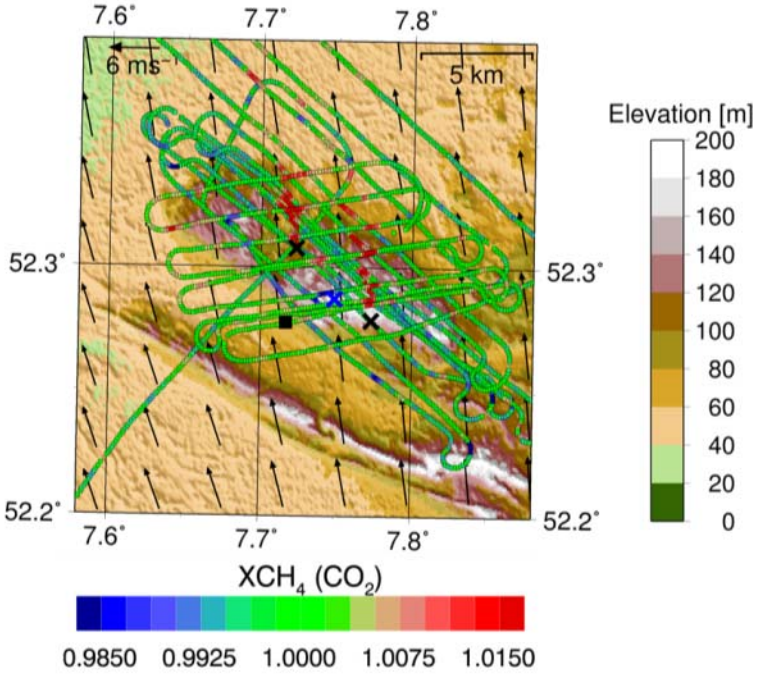

Figure 8: MAMAP flight pattern and quick-look analysis Ibbenbüren (exhaust shafts Bockradener-Schacht and Theodor-Schacht, black crosses) 19.8.2012.The two CH_4 plumes are visible as an enhancement in the XCH_4 dry column ratio. Wind field is indicated by black arrows. Topography map underneath.

The results of the quick-look data screening for MAMAP data are summarised in Table 3.

Quick looks METAIR

All data were saved on different solid state flash memories (one in each pod, one in the center, one in the camera, and one in the CH_4-monitor). Once the data are secured a quick look of data was performed in several stages:

(i) Are all data there and looking ok?
(ii) Time series or maps of core parameters.
(iii) Forwarding tracks and other data to the partners.

Normally, this is not a problem and a standard procedure. After this, a full post-processing of the data, including synchronisation and calibration, takes about twice as much time as its production, i.e. typically one working day per flight. This procedure is usually divided into steps, i.e. for distributing preliminary data (geo-referenced concentrations, winds, temperatures, etc.), so that one can post-process about four flights (two measuring days) within one working day.

A quick-look example for the Ibbenbüren flight on 19.8.2012 (see also above) is given in Figure 9.

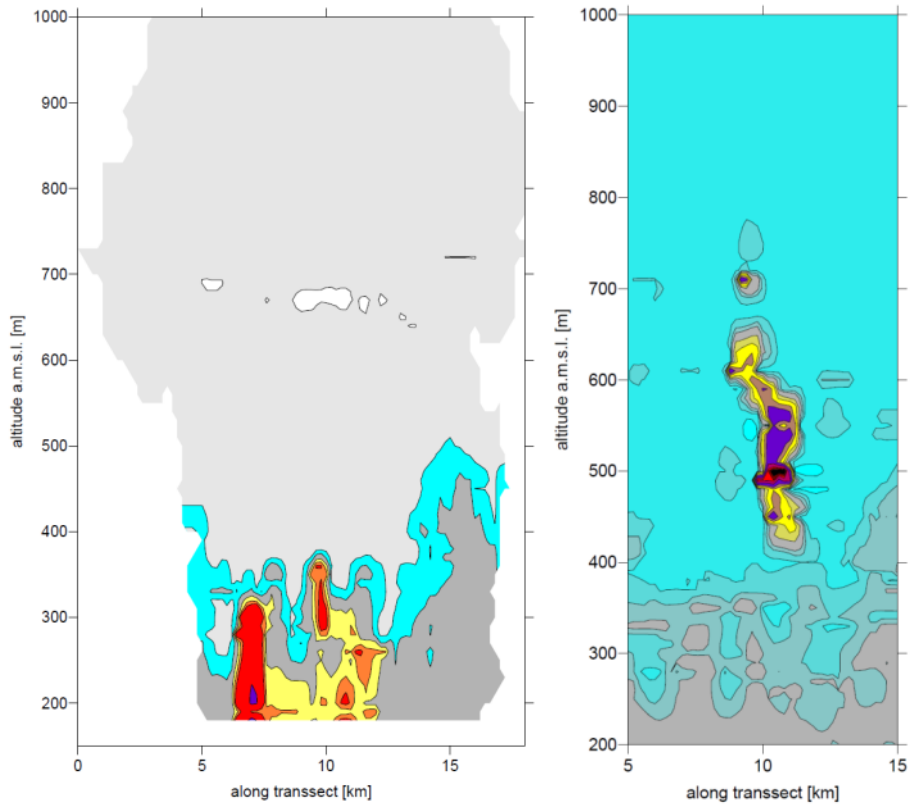

Figure 9: METAIR quick-look analysis of in-situ data over Ibbenbüren 19.8.2012. Left: CH_4 plumes from (exhaust shafts Bockradener-Schacht and Theodor-Schacht). Right: CO_2 plume from coal fired power plant Ibbenbüren, located in between the two exhaust shafts (for final analysis see Chapter 7 and compare Figure 21 and Figure 22).

The results of the quick-look data screening are summarised in Table 2.

4.4. Other relevant data

As in principle the data described above can be used stand-alone to derive emissions from large point sources, other relevant data can help to improve the data analysis or the interpretation of the data.

4.4.1. Wind and topography data

For the interpretation of the data high resolution wind fields from DWD COSMO-DE are available at IUP-UB and high resolution topography data from SRTM v2.1 was used. Together with the wind field measured by METAIR, also the validity of the COSMO-DE wind fields on small scales – as relevant for plume inversion – can be tested.

4.4.2. GOSAT Data

With the support of H. Bösch, University of Leicester, GOSAT target mode was scheduled for the campaign period and target area. JAXA implemented GOSAT target mode for parts of the campaign. The data can later be used to investigate the background GHG concentrations and in case of a perfect match, to investigate how far even GOSAT is able to detect enhanced XCO_2 in areas of very large point sources.

4.4.3. Ceilometer data

In addition and where available the DWD ceilometer network (see www.dwd.de/ceilomap) data providing information on aerosol and thin cirrus layers can be used for quick look and detailed analysis of the data. DWD already provided IUP-UB with an interactive tool to get on-line access to quick-look ceilometers data. The ceilometer data can be accessed via DWD. The ceilometer data can help to characterise the remotely sensed data w.r.t. impact of atmospheric scattering due to aerosol and cirrus clouds.

4.4.4. Emission data

Reported emissions of strong point sources will be used to independently verify the derived emissions from remotely sensed and in-situ CO_2 and CH_4 data. IUP-UB contacted Bezirksregierung Arnsberg, RWE and other local authorities of the different emitting facilities to obtain hourly reported emissions.

The Bezirksregierung Arnsberg provided data for several of the coal mine ventilation shafts for the relevant days and time of overflight comprising airflow and CH_4 concentrations (see Table 4). This included data for the RAG Anthrazit Ibbenbüren coal mine (independently for both ventilation shafts) that was used to validate the inversion results.

The company RWE Power AG is operator of most of the coal-fired power plants in the target list. RWE has kindly provided hourly values of power generation of power plant locations investigated in this study which can be used for calculation of approximate CO_2 emissions (see Table 5).

Table 4: Information on emission provided by the Berzirksregierung Arnsberg. Note that for Schacht Rossenray and Schacht Friedrich Heinrich only data at 2:00 am (CEST) was available.

Target	Date and Time [CEST]	Airflow [m^3/s]	CH_4 concentration [%]
Hünxe	13.08.2012, 8:00-12:00	210	0.10
Hünxe	15.08.2012, 9:00-15:00	207	0.10
Prosper 9	13.08.2012, 8:00-12:00	76.16	0.28
Prosper 9	15.08.2012, 8:00-15:00	81	0.30
Theodor Schacht	19.08.2012, 9:00-13:00	265	0.30
Bockraden Schacht	19.08.2012, 9:00-13:00	240	0.375
Schacht Rossenray/Schacht1 (Lüfter 2)	14.08.2012, 2:00	328.91	0.04
Schacht Rossenray/Schacht1 (Lüfter 2)	16.08.2012, 2:00	331.77	0.04
Schacht Rossenray/Schacht1 (Lüfter 2)	17.08.2012, 2:00	331.34	0.03
Schacht Friedrich Heinrich 4	14.08.2012, 2:00	154.63	0.50
Schacht Friedrich Heinrich 4	16.08.2012, 2:00	154.9	0.45
Schacht Friedrich Heinrich 4	17.08.2012, 2:00	155.11	0.46

Table 5: Sample data as provided by RWE AG, Essen for the example of power plant Weisweiler. Approximate emissions for the time of the overflight can be derived from this information.

Power plant		MWh el	Monthly amount **MWh el**	Monthly amount **CO_2 in t**	**CO_2/MW h_{el}** (monthly mean) [t/h]
Weisweiler (2 x 300 MW_{el}, 2 x 600 MW_{el})			**1042343**	**1380865**	1.32
Sat., 18. August 2012	14:00 - 15:00	1826			
	15:00 - 16:00	1829			
	16:00 - 17:00	1842			
Thu., 23. August 2012	09:00 - 10:00	1312			
	10:00 - 11:00	1313			
	11:00 - 12:00	1321			
	12:00 - 13:00	1316			
	13:00 - 14:00	1310			
	14:00 - 15:00	1308			

5. Processing of campaign data

5.1. MAMAP processing

The data processing of the campaign data from MAMAP will be performed along the lines using the already developed and tested tools as described in Gerilowski et al. 2011 and Krings et al. 2011, 2013. For the processing of MAMAP data, a modified version of the Weighting Function Modified Differential Optical Absorption Spectroscopy (WFM-DOAS) algorithm will be used to obtain vertical column information of CH_4, CO_2 and also O_2 (Level 1 data product).

It is based on a least squares fit of the logarithmic simulated radiance spectrum to the measurements after correction for dark signal and pixel-to-pixel gain. The fit parameters are:

1 atmospheric parameters of interest: partial or total columns of CH_4, CO_2 and O_2,

2 additional trace gas atmospheric parameters for spectrally interfering gases (water vapour),

3 other atmospheric parameters (temperature),

4 a low order polynomial (usually of the second or third order) in wavelength to account for spectrally smooth varying parameters which are not explicitly modelled or less well known. These parameters include, for example, the MAMAP absolute radiometric calibration function, aerosol scattering and absorption parameters, and the surface spectral reflectance,

5 and shift and squeeze parameters from an iterative wavelength calibration procedure.

The results of the algorithm are height averaged increased or decreased profile scaling factors for the respective trace gases. Model radiances and required weighting functions that refer to the sensitivity of model radiances to individual fit parameters are computed with the radiative transfer model SCIATRAN using the HITRAN 2008 spectroscopic data base. To further increase the accuracy of the retrieved data, it is planned to process at least part of the data using a newly implemented look-up-table approach accounting for varying surface elevations and solar zenith angles.

For the interpretation of the MAMAP measurements with respect to sources and sinks of the greenhouse gases CO_2 and CH_4, the column averaged dry air mole fractions (in ppm for CO_2 or ppb for CH_4) are the preferred quantity rather than the total columns (in molecules cm^{-2}). This is because dry air mole fractions are less affected by changes in surface topography, pressure and flight altitude compared to the absolute column.

Dry air mole fractions (XCH_4, XCO_2) from MAMAP column data are generally obtained by using a proxy method. Assuming light path errors at different wavelengths to cancel, XCH_4 can be computed by using CO_2 as a reference and vice versa. O_2 can be used as reference as well but, due to the larger spectral distance, correlation between light paths can be less good. Nevertheless, in the presence of spatially coinciding CO_2 and CH_4 sources, this method may become necessary.

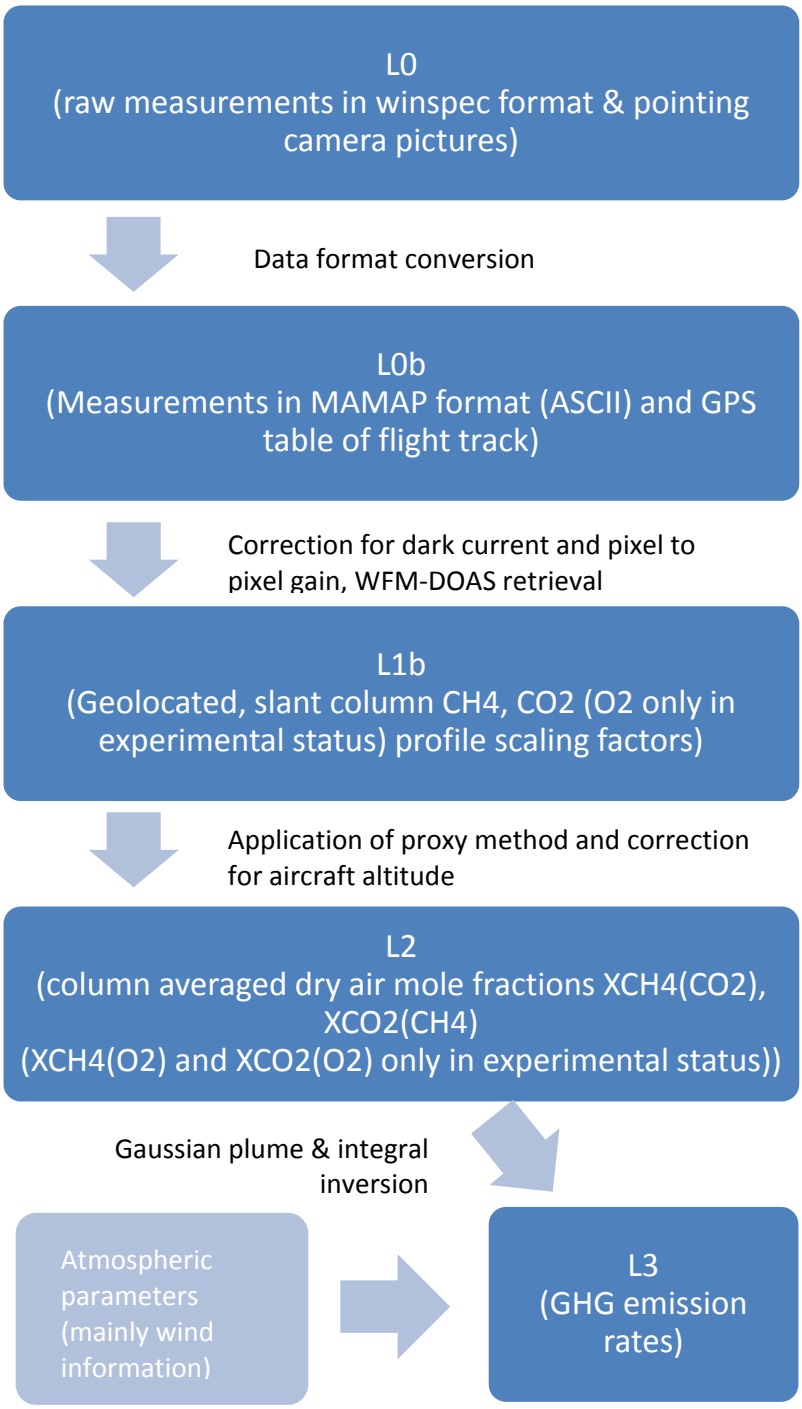

Figure 10: Data processing scheme for MAMAP data.

The MAMAP WFM-DOAS retrieval does not resolve different altitude levels. However, the retrieval has different sensitivities for different altitudes. This behavior can be characterised by the so called column averaging kernels (AK). Below the aircraft, the averaging kernels are increased by a factor of about 2 (for low aircraft altitudes) compared to above the aircraft. This is due to the fact that light from the sun passes through the absorber below the aircraft twice - once before and once after surface reflection. The higher the aircraft flies, the less pronounced the effect becomes, since the height averaged AK are about unity.

For a typical MAMAP measurement, elevated or decreased trace gas concentrations can be expected mainly below the aircraft due to activity at the surface, for example, power plants emitting CO_2 or landfills releasing CH_4. Since the retrieval is not height sensitive, the measurements will be weighted with the mean averaging kernel (ideally being close to unity). If the concentration changes occur evenly at all altitude levels, this gives the correct result. For changes only below the aircraft, this has to be accounted for in the final Level 2 product, for example, by a conversion factor. Otherwise, the column averaged mole fraction variations from the retrieval appear about twice as high as they actually are.

5.2. Processing of In-situ data

The in-situ data has three levels: Raw data that will never be changed, pre-processed data (which usually are called post-processed physical values such as temperature, wind, concentrations, etc.), and a higher level of post-processing in order to get "fluxes". Both the pre-processing and the post-processing can always be refined.

Key characteristics of the METAIR post-processing software are, that neither raw data need to be edited, nor any meta-files are produced. The results are always a one-step transformation of raw data to final results. Refining the post-processing does not mean modifying existing files, but building a new transformation which is transparently documented in a journal-file, which also contains free format comments such as a copy of the flight log and manual notes from the post-processing. Therefore, each set of results is well documented in one file.

6. Data formats and data archive

6.1. Data format and Data archive MAMAP

For the MAMAP sensor the following data products are specified and delivered:

- L0 data - raw measurements in winspec format and pointing camera pictures.
- L0b data of measurements in MAMAP format (ASCII) + gps-table data of flight path. The MAMAP data is organized in a file with structured by headers followed by the detector read outs pixel by pixel, as shown in Figure 11 and Figure 12. The Level 0b data also contains dark current spectra and white light calibration spectra, both to be applied to the data for further processing. Generally white light source spectra consist of four measurements: (1) white light source + straylight + dark current (shutter open), (2) white light source + dark current (shutter closed), (3) stray light + dark current (shutter open), (4) dark current (shutter closed).
  There are 3 ASCII files for each channel (CH4 and O2): A *-index.txt file which lists the white light source files available, *-table.txt which shows the spectra in the same format as the regular data, and additionally a *.txt file which shows for all detector pixels the average result of (1) minus (3) to normalize the data with.
- L1b processed geolocated slant column data CH_4, CO_2 for one fixed SCIATRAN reference scenario per target area/flight day, ASCII format. Each data file contains a header including the date of the measurement and a description of the data format (see also Table 6). Furthermore, relevant input parameters for the reference radiative transfer are given (surface elevation, aircraft altitude, solar zenith angle, background XCO_2 and CO_2 column, background XCH4 and CH4 column).
- L2 geolocated $XCH_4(CO_2)$, $XCO_2(CH_4)$ for one SCIATRAN reference scenario per target area/flight day, ASCII format. Each data file contains a header including the date of the measurement, description of the target, the background XCH_4 (or XCO_2) value and a description of the data format. The data is organized in columns and will cover data as specified in Table 7. Additionally the files contain a header that explains the data format and basic description of date, target and background XCO_2 or XCH_4.

MAMAP data includes the L0b spectra and GPS files, L1b data and the L2 data files for selected targets. The MAMAP data archive will be organized in subfolders for each flight day and futher subfolders for L0b, L1bL1 and L2 data. Additional readme files explain data format and content.

```
#####
# SPEC: 000001
# VERSION: 1.4.0 PROCESSED-ON: 2011-06-05
# FILENAME: open_98ms_10x1_zenith_ch4_1.SPE
# DATE: 04.06.2011 TIME: 08:16:59.4 WINSPECTIME: 08:17:52 SYSTIME: 08:18:16.6
# LAT: N 053:30:12 LON: E 008:34:16 ALT: +00003
# P: +000.000 R: +000.000 Y: +000.000
# CHN: 1024 ROWS: 0001 RO: 00010 EXP: 00.09800 ACCUMS: 0001 SHUT: 1 SAT: 0 NADIR: 0
#####
00807 00717 00966 00816 00875 00844 00838 00831 00872 00866 00963 00847 00847 00843 00912 00796 00878 00784 008
@@@
00802 00697 00962 00818 00870 00842 00829 00831 00878 00881 00973 00845 00838 00844 00902 00785 00854 00794 008
@@@
00811 00708 00954 00794 00866 00844 00841 00840 00886 00864 00966 00844 00838 00857 00901 00792 00856 00795 008
@@@
00815 00703 00954 00808 00864 00842 00819 00841 00869 00868 00973 00840 00838 00859 00901 00797 00851 00798 008
@@@
00814 00710 00956 00810 00877 00840 00833 00821 00886 00877 00963 00860 00831 00849 00896 00794 00861 00798 008
@@@
00814 00687 00961 00809 00874 00844 00827 00827 00870 00872 00950 00853 00838 00847 00895 00778 00859 00797 008
@@@
00808 00708 00962 00804 00877 00842 00830 00833 00871 00875 00969 00839 00844 00850 00908 00800 00852 00807 008
@@@
00804 00693 00960 00801 00868 00846 00835 00835 00880 00870 00965 00839 00829 00838 00902 00787 00852 00802 008
@@@
00794 00712 00959 00806 00873 00832 00841 00830 00877 00865 00979 00852 00828 00851 00909 00793 00875 00797 008
@@@
00803 00702 00938 00805 00881 00838 00844 00835 00877 00870 00975 00850 00831 00851 00905 00802 00862 00801 008
@@@
#####
# SPEC: 000002
# VERSION: 1.4.0 PROCESSED-ON: 2011-06-05
# FILENAME: open_98ms_10x1_zenith_ch4_2.SPE
# DATE: 04.06.2011 TIME: 08:17:01.6 WINSPECTIME: 08:18:17 SYSTIME: 08:18:18.7
# LAT: N 053:30:12 LON: E 008:34:16 ALT: +00003
# P: +000.000 R: +000.000 Y: +000.000
# CHN: 1024 ROWS: 0001 RO: 00010 EXP: 00.09800 ACCUMS: 0001 SHUT: 1 SAT: 0 NADIR: 0
#####
00793 00705 00948 00810 00868 00836 00850 00834 00869 00864 00963 00848 00837 00845 00906 00802 00881 00801 008
```

Figure 11: File format for MAMAP L0b spectra. The aircraft attitude (roll (R), pitch (P) and yaw (Y) is not yet implemented in the file. CHN refers to the number of pixels in a row. ROWS is 1 for a line detector. RO refers to the number of readouts in a burst (before a new header occurs), EXP the exposure time for single measurements in seconds, ACCUMS the number of stacked spectra. SHUT : 1 indicates an open shutter, whereas a value of 0 denotes a dark current measurement. NADIR is a flag for the referred port. Note that the external telescope is coupled in via the zenith sky port and the flag is hence set to 0. The tag SAT refers to a flag for saturation which however is not implemented in the L0b spectra yet. Saturated pixels will be rejected at a later stage in the retrieval itself.

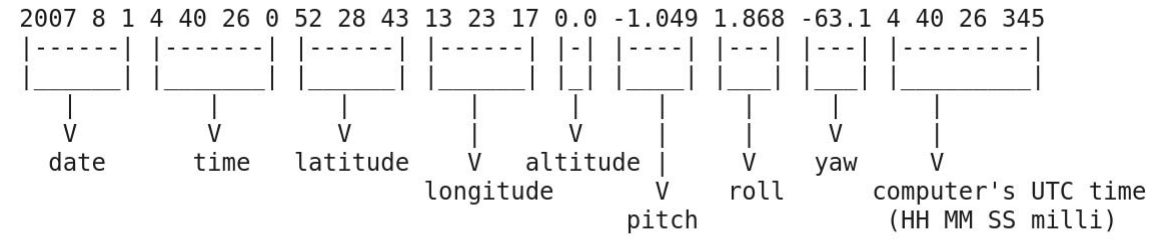

Figure 12: File format for MAMAP L0b GPS files. Latitude and longitude are given in degrees, minutes and seconds, the aircraft attitude information in degrees. The aircraft altitude is given in m.

Column	Parameter name	Parameter unit	Description
1	Longitude	degree	Ground pixel center longitude
2	Latitude	degree	Ground pixel center latitude
3	CH4	-	Scaling factor for background CH4
3	CO2	-	Scaling factor for background CO2
4	Precision	-	Measurement precision (1 σ) for scaling factors for XCH4(CO2) or XCO2(CH4)
5	RMS CH4	%	Root mean square error for CH4 fit
6	RMS CO2	%	Root mean square error for CO2 fit
7	Aircraft Altitude	m	Aircraft altitude during measurement
8	Solar zenith angle	degree	Solar zenith angle for the time and place of measurement
9	Hour	hr	UTC time
10	Minute	min	UTC time
11	Second	s	UTC time

Table 6: Data format of MAMAP L1b data. Additionally, the file may contain other auxiliary data.

Column	Parameter name	Parameter unit	Description
1	Longitude	degree	Ground pixel center longitude
2	Latitude	degree	Ground pixel center latitude
3	XCH4(CO2) or XCO2(CH4)	-	Scaling factor for background XCH4 or XCO2
4	Precision	-	Measurement precision (1 σ) for scaling factors for XCH4(CO2) or XCO2(CH4)
5	Background col.	molec./cm²	Background total column of CH4 or CO2 (depending on surface elevation)
6	Total CH4 change or Total CO2 change	molec./cm²	Total measured variation from background of CH4 or CO2
7	Elevation	m	Surface elevation
8	Aircraft Altitude	m	Aircraft altitude during measurement
9	Hour	hr	UTC time
10	Minute	min	UTC time
11	Second	s	UTC time

Table 7: Data format of MAMAP L2 data. Additionally, the file may contain other auxiliary data.

6.2. Data Format and Data Archive In-Situ (METAIR)

The standard format (Level 1b) for METAIR data are tab-delimited ASCII-Files containing all parameters after explicit time and 3-d-position. Import in Excel is directly possible. The in-situ data archive will be organized in the C-MAPExp subfolders for METAIR. Data will additionally be separated by subfolders for each day (yyyymmdd). Readme files will explain data format and content.

From all the flights and targets treated, there are results in *C_Map_Exp_MetAir_results_YYYYMMDD.zip*, in the following directories (details see Annex 3):

`docu:`

This report and other documents.

`main_grd_100:`

The main grids (concentrations, masses and fluxes above background) with 100 m resolution. This .grd format is very transparent (ASCII, with rows and columns, and ranges in the header). However, the easiest use is to download SURFER from www.goldensoftware.com, where also the demo version will open these grids as a preliminary graph (more elaborated graphics see directory pdf; examples below). When clicking of such a plot (e.g. 23_Weisw_100_CO2_T1_3flux_ex.grd), such a plot will occur, and the values can be read at the cursor position:

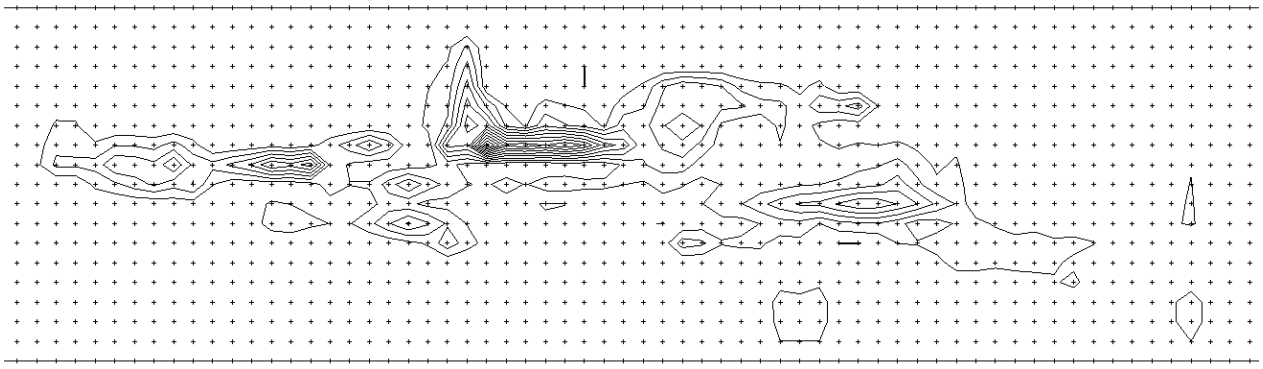

`maps:`

In this folder, all screenshots of regional views of the moving map with the flight patterns are stored.

`MetInfo:`

In this folder, information about the general weather situation can be found (charts, METAR, nearby soundings)

`other_grids:`

Additional parameters (concentrations including background, wind, and other resolutions) in the same format as in main_grd_100.

`pdf:`

All graphics that were generated either to check the post-processing, or to display selected plumes, as e.g. *23_Weisw_100_CO2_contours.pdf*, or *19_Bockrad_plus_Theo_100_near_CH4_contours.pdf*.

`results:`

All result files as described below, with very detailed meta-data, and print-plots of all the targets treated until now, with all the different resolutions. A summary is in *Results_in_situ_plumes_vYYYYMMDD.xlsx*

`selected_data:`

From every target where the emissions have been calculated, the data used is stored in these files. Some of it is plotted in plots like *15_RWE_cluster_plume_check.pdf*, or *15_RWE_cluster_plume_bubbles_CO2.pdf*.

7. The calculation of "fluxes" based on in-situ measurements of concentrations and wind

7.1. Methodology

There are exhaustive discussions in the literature about "fluxes", and their "closure" (complete treatment). However, this is mainly about vertical turbulent fluxes and budgets of energy and constituents in larger areas, where all the terms, including storage terms, are important. A concise and recent overview about this basic problem is given in Foken et al. (2009) and references therein.

However, in this study, the focus is on horizontal fluxes close to a strong point source, or groups of point sources. In this situation, the main fluxes are through a vertical plane, perpendicular to the mean flow during the measurement. In some convective situations, also the vertical flux above the source has to be considered.

When dealing with distinct sources in a limited area, where deposition, storage and other terms can be neglected, we have the following situation:

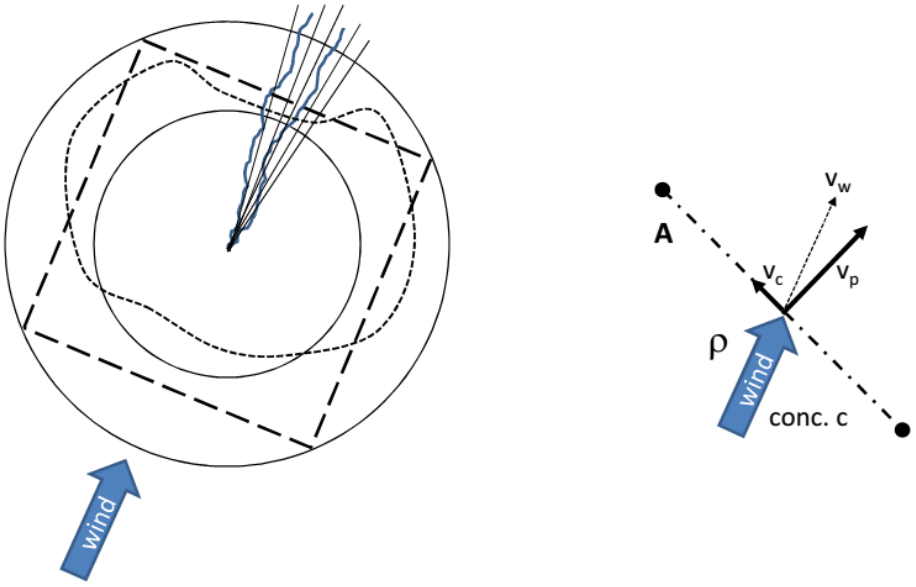

Figure 13: A two-dimensional area limited by two cylinders of different radius (fine solid lines), by a rectangular box (thick dashed line), or by an irregular boundary (shorter dashed line), with a plume leaving the area. In all these cases, the net flux out of the defined region is concentrated within the part of the boundary, where the plume is crossing. All other (background) fluxes are assumed to be balanced (same fluxes into the box as out of the box). The radial lines along the plume are indicating that instead of the length of a boundary, also angles from a polar coordinate system could be used (finally not applied, but mentioned here because it was under discussion). The detail on the right is showing the incremental calculation of any fluxes through any shape of boundary: the flux is the product of area A, the density ρ, the concentration c, and the perpendicular wind component v_p, with the wind vector v_w, and the crosswind component v_c.

Since the wind field is not homogeneous in the vertical, the conceptual model described in Figure 13 can either be applied for different layers, or the "wind vectors" and the "concentrations" are already multiplied and averaged in the vertical. The second interpretation is better, because the first one raises the question what happens if a parcel of air changes it's altitude, and hence the layer. The general statement is, that the inflow and outflow of background concentrations is balanced (sum = zero), and only the additional fluxes added to the background by known (and unknown) sources in the "box" are of interest.

Initially, we intended to apply the method with the radial coordinate system, where every flux perpendicular to a cylinder around a known source is attributed to an incremental angle of this cylinder (e.g. 1°), which is invariant with the radius. The measured fluxes would then initially have the unit $kg \cdot deg^{-1} \cdot m^{-1} \cdot s^{-1}$, where the total fluxes could be integrated over the relevant sector (where the plume was in), and over the height. However, this approach is questionable when two or more sources are in the cylinder, and has no advantages compared with the final method chosen.

A second idea was to calculate backward trajectories from background concentrations into the plume. Both options originated from work, where we flew a cylindrical flight pattern with two aircraft over a larger area, with no point sources in it (Beringer et al., 2011).

However, when working with the data, it became obvious that the concept of one single vertical cross section perpendicular to the mean flow is sufficient, more universal, and easier to explain.

Instead of a box or cylinder around the source, we put a virtual box downwind of the source(s) according to Figure 14.

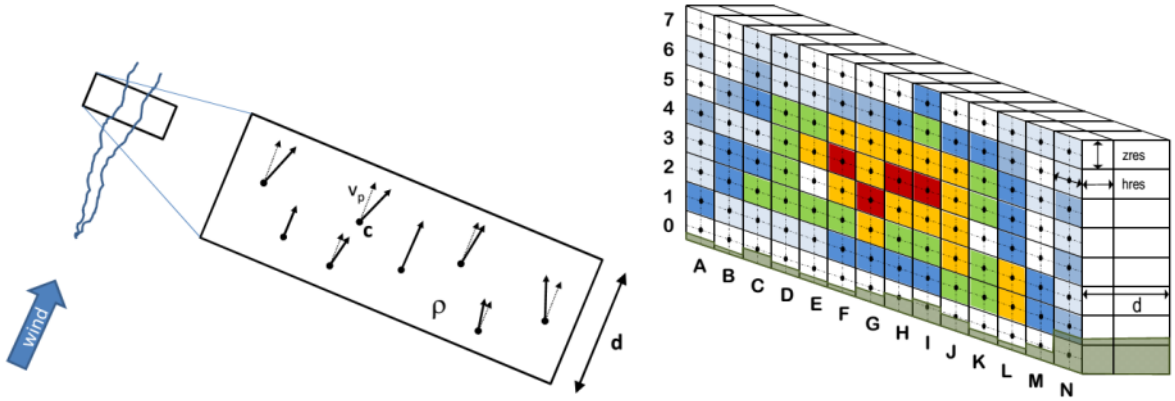

Figure 14: Left: Instead of a vertical cross-section with infinitesimal thickness, a "wall" with a defined thickness d, where the cross section was flown, was observed with the in-situ measurements. The individual fluxes are calculated from individual wind vectors and concentrations in turbulent resolution (5 Hz). In order to get a spatial distribution of the fluxes, this "wall" is divided in grid cells (right). Right: The cross section of figure left.

This "wall" has a certain depth, and was observed during a certain amount of time. The fluxes through each "brick" of that "wall" (a grid with vertical and horizontal spacing according to Figure 14, (right) are calculated straight-forward:

Each measurement of an instantaneous flux (concentration times perpendicular component of the wind) is regarded as a sample, and averaged in each grid cell. It is important to note that this includes both the "mean advective fluxes", and the "turbulent fluxes" (see key terms above). Let us call this approach the "customs approach": Each individual "parcel of air" found to cross the "wall" with the perpendicular wind component is summed up to be representative for this grid cell. In case there is a relevant turbulent flux (both horizontally and vertically from neighbouring grid cells), this is included with this approach. Maybe we would get similar results when multiplying average concentrations with average winds per grid cell. However, the fully resolved approach is better (more complete), because possible co-variances are included. To explain: If lower concentrations are associated with lower wind speeds, and vice versa, a real (turbulent) flux is there. However, when concentrations and winds are averaged first, this turbulent flux would not be detected. With the remote sensing approach, the turbulent fluxes are indirectly included when fitting the column concentrations to a Gaussian plume model. Mentioning the Gaussian plume model it is important to note that the in-situ method described here is not assuming any shape of the plume. It is a pure statistics about parcels of

air crossing an imaginary border. The assumptions and the consequences when they are hurt are discussed below.

Average concentrations and average winds per grid cell were calculated in order to plot these fields for the cross-sections. Concentration fields were calculated as absolute concentrations, and as net concentrations, with the background concentrations subtracted. How the background concentrations were calculated is described below.

For the intercomparison of the in-situ measurements with the column concentrations from the spectroscopic remote sensing data, the concentrations (i.e. the masses of CO_2 or CH_4) were summed up in vertical columns. Even then, a direct intercomparison is difficult when the flights were not simultaneous, and not on the same radial. Maybe the most robust number to compare is the mass of CO_2 or CH_4 across the plume. This would only be affected when the wind field or the emissions would have been non-stationary within the time of both observations.

The positions of the cross-sections were selected based on the flight patterns (minimum and maximum distance), and the mean wind direction. The angle of the cross-section was adjusted for a cross-wind component of 0.1 m/s or less, and the width of the cross section should include enough background concentrations.

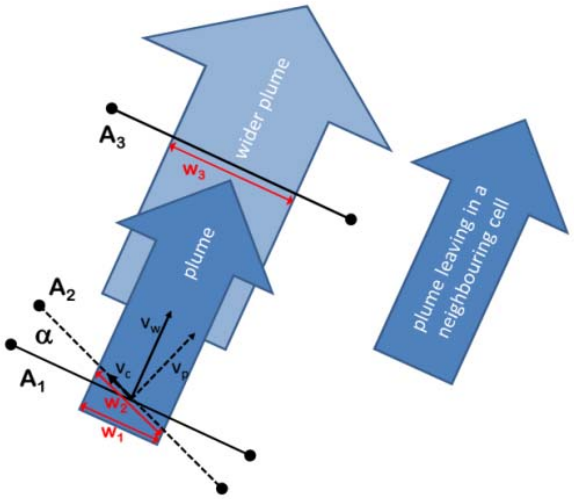

Figure 15: Discussing three possible problems assuming a misalignement of the wall, a widening of the plume within the wall, or a plume leaving the wall in another cell than it has entered. A_1 is the perfectly aligned wall element for the given wind vector v_w, with no cross wind component, where the plume crosses with a width of w_1. A_2 is misaligned by angle α with a cross wind component v_c, and A_3 is a wall element further downstream, where the plume might be wider (w_3). It is obvious from the graphics that $v_p = v_w \cdot \cos(\alpha)$, and $w_1 = w_2 \cdot \cos(\alpha)$, i.e. $w_2 = w_1/\cos(\alpha)$. Since now $v_w \cdot w_1$ and $v_p \cdot w_2$ are equal, there is the same total mass transport across the wall (air or trace gas), even when the flux (mass per area and time) is reduced when misaligned. When the plume is widening, the concentration is diluted accordingly, i.e. the total mass transport remains the same (also in two dimensions) as long as the flow (not the plume!) has no convergence or divergence within the wall. The only interesting case is when a plume does not leave the wall in the same grid cell than it has entered it. In this case, both grid cells are associated with the same flux, i.e. the mass transport is doubled. This is also the case when a plume that is smaller than one grid cell is found in both cells (splitted). Conclusions: (i) the alignment with the mean wind should be adjusted because of this third effect (this has absolute priority, i.e. the wall does not need to be aligned with the flight track, which was – in some cases – due to airspace restrictions – not crossing the plume perpendicularly); (ii) the size of the grid cells must not be too large; (iii) as stated elsewhere, the variation of the grid size is a measure for the sensitivity.

A good example is given in Figure 16 with the plume of "Weisweiler" on August-23.

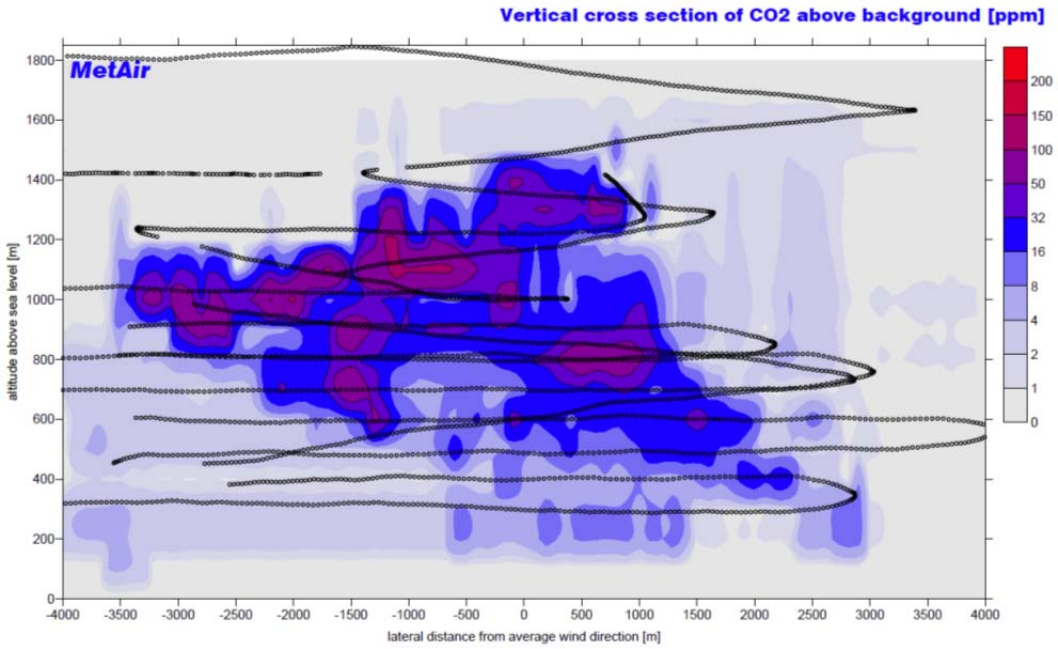

Figure 16: The CO2-plume of the coal power plant of Weisweiler (Eschweiler) was captured perfectly on August-23. The dense flight pattern (circles every second) allowed a good vertical and horizontal resolution. The background concentrations (minimum concentrations per layer) were subtracted. The extrapolation to the surface is described below.

Not all the plumes that were analysed are displayed as contour plots of concentrations and fluxes, but for 21 targets, the grid-files and the summarised results are available in the electronic data package. For the case shown in Figure 16, the details of the numerical results to be found in *23_Weisw_results.txt* are shown in the Annex 3 as an example.

Using Figure 14, most steps of the processing can be explained. Based on the flight track on the map, the minimum and maximum distance from the source was defined. The difference of these distances is the thickness of the "wall", shown as d in Figure 14. The orientation of the wall is adjusted until the amount of the average crosswind component is 0.1 m/s or less. However, as shown in Figure 15, even larger crosswind components would not be a problem. However, it makes sense to adjust the cross section perpendicular to the average wind direction. In a second step, the lateral boundaries are chosen. They should be clearly outside of the plume, but not too far away since this would increase the uncertainty about the background concentration. The wider the cross section the more likely secondary sources are included in the flux calculation (see below, when discussing the background).

The horizontal and vertical resolution "hres" and "zres" was either 50 or 100 m until now. All calculations were done in vertical columns of hres x hres, i.e. all the measurements within d – which is in in the order of a few hundred meters - were projected onto a "wall" of thickness hres. In the vertical, the grid spacing was zres. Therefore, the calculations were done in grid cells with the dimension hres x hres x zres, using data in the volumes hres x d x zres.

In Figure 14 (right), all grid cells containing data are coloured and cells with no data are left blank. The algorithm that interpolates the cross section begins on the top level, where measurements might be sparse. In the example shown, the cells E7 to H7 and J7 to K7 would be interpolated linearly, where A7 to B7 would be kept at the value of C7. Missing values in E3 and K3 would be interpolated vertically from neighbouring grid cells E2/E4 and K2/K4 respectively. The same for A5, M3, M4 and

M6. Of course we could have applied standard interpolation methods like "anisotropic inverse distance averaging" or "Kriging" which are included in the software package Surfer (goldensoftware.com) used for the graphs. However, the linear interpolations and extrapolations were sufficient for filling the grids (mainly for graphical reasons), because our focus was on measured data, and the results should not depend too much from interpolations and extrapolations. However, varying the resolution of the grid (e.g. 100 m instead of 50 m for hres and zres) is a good sensitivity test for assessing the robustness of the results.

Two examples, for those plumes shown in Figure 16 and Figure 17:

case	hres and zres 100 m	hres and zres 50 m	hres and zres 200 m	hres and zres 100 m, no_ext
Weisweiler_23 with good coverage	21.43 Mt/a	21.17 Mt/a -1.2%	22.05 Mt/a +2.9%	21.27 Mt/a -0.75%
Weisweiler_18 with less coverage	15.58 Mt/a	13.76 Mt/a -11.7%	12.46 Mt/a -20.9%	14.16 Mt/a -9.1%

The reference in both cases is 100 m resolution, with extrapolations to the surface (both) and extrapolation to the inversion (Weisweiler_18). However, the extrapolation is a minor uncertainty; the different resolutions are causing larger differences. The measurement on August 23 is robust, with a total uncertainty of less than 5% (coarse estimate), whereas the measurement on the 18th seems to have an uncertainty in the order of 20 to 30 %. These two examples are showing that the main uncertainty is not resulting from the uncertainties of the measurements (wind speed 0.5 m/s; CO_2 concentration 0.5 ppm), but, from the flight pattern.

Extrapolation to the surface

Usually there was a gap between the lowest flight track, and the surface (taken from SRTM). The maximum of the DTM below the flight track was taken as the terrain elevation below the column. The different parameters were treated differently:

Concentrations: Kept constant in the grid cells below the lowest flight track. This might cause an underestimation for CH_4 (sources near the surface), and an overestimation for CO_2. However, both is not very relevant, and we just do not know it better. See the comment concerning fluxes.

Masses for column concentrations: Proportional to the gap, i.e. in cell C0 in Figure 14 (right), about 55% of the mass of cell C1 is taken.

The wind is zero below the DTM. However, the fluxes above the surface are taken from the layer above. For CO_2 this is irrelevant, since the plumes did not reach the surface, and we flew in the background concentrations below the plume in most cases. For CH_4 this choice is considering the fact that concentrations tend to increase towards the surface, compensating the lower wind speeds. Empirically, we very often observed the same wind speeds at 10 m height (reported from the airfields) as we have measured in flight 150 m or higher above the ground, i.e. the "logarithmic wind profile" is very shallow, close to the surface. Anyhow, this extrapolation should not be important. The fraction of fluxes compared with the truly measured flux is indicated as a percentage in the numerical results.

Extrapolation above the highest flight track

In two cases, the "curtain" flown did not reach the top of the plume. However, there were strong inversions above, allowing the conclusion that the plume did not extend higher than this. In these cases, the altitude of the inversion was known, leading to a linear interpolation between the highest flight track (e.g. at 1050 mAMSL) and the 1300 mAMSL (altitude of the inversion) as shown in Figure 17.

Background concentrations

The background concentrations were assumed to be the minimum concentrations in each layer (1 to 7 in Figure 14 right). It is clear that the background is not just one concentration for all altitudes. However, it is clear that this is a sensitive parameter. Taking the minimum per layer means that any enhancement above this lowest possible background concentration is considered to be a flux from the source(s) under study. However, concentrations exceeding the background could also be caused by sources far away, or convective mixing from the boundary layer. Taking the minimum tends to overestimate the local fluxes. However, in clear cases like in Figure 16 and others this should not be a problem. It might be a problem when the concentrations are not strongly enhanced (as e.g. on the far cross section in Figure 22), or when the coverage by measurements is poor (also Figure 22f). Another approach to calculate background concentrations would be to take the 10% or 20%-percentile of lowest concentrations per layer. However, the difference in clear cases would not be relevant, and the minimum concentration is the best estimate for the background concentrations on a larger scale, especially because the measurements are accurate (both CO_2 and CH_4), and we do not have to consider artefacts in minimum concentrations. They are at least averaged in the 50 x 50 or 100 x 100 m grid cells.

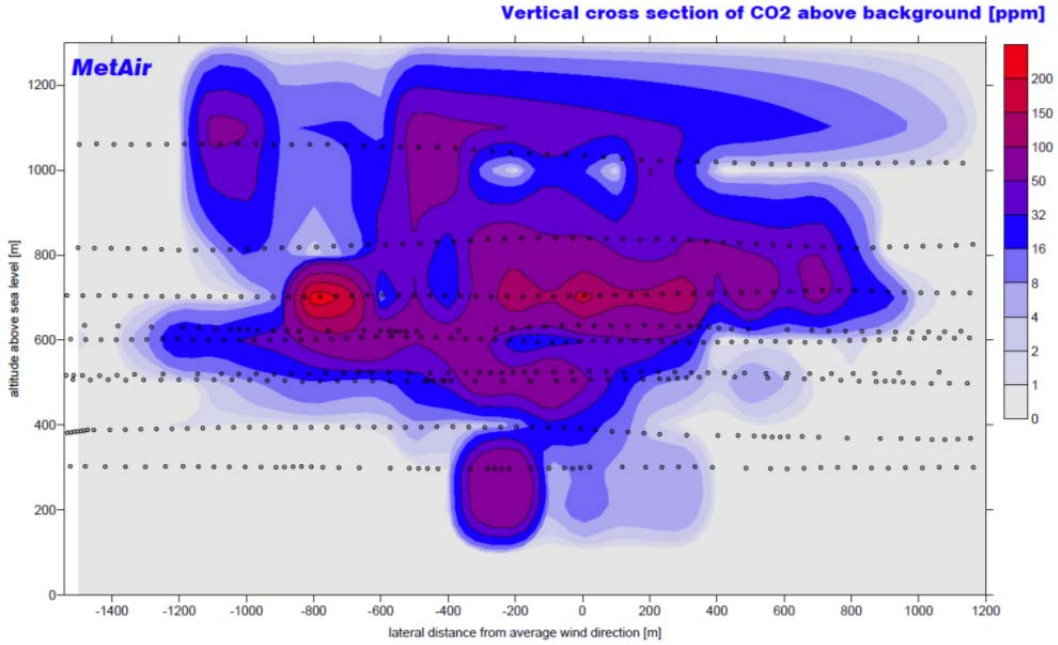

Figure 17: The CO_2-plume of the coal power plant of Weisweiler (Eschweiler) was not captured completely on August-18. The highest traverse flown was at about 1050 mAMSL, while an inversion was present at 1300 mAMSL (radio sounding of Essen) Therefore, the concentrations measured on 1050 mAMSL were linearly interpolated to background concentrations on 1300 mAMSL. The higher concentrations above the highest flight track at 1100 mAMSL are looking like an artefact. However, they are not. This is due to the fact that the grid resolution is 100 m, and the concentrations measured at 1050 mAMSL or higher were averaged in the grid cell centred at 1100 mAMSL (see Figure 14 right). The same is true for the 300 m level, where the measurements at

about 330 mAMSL are attributed to. Below, the interpolation goes to zero (background) below the digital terrain model (not visible here). The percentage of extrapolations of the CO_2 fluxes above and below the explicit measurements was only 9% (6% on top; 3% below).

7.2. Ibbenbüren August-19, with CO_2- and CH_4-sources

The three plumes in the region of Ibbenbüren form one small coal power plant Ibbenbüren and two coal mine ventilation shafts Bockraden and Theodor were an interesting set of sources documented on August-19 (see Figure 18).

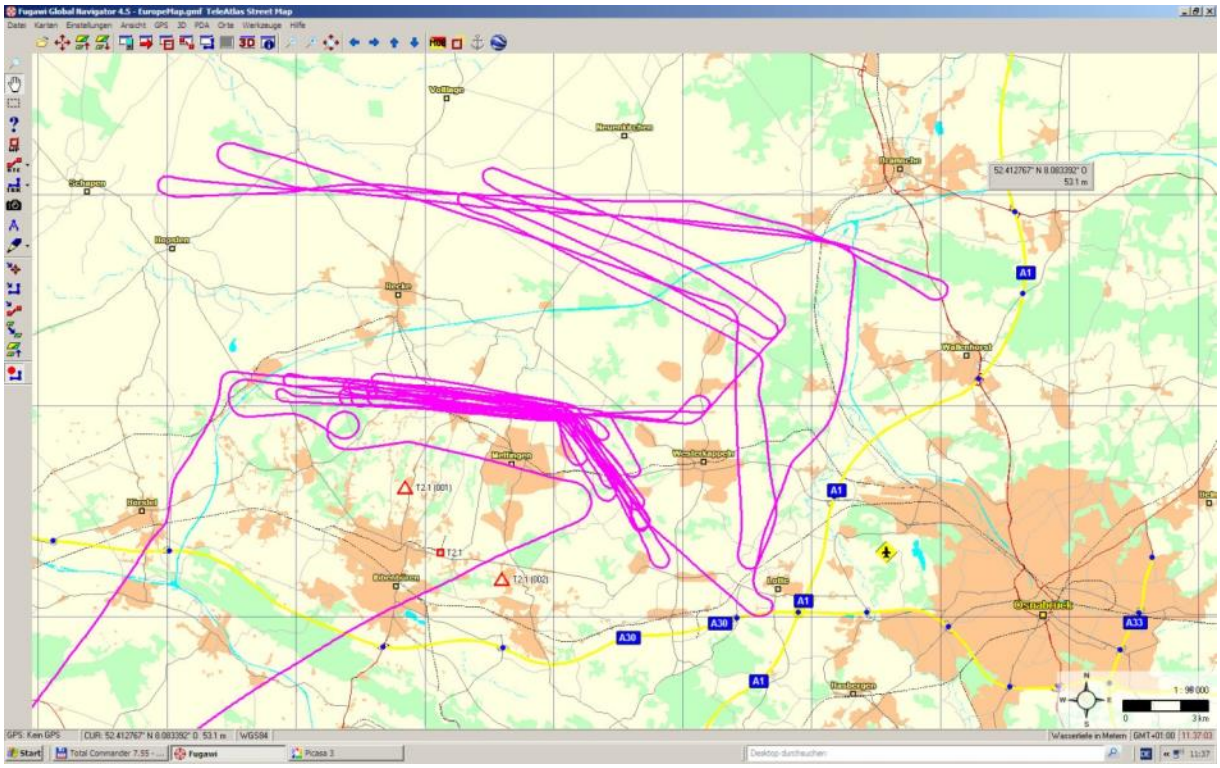

Figure 18: The CO_2-plume of the coal power plant of Ibbenbüren (T2.1) and the two shafts Bockradener_Schacht (T2.1(001)) and Theodorschacht (T2.1(002)) with two curtains flown. The first one is roughly 5 km away from the sources, and the second one roughly 12 km. The CO_2 plume from T2.1 was captured well in both cross sections (Figure 19 and Figure 20), whereas the CH_4-sources are well captured in the near range (Figure 21), leading to some questions on the second cross section (Figure 22).

For the power plant Ibbenbühren the results for the two cross sections in Figure 19 and Figure 20 were in very good agreement: 6.71 Mt/a and 6.50 Mt/a. This is an indication that the flux calculations based on the in-situ measurements are quite accurate and robust.

The CH_4 fluxes of Bockradener Schacht and Theodorschacht in the first cross section (Figure 21) was 22.74 kt/a and 19.44 kt/a respectively. However, the sum in the more distant cross section (Figure 22), where the plumes were overlapping, was calculated to be 72.49 kt/a. It is obvious that some significant overestimation was from the western part above 500 mAMSL, where there were no measurements, and the top-down interpolation led to artefacts. Additionally, plumes and enhanced concentrations in the boundary layer from other sources might have been captured as well.

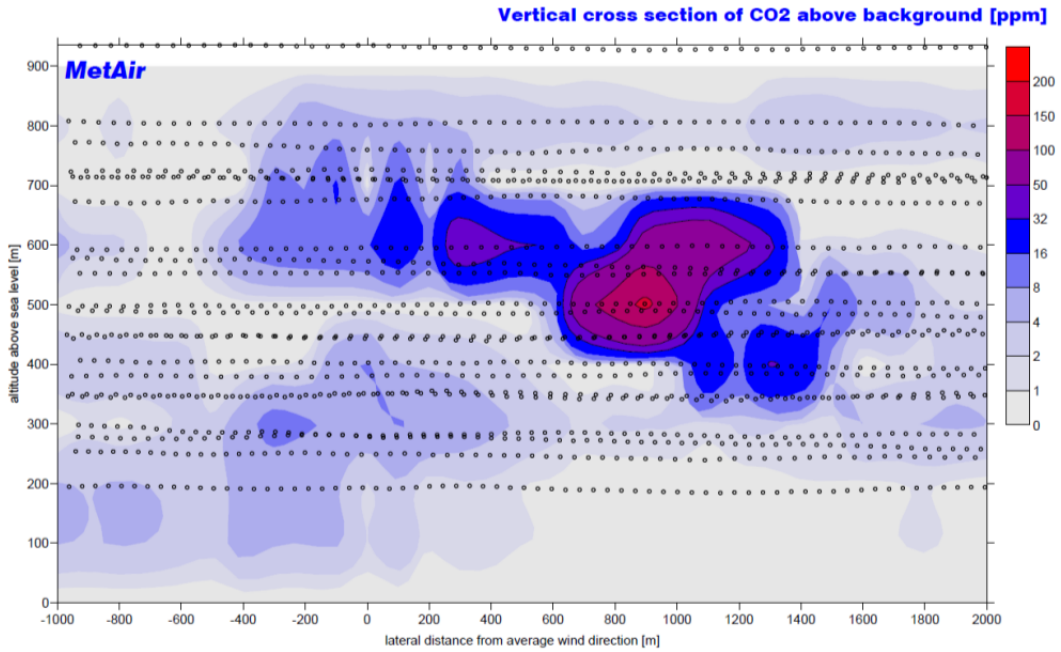

Figure 19: The plume of the coal power plant of Ibbenbüren captured on the nearer cross section.

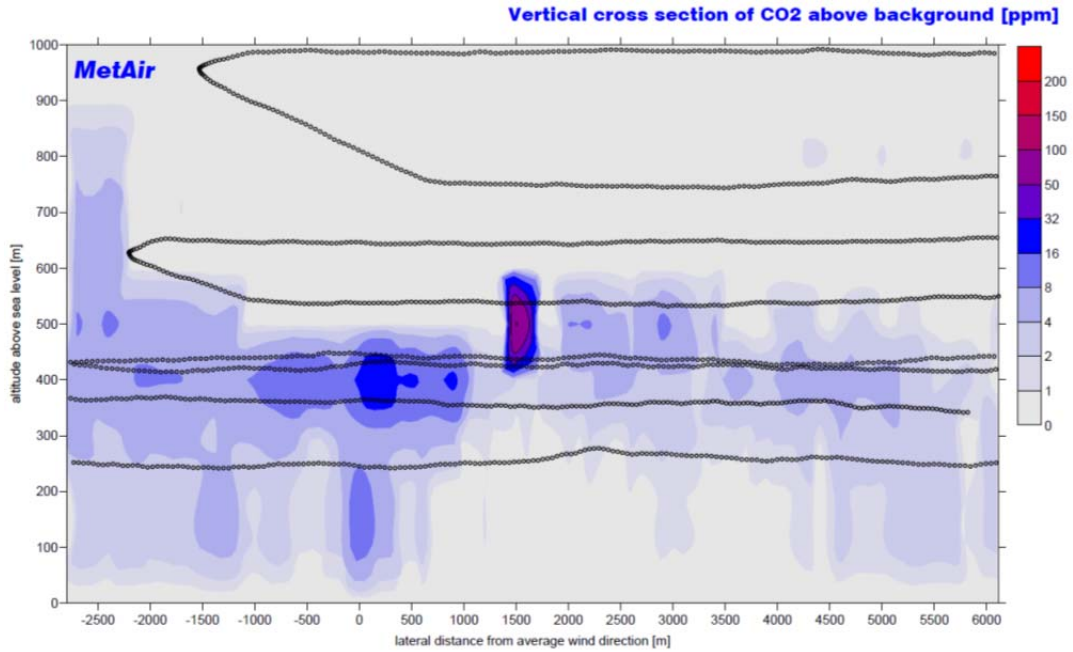

Figure 20: The same plume as in Figure 19 on the second cross section.

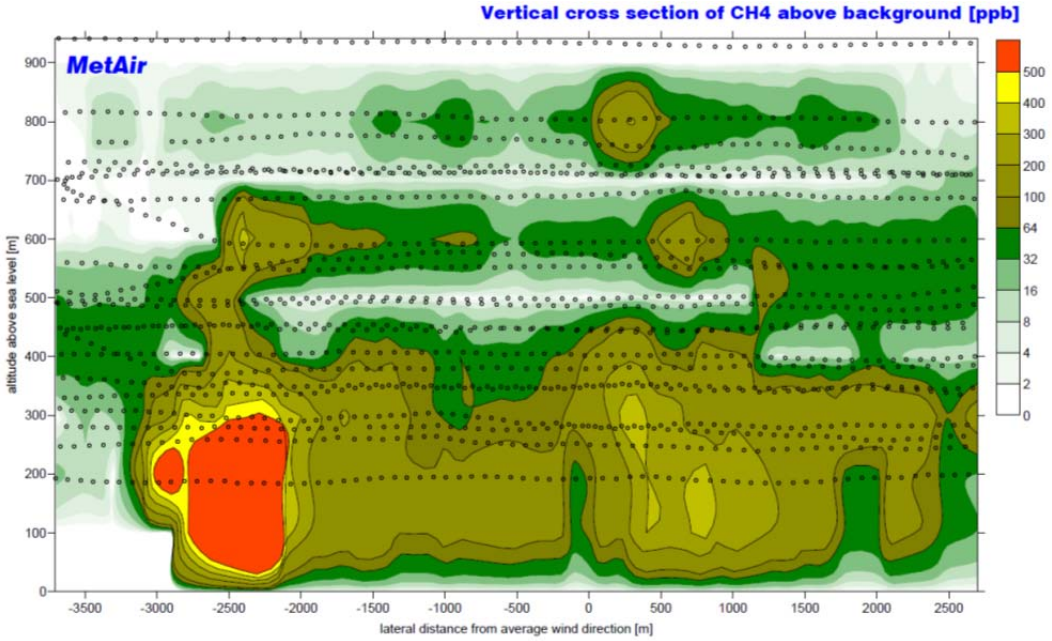

Figure 21: The two CH4-plumes of Bockradener Schacht and Theodorschacht in 5 km distance from the sources.

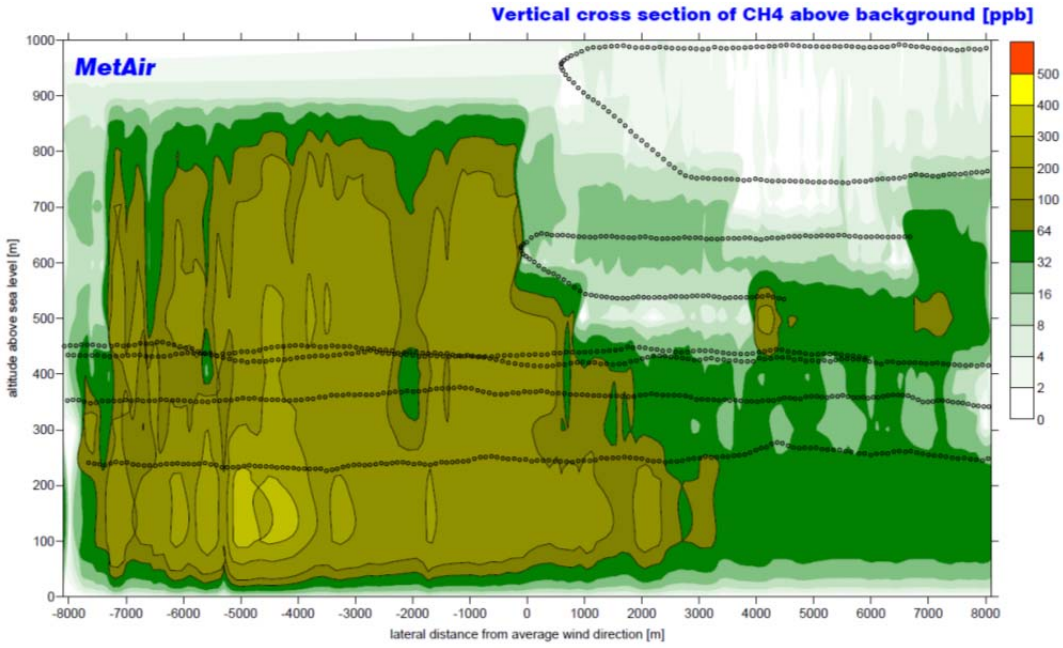

Figure 22: The two CH_4-plumes of Bockradener Schacht and Theodorschacht in 12 km distance from the sources. The flight track was not covering the western part of the altitude range above 500 mAMSL, leading to artefacts and inconsistent results.

The main conclusion in this case is, that very remote cross sections, with incomplete coverage, do not deliver reliable measurements.

7.3. The cluster of four power plants near Neurath - Niederaussem

These targets were documented during four days (August-15/16/17/18), delivering estimates of 53 Mt/a, 49 Mt/a, and 50 Mt/a for August-16 to 18 (August-15 not yet evaluated), which seems quite consistent. However, these cases were completely different (see Figure 23).

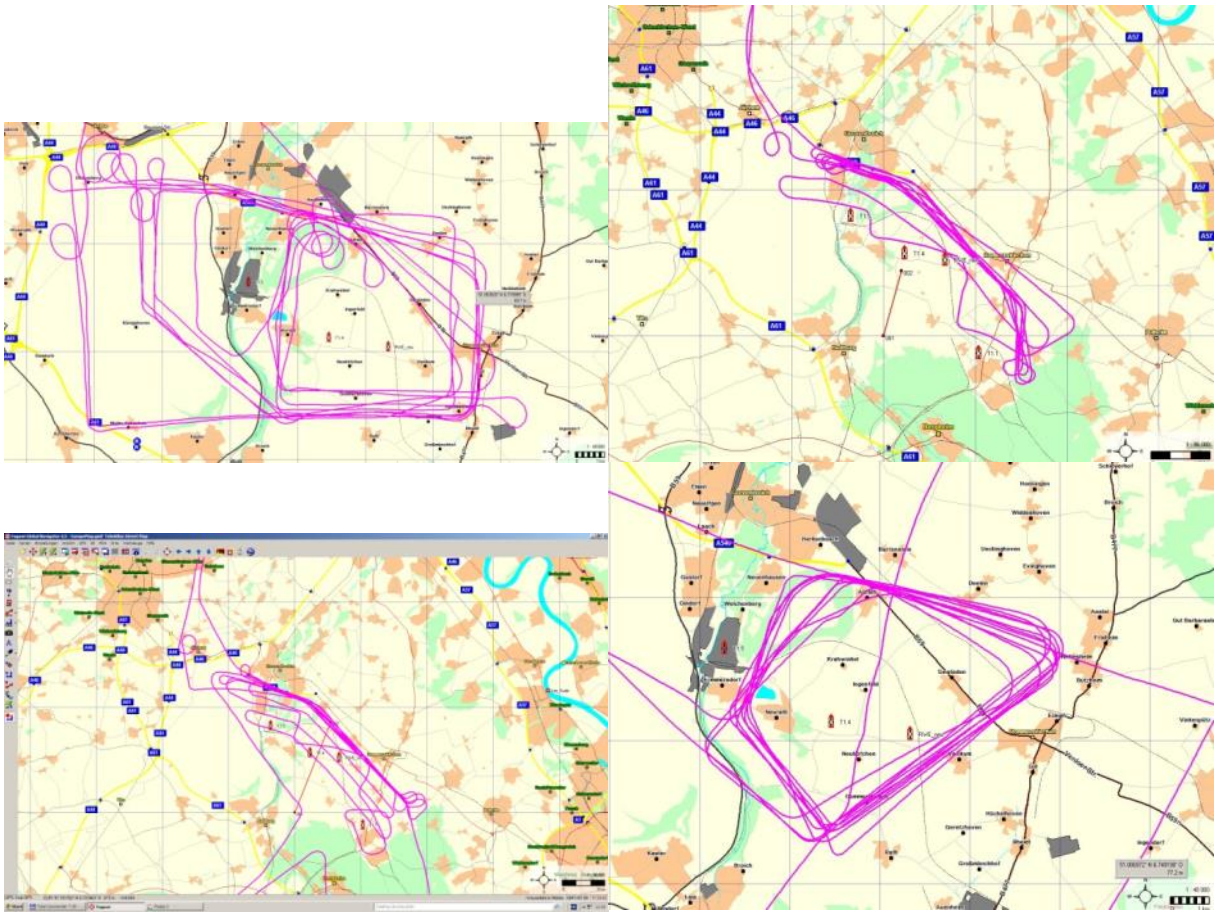

Figure 23: RWE cluster Neurath-Niederaussem flown on four days (August-15 top left, 16 top right, 17 bottom left, and 18 bottom right. On the 16th and 17th, relevant convective fluxes were visible and were included in the calculations. On August-18 it was possible to separate the emissions of T1.5 and the other sources.

Figure 24: Two photographs of sources shown in Figure 23.

For all the details, please refer to the files containing the results, and the grid-files. In the following, only some examples of cross sections of plumes are shown.

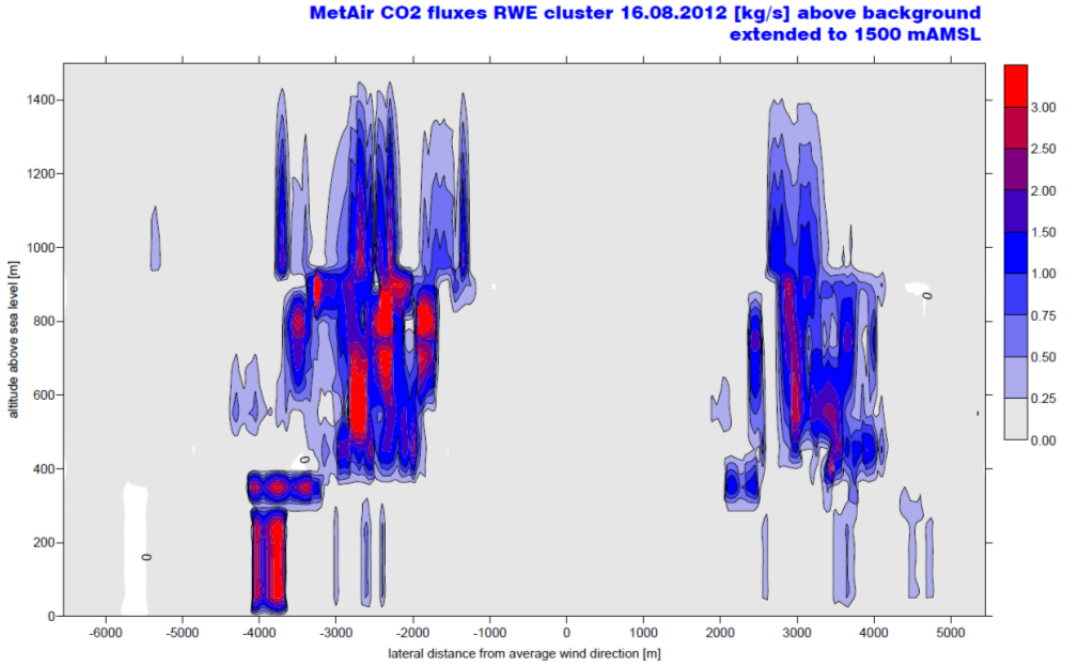

Figure 25: CO_2 plumes of the four sources in the RWE cluster on August-16. The measurements were extrapolated up to the inversion on 1500 mAMSL. This extrapolation contained about 20% of the emissions.

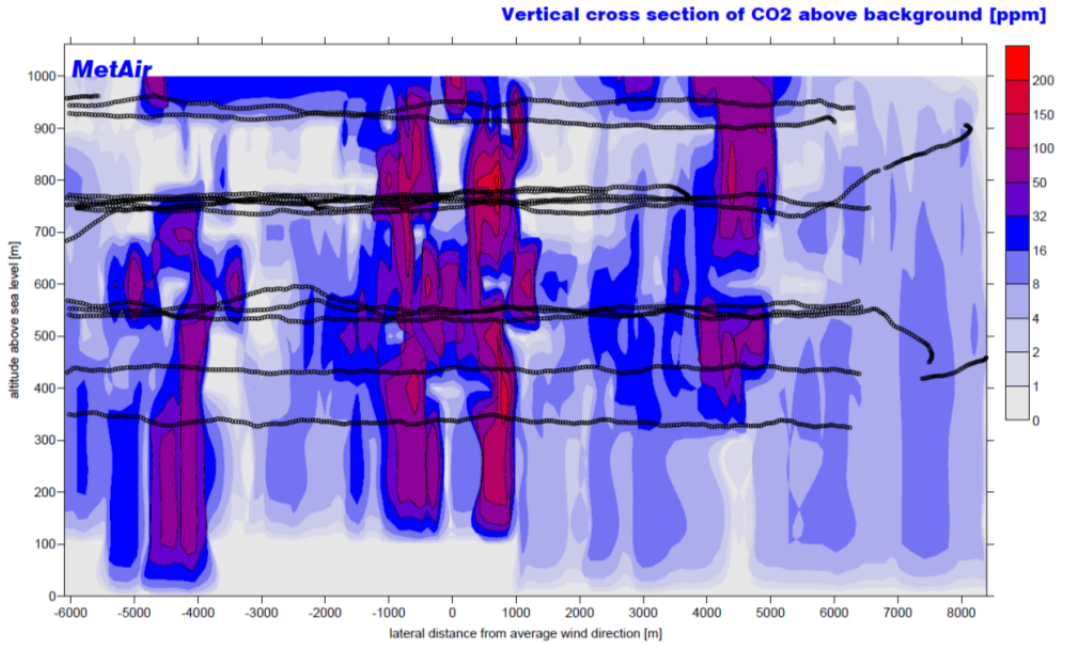

Figure 26: CO_2 plumes of the four sources in the RWE cluster on August-17.

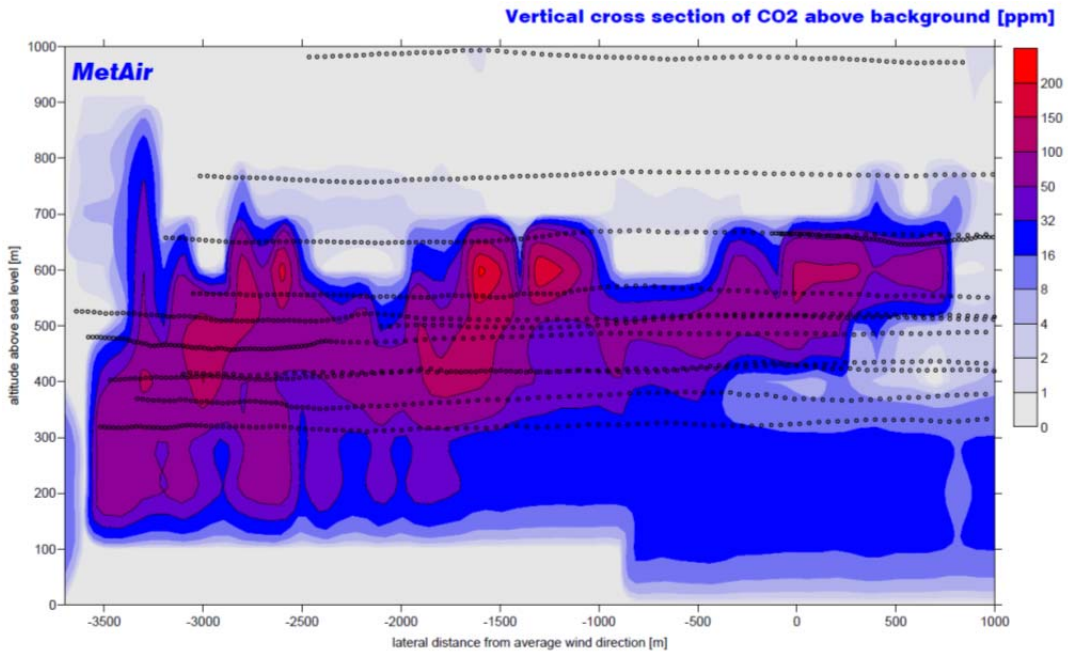

Figure 27: CO_2 plumes of the four sources in the RWE cluster on August-18.

7.4. Discussion about the main uncertainties

7.4.1. Measurement errors

The wind components have an accuracy of 0.5 m/s, the CO_2 concentrations have an accuracy of better than 1 ppm, and the CH_4 of better than 5 ppb. Meanwhile we also got the analysis of the flask-samples, which would allow to increase the absolute accuracy by a factor of two. However, since the background is removed, the absolute concentrations are not important, remaining with uncertainties in terms of "precision" (stability of the parameters within an hour), which leaves us with maximum uncertainties of 0.5 ppm CO_2 and 2 ppb CH_4 (very conservative). The uncertainties of the wind measurements remain in the order of 0.5 m/s. However, the main uncertainty is the crosswind component. When flying back and forth through any plume on a similar altitude, then this error is averaged out.

However, we make a coarse error assessment with these numbers. Then the relative error based on the wind measurement is 10 % at wind speeds in the order of 5 m/s, increasing with weaker winds, and decreasing with higher wind speeds. For CO_2, a plume with moderate 50 ppm above background (we observed up to 300 ppm) only adds another percent (or less), and the uncertainty of the excessive CH_4 is in the order of a permille. Considering the fact that all estimates were rather overestimating the possible errors, we remain with a relative error from the measurements of less than 10 %. It is possible to reduce this uncertainty by further inspection and optimisation (for each flight, the parameters for the complex wind calculations could be reviewed).

The estimate of 10 % was confirmed by adding these errors (wind and concentration) to the individual measurements of a specific case (15_RWE_cluster). This was a worst-case addition of errors in the plume, i.e. without changing the background, and without applying any statistical distribution of errors and their sign. An improved version of the software could introduce a Monte-Carlo-Error on each individual measurement in order to assess the influence on the result. An

analytical assessment of the error propagation is not possible. Therefore, we remain with this worst-case estimate for this stage of the work.

7.4.2. Methodological limitations

As the sensitivity analysis shows, the main uncertainties are dependent from the meteorological conditions and the flight patterns. This uncertainty is quantified in the table. "10 %" means, that the ratio between the highest and the lowest value was 1.10. This is +/- 5 % for the average. However, we leave this doubled percentage as a conservative estimate for the methodological uncertainty.

In summary, the accuracy for the fluxes for those cases, where the meteorological conditions and the flight pattern was favourable, is in the order of 10 % or less. However, there are cases in the "middle field", where the relative uncertainty is in the order of 20 %, and some cases like T2.2 Prosper_9 on Aug-15, where it is obvious that the method does not deliver reliable estimates.

A closer look into these cases with low or high sensitivity makes clear that an ideal flight pattern is covering the plume as complete as possible, which is trivial. For the CO_2 plumes, the minimum height of 50 m or more above ground was never a problem, because the sources were from high chimneys. However, for the CH_4 sources, this might be a problem. In two cases, we did not reach the top of the plume due to air space restrictions or other reasons. This was not ideal, but the inversion not far above was known, and allowed a reasonable closure. Due to reasons discussed above, when explaining the method with the "gridded wall", it is clear that the "wall" should be as thin as possible, because otherwise, artefacts could occur.

7.4.3. Other sources for errors

An obvious problem is instationarity. It is clear that the extrapolations to annual emissions are useless when the source strengths are varying from day to day, or even by the hour. In such cases, we should either compare daily declarations of emissions, or a percentage of the possible variation should be known.

Another type of instationarity is caused by the atmospheric turbulence on the scale of a few hundred metres. Especially convection, but also shear turbulence, can cause intermittent concentrations. This effect is statistically minimised when at least the legs in the core of the plume were flown several times.

Of course we could imagine other special flows, or a combination with instationarities, that would cause specific artefacts.

Bottom line: It is possible to measure a source strength representative for one or more hours with a well-adapted flight pattern with an accuracy in the order of 10 %. In some cases, a detailed inspection of the individual uncertainties, with improved post-processing of the wind, it should even be possible to reach 5 %. On the other hand, non-stationary conditions and non-ideal flight tracks (e.g. caused by air space restrictions or pure lack of time), the error can grow above 20 %.

7.5. Summary of flux estimates based on in-situ data

The results are summarised in Table 8. All plumes (CO_2 and CH_4) that were found in the raw data were attributed to sources or groups of sources, classified by intensity and labelled with the time (full hour Central European Summer Time) when it was measured.

		13	14	15	16	17	18	19	23	Mt/a CO_2 50 / 100 / 200	kt/a CH_4 50 / 100 / 200	av_wind m/s	accuracy %	remarks
	Lee von Koeln						X							
	sum of T1.1+T1.4+RWE_neu			15						42.74 / 31.70 / 36.66		8,3	35	
	sum of T1.1+T1.4+T1.5+RWE_neu			15						52.33 / 54.38 / 55.12		8,3	5	only 5 % of the total flux is extrapolated (to surface only)
					12					53.01 / 50.27 / 56.46		3,8	12	about 25 % of the flux was extrapolated below the inversion
						12				41.03 / 47.54 / 49.10		3,5	20	about 18 % of the flux was vertical flux above the sources
							11			50.33 / 47.24 / 47.07		8,3	7	only 15 % of the total flux is extrapolated (to surface only)
	RWE neu			15		12	11							
T1.1	RWE Kraftwerk Niederaussem			15						19.74 / 24.54 / 22.88		7,8	24	only 5 % of the total flux is extrapolated (to surface only)
						12								single source is possible to extract; not yet done
							11			37.38 / 37.18 / 36.33		9,5	3	
T1.4	RWE Kraftwerk Neurath			15		12	11							
T1.5	RWE Kraftwerk Fimmersdorf			15		12	11							
T1.2	RWE Kraftwerk Goldenberg					X	12							
T1.3	RWE Kraftwerk Eschweiler						16			13.76 / 15.58 / 12.46			25	about 10 % of the flux was extrapolated below the inversion
									13	21.17 / 21.43 / 22.05		2,9	4	no extrapolations, even not to the surface
T1.6	Salzgitter Flachstahl GmbH													
T1.7	Kraftwerk Scholven	17								7.34 / 6.8 / 6.14	10.18 / 13.24 / 8.81	1,5	20 / 50	about 50 % of the flux was vertical flux above the source
T1.7	Kraftwerk Scholven			14										
T2.1	RAG Anthrazit Ibbenbühren							11		5.95 / 6.71 /6.28		6,8		main cross section in about 6 km distance
T2.1	Bockradener Schacht							11			22.74 / 22.69 / 15.65	4,4	45	
T2.1	Theodorschacht							11			20.97 / 19.44 / 14.25	4,9	47	
	sum of all three T2.1 on the far cross section							11		8.34 / 6.50 / 7.62	101.28 / 89.92 / 77.31	4,7	28 / 31	consistent sum for CO_2, however, not for CH_4 close to surfac
T2.2	RAG Bergwerk Prosper-Haniel	X		13		11		10						
T2.2	Schacht Hünxe	X		13										
								10			6.88 / 6.57 / 5.88	5,1	17	
T2.2	Schacht Prosper - 9	14		17		11	10							
				17							10.6 / 20.11 / 28.63	13,5	100	very unstable solution, i.e. about +/- 50 % of average
								14			7.17 / 7.84 / 7.26	6,2	9	
T2.2	Haniel Schacht 1	X		17		11		10						
T2.2	Förderberg	X				11		10						
T2.3	RAG Bergwerk West		13		17	X								
T2.3	Rossenray / Schacht 1		13		17	X								
T2.3	Schacht Friedrich Heinrich - 4		13											
					14						11.55 / 10.47 / 12.03	5,2	15	far cross section (>2.5 km)
					14						7.09 / 8.00 / 5.24	3,4	53	nearer cross section (<2.5 km)
					17						8.44 / 8.53 / 7.97	3,5	7	near
						14					7.03 / 8.39 / 7.78	3,6	19	near
T2.4	RAG Bergwerk Auguste Victoria	16												
T2.4	Schacht AV 7	X												
T2.4	Schacht AV 8	X	X											
T2.5	AVG Zentraldeponie Vereinigte Ville					X	X							
T2.6	Deponie Watenbüttel BS													
T2.7	ABZ Hannover/Lahe													
T2.8	Deponie Schöneicher Plan													
T2.9	Ruhr Öl Gelsenkirchen	X		X										
T2.10	Rheinland Raffinerie Godorf						X							
T2.11	EXXON Grossenkneten		X											
T2.12	EXXON NEAG		X											
T2.13	EXXON Voigtei		X											
T2.14	EXXON Dötlingen		X											
T2.15	WINGAS Rehden		X											
T2.16	EXXON Rühlermoor													
	FLEX Selhausen								X					
	FLEX Altendorf								X					

	This table shows all targets flown by METAIR. The color codes were based on the quick-looks:	Days in August 2012 (Aug-13 to Aug-23). The numbers in the fields below are the times (rounded hours CEST) where these targets have been characterised.
	high concentrations above background	Results of the flux calculations as described and discussed in the report. The results are given for grid resolutions of 50, 100, and 200 m, which shows the sensitivity. The "accuracy" is given as the percentage between the highest and the lowest value. av_wind is the average wind when dividing the total flux by the total net column mass for the reference case with 100 m grid resolution.
	enhanced concentrations visible	
	no or very weak enhancement	

All marked targets/days are suitable for flux calculations; those targets written in red were not possible to assess (time, weather, air space, or other reasons)

Table 8: Summary of preliminary results on of flux estimates based on in-situ data.

This first screening was only based on maximum concentrations and could not lead to any ranking about "best data sets". A pre-assessment was possible by remembering the cases, and by looking into the flight tracks. However, the first priority for the post-processing was given by those targets that were also successfully measured with MAMAP.

The two main cases were the power plant Eschweiler/Weisweiler (T1.3) on August-18, and the group of sources for CO_2 (Ibbenbüren, T2.1) and CH_4 (Theodor and Bockradener Schacht; T2.1x) on August-19. These are the main cases for intercomparison.

However, Eschweiler/Weisweiler (T1.1) was measured in-situ also on August-23 even under better conditions, and the cluster of power plants near Niederaussem (T1.1, T1.4, T1.5 and a new plant named RWE_neu). This cluster was documented on four days, and allowed to isolate single sources on two days.

During this work, also other sources were assessed by curiosity, like e.g. T1.7 (power plant Scholven), where we knew that the convection above the source was quite relevant. This was also the case for the RWE_cluster on August-17. The individual results with many meta-data can be found in the files *date_target_results.txt* in the METAIR part of the CMAPEXP data package. They are summarised Table 8.

The main results are the Mt/a CO_2, or kt/a CH_4, i.e. the kg/s measured during the very limited time of the measurements (typically half an hour up to two hours for a cluster). The method how this was done is explained above. For the table, a systematic sensitivity study was made, using grid sizes of 50, 100, and 200 m (see discussion about uncertainties in the next chapter). Another key parameter is the average wind. This is the total flux divided by the total mass of the plume in the cross section, i.e. this av_wind could directly be applied to total column mass concentrations measured by MAMAP, or vice versa to divide the fluxes based on the MAMAP-inversion to get the total mass of the plume in the cross section. All concentrations, masses and fluxes are "above background" if not specified otherwise.

8. Inversion of emission rates from MAMAP measurements using model and airborne in-situ data to constrain wind speed estimates

8.1. Power plant Weisweiler

8.1.1. Target description

On August 18, 2012 measurements were performed at the coal and gas fired power plant Weisweiler in North Rhine-Westphalia, Germany. In 2012, the power plant had an installed base load power of 2100 MW (lignite) and a mid-load and peak load power of 540 MW (gas) (RWE Power AG, http://www.rwe.com/web/cms/de/60142/rwe-power-ag/standorte/braunkohle/kw-weisweiler/, last access: December 2013). Reported CO_2 emissions were about 19.3 Mt CO_2 in 2011 (E-PRTR, http://prtr.ec.europa.eu/, last access: January, 2014). In the vicinity of the power plant is a waste incineration plant with considerably lower emissions of about 148 kt CO_2 in 2011 (E-PRTR, http://prtr.ec.europa.eu/, last access: January, 2014).

The power plant has a number of stacks distributed on an about 300 m wide area releasing flue gas to the atmosphere including three large cooling towers of about 120 m height. The surrounding of the power plant is mostly flat but exhibits two depressions from open cut mining which however do not spacially coincide with the CO_2 plume originating at the power plant (see below). Time of overflight was approximately from 13:35 UTC to 14:33 UTC. Local time was 15:35 to 16:33 (CEST).

8.1.2. Measurement data

The column averaged dry air mole fractions of CO_2 were retrieved using methane (CH_4) as a proxy: $XCO_2(CH_4)$. The corresponding background profiles for the linearization points are based on the U.S. standard atmosphere (U.S. Committee on Extension to the Standard Atmosphere, 1976) scaled to actual values. Background XCO_2 was set to 389 ppm based on the SECM model presented by Reuter et al (2012). The methane background XCH_4 was estimated to about 1.76 ppm. An assumed uncertainty of the ratio of the background columns of 1% accounts for possible deviations from these values.

Aircraft altitude during the measurements was almost constant at 1600 m (+/-25m), which was also selected for the reference radiative transfer. Assuming a constant aircraft velocity of 200 km/h, the ground scene size is about 22m x 54m (cross track x along track). Thereby the along track ground scene size describes the full width at half maximum for the sensitivity along the flight track. During the measurements, the solar zenith angle varied from about 45.2° to 52.4°.

The radiative transfer model was interpolated using a two dimensional look-up table (LUT) based on solar zenith angle and surface elevation. For that the SRTM digital elevation model (Shuttle Radar Topography Mission (SRTM) version 2.1, http://dds.cr.usgs.gov/srtm/version2_1/), a collaborative effort from NASA, NGA as well as the German and Italian Space Agencies) was used. Due to the changing measurement geometry, also the conversion factor *k* to correct for the altitude sensitivity effect (Krings et al, 2011) has to be determined for each measurement independently using also a LUT. On average, the conversion factor for the present measurements is about 0.49.

Due to the instrument improved instrument performance reported in Krings et al (2013) basically no filtering based on the fit quality needs to be applied. Only measurements in saturation or with low signals, for example, over water which has a very low spectral reflectance in the short-wave infrared, are rejected from further processing. Figure 28 shows the fit root mean square (RMS) error for all

measurements in the vicinity of the power plant ordered by size. The RMS is generally very low except for a few measurements most of which are caused by bad signal strength.

The precision in the measurement area is approximately 0.28% determined as standard deviation of the data.

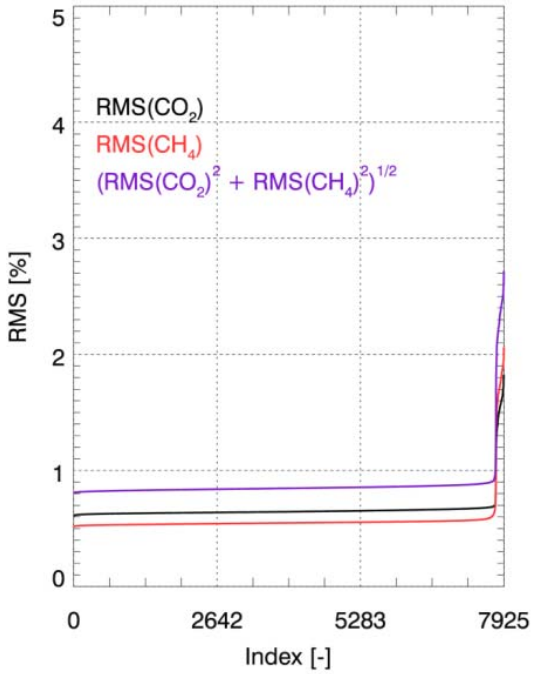

Figure 28: Fit quality based on the root mean square (RMS) values of the fit for CO_2 and CH_4 measured in the vicinity of the power plant Weisweiler. Basically no quality filter based on the RMS was applied.

Figure 29 shows the $XCO_2(CH_4)$ data acquired over the power plant Weisweiler plotted as a 3-point moving average on top of a topography map that was used for the surface elevation look-up table approach. Clearly visible is the CO_2 plume originating at the power plant's location and advected in downwind direction towards North. The arrows indicate the wind field of the COSMO-DE model operated by the German Weather Service (DWD) based on the COSMO model (Doms, 2011) at model layer 45 which is approximately 350m above sea level. The two large depressions North and North-East of the power plant are lignite open cut mines.

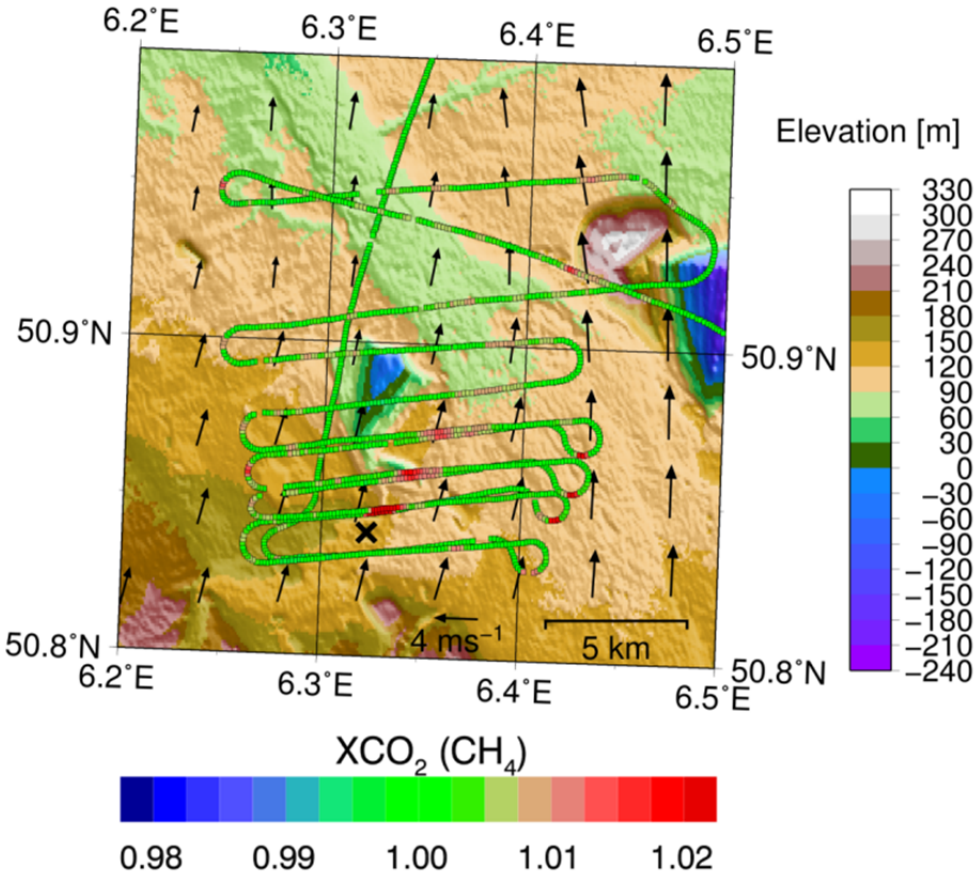

Figure 29: MAMAP $XCO_2(CH_4)$ and surface elevation for the area of power plant Weisweiler. The power plant position is denoted by a black cross. MAMAP data have been smoothed by a 3-point moving average. The arrows denote wind speed and direction in altitude layer 45 of the COSMO-DE model, i.e. approximately at 350m above sea level. (Maps in UTM projection. Topographic data were obtained from the Shuttle Radar Topography Mission (SRTM) version 2.1 (http://dds.cr.usgs.gov/srtm/version2_1/), a collaborative effort from NASA, NGA as well as the German and Italian Space Agencies.)

8.1.3. Atmospheric conditions and wind information from model data

Very important for the dispersion of trace gases in the atmospheric boundary layer are wind speed and direction, atmospheric stability and boundary layer height. While wind direction and atmospheric stability can generally be retrieved from the data directly (Krings et al, 2011, 2013), the boundary layer height and in particular wind speed need to be determined from external data.

The boundary layer or mixing layer is separated from the free troposphere by a zone that largely prevents further vertical propagation. The mixing layer is usually characterized by constant (virtual) potential temperature due to convective mixing whereas an increase of potential temperature with altitude indicates a stable layering that can inhibit further convection. Since wind speed is generally not constant with altitude, boundary layer height and associated final plume rise can be an important parameter when estimating the average wind speed the trace gas plume is subject to.

Figure 30 shows the COSMO-DE result for temperature and virtual potential temperature for the model grid point North-West of the power plant location. Potential temperature refers to the temperature an air parcel would have if brought adiabatically to a pressure of 1000hPa, while the

virtual potential temperature is the temperature a dry air parcel must have when having the same density and pressure as moist air.

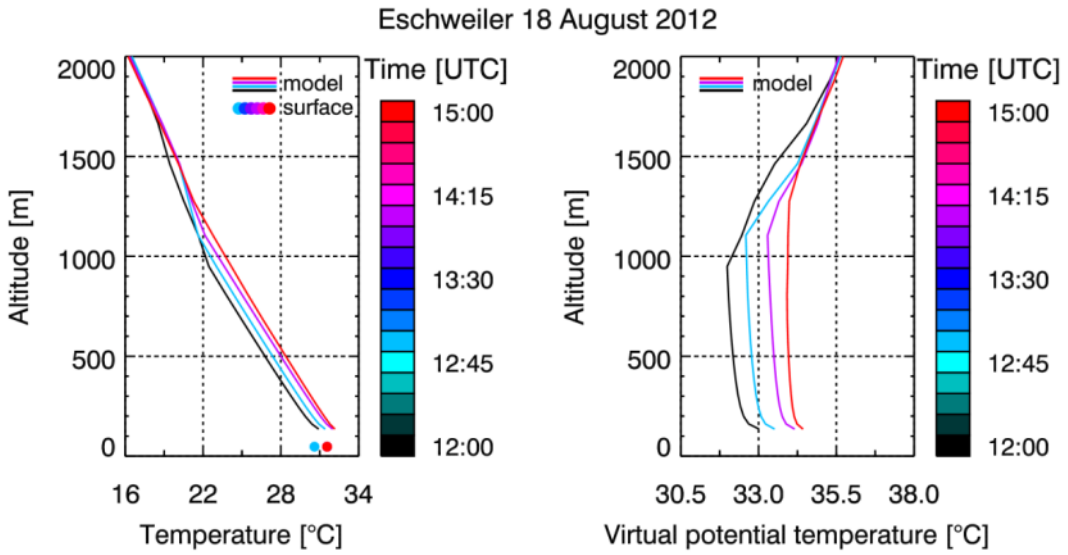

Figure 30: Temperature (left) and virtual potential temperature (right) for the COSMO-DE model grid point North-West of the power plant. Surface in situ data for temperature was obtained from Düsseldorf airport (EDDL) located approximately 60 km North-East of Weisweiler power plant.

In a first approximation the boundary layer height can be identified by a sharp increase in virtual potential temperature. According to Figure 30, the boundary layer altitude is evolving from about 1000m altitude above ground at 13:00 UTC to about 1150m altitude above ground at 15:00 UTC. This can only be a very crude approximation as the transition between boundary layer and free troposphere is not a sharp boundary, but rather an area in which vertical dispersion decreases depending also on other parameters such as wind speed and wind shear, which so far are not considered here.

Figure 31 shows wind speed and direction for the same model grid point. In general, also the wind speed changes when reaching the boundary layer height which can also be seen in the figure. The wind speed ranges from about 2.5m/s to 6m/s for the time and altitude range of the overflight.

To obtain an adequate estimate of the average wind speed which transports the plume in downwind direction, a weighted mean of the wind profile was computed considering the vertical Gaussian dispersion of the plume based on the stability derived from the MAMAP data and dynamically taking into account the evolving boundary layer. This is achieved by computing the effective wind speed for each MAMAP transect which is averaged for the Gaussian plume model inversion, whereas for the integral method each track is evaluated independently and the resulting emission rates subsequently averaged.

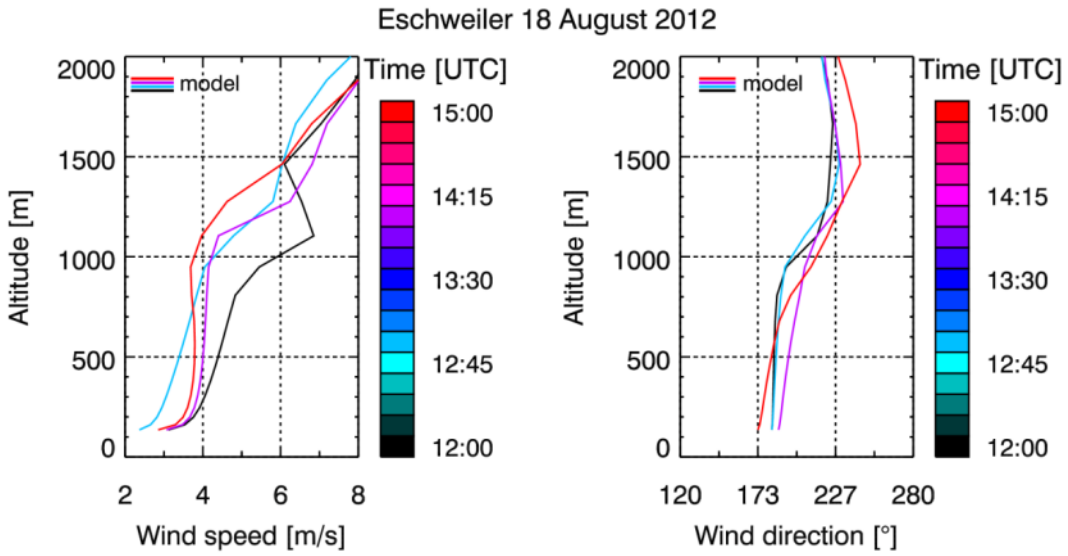

Figure 31: Wind speed (left) and direction (right) for the model grid point North-West of Weisweiler power plant.

8.1.4. Inversion for emission data

Preparation and performance of the Gaussian plume inversion and the integral inversion method is very much in line with Krings et al (2011, 2013).

Before the inversion the data were gridded to pixels of 100m x 100m. There was no additional smoothing or filtering, beside the signal filter described in Section 8.1.2. The measurements were normalised to background using as reference an upwind area defined by -2000m < x < 0m and -2000m < y < 2000m for the coordinate system that has been rotated so that wind direction points to positive x-direction. Since the power plant site exhibits various stacks where it is not clear if they are emitting CO_2 or not, basically the whole area was treated as a homogenous source with a cross section of 300m perpendicular to wind direction. The cooling tower height is about 128m above ground which was hence assumed as injection altitude for the CO_2. Note that source width and injection altitude matter explicitly only for the Gaussian plume model inversion, whereas the integral method is independent of these parameters.

Wind direction was determined empirically from the measured data to about 219°. When fitting the stability parameter to the retrieved XCO_2 this yields a=220.2 (+/- 3.0% statistical error), i.e. very unstable atmospheric conditions (stability class A), independent of wind speed. Using this stability as input for a vertical Gaussian dispersion model as a function of distance to source to compute a weighted mean of the wind profile, an average wind speed of 3.96m/s was obtained for the plume area covered by MAMAP data.

Applying this wind speed to the Gaussian plume inversion, the result for the average emission rate for the time of the overflight is 16.35 Mt CO_2/yr with a statistical error of +/- 2.6%. The contour lines as an overlay on the retrieved XCO_2(CH_4) can be seen in Figure 32.

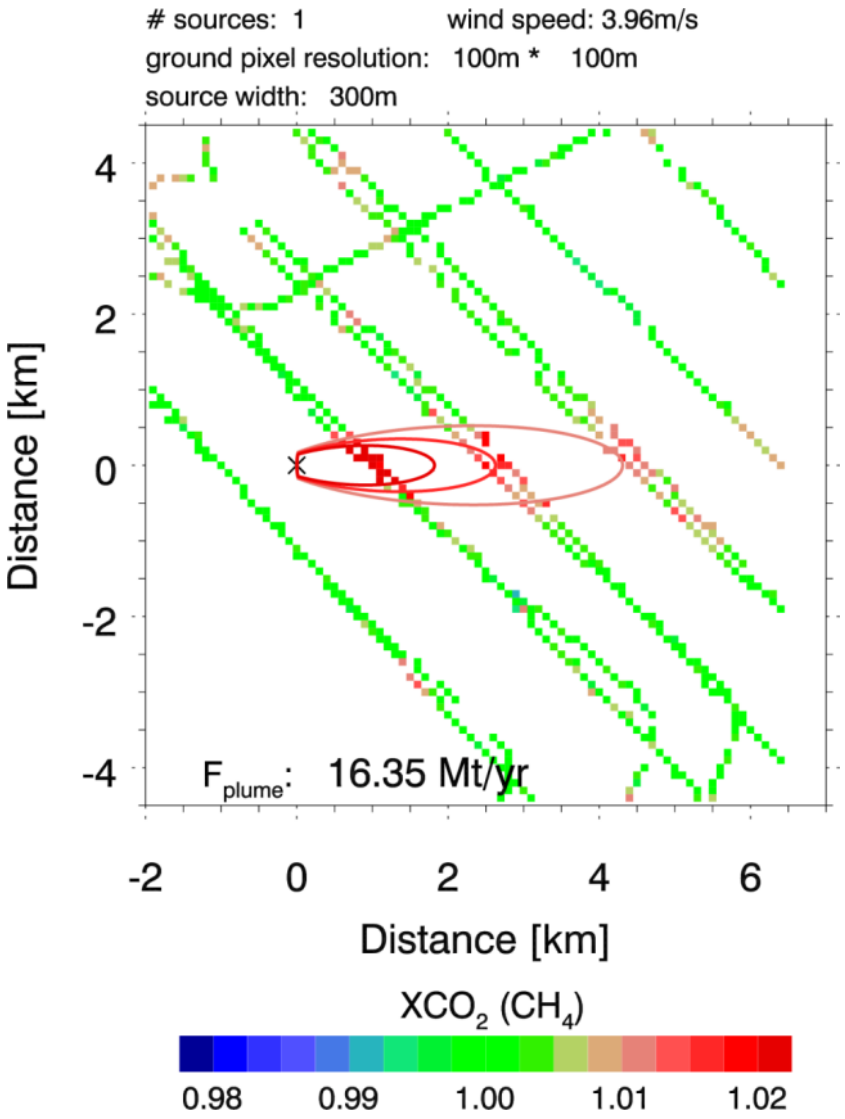

Figure 32: MAMAP $XCO_2(CH_4)$ data as used for the inversion rotated so that wind direction points to positive x-direction. The contour lines indicate the result of the Gaussian plume inversion with a resulting emission of 16.35 Mt CO_2/yr for the time of the overflight.

Since the upwind area was basically defined as background, the upwind transect has not been used for the integral inversion. When evaluating the individual flight tracks with the integral method, there are substantial variations in the inversion result most likely due to convective cells that are not homogeneously distributed in time and space. This is in line with the idea of the Gaussian plume model, which is only a good approximation on average. When taking the mean of the single track inversions with independent wind speed calculations for each track (see Figure 33 - Figure 35), the result for the integral method is about 15.83 Mt CO_2/yr and hence very close to the result for the Gaussian plume inversion.

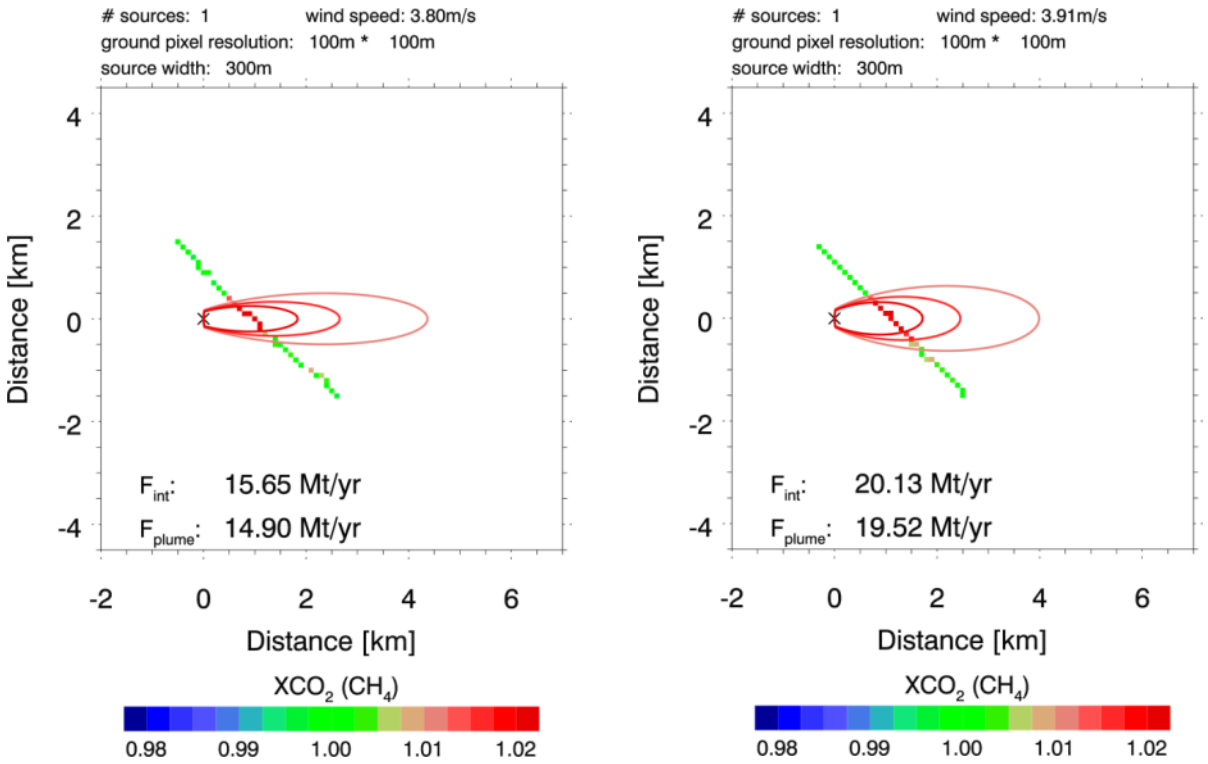

Figure 33: Result of integral (F_{int}) and Gaussian plume model inversion (F_{plume}) for each of the 6 flight tracks under consideration independently evaluated. Each figure shows a different track with independently computed wind speed given in the header. The results are continued in Figure 34 and Figure 35.

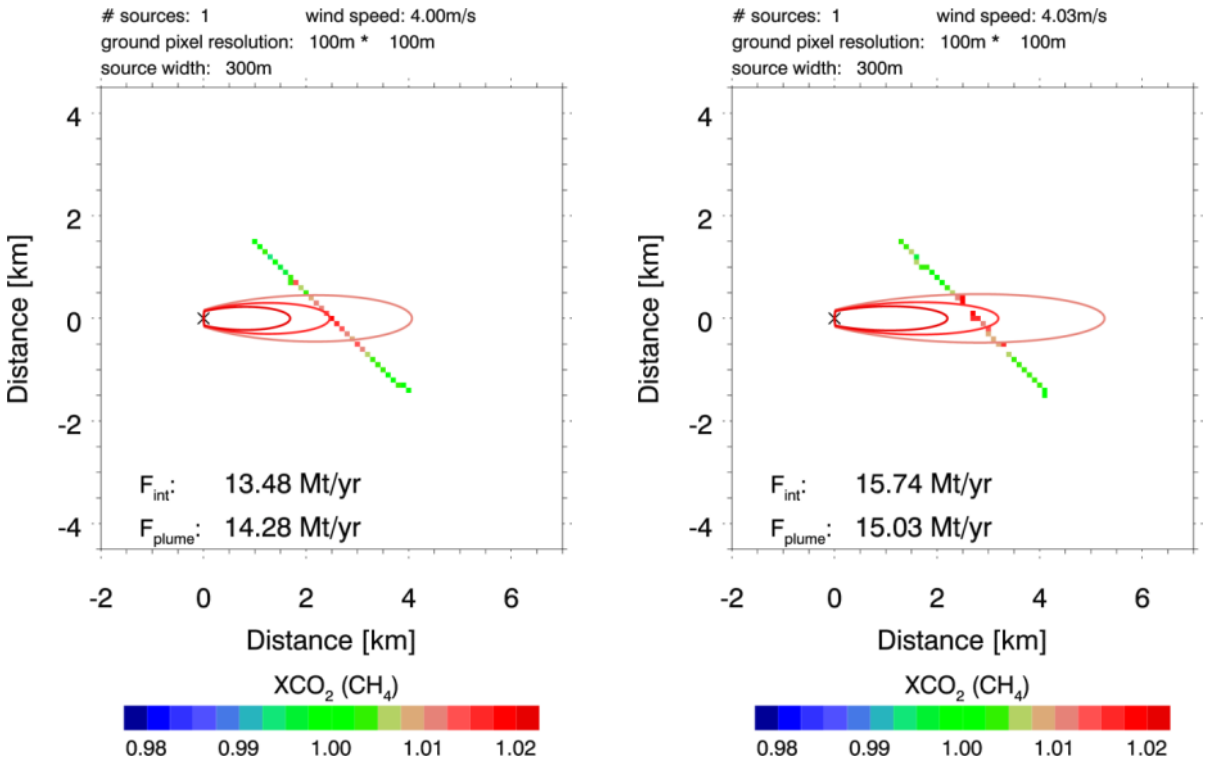

Figure 34: Continuation of Figure 33.

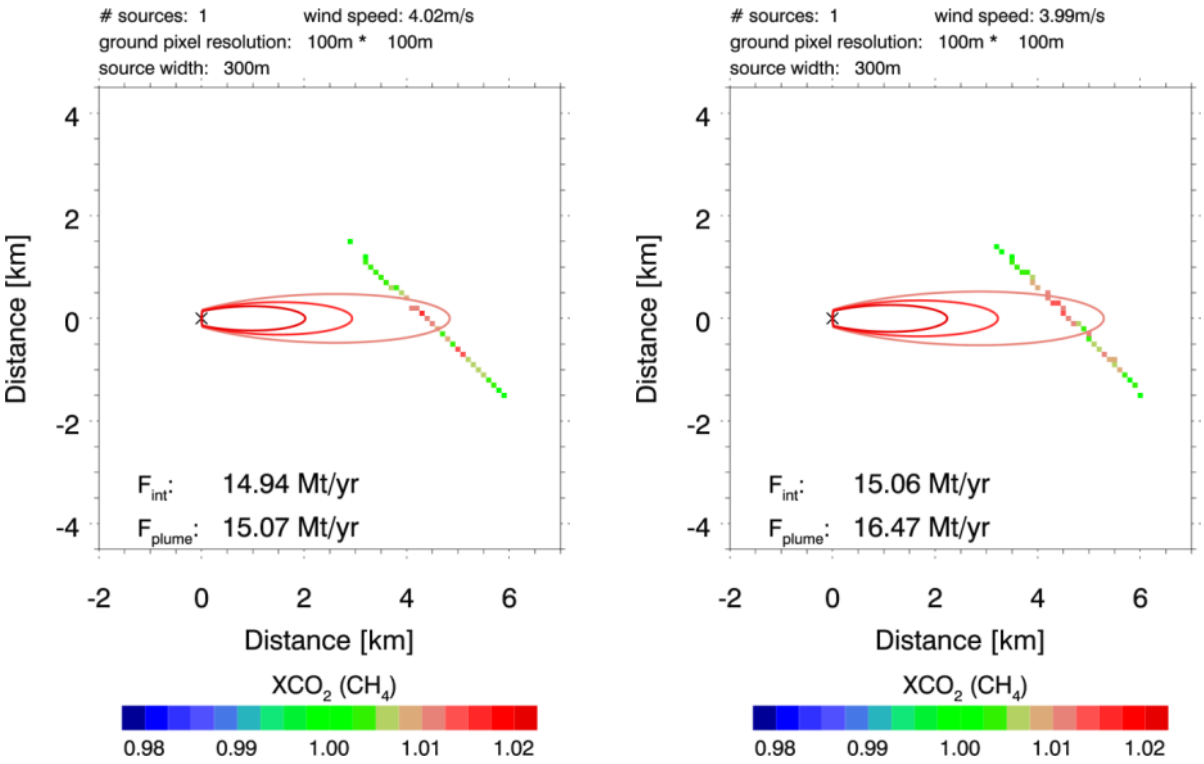

Figure 35: Continuation of Figure 33.

In principal, also the Gaussian plume inversion can be applied to individual flight tracks instead of on all data at once (see Figure 33-Figure 35). The average result of 15.88 Mt CO_2/yr for the time of the overflight is very similar to before showing that the inversion is rather stable.

8.1.5. Incorporation of atmospheric in situ information

The precision of the wind model was roughly estimated to about 0.9 m/s (1σ) with negligible bias for the case described in Krings et al (2011). Assuming the same error holds in the present study, this leads to a relative error (1σ) on the inversion of about 23%.

This error can potentially be drastically reduced when on-site wind information is available, e.g. from airborne turbulence measurements as they were used in Krings et al (2013) and that were also performed during the C-MAPExp campaign. Furthermore, an aircraft can acquire information on additional atmospheric parameters that can be used to validate and potentially correct model estimates for the boundary layer height.

Figure 36 shows the flight pattern of the in-situ measurements performed at the Weisweiler power plant location. The measurements concentrate on transects at several altitude layers downwind of the source from about 150m above ground to about 960m above ground. The acquired temperature data as compared to the corresponding model data is shown in Figure 37 for the temperature and in Figure 38 for the virtual potential temperature. It can be seen that there is an offset between measurement and model most likely caused by an offset in the model data. This is supported by the fact that several independent measurement devices on-board the aircraft recorded similar temperatures.

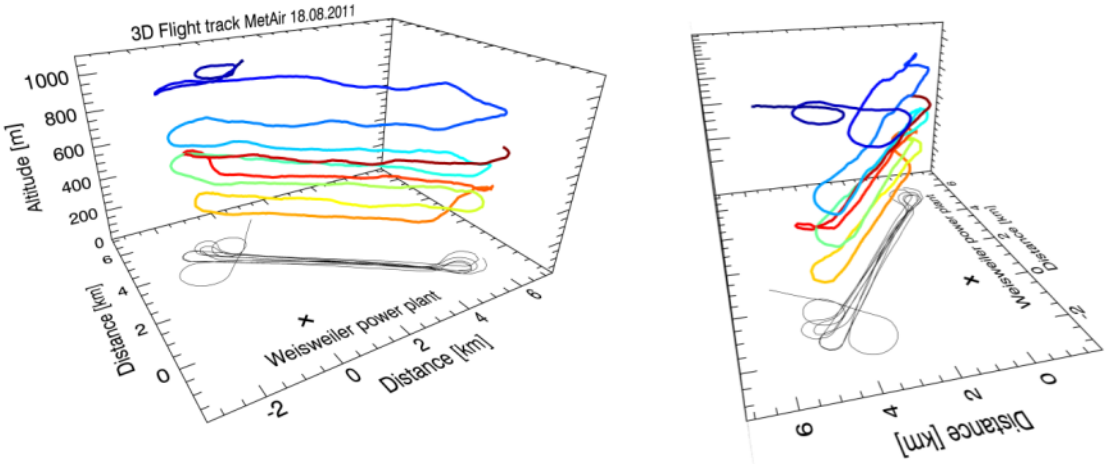

Figure 36: Flight track of in-situ measurements displayed from two different viewing angles. Location is in UTM projection relative to the power plant location. The colors indicate the temporal progression from dark blue to dark red, while the thin black lines denote the projection of the flight tracks on the surface.

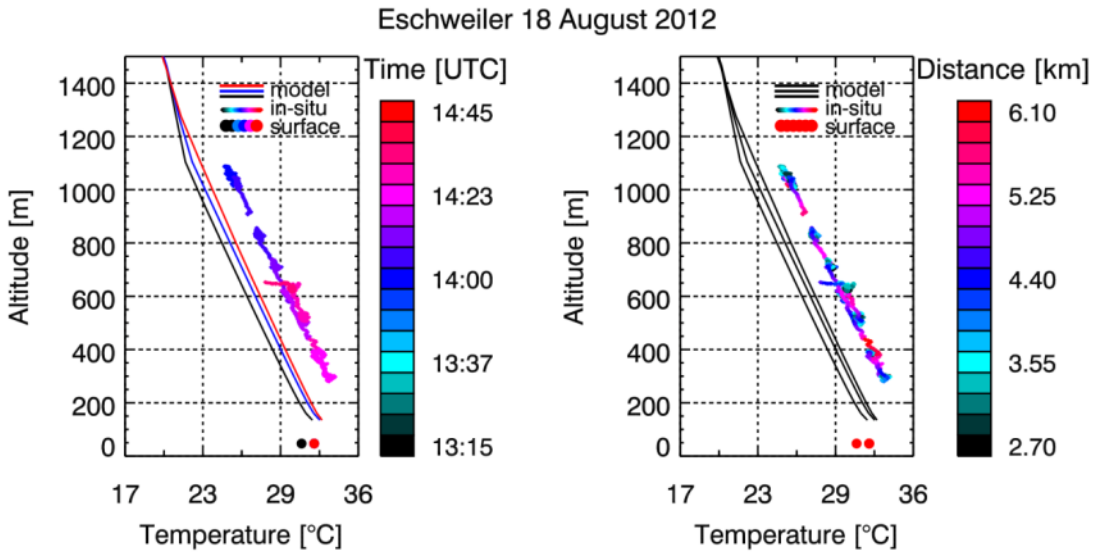

Figure 37: Temperature as given by the COSMO-DE model grid point North-West of Weisweiler power plant (straight lines), airborne and ground based in-situ measurements (discs). Data is colour coded for time (left) and distance to the source (right). Ground based measurements from Düsseldorf Airport (60km North-East of the power plant) have been obtained through Weather Underground (www.wunderground.com).

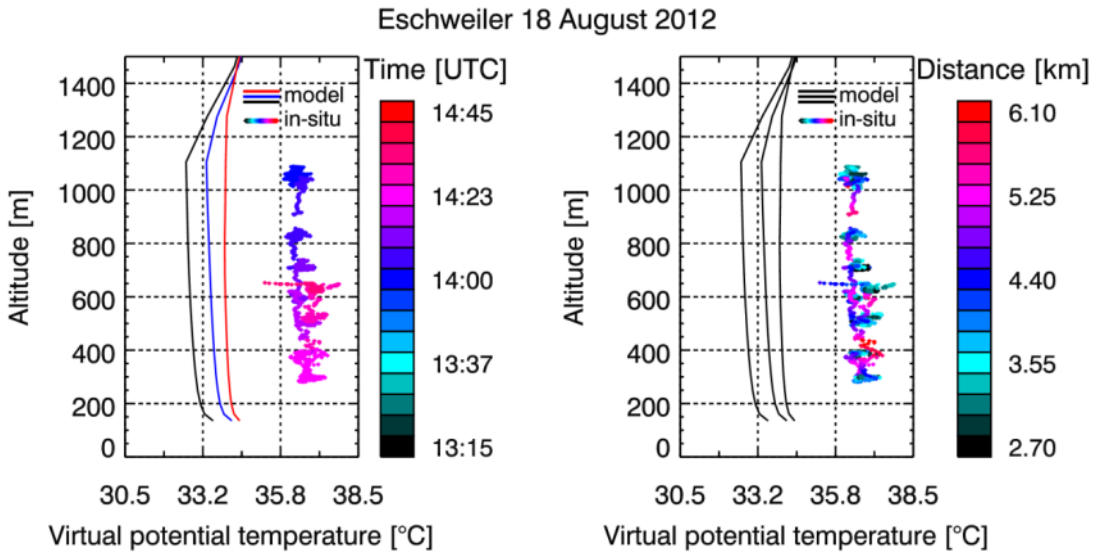

Figure 38: Virtual potential temperature as given by the COSMO-DE model grid point North-West of Weisweiler power plant (straight lines), airborne and in-situ measurements (discs). Data is colour coded for time (left) and distance to the source (right).

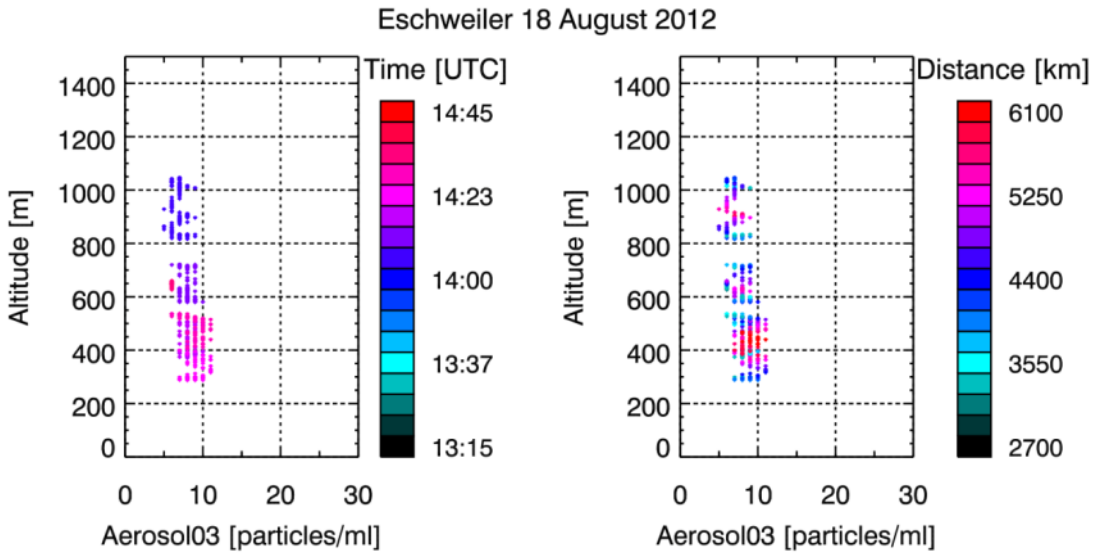

Figure 39: Vertical aerosol distribution measured in-situ for aerosol particles larger than 3µm. Data is colour coded for time (left) and distance to the source (right).

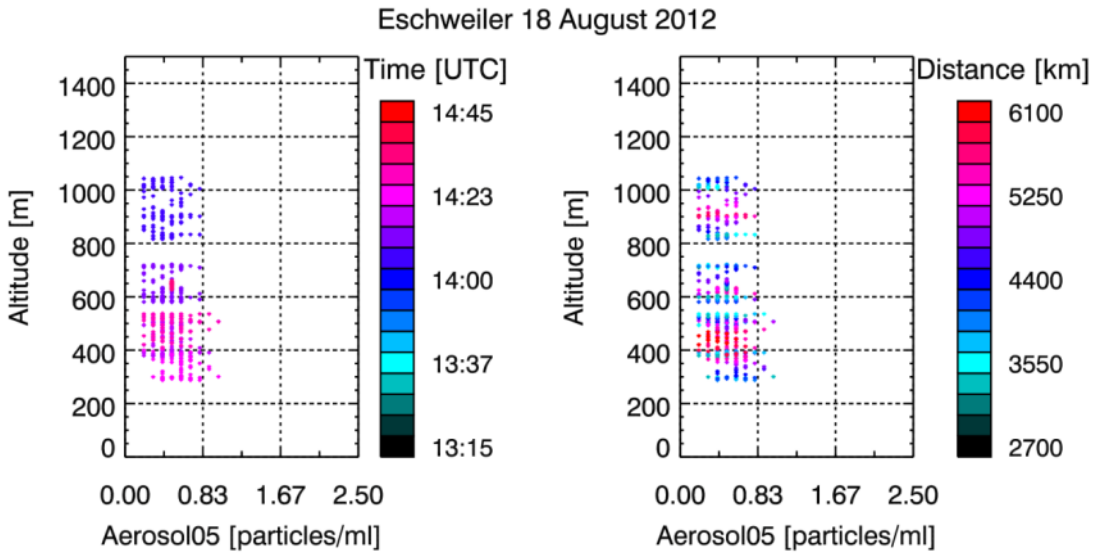

Figure 40: Vertical aerosol distribution measured in-situ for aerosol particles larger than 5µm. Data is colour coded for time (left) and distance to the source (right).

Although an offset would not hamper an approximation of the boundary layer height, the in-situ data unfortunately do not cover the complete boundary layer. It is therefore not possible to validate the boundary layer height estimate by the model data. This is also confirmed by inspecting the recorded vertical aerosol distribution for particles larger than 3 µm (Figure 39) and for particles larger than 5 µm (Figure 40) outside the plume area. Changes in vertical aerosol concentrations can in principal be used as a proxy for the boundary layer height, because aerosols are largely trapped in the mixing layer. However, the probed altitude layers show a rather even distribution of particles with height indicating that the boundary layer height was not reached.

The comparison of wind speed and direction is shown in Figure 41 and Figure 42 for 1 Hz temporal resolution of the in-situ data and in Figure 43 and Figure 44 for a 60 s moving average. The in-situ wind speed is significantly varying, but it appears that the model underestimates the wind speed on average for the time of the overflight. To quantify this underestimation, the probed altitude range has been divided into five equally thick layers in which the deviation between the in-situ measurements on the one hand and the associated model data interpolated in time and space on the other hand were quantified and subsequently averaged over the altitude layers. For the available model and measurement data at the target area and time, this yields an average underestimation of about 0.23m/s, i.e. about 5.4%. The target area and time were defined by a maximum distance to the source of 7.5km in a time interval between 13:35 and 14:33 UTC. The complete results are shown in Table 9. Note that the results do not directly relate to Figure 41 and Figure 43 which only shows the model wind speed at the North-West COSMO-DE grid point while model wind data from the whole measurement area enters the computations in Table 9.

Table 9: Results of the wind speed comparison between model and airborne in-situ data for Weisweiler power plant.

Altitude range a.s.l. [m]	Model wind speed [m/s]	In-situ wind speed [m/s]	Wind speed difference [m/s]	Relative wind speed difference [%]
282 – 443	4.07	4.66	+0.60	+14.7
443 – 605	4.23	4.62	+0.39	+9.2
605 – 766	4.29	5.04	+0.75	+17.4
766 – 928	4.34	3.32	-1.01	-23.4
928 – 1089	4.37	4.80	+0.43	+9.9
			Average: +0.23m/s	Average: +5.4%

Following these calculations, the inversion results for the CO_2 emissions of the power plant need to be adjusted upwards by +5.4%. This leads to an emission rate of 17.23 Mt CO_2/yr (Gaussian plume inversion) and 16.68 Mt CO_2/yr (integral method) for the time of the overflight.

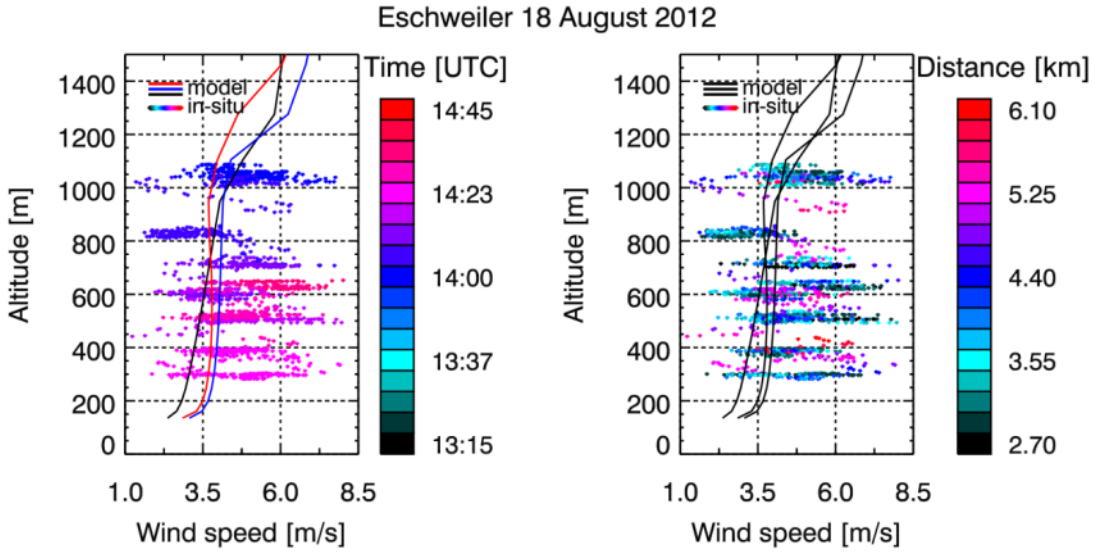

Figure 41: Wind speed as given by the COSMO-DE model grid point North-West of Weisweiler power plant (straight lines) and airborne in-situ measurements (discs). Data is colour coded for time (left) and distance to the source (right).

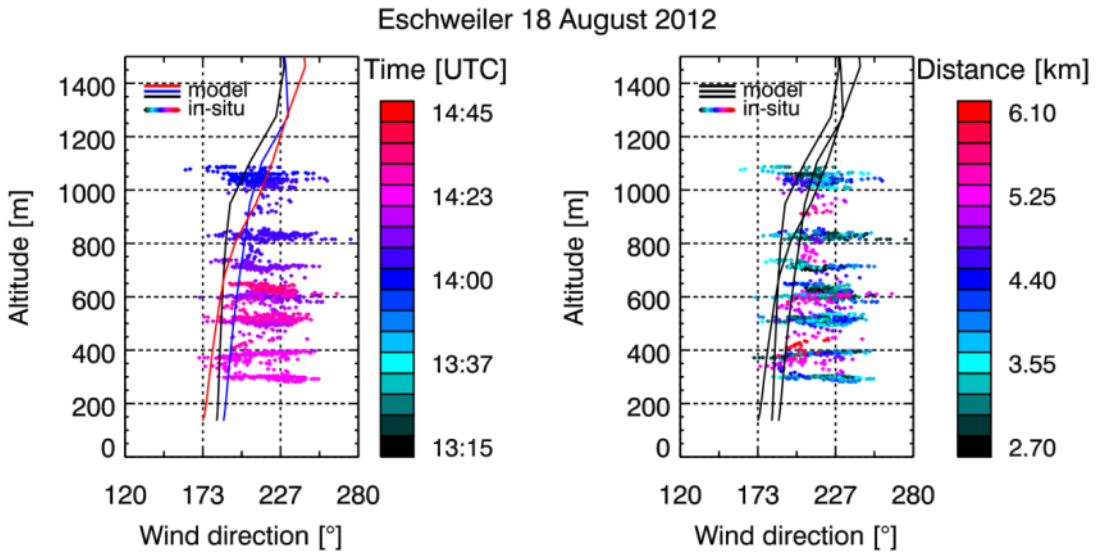

Figure 42: Wind direction as given by the COSMO-DE model grid point North-West of Weisweiler power plant (straight lines) and airborne in-situ measurements (discs). Data is colour coded for time (left) and distance to the source (right).

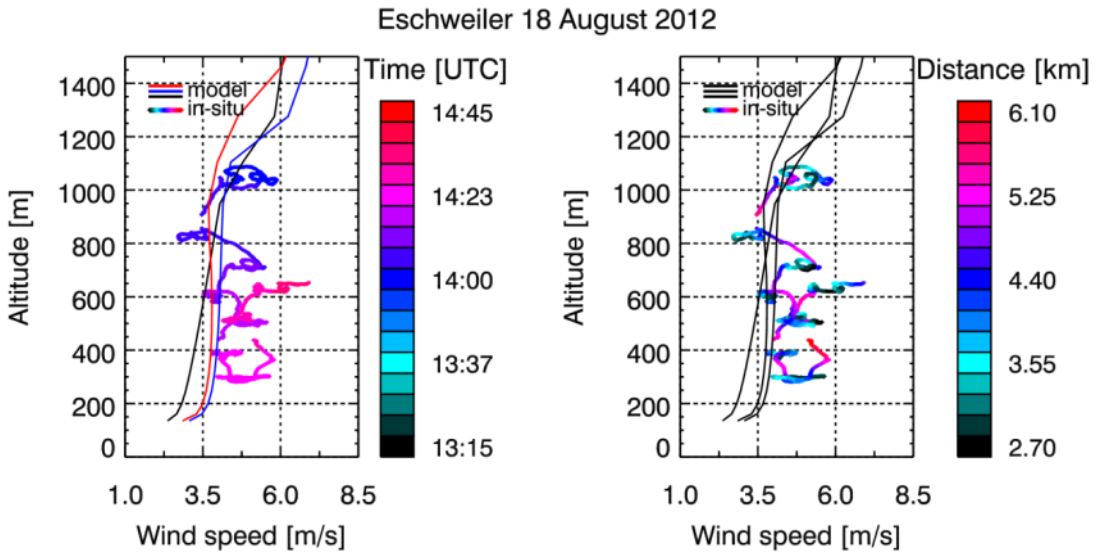

Figure 43: As Figure 41 but smoothed by a 60s moving average.

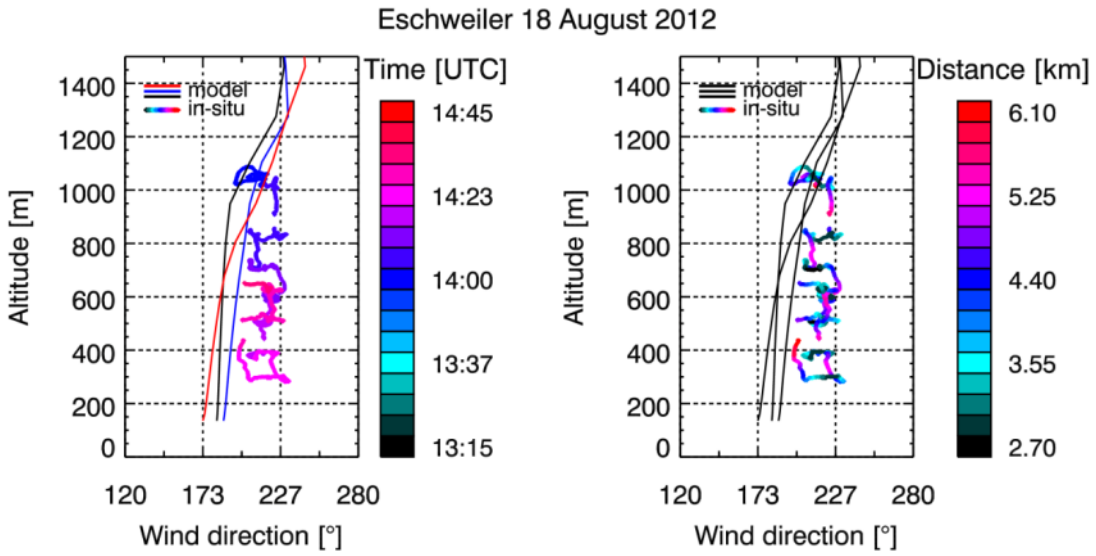

Figure 44: As Figure 42 but smoothed by a 60s moving average.

8.1.6. Error discussion

The main error arises from uncertainty of wind speed. This error is composed of the uncertainty of the model and the in-situ measurements (ca. 0.5m/s) and on assumptions that are made to estimate the average, vertically integrated wind speed throughout the plume. One example is the boundary layer height estimate, which in this case has been estimated from the model data only as there are no in-situ data available for the relevant altitudes. However, changing the boundary layer height has only a small impact. Changing the boundary layer height by +/- 200m only results in an average wind speed change of +1.8%/-0.25%. Hard to quantify is the impact of the vertical distribution that may not be Gaussian as assumed for the estimation. However, on average the Gaussian distribution is likely a good assumption.

Another source of uncertainty is the source extension. The power plant area exhibits a number of stacks of different diameter and height, so that not each stack has been considered independently but rather an effective emission area and injection height. However this affects mainly the Gaussian plume model. Since the results of integral and plume model inversion are very similar a systematic error due to this effect is probably rather low.

8.2. CH_4 from coal mine ventilation shafts Ibbenbüren

8.2.1. Target description

On August 19, 2012 measurements were performed at the ventilation shafts of RAG Anthrazit Ibbenbüren GmbH coal mine in western Germany. The features of this coal mine were described in detail in Krings et al (2013) and are only briefly summarized here.

The mine gas, which consists to a large part of methane (CH_4), is released by the two ventilation shafts Theodor Shaft and Bockraden Shaft that are about 4.5 km apart. The ventilation shafts are approximately 15m high and have a diameter of about 7m. Reported CH_4 emissions of the mine were about 41.8 kt CH_4 in 2011 (E-PRTR, http://prtr.ec.europa.eu/, last access: January, 2014).

In between the two ventilation shafts, a small coal fired power plant is located with an installed power of about 800MW (http://www.rwe.com/web/cms/de/1770936/rwe-generation-se/standorte/deutschland/kw-ibbenbueren/, last access: January, 2014) which emitted about 5.02 Mt CO_2 in 2011 (E-PRTR, http://prtr.ec.europa.eu/, last access: January, 2014).

Time of overflight was approximately from 08:25 UTC to 10:49 UTC. Local time was 10:25 to 12:49 (CEST).

8.2.2. Measurement data

The column averaged dry air mole fractions of CH_4 were retrieved using carbon dioxide (CO_2) as a proxy: $XCO_4(CH_2)$. The corresponding background profiles for the linearization points are based on the U.S. standard atmosphere (U.S. Committee on Extension to the Standard Atmosphere, 1976) scaled to actual values. Background XCO_2 was set to 389 ppm based on the SECM model presented by Reuter et al (2012). The methane background XCH_4 was estimated to about 1.76 ppm based on previous measurements in the same area (Krings et al, 2013). An assumed uncertainty of the ratio of the background columns of 1% accounts for possible deviations from these values.

Aircraft altitude during the measurements was almost constant at about 2135 m (+/- 40 m), which was also selected for the reference radiative transfer. Assuming a constant aircraft velocity of 200 km/h, the ground scene size is about 30m x 54m (cross track x along track). Thereby the along track ground scene size describes the full width at half maximum for the sensitivity along the flight track. During the measurement, the solar zenith angle varied from about 40° to 53°.

The radiative transfer model was interpolated using a two dimensional look-up table (LUT) based on solar zenith angle and surface elevation. For that the SRTM digital elevation model (Shuttle Radar Topography Mission (SRTM) version 2.1, http://dds.cr.usgs.gov/srtm/version2_1/), a collaborative effort from NASA, NGA as well as the German and Italian Space Agencies) was used. Due to the changing measurement geometry, also the conversion factor *k* to correct for the altitude sensitivity effect (Krings et al, 2011) has to be determined for each measurement independently using also a LUT. On average, the conversion factor for the present measurements is about 0.61.

Due to the instrument enhancement reported in Krings et al (2013) basically no filtering based on the fit quality needs to be applied. Only measurements in saturation or with low signals, for example, over water which has a very low spectral reflectance in the short-wave infrared, are rejected from further processing. Figure 45 shows the fit root mean square (RMS) error for all measurements in the vicinity of the power plant ordered by size. The RMS values are very low except for a few measurements that mostly did not pass the subsequent signal filter.

The $XCH_4(CO_2)$ precision in the measurement area is approximately 0.45% determined as standard deviation of the data just outside the measurement area.

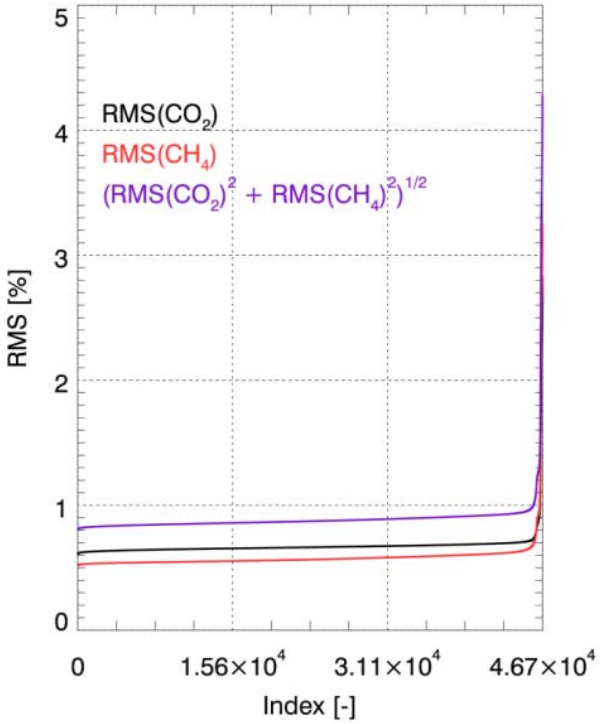

Figure 45: Fit quality based on the root mean square (RMS) values of the fit for CO_2 and CH_4 for the flight on 19 August 2013. Basically no quality filter based on the RMS was applied.

Figure 46 shows the $XCH_4(CO_2)$ data acquired over the coal fired power plant plotted as a 3-point moving average on top of a topography map that was used for the surface elevation look-up table approach. Clearly visible are the CH_4 plumes originating at the ventilation shafts Theodor in the North-West and Bockraden in the South-East and advected in downwind direction towards North. The CO_2 emissions from the small power plant in between are far less striking as an apparent small decrease in XCH_4 downwind. The arrows indicate the wind field of the COSMO-DE model at model layer 48 which is approximately 190m above sea level.

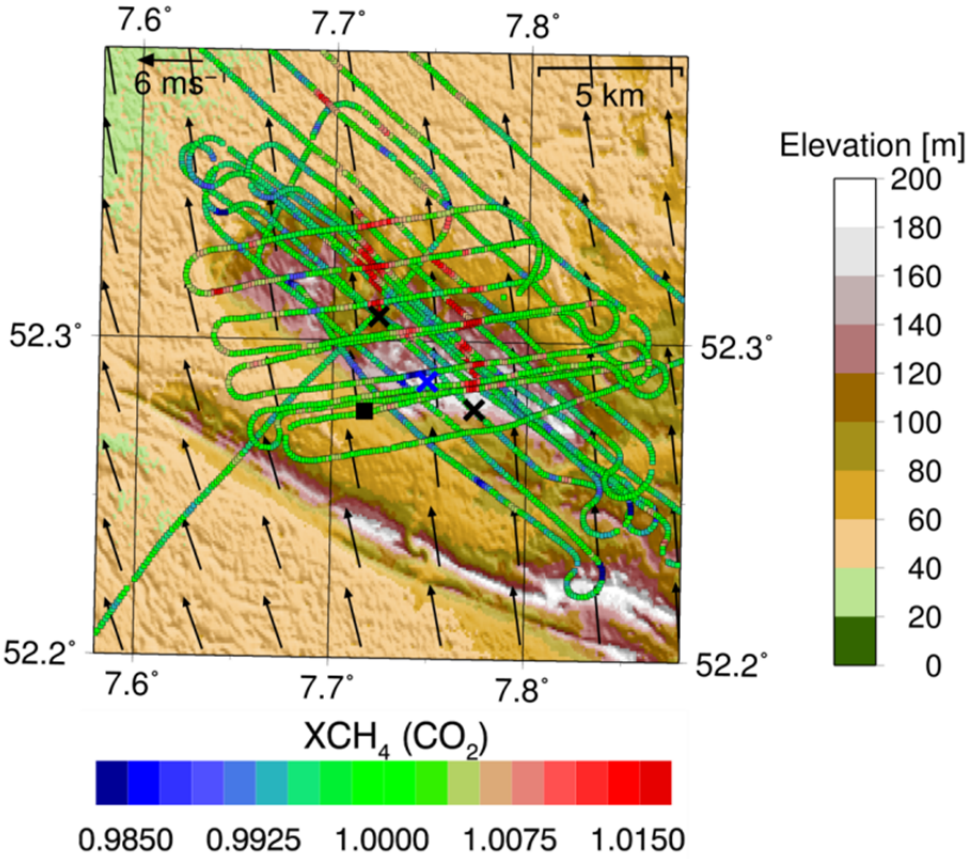

Figure 46: MAMAP $XCH_4(CO_2)$ and surface elevation for the area of Ibbenbüren coal mine. MAMAP data have been smoothed by a 3-point moving average. The North-Western Theodor Shaft and the South-Eastern Bockraden Shaft are denoted by black crosses. The blue cross in between denotes the small coal fired power plant. The arrows denote wind speed and direction in altitude layer 48 of the COSMO-DE model, i.e. approximately at 190m above sea level. (Maps in UTM projection. Topographic data were obtained from the Shuttle Radar Topography Mission (SRTM) version 2.1 (http://dds.cr.usgs.gov/srtm/version2_1/), a collaborative effort from NASA, NGA as well as the German and Italian Space Agencies.)

8.2.3. Atmospheric conditions and wind information from model data

As mentioned in Section 8.1.3, wind speed is an important input parameter for the inversion. For that also the boundary layer height is needed.

Figure 47 shows the COSMO-DE result for temperature and virtual potential temperature for the model grid point North-West of the small power plant location (in the centre of the measurement area).

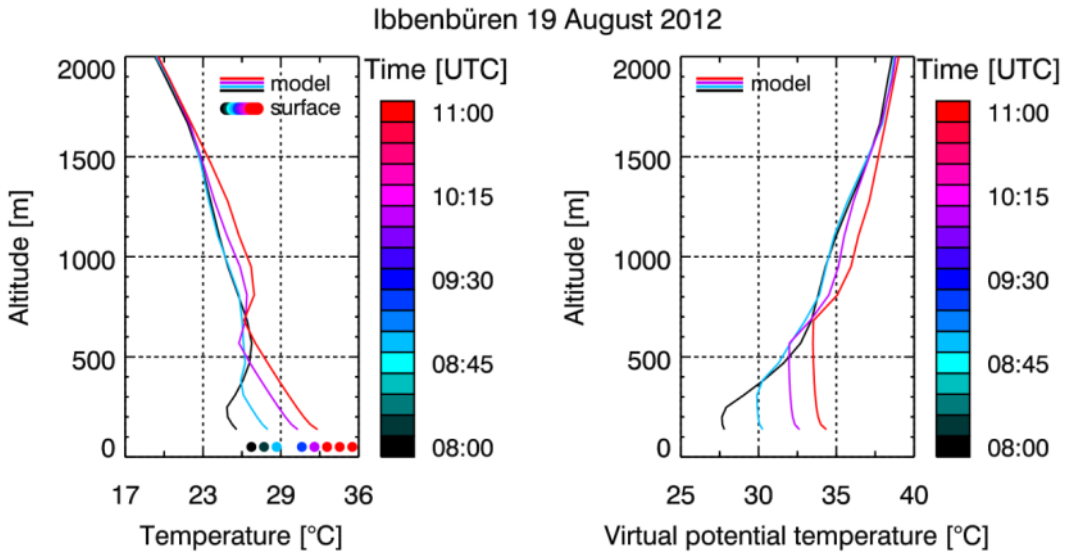

Figure 47: Temperature (left) and virtual potential temperature (right) for the COSMO-DE model grid point North-West of the small power plant in the centre of the measurement area. Surface in situ data for temperature was obtained from Münster/Osnabrück airport (EDDG) located approximately 10km South of the coal mine ventilation shafts.

In a first approximation the boundary layer height can be identified by a sharp increase in virtual potential temperature. According to Figure 47, the boundary layer altitude is evolving from about 100m altitude above ground at 08:00 UTC to about 550m altitude above ground at 11:00 UTC. As in Section 8.1.3, this can only be a very crude approximation.

Figure 48 shows wind speed and direction for the same model grid point. At the boundary layer height wind speed and direction also changes. The wind speed ranges from about 4m/s to 12.5m/s for the time and altitude range of the overflight.

To obtain an adequate estimate of the average wind speed which transports the plume in downwind direction, a weighted mean of the wind profile was computed taking into account the vertical Gaussian dispersion of the plume based on the stability derived from the MAMAP data and dynamically taking into account the evolving boundary layer. This is achieved by computing the effective wind speed for each transect which is averaged for the Gaussian plume model inversion. For the integral method each track is evaluated independently and the resulting emission rates subsequently averaged.

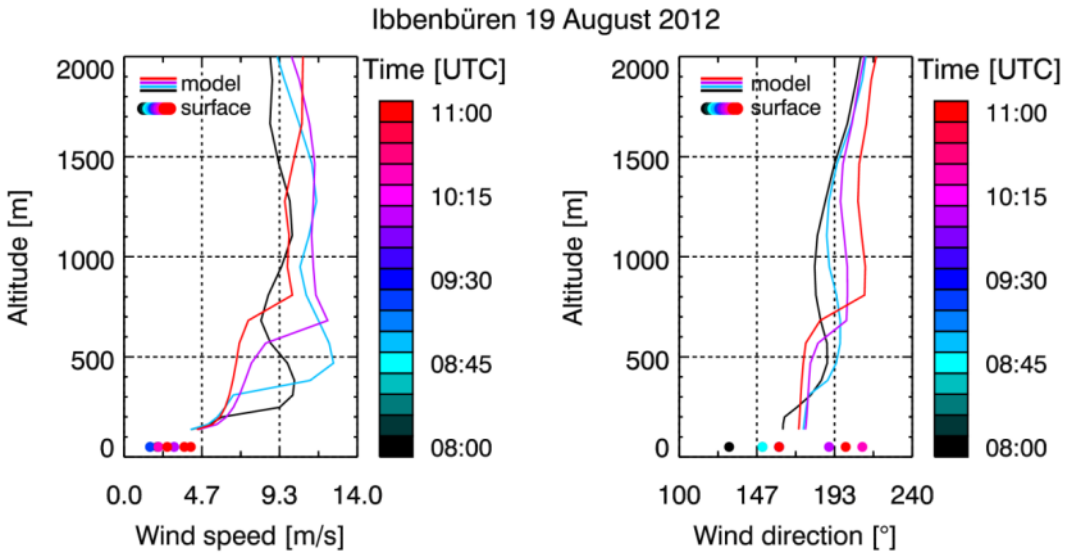

Figure 48: Wind speed (left) and direction (right) for the model grid point North-West of the small power plant in the center of the measurement area.

8.2.4. Inversion for emission data

Preparation and performance of the Gaussian plume inversion and the integral inversion method is very much in line with Section 8.1.4 and Krings et al (2011, 2013).

Before the inversion the data were gridded to pixels of 100m x 100m. There was no additional smoothing or filtering, beside the signal filter described in Section 8.2.2. The measurements were normalised to background using as reference an upwind area defined by -2000m < x < 0m and -2000m < y < 2000m for Theodor Shaft and -1000m < x < 0m and -1000m < y < 1000m for Bockraden Shaft. In both cases this is applied for the coordinate system that has been rotated so that wind direction points to positive x-direction.

Wind direction was determined empirically from the measured data to about 175° for both ventilation shafts. When fitting the stability parameter to the retrieved XCH_4 at Theodor Shaft this yields a=122.8 (+/- 7.1% statistical error), i.e. stability class B/C (between moderately and slightly unstable atmospheric conditions), independent of wind speed. In case of Bockraden Shaft, the retrieved stability parameter is a=138.4 (+/- 6.5% statistical error), i.e. also stability class B/C.

Using this stability as input for a vertical Gaussian dispersion model as a function of distance to source to compute a weighted mean of the wind profile, average wind speeds of 5.85m/s (Theodor) and 5.49m/s (Bockraden) were obtained for the two plume areas covered by MAMAP data.

Applying this wind speed to the Gaussian plume inversion, the result for the average emission rate for the time of the overflight is 13.08 kt CH_4/yr with a statistical error of +/- 5.9% for Theodor Shaft and 18.34 kt CH_4/yr (+/- 5.6%) for Bockraden Shaft. The contour lines as an overlay on the retrieved $XCH_4(CO_2)$ can be seen in Figure 49 and Figure 50.

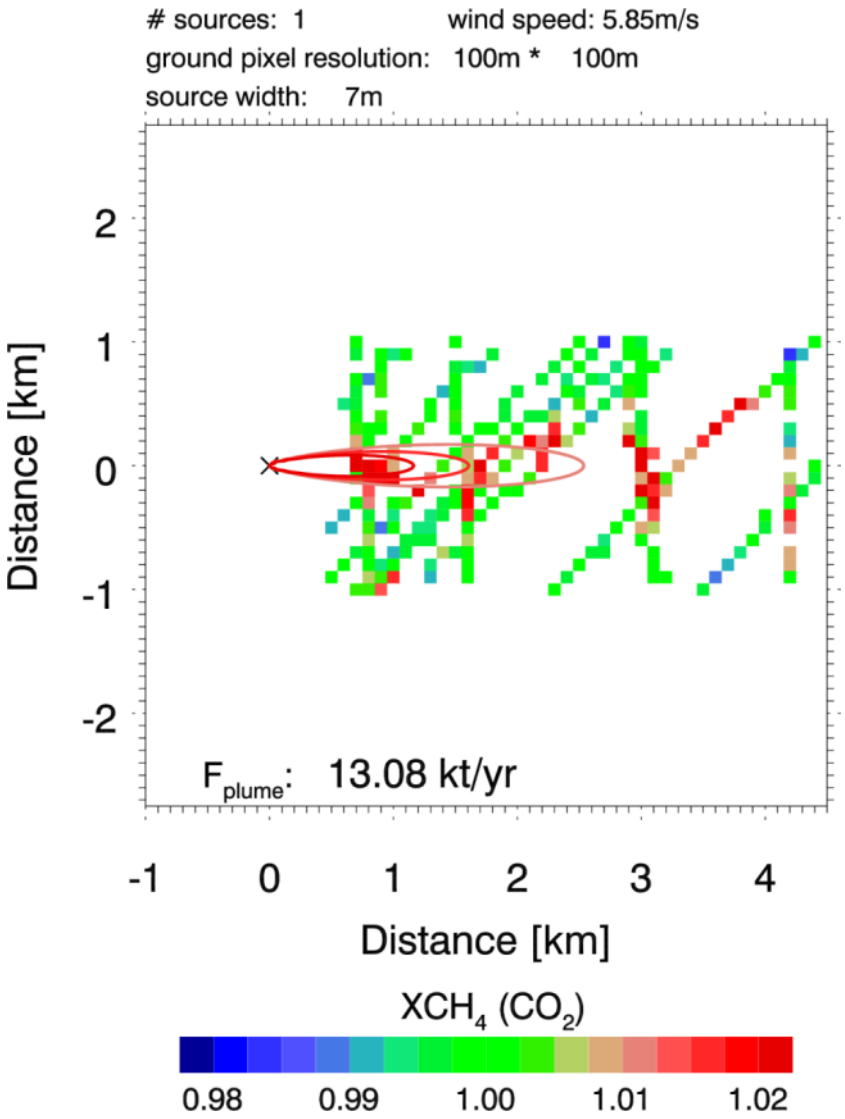

Figure 49: Theodor Shaft MAMAP $XCH_4(CO_2)$ data as used for the inversion. Data are rotated so that wind direction points to positive x-direction. The contour lines indicate the result of the Gaussian plume inversion with a resulting emission of 13.08 kt CH_4/yr for the time of the overflight.

Since the upwind area was basically defined as background, the upwind transect data have not been used for the integral inversion. When evaluating the individual flight tracks with the integral method, there are substantial variations in the inversion result most likely due to convective cells that are not homogeneously distributed in time and space. This is in line with the idea of the Gaussian plume model, which is only a good approximation on average. When taking the mean of the single track inversions with independent wind speed calculations for each track (examples see Figure 51 and Figure 52), the results for the integral method are about 12.49 kt CH_4/yr for Theodor Shaft and 16.87 kt CH_4/yr for Bockraden Shaft and hence very close to the result for the Gaussian plume inversion. The emission rate estimates for individual tracks are partly below zero. This might be due to the fact, that inhomogeneous convective movement lead to a discontinuous plume distribution where noise can dominate the inversion result.

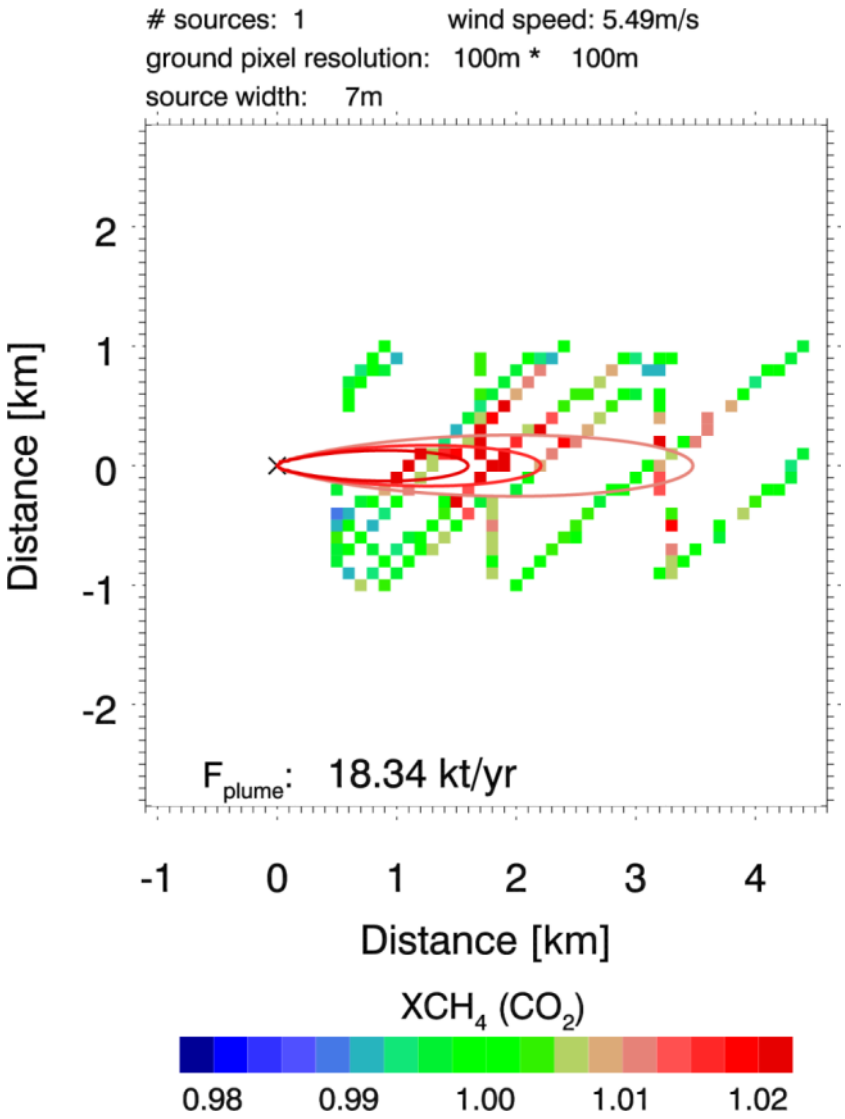

Figure 50 : Bockraden Shaft MAMAP $XCH_4(CO_2)$ data as used for the inversion rotated so that wind direction points to positive x-direction. The contour lines indicate the result of the Gaussian plume inversion with a resulting emission of 18.34 kt CH_4/yr for the time of the overflight.

As for Weisweiler power plant in Section 8.1.4, in principal, also the Gaussian plume inversion was applied to individual flight tracks instead of on all data at once (example see Figure 51 and Figure 52).

The average result of 16.51 kt CH_4/yr (Theodor) and 19.71 kt CH_4/yr (Bockraden) for the time of the overflight differs in particular for Theodor Shaft from the result when considering all data at once. This could be due to the fact that the plume dispersion in the target area appears to be very discontinuous as can be seen from the individual single track results for Gaussian plume and integral inversion. In this case it is more reliable to invert all data at once so that a statistically correct treatment of data following an optimal estimation procedure is ensured.

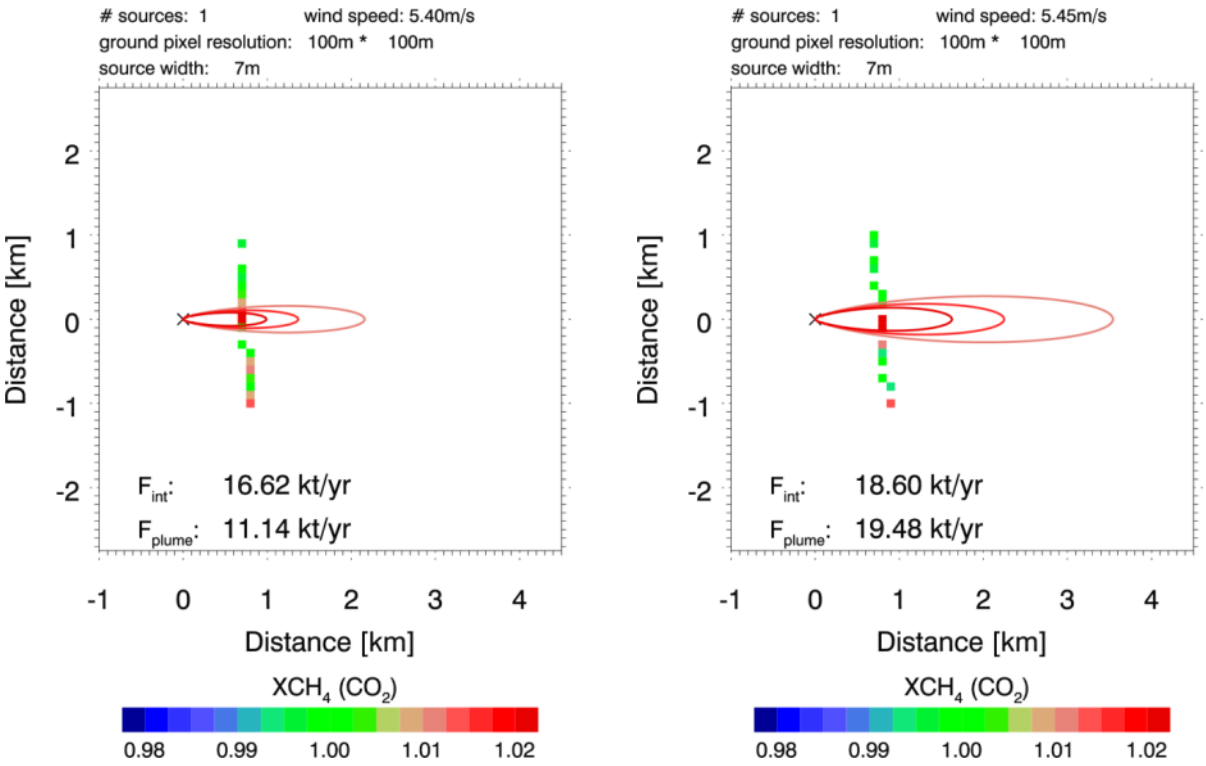

Figure 51: Example for result of integral (F_{int}) and Gaussian plume model inversion (F_{plume}) for individual tracks under consideration for Theodor Shaft independently evaluated. Each figure shows a different track with independently computed wind speed given in the header.

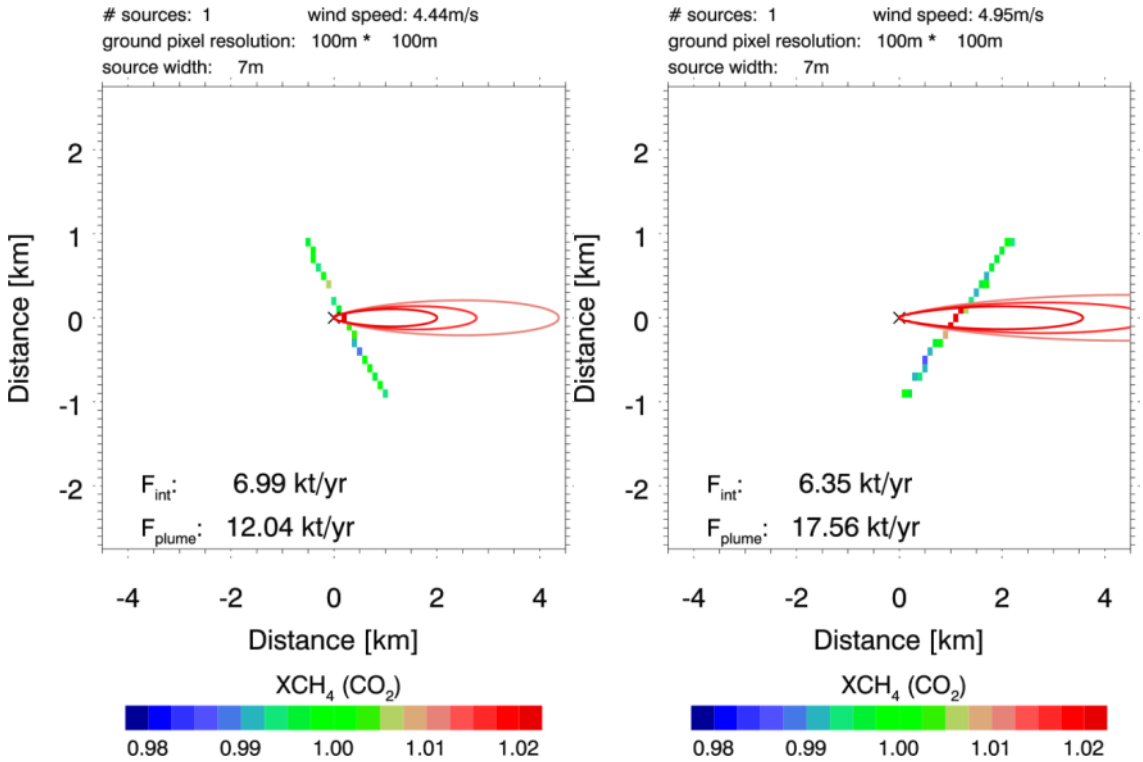

Figure 52: Example of results of integral (F_{int}) and Gaussian plume model inversion (F_{plume}) for individual tracks under consideration for Bockraden Shaft independently evaluated. Each figure shows a different track with independently computed wind speed given in the header.

8.2.5. Incorporation of atmospheric in situ information

The precision of the wind model was roughly estimated to about 0.9 m/s (1σ) with negligible bias for the case described in Krings et al (2011). Assuming the same error holds in the present study, this leads to a relative error (1σ) on the inversion of about 15-16%.

This error can potentially be drastically improved when on site wind information is available, e.g. from airborne turbulence measurements as they were used in Krings et al (2013) and that were also performed during the C-MAPExp campaign.

Figure 53 shows the flight pattern of the in-situ measurements performed at the Ibbenbüren coal mine location. The measurements concentrate on transects at several altitude layers and two distances downwind of the source from about 180 m to about 990 m above sea level.

The acquired temperature data as compared to the corresponding model data is shown in Figure 54 for the temperature and in Figure 55 for the virtual potential temperature. In general, model and in-situ measurements agree rather well. It is however hard to validate the selected boundary layer heights (see Section 8.2.3). Inspecting the aerosol vertical profiles (see Figure 56 and Figure 57) gives a clearer on boundary layer height showing a drop in aerosol concentrations at about 500m altitude for particles larger than 3µm for about 10:00 UTC. This is in good agreement with the boundary layer height derived from modelled virtual potential temperature. However, the exact boundary layer height is not critical because when for comparison running the wind speed computation without any boundary layer at all, the wind speed only differs by +3% (Theodor) and +4% (Bockraden) which is well below the wind uncertainty.

The comparison of wind speed and direction is shown in Figure 58 and Figure 59 for 1 Hz temporal resolution of the in-situ data and in Figure 60 and Figure 61 for a 60 s moving average. The in-situ wind speed is significantly varying, but it appears that the model overestimates the wind speed for the time of the overflight. To quantify this overestimation, the probed altitude range has been divided into 5 equally thick layers in which the deviation between the in-situ measurements on the one hand and the associated model data interpolated in time and space on the other hand were quantified and subsequently averaged over the altitude layers. For the available model and measurement data at the target area and time, this yields an average overestimation of about 3.03m/s, i.e. about 28.1%. Thereby the target area and time were defined by a maximum distance to the centre of the measurement area of -15km < x,y < 15km in a time interval between 08:25 and 10:49 UTC. The complete results are shown in Table 2. Note that the results do not directly relate to Figure 58 and Figure 60 which only show the model wind speed at the North-West COSMO-DE grid point while model wind data from the whole measurement area enters the computations in Table 2.

However, in contrast to the conditions at Weisweiler power plant (see Section 8.1.5), the wind profile shape of model and in-situ measurements significantly differ. In this case it would be helpful to weight the individual height layers due to their importance for the dispersion. For that, the most important layers would be the surface layer and the lowest layers in Table 10. This is further supported by the fact, that the computed average wind speed from the model is about 5-6m/s (basically independent of boundary layer height). The surface layer is about 100m thick and was not probed by the airborne instrument, so that this option is not feasible without strong assumptions. A simple approximation would be to assume that the relative wind difference in the lowest layer of Table 10 is also valid for the surface layer, so that the model alone overestimates the wind speed by about 28%.

If this information is used to correct the inversion results from the previous chapter this yields for the Gaussian plume inversion 9.42 ktCH_4/yr (Theodor) and 13.20 ktCH_4/yr (Bockraden). For the integral

inversion the emission rate estimates change to 8.99 $ktCH_4/yr$ (Theodor) and 12.15 $ktCH_4/yr$ (Bockraden).

Table 10: Results of the wind speed comparison between model and airborne in-situ data for Ibbenbüren.

Altitude range a.s.l. [m]	Model wind speed [m/s]	In-situ wind speed [m/s]	Wind speed difference [m/s]	Relative wind speed difference [%]
183 – 345	6.68	4.82	-1.85	-27.8
345 – 507	11.52	6.17	-5.35	-46.1
507 – 668	12.61	8.40	-4.21	-33.3
668 – 830	11.88	9.45	-2.43	-20.4
830 – 992	11.21	9.91	-1.31	-11.6
			Average: -3.03m/s	Average: -28.1%

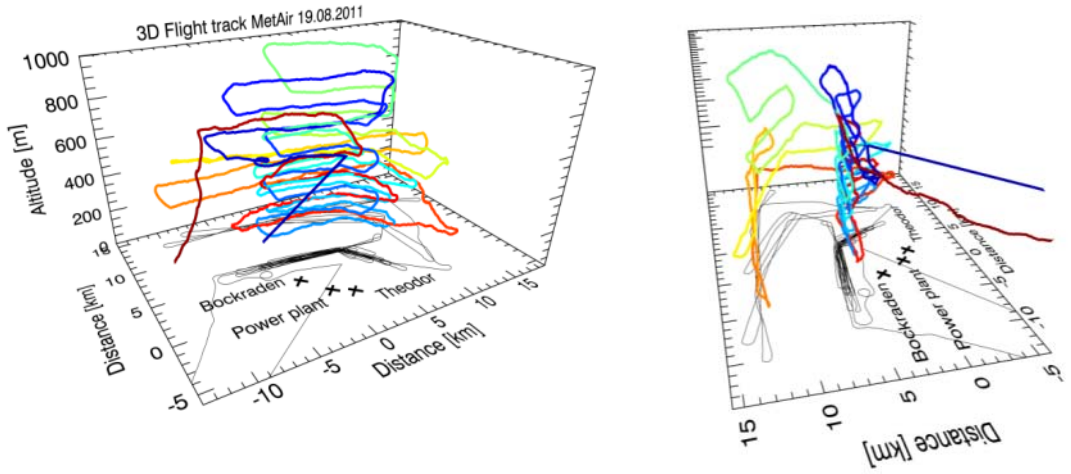

Figure 53: Flight track of in-situ measurements. Location is in UTM projection relative to the power plant location. The colours indicate the temporal progression from dark blue to dark red, while the thin black lines denote the projection of the flight tracks on the surface.

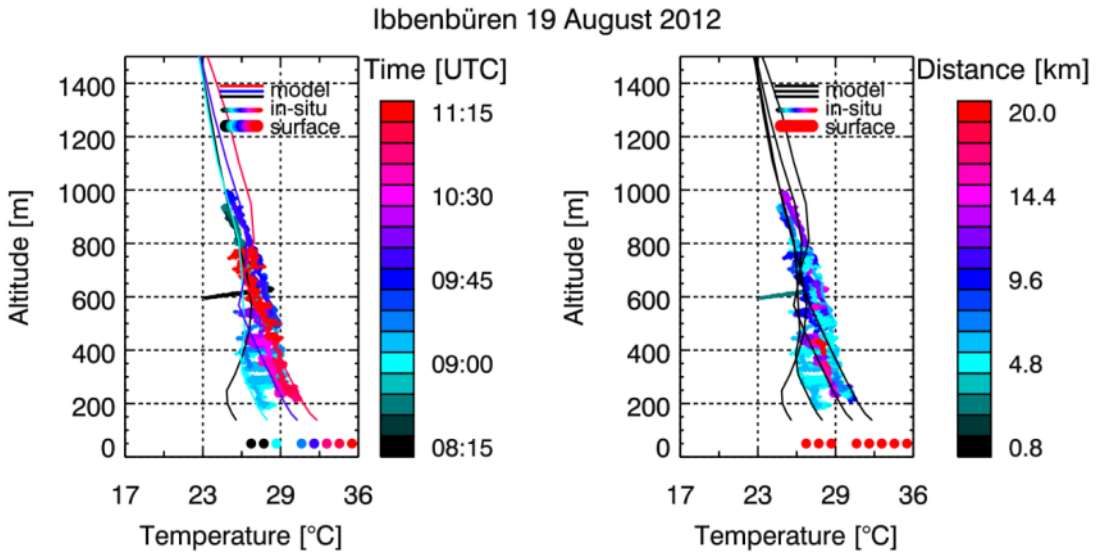

Figure 54: Temperature as given by the COSMO-DE model grid point North-West of the small power plant in the centre of the measurement area (straight lines), airborne and ground based in-situ measurements (discs). Ground based measurements from Münster/Osnabrück Airport (10km South of the measurement area) have been obtained through Weather Underground (www.wunderground.com). Data is colour coded for time (left) and distance to the source (right).

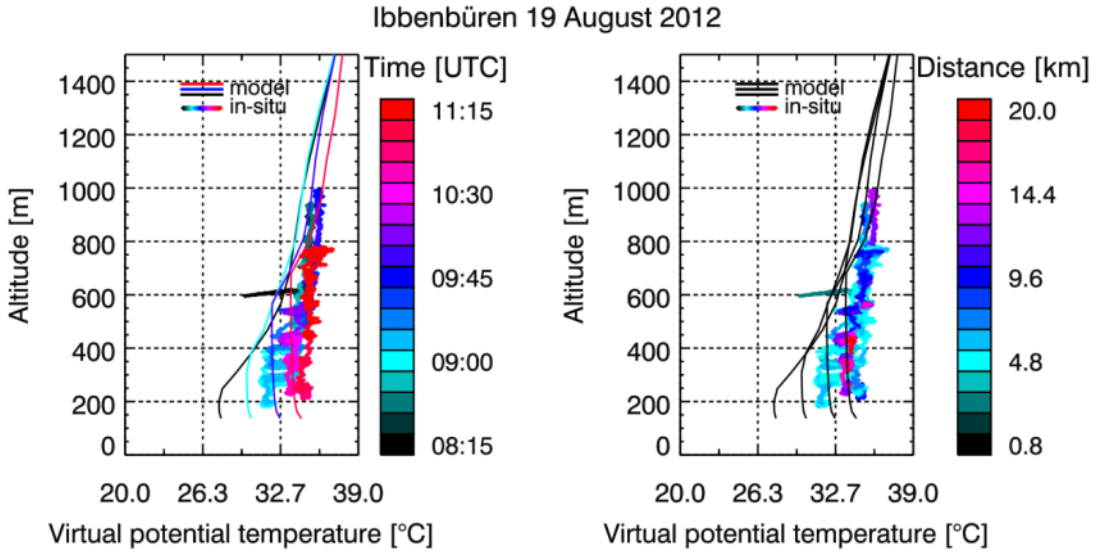

Figure 55: Virtual potential temperature as given by the COSMO-DE model grid point North-West of the small power plant in the centre of the measurement area (straight lines) and airborne in-situ measurements (discs). Data is colour coded for time (left) and distance to the source (right).

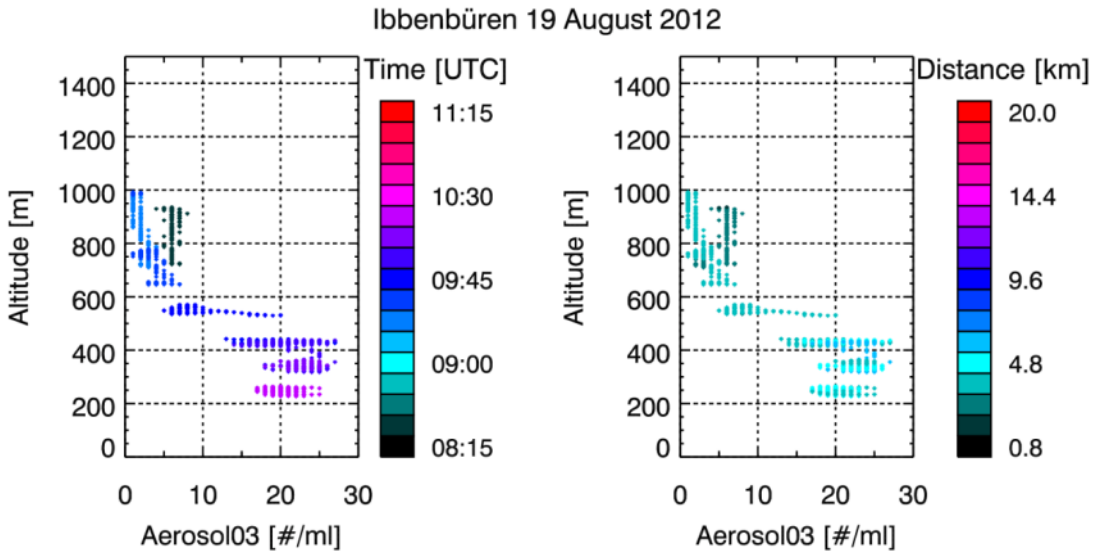

Figure 56: Vertical aerosol distribution measured in-situ for aerosol particles larger than 3µm. Data is colour coded for time (left) and distance to the source (right).

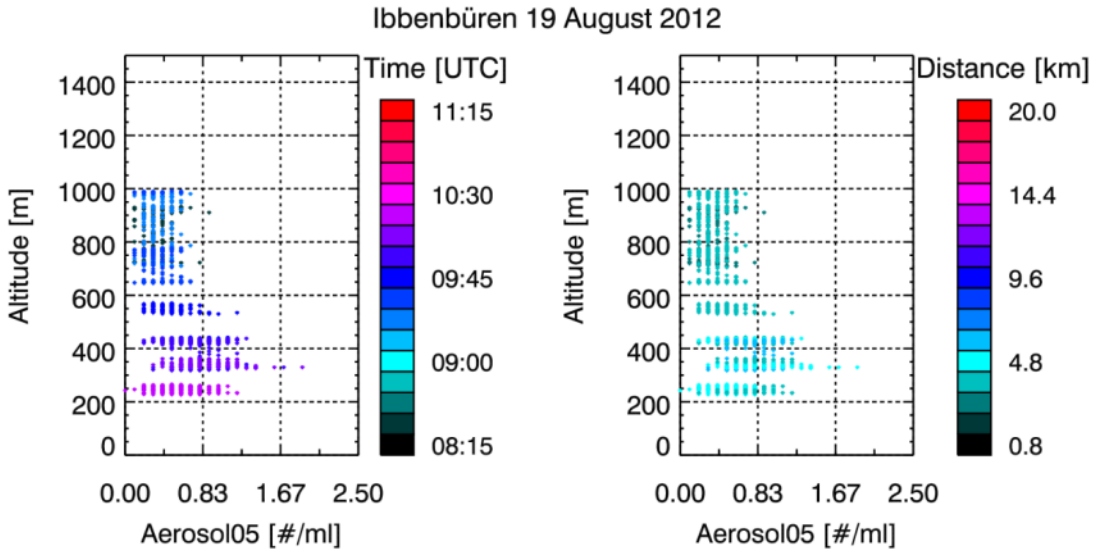

Figure 57: Vertical aerosol distribution measured in-situ for aerosol particles larger than 5µm. Data is colour coded for time (left) and distance to the source (right).

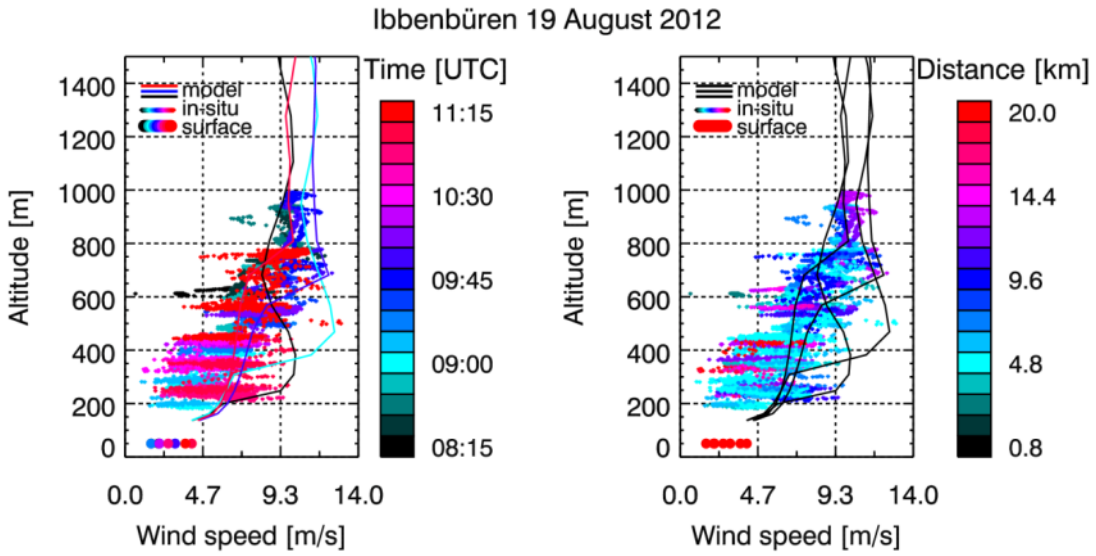

Figure 58: Wind speed as given by the COSMO-DE model grid point North-West of the small power plant in the centre of the measurement area (straight lines) airborne and ground based in-situ measurements (discs). Ground based measurements from Münster/Osnabrück Airport (10km South of the measurement area) have been obtained through Weather Underground (www.wunderground.com). Data is colour coded for time (left) and distance to the source (right).

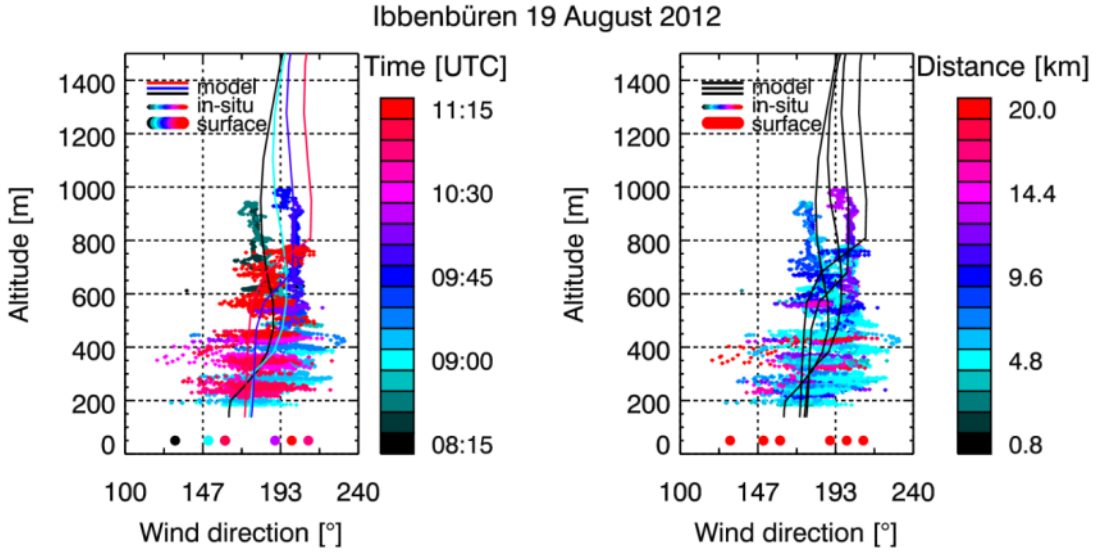

Figure 59: Wind direction as given by the COSMO-DE model grid point North-West of the small power plant in the centre of the measurement area (straight lines) airborne and ground based in-situ measurements (discs). Ground based measurements from Münster/Osnabrück Airport (10km South of the measurement area) have been obtained through Weather Underground (www.wunderground.com). Data is colour coded for time (left) and distance to the source (right).

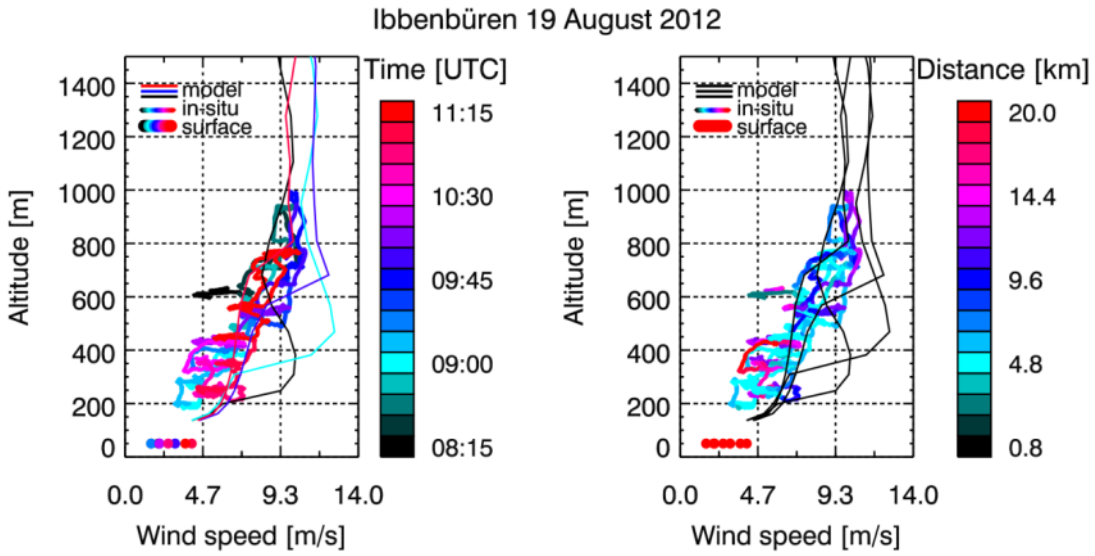

Figure 60: As Figure 58 but smoothed by a 60s moving average.

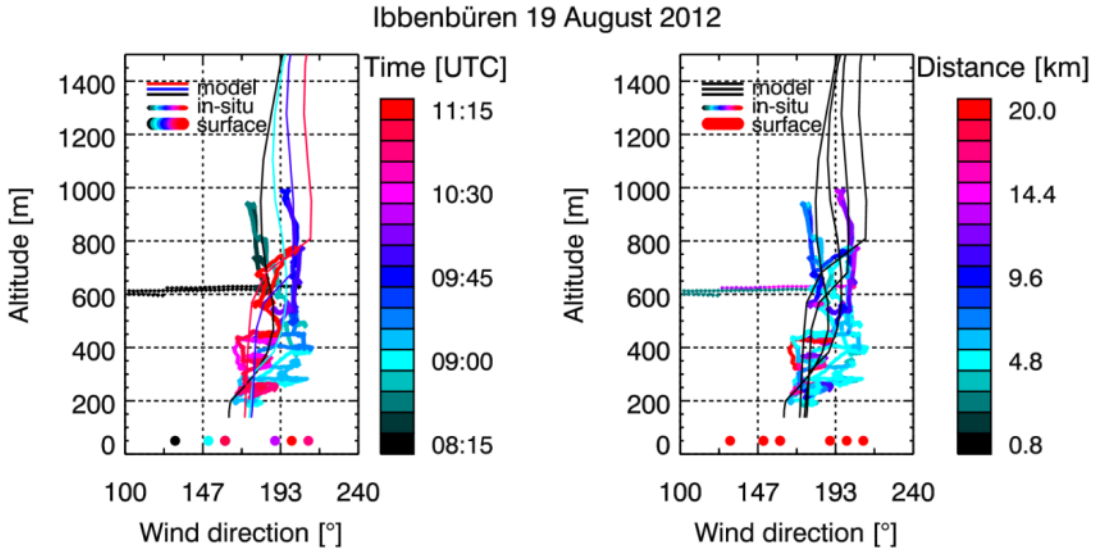

Figure 61: As Figure 59 but smoothed by a 60s moving average.

8.3. Conclusions for the remote sensing inversions

The results from the measurements performed over Weisweiler power plant on August 18, 2012 and over the coal mine ventilation shafts of the coal mine RAG Anthrazit Ibbenbüren on August 19, 2012 are summarized in Table 11.

Table 11: Results of the data analysis for CO_2 emissions from Weisweiler power plant and CH_4 emissions from coal mine ventilation shafts of the coal mine RAG Anthrazit Ibbenbüren.

Data basis	**MAMAP and COSMO-DE**			**MAMAP, COSMO-DE and airborne in-situ**			**Reported in 2011**	**Reported for the time of the overflight**
Target	Gaussian plume	Integral	Approx. wind error	Gaussian plume	Integral	Approx. wind error		
Weisweiler power plant	16.35 $MtCO_2/yr$ (+/- 2.6%)	15.83 $MtCO_2/yr$	23%	17.23 $MtCO_2/yr$ (+/- 2.6%)	16.68 $MtCO_2/yr$	12%	19.3 $MtCO_2/yr$	21.2 Mt $MtCO_2/yr$
Ibbenbüren: Theodor Shaft	13.08 $ktCH_4/yr$ (+/- 5.9%)	12.49 $ktCH_4/yr$	15%	9.42 $ktCH_4/yr$ (+/- 5.9%)	8.99 $ktCH_4/yr$	12%	41.8 $ktCH_4/yr$	16.4 $ktCH_4/yr$
Ibbenbüren: Bockraden Shaft	18.34 $ktCH_4/yr$ (+/- 5.6%)	16.87 $ktCH_4/yr$	16%	13.20 $ktCH_4/yr$ (+/- 5.9%)	12.15 $ktCH_4/yr$	13%		18.2 $ktCH_4/yr$

The highest uncertainties are expected to result from uncertainty in wind speed and estimation of an average wind speed and are denoted in Table 11 along with the statistical uncertainties based on the instrument precision for the plume inversion. In case of Weisweiler power plant, the COSMO-DE model wind speed was biased low compared to the measurements. Adjusting for this bias leads to emission rates that are about 5.4% higher than the results considering only MAMAP measurements and COSMO-DE model data. The emission rate estimate for the time of the overflight is about 20% lower than the emission ratecomputed from data provided by RWE.

In case of the coal mine ventilation shafts, the wind profiles between airborne in-situ measurements and model significantly differed. However, the lowest atmospheric layer which contains a large part of the emitted CH_4 was not probed. Assuming that the bias in the lowest atmospheric layer is as in the lowest probed layer, the inverted emission rates need to be adjusted by -28%.

The emission rate estimate for the two ventilation shafts combined is then about 46-49% lower than the average emission rate for 2011. Generally the CH_4 emissions in coal mines are related to cutting of fresh coal with a resulting maximum emission rate on Friday evening and a minimum on Monday morning (EnergieAgentur.NRW, 2009). Hence, an emission rate that is lower than the yearly average is likely for a Sunday when the present measurements were performed and assuming that the interannual variations of CH_4 emissions of the coal mine are low. However,compared to the actual emissions as provided by the Bezirksregierung Arnsberg, the result is biased by about -37%.

Main error source is the uncertainty of wind information which is roughly between 10% and 20%. An additional uncertainty arises from the computation of an average wind speed which is challenging especially in case of Ibbenbüren where the wind profile significantly differs from the model wind profile (see Section 8.2.5).

9. Comparison of inversion results using in-situ and remote sensing

9.1. Comparison of columns

The in-situ measurements converted to vertical columns and projected on straight lines are shown in Figure 62 for Weisweiler power plant and in Figure 65 for the coal mine ventilation shafts Ibbenbüren.

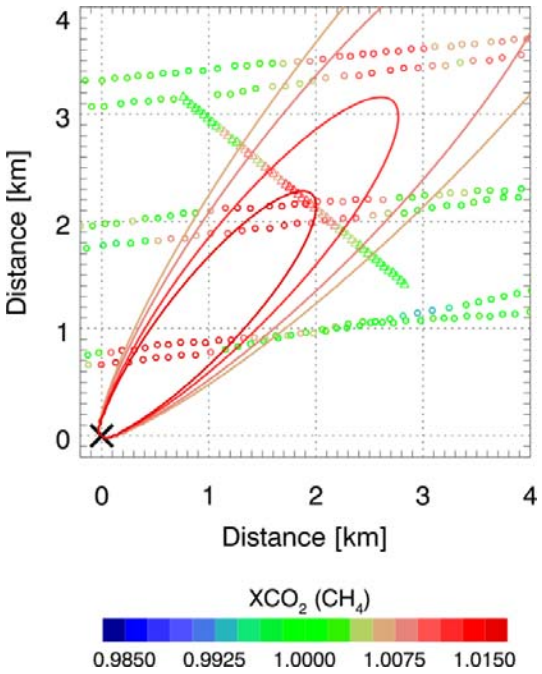

Figure 62 : Comparison between remote sensing measurements of XCO_2 (circles) at Weisweiler power plant with in-situ measurements converted to vertical columns projected on a straight line (triangles).

For Weisweiler power plant, the location of the plume between remote sensing and in-situ measurements coincide very well. The horizontal cross section of the in-situ data is additionally shown in Figure 63. For comparison also the cross sections of the remote sensing data closest to the projected in-situ measurements are shown in Figure 64, showing similar values in both cases. However, the remote sensing results appear to be somewhat higher which is also reflected in the inversion result of the in-situ data (see Section 9.2). An exact agreement between in-situ and remote sensing is not to be expected. On the one hand this is because the measurements were not performed at the same time and on the other hand the vertical columns computed from the in-situ measurements are only virtual columns that have been obtained from numerous measurements performed at various altitudes at different times.

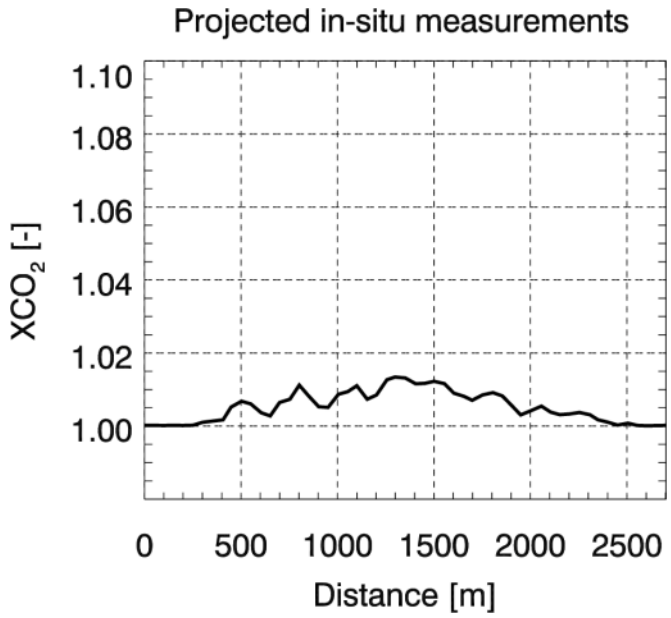

Figure 63 : Cross section of in-situ measurements converted to column averaged dry air mole fractions at power plant Weisweiler.

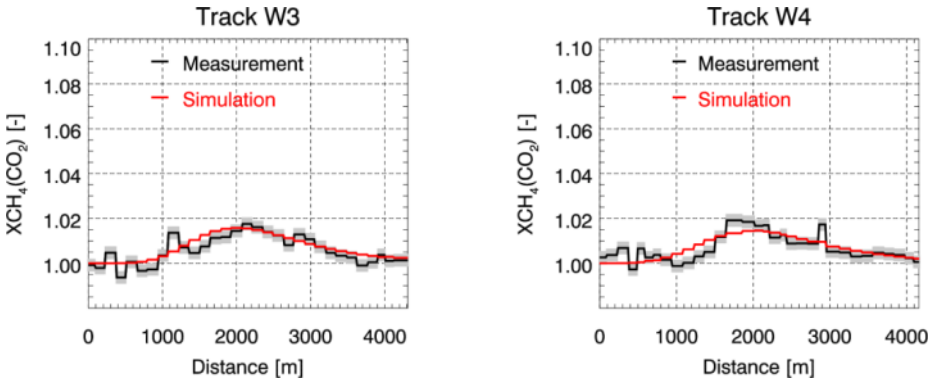

Figure 64 : Cross sections of remote sensing column averaged dry air mole fractions at power plant Weisweiler closest to the in-situ measurements. Measurements are shown in black, while the result of the model based on the inverted emission rate using the plume model and sampled like the measurement is shown in red.

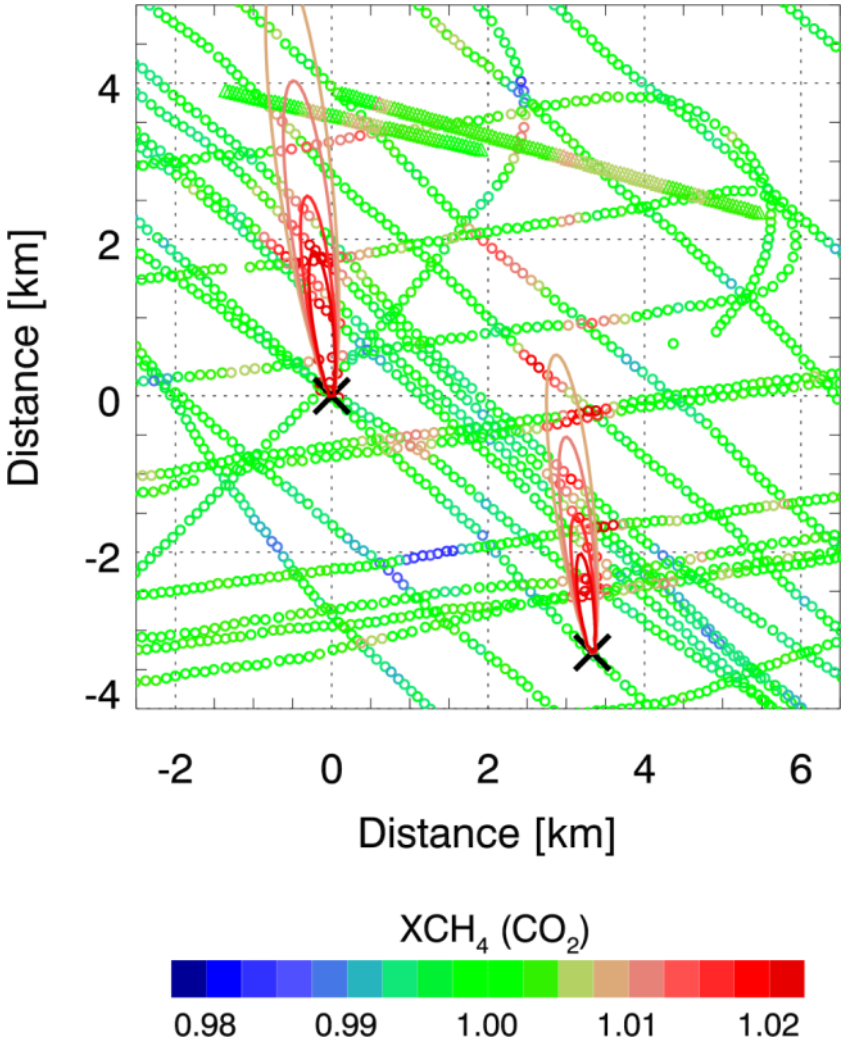

Figure 65 : Comparison between remote sensing measurements of XCH_4 (circles) at coal mine ventilation shafts Ibbenbüren with in-situ measurements converted to vertical columns projected on a straight line (triangles) for each shaft.

The in-situ cross section for the two ventilation shafts of the coal mine Ibbenbüren are shown in Figure 66, the relevant remote sensing cross sections in Figure 67 for Theodor Shaft and in Figure 68 for Bockraden Shaft. From all masurements it can be seen that the plume has not a Gaussian profile but appears to be rather ragged. This makes a comparison between remote sensing and in-situ particularly difficult. Nevertheless, the order of magnitude of obtained column mole fractions are similar.

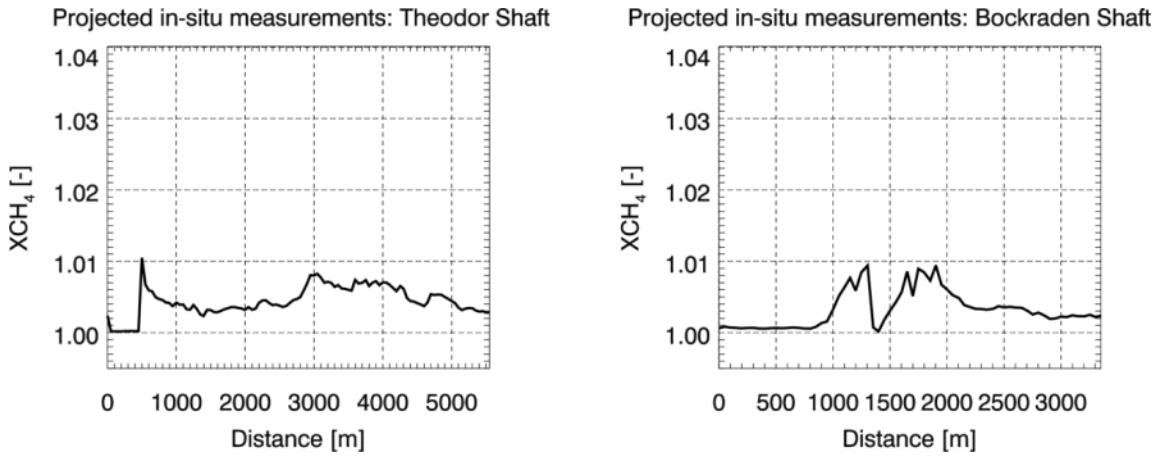

Figure 66 : Cross section of in-situ measurements converted to column averaged dry air mole fractions at Theodor Shaft (left) and Bockraden Shaft (right).

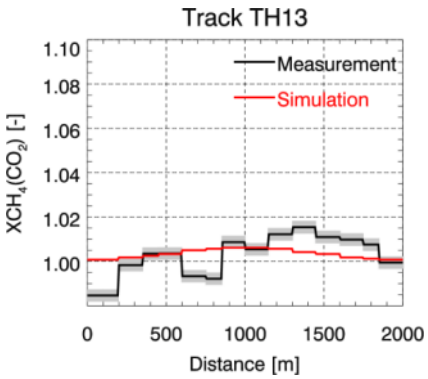

Figure 67 : Cross section of remote sensing column averaged dry air mole fractions at Theodor Shaft closest to the in-situ measurements. Measurements are shown in black, while the result of the model based on the inverted emission rate using the plume model and sampled like the measurement is shown in red. However this track is more than 1km closer to the source than the projected in-situ measurements.

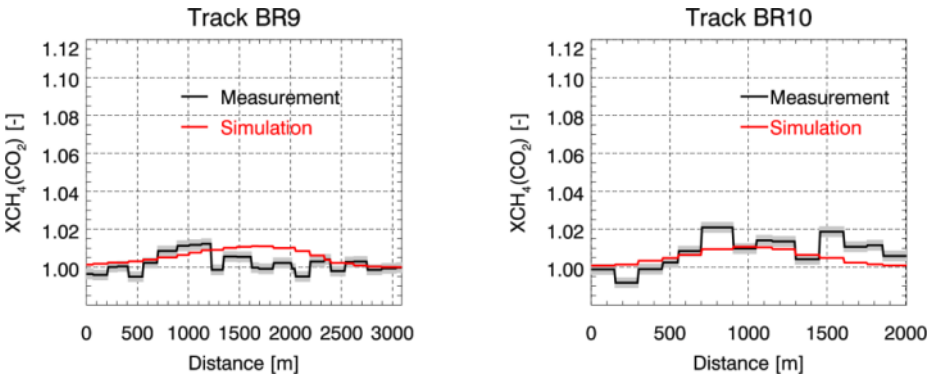

Figure 68 : Cross sections of remote sensing column averaged dry air mole fractions at Bockraden Shaft closest to the in-situ measurements. Measurements are shown in black, while the result of the model based on the inverted emission rate using the plume model and sampled like the measurement is shown in red.

9.2. Preliminary Comparison of Inversion Results

Preliminary inversion results for remote sensing and in-situ measurements are shown in Table 12. In case of CO_2 emissions from Weisweiler power plant, the remote sensing results incorporating the in-situ meteorological data are about 17 $MtCO_2$/yr for the time of the overflight. The in-situ result (for a horizontal resolution of 50m as defined in Section 7.1) is significantly lower at about 13.8 $MtCO_2$/yr. The total emissions in 2011 as reported within the framework of emission release registers were about 19.3 $MtCO_2$/yr (E-PRTR, http://prtr.ec.europa.eu/, last access: January, 2014). Reported emissions for the time of the overflight as inferred from data provided by RWE are about 21.2 $MtCO_2$/yr

In case of Ibbenbüren, the in-situ results for the near and far track strongly differ by a factor of about 2.3. The reason for that is not clear (see also Section 7.2 for a discussion). Compared to the reported data provided by the Bezirksregierung Arnsberg, the near in-situ tracks overestimate the emissions by about 26%, the far track by about 193%. The inversion using remote sensing data on the other hand underestimates the emissions by about 47%. In case of the remote sensing result, this bias is larger than the expected errors. Possible reasons for that will be discussed in Section 9.3.

The columns of CO_2 and CH_4 computed from the in-situ data by Metair can of course also be used with the IUP inversion approaches applied for the remote sensing data. The average inversion result for Weisweiler is then 12.1 $MtCO_2$/yr for the time of the overflight and hence very close to the in-situ inversion result by Metair. The results for Theodor Shaft using the IUP remote sensing inversion techniques applied to the in-situ data yields about 24.1$ktCH_4$/yr which is about 15% higher than the in-situ inversion. For Bockraden Shaft on the other hand the IUP inversion using the in-situ data leads to an emissions estimate of about 14.1$ktCH_4$/yr, that is 35% lower than the Metair result.

Data basis	MAMAP and COSMO-DE				MAMAP, COSMO-DE and airborne in-situ wind information				In-situ (Metair)					Reported
Target	Gaussian plume	Integral	Wind speed	Approx. wind error (+)	Gaussian plume	Integral	Wind speed	Approx. wind error (+)	Near field inversion (*)	Far field inversion (*)	Wind speed		Approx. wind error (+)	
											Near field	Far field		
Weisweiler power plant	16.35 $MtCO_2$/yr (+/- 2.6%)	15.83 $MtCO_2$/yr	3.96 m/s	23%	17.23 $MtCO_2$/yr (+/ - 2.6%)	16.68 $MtCO_2$/yr	4.19 m/s	12%	13.76 $MtCO_2$/yr		4.91 m/s		10%	21.2 $MtCO_2$/yr
Ibbenbüren: Theodor Shaft	13.08 $ktCH_4$/yr (+/- 5.9%)	12.49 $ktCH_4$/yr	5.85 m/s	15%	9.42 $ktCH_4$/yr (+/- 5.9%)	8.99 $ktCH_4$/yr	4.21 m/s	12%	20.97 $ktCH_4$/yr	101.28 $ktCH_4$/yr	4.9 m/s	4.25 m/s	10/12%	16.4 $ktCH_4$/yr
Ibbenbüren: Bockraden Shaft	18.34 $ktCH_4$/yr (+/- 5.6%)	16.87 $ktCH_4$/yr	5.49 m/s	16%	13.20 $ktCH_4$/yr (+/- 5.9%)	12.15 $ktCH_4$/yr	3.95 m/s	13%	22.74 $ktCH_4$/yr		4.38 m/s	3.42 m/s	11/14/%	18.2 $ktCH_4$/yr

Table 12: Preliminary comparison of inversion results for remote sensing and in-situ measurements. The results for remote sensing are splitted according to the used meteorological data. Explanations: (+) Approximate wind error is computed from the errors of 0.9m/s for COSMO-DE and 0.5m/s for the in-situ wind data. For the in-situ inversion the wind speed is only an effective wind speed computed in the post-processing and is not used as such for the inversion. (*) "Near field" and "Far field" refers to the in-situ measurement tracks flown at different distances from the source. The far field inversion in case of Ibbenbüren in-situ data includes emissions from both shafts. For Weisweiler there is only one track for in-situ column data, therefore it is not distinguished between near and far field.

Powerplant	Date	Emnissions at Time of Overpass [$MtCO_2/yr$]		
		Derived from Energy Production Data	In-situ	Remote Sensing
Weisweiler	18.08.2012	21.2	13.8 ±25%	15.5 ± 25%
	23.08.2012	15.2	21.2 ± 4%	--
Niederaußem	15.08.2012	25.7	24.5 ± 24%	--
	18.08.2012	22.5	37.2 ± 3%	--
Gesamt-emissionen: Niederaußem + Neurath + Frimmersdorf	15.08.2012	69.8	54.4 ± 4%	--
	16.08.2012	71.0	50.3 ± 12%	--
	17.08.2012	64.0	47.5 ± 20%	--
	18.08.2012	46.2	47.2 ± 7%	--
Ibbenbüren	19.08.2012	3.9	6.7 ± 6.8%	--

Table 13: Comparison of inverted emissions with emissions derived from energy production.

Table 13 compares the emissions inverted from the in-situ data set to the emissions reported at the time of the overpass. Due to the larger effort of inverting the remote sensing data, only data from Weisweiler could be evaluated in this project. Further investigations on the observed commonalities and differences are out of scope of this campaign project (main focus was data acquisition), but it indicates that further investigations on the data set are required and will lead into new insights into the field of determining point source emissions from remote sensing data.

9.3. Possible bias in the inversion of remote sensing data due to assumptions in background correction

It is evident that the inversion of remote sensing data in case of Ibbenbüren strongly underestimates the reported emissions. The difference is about -47%. The most likely candidate that can potentially have such an impact is the choice of the normalisation of MAMAP data. The MAMAP instrument is not absolutely calibrated and therefore needs a normalisation to the designated background. General procedure is to divide (normalise) the data by the median of a region that is trusted to be at background concentration level.

In case of Ibbenbüren the data region for normalisation was selected upwind of the measurement area, stated in detail in Section 8.2.4. A revised normalisation was tested afterwards that uses the same normalisation for both ventilation shafts using the complete surrounding area of the shafts excluding the plume area, while the plume area is approximated empirically (see Figure 69). Since this data also includes several turns of the airplane it is useful to include an inclination filter rejecting all data for instrument inclination geometries of more than 5° off nadir. The advantage of this method is that significantly more data is taken into account giving potentially a better average. In this way also variations during flight, e.g. due to changing atmospheric conditions (clouds, aerosols, …) are taken into account to some degree. The disadvantage is that upwind sources cannot be completely separated anymore from the source of interest. However, this is not critical for Ibbenbüren since there are no significant (localised) sources upwind of the ventilation shafts. For the former normalisation method, the normalisation factor was about 0.981 (Theodor Shaft) and 0.980 (Bockraden Shaft). Using the revised normalisation method, this factor becomes 0.978 for both shafts. This result is rather stable with respect to the excluded plume area leading to varying inversion results of less than 1.5% for a reasonable modification of the selected data for normalisation. The cross sections for all tracks in comparison with data using the former normalisation are shown in Figure 70 to Figure 76. It is apparent that the scatter due to noise appears to be rather high making a determination of background by eye quite difficult.

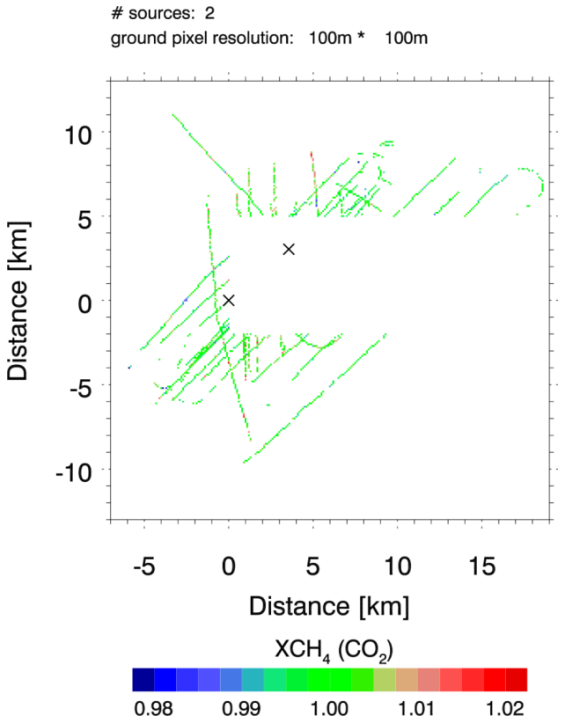

Figure 69 : Remote sensing data used for the revised normalization method for data at Ibbenbüren coal mine. The methane plume area originating at the two ventilation shafts is excluded.

In doing so, the emission rate estimates are significantly higher (see Table 14). For Theodor Shaft, the emission rate is about 14.76 $ktCH_4/yr$ (integral method) and 12.30 $ktCH_4/yr$ (Gaussian plume inversion). For Bockraden emissions are estimated to 15.30 $ktCH_4/yr$ (integral) and 16.05 $ktCH_4/yr$ (plume). All in all the bias is decreased to an underestimation of 16% relative to the reported emissions.

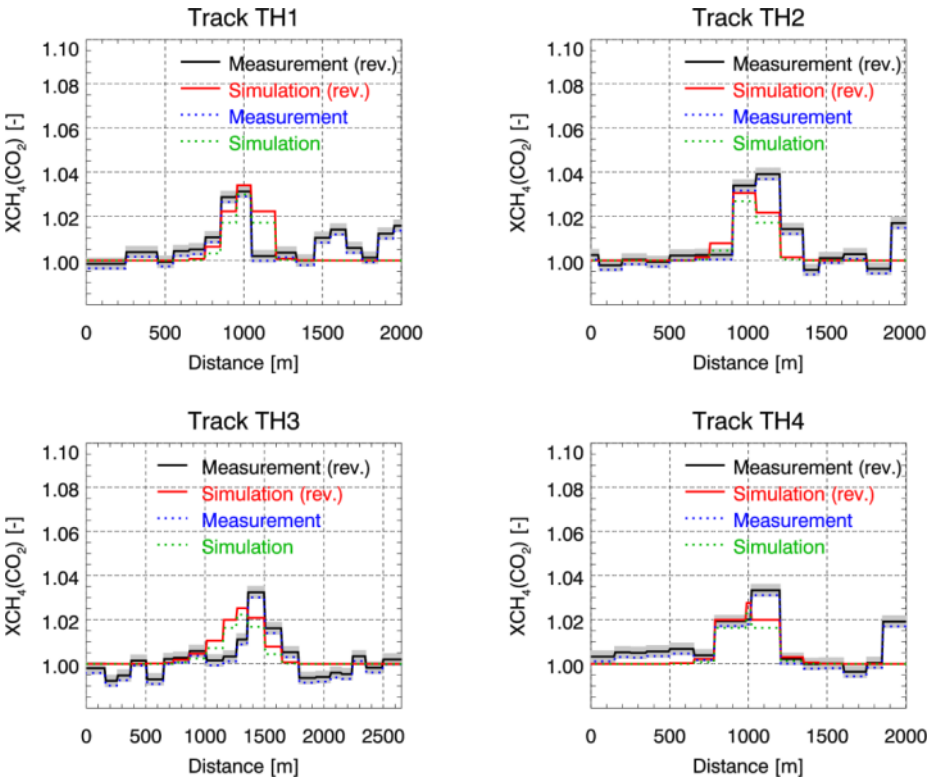

Figure 70 : Cross sections of remote sensing column averaged dry air mole fractions at Theodor Shaft. Measurements with revised normalization are shown in black, while the result of the model based on the inverted emission rate using the plume model and sampled like the measurement is shown in red. Measurement and simulation based on the former nomalisation are shown in blue and green dotted lines respectively.

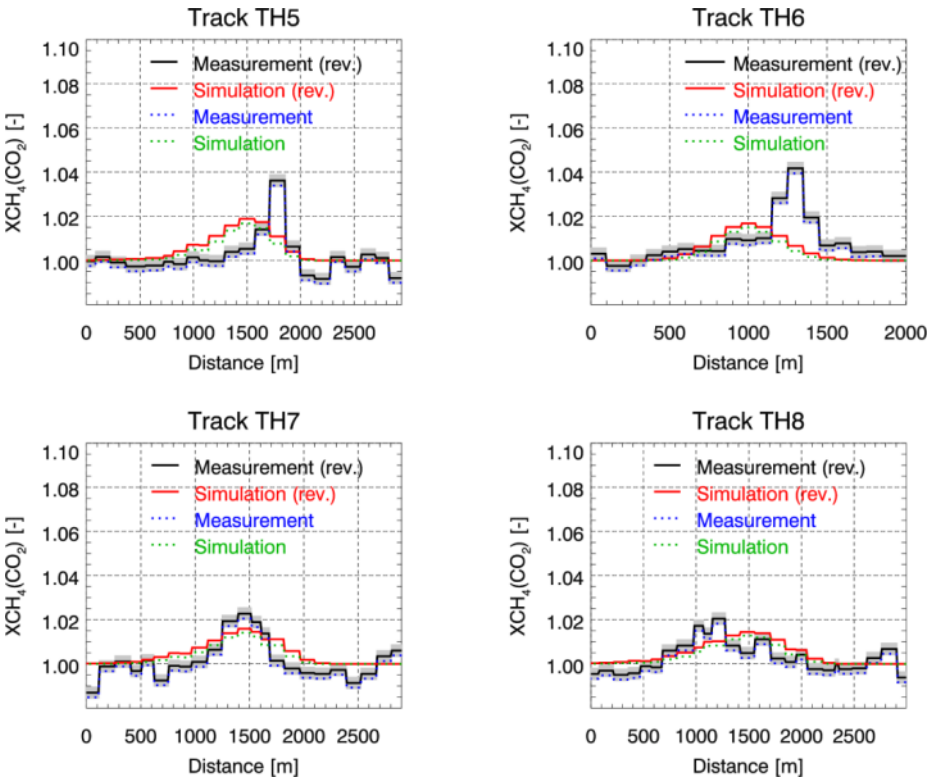

Figure 71 : Continuation of Figure 70.

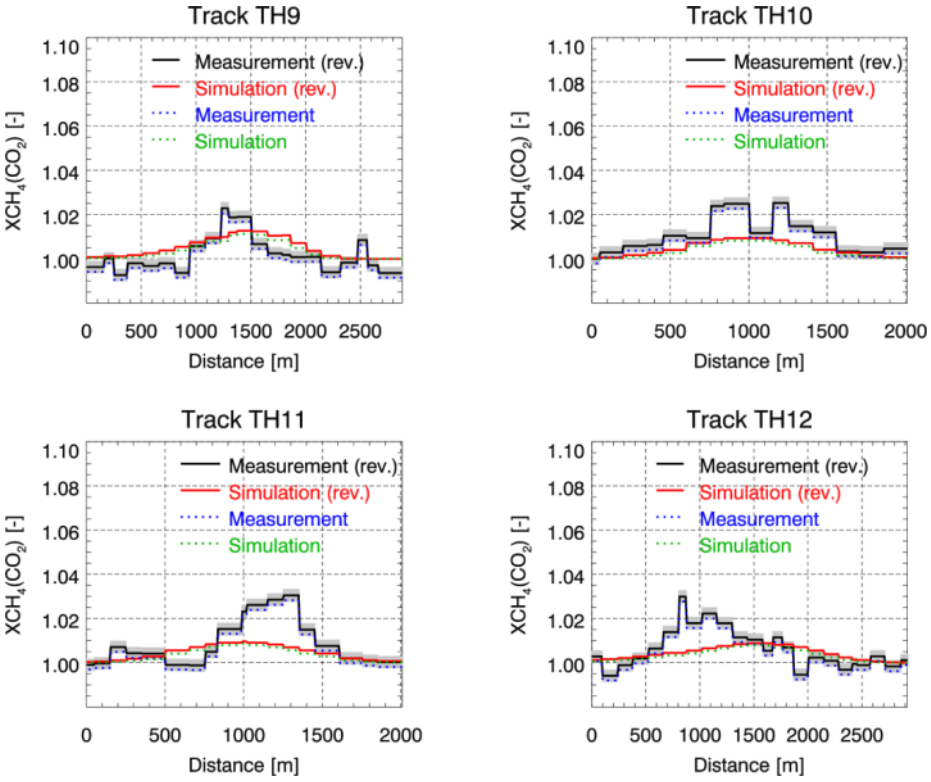

Figure 72 : Continuation of Figure 70.

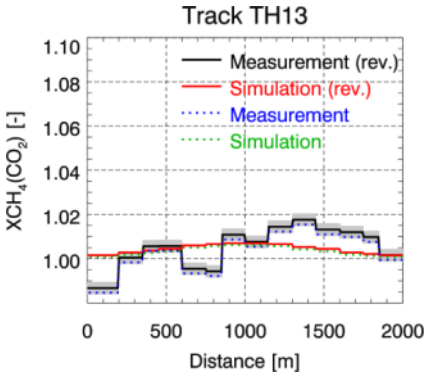

Figure 73 : Continuation of Figure 70.

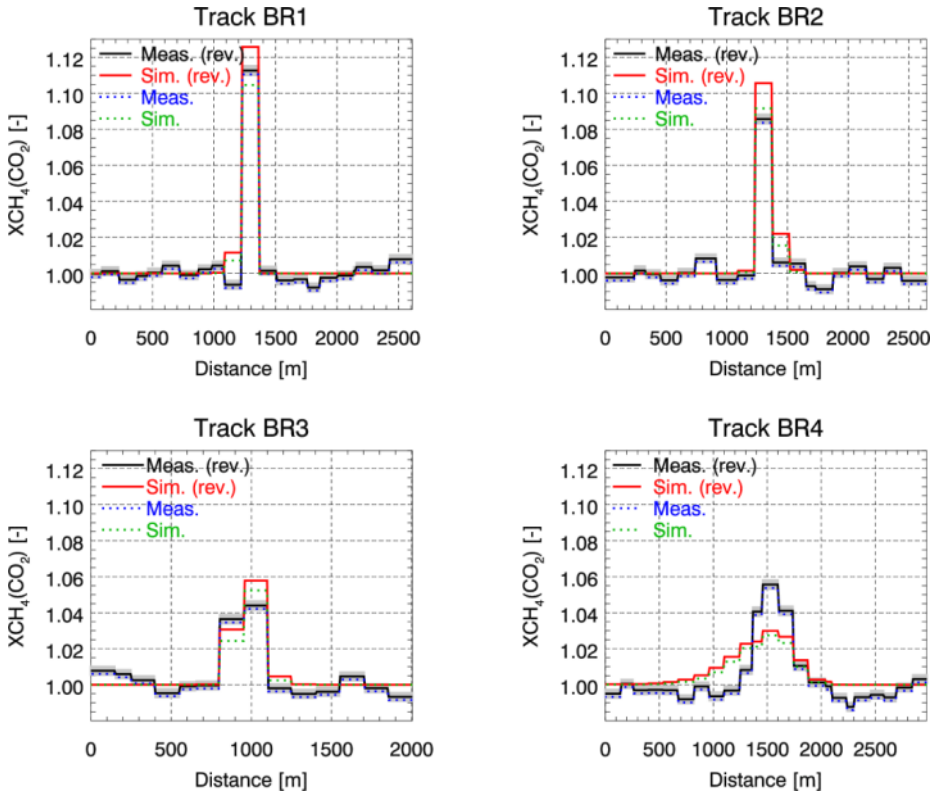

Figure 74 : Cross sections of remote sensing column averaged dry air mole fractions at Bockraden Shaft. Measurements with revised normalization are shown in black, while the result of the model based on the inverted emission rate using the plume model and sampled like the measurement is shown in red. Measurement and simulation based on the former nomalisation are shown in blue and green dotted lines respectively.

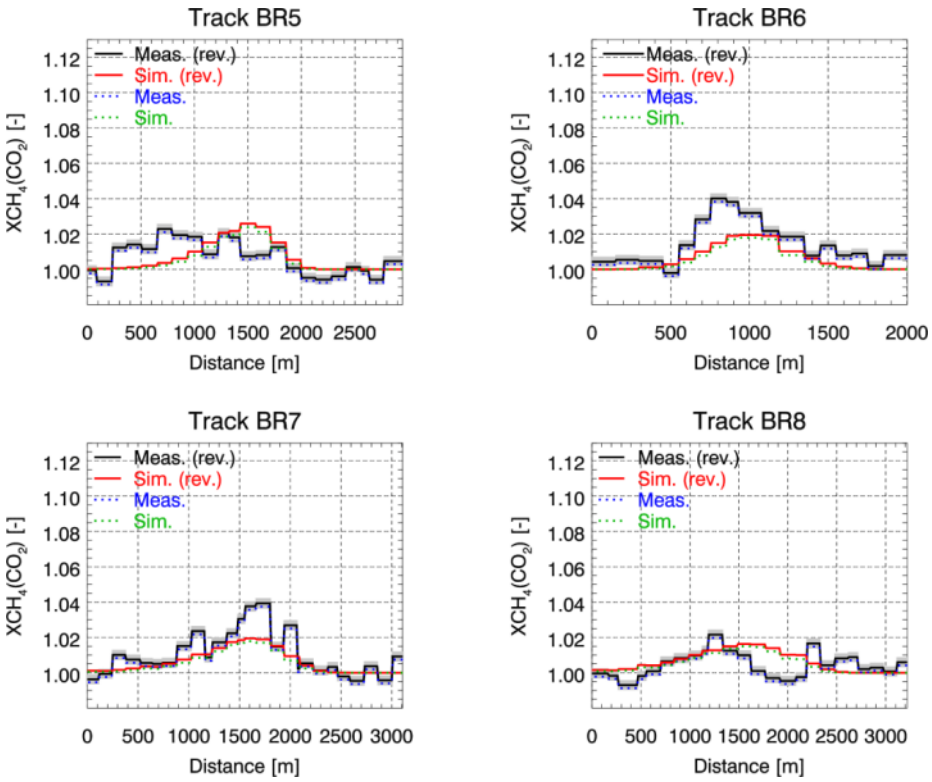

Figure 75 : Continuation of Figure 74.

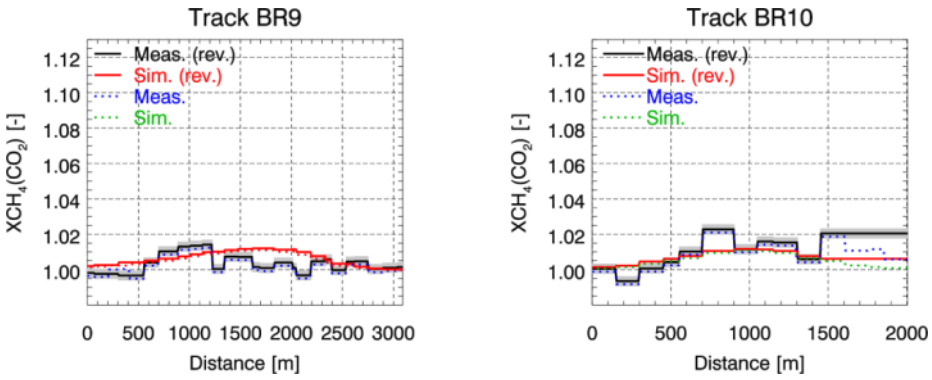

Figure 76 : Continuation of Figure 74. Note that track BR10 has not been taken into account for the mean of the integral method, because of rejected data at the end of the track (due to the applied inclination filter).

For this method to be consistent it should also be applied in case of Weisweiler power plant and the results compared with the reported emissions (see Table 14). Using the revised normalisation (Figure 77), the normalisation factor changes from about 1.024 to about 1.026 leading to decreased emission results of 15.08 $MtCO_2$/yr (integral) and 15.93 $MtCO_2$/yr(plume). This is about 9% lower than before.

In case of the power plant Weisweiler this modification increases the bias to about -27% but with the new result being closer to the in-situ inversion results by Metair which are still lower. The cross sections are shown in Figure 78 and Figure 79 exhibiting less noisy data that fit the simulated Gaussian plume well.

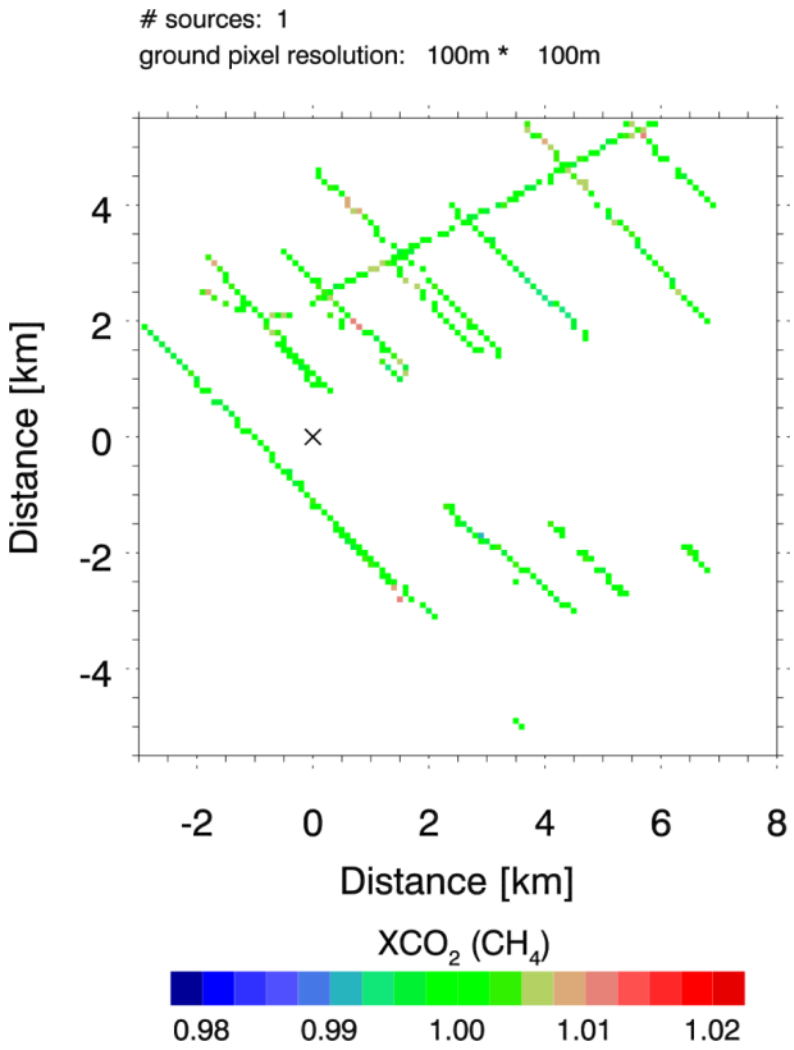

Figure 77 : Remote sensing data used for the revised normalization method for data at Weisweiler power plant. The methane plume area originating at the two ventilation shafts is excluded.

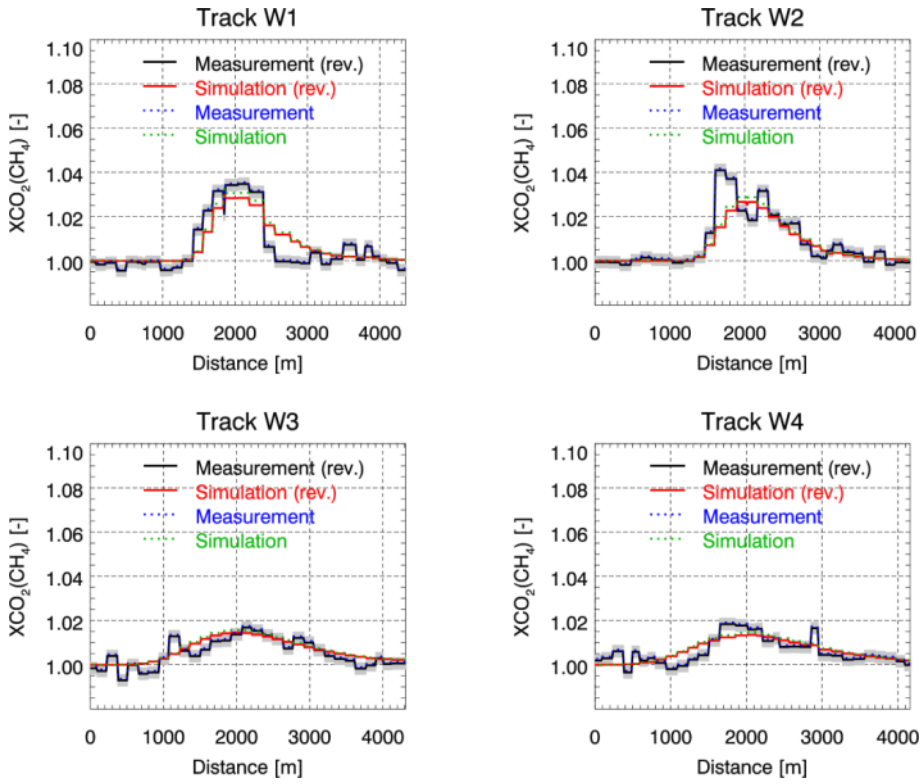

Figure 78 : Cross sections of remote sensing column averaged dry air mole fractions at Weisweiler power plant. Measurements with revised normalization are shown in black, while the result of the model based on the inverted emission rate using the plume model and sampled like the measurement is shown in red. Measurement and simulation based on the former nomalisation are shown in blue and green dotted lines respectively.

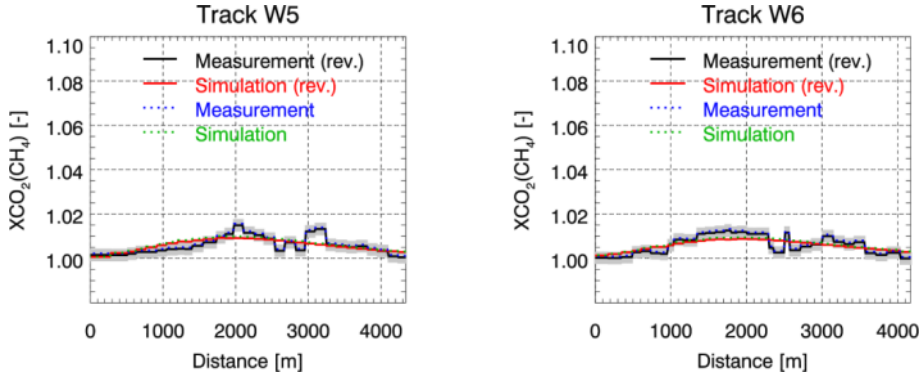

Figure 79 : Continuation of Figure 78.

Data basis	MAMAP and COSMO-DE (updated normalisation)				MAMAP, COSMO-DE and airborne in-situ wind information (updated normalisation)				In-situ (Metair)					Reported
Target	Gaussian plume	Integral	Wind speed	Approx. wind error (+)	Gaussian plume	Integral	Wind speed	Approx. wind error (+)	Near field inversion (*)	Far field inversion (*)	Wind speed		Approx. wind error (+)	
											Near field	Far field		
Weisweiler power plant	15.06 $MtCO_2/yr$ (2.8+/- %)	14.25 $MtCO_2/yr$	3.96 m/s	23%	15.93 $MtCO_2/yr$ (+/- 2.8%)	15.08 $MtCO_2/yr$	4.19 m/s	12%	13.76 $MtCO_2/yr$		4.91 m/s		10%	21.2 $MtCO_2/yr$
Ibbenbüren: Theodor Shaft	17.08 $ktCH_4/yr$ (+/- 4.9%)	20.50 $ktCH_4/yr$	5.85 m/s	15%	12.30 $ktCH_4/yr$ (+/- 4.9%)	14.76 $ktCH_4/yr$	4.21 m/s	12%	20.97 $ktCH_4/yr$	101.28 $ktCH_4/yr$	4.9 m/s	4.25 m/s	10/12%	16.4 $ktCH_4/yr$
Ibbenbüren: Bockraden Shaft	22.29 $ktCH_4/yr$ (+/- 4.9%)	21.27 $ktCH_4/yr$	5.49 m/s	16%	16.05 $ktCH_4/yr$ (4.9+/- %)	15.30 $ktCH_4/yr$	3.95 m/s	13%	22.74 $ktCH_4/yr$		4.38 m/s	3.42 m/s	11/14/%	18.2 $ktCH_4/yr$

Table 14: Preliminary comparison of inversion results for remote sensing and in-situ measurements. For the remote sensing data the background correction as described above was applied. The results for remote sensing are splitted according to the used meteorological data. Explanations: (+) Approximate wind error is computed from the errors of 0.9m/s for COSMO-DE and 0.5m/s for the in-situ wind data. For the in-situ inversion the wind speed is only an effective wind speed computed in the post-processing and is not used as such for the inversion. (*) "Near field" and "Far field" refers to the in-situ measurement tracks flown at different distances from the source. The far field inversion in case of Ibbenbüren in-situ data includes emissions from both shafts. For Weisweiler there is only one track for in-situ column data, therefore it is not distinguished between near and far field.

10. Evaluation of C-MAPExp data on the scales probed by CarbonSat

While the data analysis concept for MAMAP remote sensing data and CarbonSat measurements is in principle rather similar, the spatial scales differ by an order of magnitude. MAMAP observations have a ground scene size in the order of 100 m x 100 m depending on aircraft altitude, velocity and the used telescope. For CarbonSat ground scenes are considerably larger at about 2 km x 2 km. Furthermore, MAMAP data is more sparse than data from the imaging CarbonSat instrument.

Consequently, gridding sparse MAMAP data to CarbonSat resolution has limitations. To better assess what to expect from CarbonSat measurements for sources that have been surveyed during the C-MAPExp campaign two approaches were made. The first is the simple regridding of MAMAP data to CarbonSat measurement ground scene size. This of course yields no observations in grid boxes where there are no MAMAP measurements. In some cases this could potentially also lead to overestimation or underestimation of the vertical column if the available MAMAP data is not representative for the respective CarbonSat ground scene. The second approach uses a 2D interpolation method (Kriging) to fill the gaps in the MAMAP data. In cases where MAMAP data is too sparse this can lead to artifacts, in particular at the edges of the measurement patterns. To avoid too strong artifacts a filtering approach was chosen for data analysis similar as in Chapter 9.3. The additional filter is based on the inclination angle of the instrument. While for the previous analysis the data was mainly evaluated on the straight flight lines that cross the plume, for the 2D interpolation also the data at the edges of the pattern that are mostly formed by aircraft turns are important. Therefore data was only accepted for the analysis, if the inclination did not deviate more than 10° from the vertical.

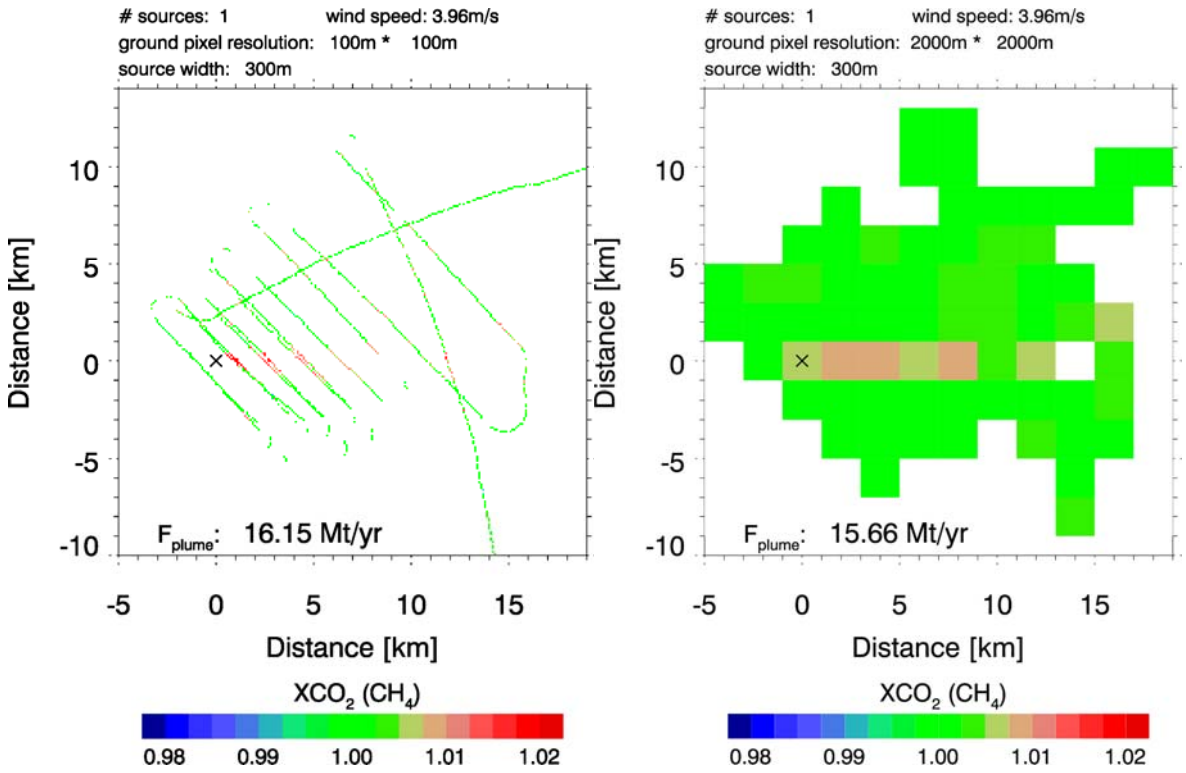

Figure 80: Left: MAMAP data gridded to 100 m x 100 m that has been used for the analysis. An inclination filter was applied that filtered most of the aircraft turning events. F_{plume} denotes the inversion result for CO_2 for the data shown. Right: Same data but gridded to 2 km x 2 km.

The resulting data for power plant Weisweiler is shown in Figure 80 (left). Applying the Gaussian plume inversion method, this results in an emission rate of 16.15 $MtCO_2$/yr. Note that this result is slightly different from the result in Chapter 9.3, due to the fact that a larger region was used as well as a different filtering. When gridding the data to a larger footprint of about 2 km x 2 km there are regions that are not covered by measurements (see Figure 80, right). However, the remaining pixels clearly visualize the plume extend downwind of the power plant location. The resulting emission rate using the 2 km x 2 km data is 15.66 $MtCO_2$/yr for the time of the overflight and – with respect to the errors involved – very close to the original result.

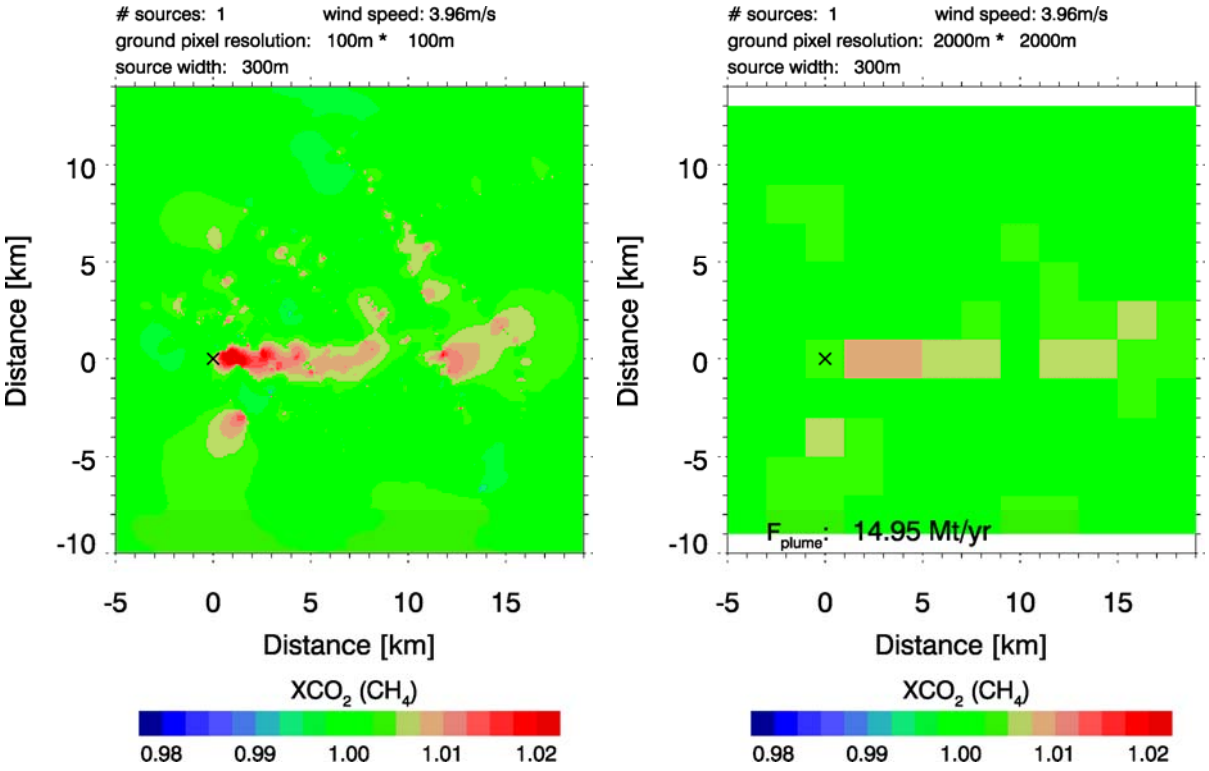

Figure 81: Left: 2D interpolation (Kriging) of MAMAP data shown in Figure 80 (left). Right: Interpolated data gridded to CarbonSat resolution. F_{plume} denotes the inversion result for CO_2 for the data shown.

Instead of directly gridding the MAMAP data to 2 km x 2 km CarbonSat resolution, the gaps in observations can be filled using a 2D interpolation approach. For this, the Kriging method (spherical weighting, range=15km, nugget=0) was used. The result is shown in Figure 81 (left). The plume structure is better visible than in the sparse MAMAP data but also few artifacts are present. As before, this data can now be gridded to CarbonSat resolution (see Figure 81, right). Inverting this data yields an emission rate estimate (14.95 $MtCO_2$/yr) that is very close to the inversion result at MAMAP resolution and to the inversion result for the simple regridding approach. This gives some confidence that the scaling was performed appropriately. For other, less adequate flight patterns the degree of agreement between the inversions could be significantly less. This approach does not consider the CarbonSat preicision. Instead the gridded MAMAP data will be slightly smoother than to be expected from measurements of a single overpass with CarbonSat.

11. Summary

During August 2012 the C-MAPExp campaign was performed to quantify “gradients” in atmospheric CO_2 and CH_4 from strong local greenhouse gas sources e.g. from coal-fired power plants, localized industrial complexes, landfills, etc. with the overall goal to demonstrate that CO_2 and CH_4 emissions from atmospheric gradient measurements can be derived. The campaign was performed in support of the mission definition of CarbonSat EE8 candidate.

Within a unique campaign set-up – to the knowledge of the authors it is the first ever set-up of this type - using one aircraft with the XCO_2 and XCH_4 remote sensing instrument MAMAP probing the partial column of the gases below the aircraft in combination with another aircraft equiqed with in-situ sensors for atmospheric CO_2 and CH_4 concentration as well as wind speed and direction probing the CO_2 and CH_4 plumes in the boundary layer, over 20 targets were successfully probed. This included the collection, processing and preliminary analysis of airborne remote sensing and airborne in-situ data from CH_4 and CO_2 emitting targets of different but mostly known emission strength.

During the eight observation days, the in-situ airplane (MetAir) documented 52 plumes, from which 18 were very clear, 28 detectable as well, but less pronounced or less densely flown, and 6 targets observed turned out not to emit detectable amounts of CO_2 or CH_4 during the time of observations.

The remote sensing airplane (Cessna FUB with MAMAP) documented during the same period 39 plumes, from which 16 were clear and of good quality for flux inversion, and 23 were not well suited for flux inversion either due to a plume at or below the detection limit or due to non-optimum meteorological conditions (partly cloudy, strong boundary layer disturbances etc.).

The flight conditions during campaign were very good. The data quality of the collected data set is generally high. The data set was processed and a data archive was delivered to ESA.

For two selected targets an end-to-end data analysis up to fluxes was performed. This was done individually for both the in-situ and the remote sensing data set alone, but also using in-situ meteorological data to better constrain the flux inversion from the remote sensing data. In addition to assess consistency w.r.t. atmospheric “gradients”, the in-situ data was “integrated” and analysed with the same approach as the remote sensing data. For both targets an independent emission rate estimate for validation was based on reported emissions and energy production data, respectively, and was then used to further assess the results for the different inversion techniques.

For the remote sensing data set it was identified that – beside other error sources already known and controlled - the background correction can result in significant biases and a new background correction scheme was successfully developed and applied.

From the preliminary data analysis it can be concluded that the campaign data set is of high data quality. It allows from both in-situ and remote sensing data to derive emissions of point sources as documented for two examples and results on emissions compare well within error bars (approx. 20-30%) with reported emissions. Re-gridding/interpolating the C-MAPExp data to the CarbonSat spatial scale and sucsessive plume inversion established the linkage between the scales and demonstrates the value of CarbonSat data to constrain point source emissions.

Campaign results were already highlighted in an ESA web-story:

http://www.esa.int/Our_Activities/Observing_the_Earth/The_Living_Planet_Programme/Campaigns/Pinpointing_sources_of_greenhouse_gases

12.Recommendations and Lessons Learned

12.1. Future analysis of the campaign data set

As the main focus of this campaign project was the collection of a unique CO_2 and CH_4 in-situ and remote sensing data set around strong point sources, the analysis of the data set could only be done in some depth for the combined data set for two sources.

There is therefore the obvious need to perform a full data analysis & interpretation of the whole data set. This should focus on the point sources, but could also include analysis of MAMAP data from longer transfer flights to characterise larger scale gradients and compare them with gradients from mesoscale modelling.

Future activities should include for the point sources:

- Refinement of in-situ data pre-processing
    - (i) individual optimisation of wind, (ii) more accurate calibrations for the concentrations using the few flask-samples available, and (iii) a more thorough inspection of the whole data set. This would improve the accuracy and the precision above the basic specifications.
- Refinement of the in-situ post-processing to fluxes, especially w.r.t. better take into account the boundary layer structure and improved background corrections.
- Calculate emissions from additional sources and for additional constitutents (like CO, NOx, and water vapour) could be included as well.
- Refinement of remote sensing flux inversion w.r.t. background correction
- Refinement of the computation of an average wind speed, in particular for cases where modelled and measured wind profiles significantly differ
- Extension of remote sensing flux inversion to all “good” targets, with the goal to investigate consistency of methodology under different conditions.
- Common analysis using both in-situ and remote sensing data for all “good” targets, incl. Gaussian plume fit to the in-situ measurements (initial results see chapter 9).
- Compare in-situ and remote sensing data to LES simulations to gain more detailed insight into plume mixing and entrainment processes.
- Comparison of inversion results for the “good” targets to the independent data of reported respectively computed emissions based on provided data from federal governments and companies.

Future activities should include for larger scale gradients:

- Generate high quality concentration transects for transfer flight from remote sensing data. This also has to include refinement of MAMAP Level 2 data analysis w.r.t. the usage of the O2-A band to characterise scattering effects.
- Compare measured concentration gradient with concentration gradient from mesoscale models to judge on the variability in CO_2 and CH_4.

12.2. Lessons learned

The team operated an ideal combination of methods very efficiently, and preliminary results presented in this report are better than expected, and a future campaign could build upon these experiences.

The separation of remote sensing sensors on one aircraft flying above the boundary layer and in-situ sensors on another aircraft probing curtains in the boundary layer, is a set-up which can be recommended for any future campaign focussing on collecting data for flux inversion (GHG and GRG).

However, to better compare in-situ and remote sensing columns and also flux estimates the sensors should measure at the same time and location. While the in-situ sensor completes measuring the "curtain", the remote sensing instrument should measure above this curtain several times. This will provide optimal conditions to ensure that both instruments are probing the same plume and better assess differences in the individual measurement techniques. Another advantage of the co-location in time and space will be the improved applicability of the obtained in-situ wind information.

Of course, if the main goal is only to obtain accurate emission estimates for a source that is known to be constant in time, then the observations could be decoupled. While the remote sensing measurements are restricted to cloud free conditions, this does not interfere with in-situ measurements. Then, each system could be active when the conditions for the method are ideal.

This would allow to further increase the number of optimum measurements for each method for temporal constant sources.

One area of uncertainty introduced in the in-situ flux inversion is the lack of knowledge of the concentrations below the lowest flight track, which was a problem for high stack emissions. For future campaigns it is recommended to mitigate by establishing ground based in-situ measurements (ideally a mobile tower). For smaller plumes, the use of a mid-size RPAS like ZHAW-UMARS[1] might be possible.

The inversion of the remote sensing data suffers most from unknown wind profiles. The fine structure of the wind profile also from very advanced and highly resolved models such as COSMO-DE are known to significantly differ from actual winds at local scales. However it still needs to be investigated more closely, how modelled and in-situ data can be combined most effectively to give a better estimate for the average wind speed for the purposes outlined in this study.

In principle, however, LIDARs would be very interesting for a "real" wind model calibration and quality assessment study. This might be even of advantage for future analysis of CarbonSat data.

[1] http://www.imes.zhaw.ch/en/engineering/institutes-centres/imes/projekte/leichtbautechnik/umars/project-status.html

13. Acknowledgements

The official reference values for methane emission rates from Ibbenbüren coal mine for the time of the overflight were kindly provided by the Bezirksregierung Arnsberg, Abteilung Bergbau und Energie in NRW.

The reference values for CO_2 emission rates of the power plants were derived from power generation values of each power plant location kindly provided by RWE AG, Essen, Germany.

The tremendous job performed by the pilots of METAIR and FUB is greatly acknowledged.

14.References

Beringer et al., 2011 Savanna patterns of energy and carbon integrated across the landscape, Bulletin of the Americsn Meteorological Society, 1467-1485, Nov. 2011.

Bovensmann, H., Buchwitz, M., Burrows, J. P., Reuter, M., Krings, T., Gerilowski, K., Schneising, O., Heymann, J., Tretner, A., and Erzinger, J.: A remote sensing technique for global monitoring of power plant CO2 emissions from space and related applications, Atmos. Meas. Tech., 3, 781-811, 2010.

Doms, G.: A Description of the Nonhydrostatic Regional COSMO-Model, Deutscher Wetterdienst, Technical Report (http://www.cosmo-model.org/), last access: October 2012, 2011.

EnergieAgentur.NRW: Grubengas. Ein Energieträger in Nordrhein-Westfalen, Ministerium für Wirtschaft, Mittelstand und Energie des Landes Nordrhein-Westfalen, 36 pp., 2009.

Foken et al. , Results of a panel discussion about the energy balance closure correction for trace gases, BAMS, ES13-ES18, 2009.

Gerilowski, K., A. Tretner, T. Krings, M. Buchwitz, P. P. Bertagnolio, F. Belemezov, J. Erzinger, J. P. Burrows, and H. Bovensmann, MAMAP – a new spectrometer system for column-averaged methane and carbon dioxide observations from aircraft: instrument description and performance analysis, Atmos. Meas. Tech., 4, 215-243, 2011.

Rebecca V. Hiller, Bruno Neininger, Dominik Brunner, Christoph Gerbig, Daniel Bretscher, Thomas Künzle, Nina Buchmann, Werner Eugster (2014): Aircraft based CH4 flux estimates for validation of emissions from an agriculturally dominated area in Switzerland. Journal of Geophysical Research: Atmospheres 03/2014; DOI:10.1002/2013JD020918.

Krings, T., Gerilowski, K., Buchwitz, M., Reuter, M., Tretner, A., Erzinger, J., Heinze, D., Pflüger, U., Burrows, J. P., and Bovensmann, H.: MAMAP – A new spectrometer system for column-averaged methane and carbon dioxide observations from aircraft: retrieval algorithm and first inversions for point source emission rates, Atmos. Meas. Tech., 4, 1735–1758, doi:10.5194/amt-4-1735-2011, 2011.

Krings, T., Gerilowski, K., Buchwitz, M., Hartmann, J., Sachs, T., Erzinger, J., Burrows, J. P., and Bovensmann, H.: Quantification of methane emission rates from coal mine ventilation shafts using airborne remote sensing data, Atmos. Meas. Tech., 6, 151-166, doi:10.5194/amt-6-151-2013, 2013.

Reuter, M., Buchwitz, M., Schneising, O., Hase, F., Heymann, J., Guerlet, S., Cogan, A. J., Bovensmann, H., and Burrows, J. P.: A simple empirical model estimating atmospheric CO_2 background concentrations, Atmos. Meas. Tech., 5, 1349-1357, doi:10.5194/amt-5-1349-2012, 2012.

U.S. Committee on Extension to the Standard Atmosphere: U.S. Standard Atmosphere, 1976, National Oceanic and Atmospheric Administration, National Aeronautics and Space Administration, United States Air Force, Washington D.C., 241 pp., 1976.

Krings, T., Gerilowski, K., Buchwitz, M., Reuter, M., Tretner, A., Erzinger, J., Heinze, D., Pflüger, U., Burrows, J. P., and Bovensmann, H.: MAMAP – a new spectrometer system for column-averaged methane and carbon dioxide observations from aircraft: retrieval algorithm and first inversions for point source emission rates, Atmos. Meas. Tech., 4, 1735-1758, doi:10.5194/amt-4-1735-2011, 2011.

15. Acronyms and abbreviations

Acronym	Meaning
AOD	Aerosol Optical Depth
BESD	Bremen optimal EStimation DOAS
CarbonSat	Carbon Monitoring Satellite
DOAS	Differential Optical Absorption Spectroscopy
DWD	Deutscher Wetterdienst
ENVISAT	Environmental Satellite
FLEX	Fluorescence Explorer
GHG	Greenhouse Gas
GRG	Global Reactive Gases
GOSAT	Greenhouse Gases Observing Satellite
IUP-UB	Institute of Environmental Physics (Institut für Umweltphysik), University of Bremen, Germany
MAMAP	Methane Airborne MAPper
MRD	Mission Requirements Document
RMSE	Root Mean Square Error
SCIAMACHY	Scanning Imaging Absorption Spectrometers for Atmospheric Chartography
SNR	Signal to Noise Ratio
TOA	Top of atmosphere

Annex 1: Overview of targets

Annex 2: C-MAPExp Flight Documentation (day-by-day), incl. Photographic Material

Annex 3: Content of the in-situ result files (METAIR)

C-MAPExp
Final Report
Annex 1-3

ESA Study

"Scientific and Technical Assistance for the Deployment of a flexible airborne spectrometer system during C-MAPExp"

ESTEC Contract No. 4000106993/12/NL/FF/lf

Lead author:

Heinrich.Bovensmann@iup.physik.uni-bremen.de

Institute of Environmental Physics (IUP) / Institute of Remote Sensing (IFE), University of Bremen (UB), Bremen, Germany

Co-Author:

T. Krings, K. Gerilowski, Institute of Environmental Physics (IUP), University of Bremen (UB), Bremen, Germany

Bruno Neininger, METAIR AG, Switzerland

Thomas Ruhtz, Carsten Lindemann, Free University of Berlin, Germany

Change log

Version	Date	Status	Authors	Reason for change
Draft 0.3	20.1.2014	To Team	H. Bovensmann	Initial internal version
Draft 0.9	02.5.2014	To Team	T. Krings, B. Neininger, H. Bovensmann	Internal full draft final for final internal revision
Final 1.0	4.5.2014	To ESA	See cover	Delivery to ESA

Table of Contents

Annex 1: Overview of targets

As the focus of the campaign is on strong point source targets, a number of targets were pre-selected according to the source strength, source type (CO_2, CH_4) and the expected knowledge about the source strength.

As the methodology of determining emission source strength of CO_2 and CH_4 using remote sensing data is quite new, highest priority will be given to those targets with well known and high emissions. For CO_2, these are typically coal fired power plants with emissions larger than 10 $MtCO_2$ per year, and for CH_4, these are typically ventilation shafts of active coal mining areas with emission larger then 5-10 kt CH_4/year. These targets will be used to establish and demonstrate the methodology to derive source strength using RS in comparison to in-situ sensors.

Medium priority targets are those where the expected emission might be high but with larger uncertainty on emission information, or well known emitters with emissions near the detection limit of the RS sensor (see below). These are, for example, landfills for CH_4 and steel production facilities and smaller power plants for CO_2.

Low priority targets are those whose emission strengths are not well-known but with expected emissions near the detection limit of the RS sensor (see below).

The data about the reported emissions as documented in European Pollutant Release and Transfer Register (E-PRTR) for 2010 were used to categorise the targets w.r.t. their source strength.

Beside the point source targets there is one city target (Cologne) and the TCCON station at IUP Bremen.

The tables below summarize the preselected targets, with their respective emission strength, position and priority according to the above mentioned criteria.

	CO_2 Emitters	Emissions in E-PRTR 2010	Coordinates		Distance to Airfield	Priority
Target #		Mt/year	E [°]	N [°]	[km]	
T1.1	RWE Kraftwerk Niederaussem	28	6,66882	50,99213	70.7	High
T1.2	RWE Kraftwerk Goldenberg	*26*	6,84098	50,85720	84.4	High
T1.3	RWE Kraftwerk Eschweiler/Weisweiler	20	6,32385	50,83895	94.2	High
T1.4	RWE Kraftwerk Neurath	17	6,61523	51,03771	66.5	High
T1.5	RWE Kraftwerk Frimmersdorf	14,4	6,57578	51,05481	65.5	High
T1.6	Salzgitter Flachstahl GmbH	7,5	10,40308	52,15475	251.1	Medium
T1.7	EON Kraftwerk Scholven	9,4	7,00947	51,60275	10.4	High
T1.8	Kraftwerk Voerde OHG	6,2	6,68192	51,57850	13.1	Medium
T1.9	ThyssenKrupp Steel AG Werk Schwelgern	5,5	6,73591	51,50369	15.2	Medium
T1.10	ThyssenKrupp AG Werk Hamborn	3,8	6,72648	51,49125	16.7	Medium

Table 1: C-MAPExp CO_2 targets.

	CH_4 Emitter	Emissions in E-PRTR 2010	Coordinates		Distance to Airfield	Priority
		[kt/year]	E [°]	N [°]	[km]	
	Coal Mining					
T2.1	RAG Anthrazit Ibbenbüren	37,4	7,74155	52,28712	96.1	High
	Bockradener Schacht		7,72320	52,30757	97.1	
	Theodorschacht		7,77287	52,27859	96.8	
T2.2	RAG Bergwerk Prosper-Haniel	24	6,97500	51,51600	13.6	High
	Schacht Hünxe		6,78248	51,62828	5.6	
	Schacht Prosper - 9		6,90598	51,56699	6.3	
	Haniel Schacht 1		6,88067	51,54383	8.1	
	Förderberg		6,95861	51,52061	12.6	
T2.3	RAG Bergwerk West	23	6,54694	51,49276	25.7	High
	Rossenray / Schacht 1		6,55859	51,51774	23.6	
	Friedrich Heinrich - 4		6,47228	51,51745	29.1	
T2.4	RAG Bergwerk Auguste Victoria	2	7,11087	51,68864	19.1	Low
	Schacht AV 7		7,11051	51,68520	18.9	
	Schacht AV 8		7,09591	51,74732	21.9	
	Landfill					
T2.5	AVG Zentraldeponie Vereinigte Ville	5	6,83080	50,84081	86.2	High
T2.6	Deponie Watenbüttel BS	2,6	10,43179	52,31655	257.4	Medium
T2.7	ABZ Hannover/Lahe	4,4	9,85792	52,41068	223.9	Medium
T2.8	Deponie Schöneicher Plan	*4,9*	13,52829	52,23947	463.6	Medium

Table 2: C-MAPExp CH_4 targets part 1.

	CH_4 Emitter	Emissions in E-PRTR 2010	Coordinates		Distance to Airfield	Priority
		[kt/year]	E [°]	N [°]	[km]	
	Refineries (Oil & Gas)					
	Oil Refineries					
T2.9a	Ruhr Öl Gelsenkirchen (Werk Scholven)	????	7,02309	51,60000	11.4	Medium
T2.9b	Ruhr Öl Gelsenkirchen (Werk Horst)		7.04556	51,53827	15,5	Medium
T2.10	Rheinland Raffinerie Nord, Godorf	????	6,97685	50,85499	85.0	Medium
T2.11	Rheinland Raffinerie Süd, Wesseling	????	7,00576	50,81411	89.7	Medium
	Gas Refineries					
T2.12	EXXON Grossenkneten	????	8,22800	52,95500	175.8	Medium
T2.13	EXXON NEAG	????	8,88700	52,62300	178.3	Medium
	Gas Production					
T2.14	EXXON Voigtei	????	8,95100	52,60100	180.3	Low
	Gas Storage					
T2.15	EXXON Dötlingen	????	8,35497	52,94444	179.5	Low
T2.16	WINGAS Rehden	????	8,49300	52,61500	157.6	Low
	Oil Production					
T2.17	EXXON Rühlermoor	????	7,19600	52,66700	119.2	Low

Table 3: C-MAPExp CH_4 targets part 2.

	Other targets	**Coordinates**		**Distance to Airfield**	**Priority**	Comment
		E [°]	N [°]	[km]		
T3.1	Flugplatz Dinslaken Schwarze Heide	6,859	51,616	0		Baseline Airfield
T3.2	Forschungszentrum Jülich	6,4083	50,90758	86	Medium	HyFLEX
T3.3	TCCON Bremen	8,84965	53,10365	214	Low	Total column validation target, MAMAP only
T3.4	Cologne	6,96285	50,9395	76 30 km flight diamter	Medium-Low	City Target, only when easterly winds, otherwise contamination from T1.1-T1.5

Table 4: C-MAPExp other targets.

Annex 2: C-MAPExp Flight Documentation (day-by-day), incl. Photographic Material

Overview

Date	Day of Week	Activity	Comment
10.8.2012	Fri	Integration MAMAP into Cessna	
11.8.2012	Sat	1st Test Flight Berlin	Minor issues with O2 band channel, fixed on-site
12.8.2012	So	2nd Test Flight MAMAP Berlin and Transfer to Dinslaken, Arrival METAIR at Dinslaken	
13.8.2012	Mo	Aircrafts ready at Dinslaken, Test flight T1.7, T2.2, T2.4, 2.9	**Start Data Acquisition Phase**
14.8.2012	Tue	T2.3, 2.4, DIMO pre-screening T2.11-2.15	
15.8.2012	Wed	Targets: 1.1, 1.4, 1.5, 1.7, 2.2, 2.9	
16.8.2012	Thu	Targets: 1.1, 1.4, 1.5, 2.3	
17.8.2012	Fri	Targets: 1.1, 1.2, 1.4, 1.5, 2.2, 2.3, 2.5	
18.8.2012	Sat	Targets: 1.1 - 1.5, 2.2, 2.5, 2.10	
19.8.2012	Sun	Targets: 2.1, 2.2	
20.8.2012	Mo	No Flights	
21.8.2012	Tue	No Flights	
22.8.2012	Wed	No Flights	
23.8.2012	Thu	T1.4, FLEX Selhausen/Altendorf	
24.8.2012	Fri	End of Acquisition Phase, dis-integration	
25.8.2012	Sat		

Table 5: Campaign schedule as executed. Details of the targets flown by METAIR-DIMO and MAMAP/Cessna.

Flight Day 12.08.2012

MAMAP

Target(s): Schöneiche (LF)

Flight ID : 2012_08_12_1

Start of Measurement: 07:57 UTC

End of Measurement: 08:34 UTC

Spectrometer Temperature: 28°C

Weather Conditions: clear sky, calm wind from East, ca. 3 n/sec., BL ca. 500 m (estimated visually).

Figure 1: Clear Sky over Schöneiche.

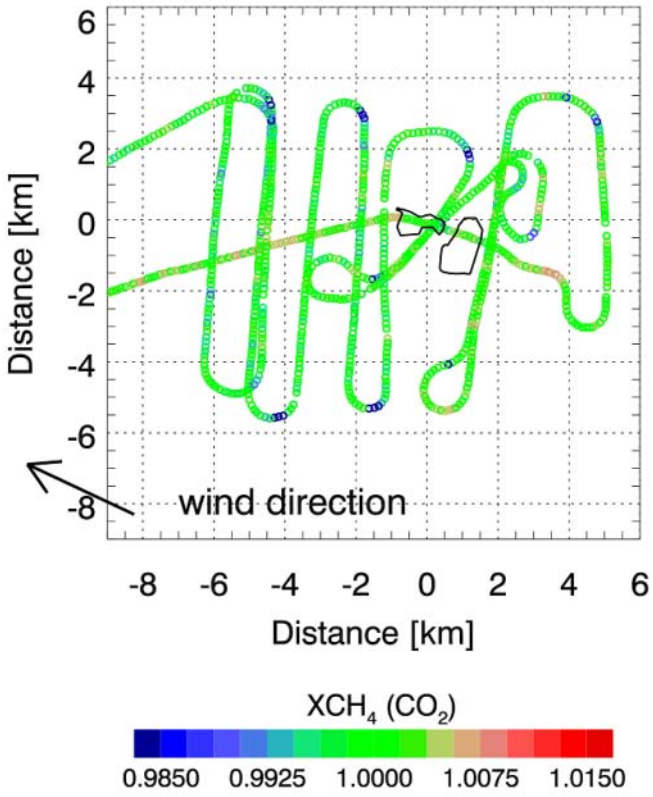

Figure 2: MAMAP flight pattern and quick-look analysis Schöneiche 12.8.2012

Flight Day 13.08.2012

MAMAP

Target(s): Prosper-Haniel (CM), Auguste-Victoria (CM), Ruhr Oil Gelsenkirchen (RF)

Flight ID : 2012_08_13_1

Start of Measurement: 08:57 UTC (Prosper-Haniel)

End of Measurement: 10:00 UTC (Prosper-Haniel)

Start of Measurement: 10:00 UTC (Ruhr Oil Gelsenkirchen)

End of Measurement: 10:13 UTC (Ruhr Oil Gelsenkirchen)

Start of Measurement: 10:13 UTC (Auguste-Victoria)

End of Measurement: 10:40 UTC (Auguste-Victoria)

Spectrometer Temperature: 28°C

Weather Conditions: slight to medium/strong Cirrus, wind from SW, ca. 4m/sec, BL ca. 600 m (estimated visually).

Figure 3: Cloud situation over Prosper-Haniel and Auguste-Victoria, 13.8.2012.

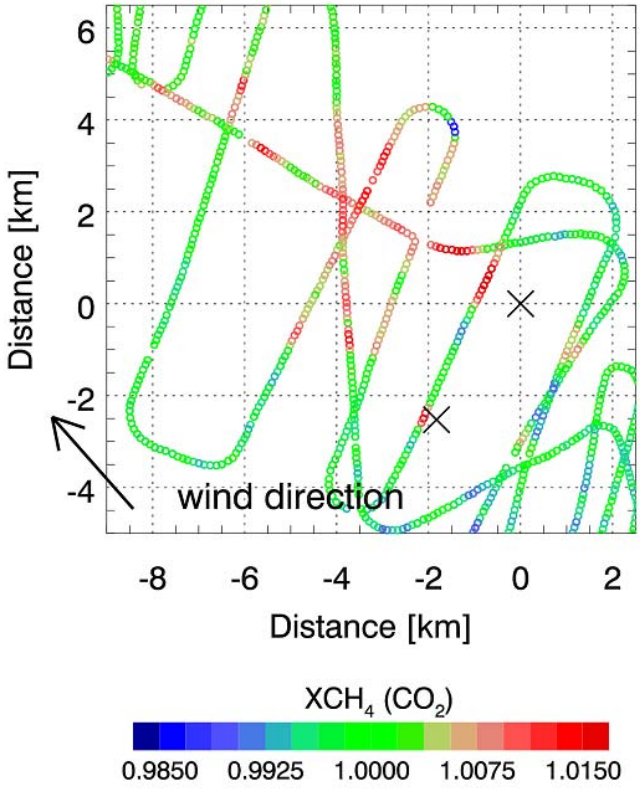

Figure 4: MAMAP flight pattern and quick-look analysis Prosper-Haniel (Prosper-9 and Schacht-1 exhaust shafts) 13.8.2012.

METAIR

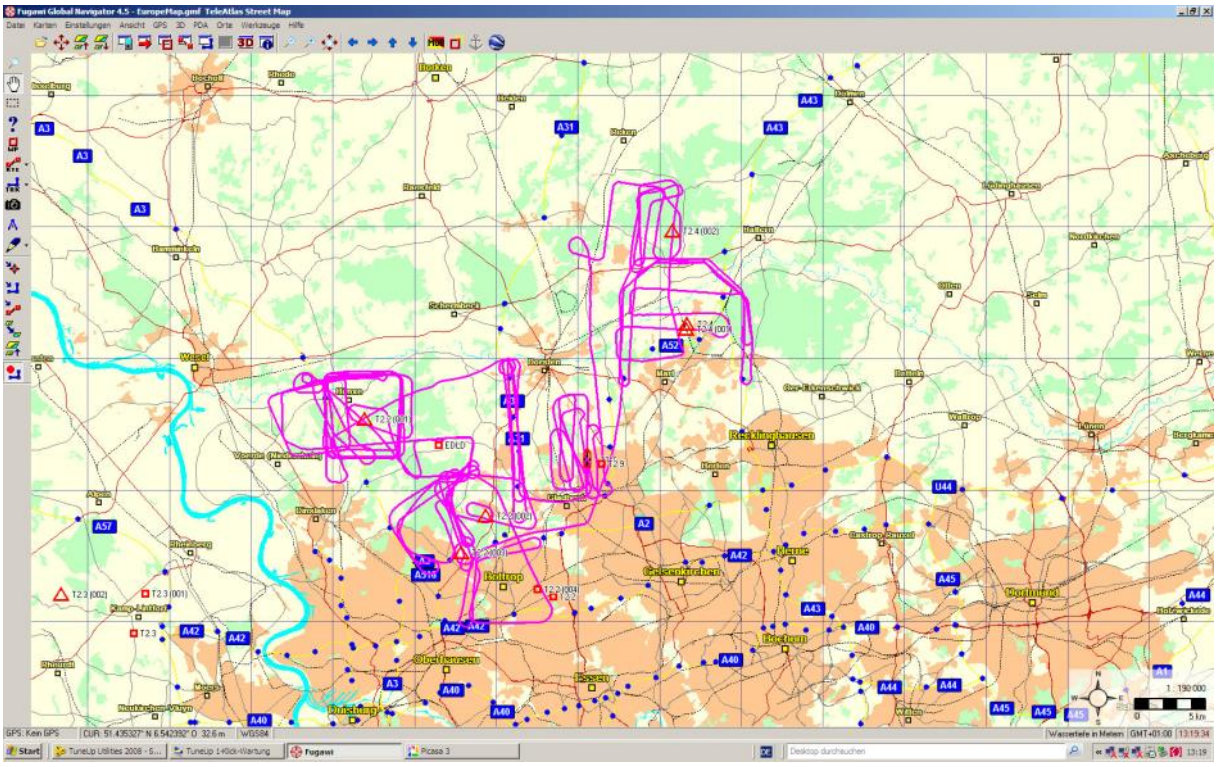

Flight Day 14.08.2012

MAMAP

Target(s): Niederaussem (PG), Neurath (PG), Fimmersdorf (PG), Bergwerk-West (CM)

Flight ID : 2012_08_14_1

Start of Measurement: 08:45 UTC (Bergwerk-West)

End of Measurement: 09:32 UTC (Bergwerk-West)

Spectrometer Temperature: 32°C

Weather Conditions: flight over Niederaussem, Neurath, Fimmersdorf aborted due to strong clouds. Medium to stronger Cirrus over BW-West (Cirrus stronger in comparison to 13.8.2012), wind from SSW, no additional measurements over CM Prosper Haniel due to strong Cirrus.

Figure 5: Cloud situation over CM BW-West at the beginning of the flight. Cloud situation during the later measurements over the Power-Plants comparable as shown on the pictures for the beginning of the flight.

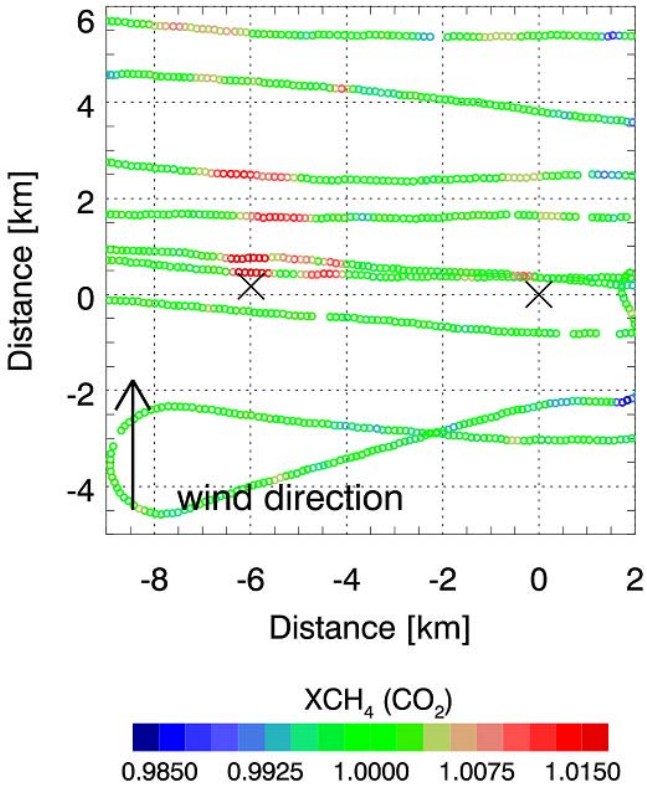

Figure 6: MAMAP flight pattern and quick-look analysis Bergwerk-West (CM) (Friedrich-Heinrich-4 and Rossenray exhaust shafts) 14.8.2012.

METAIR

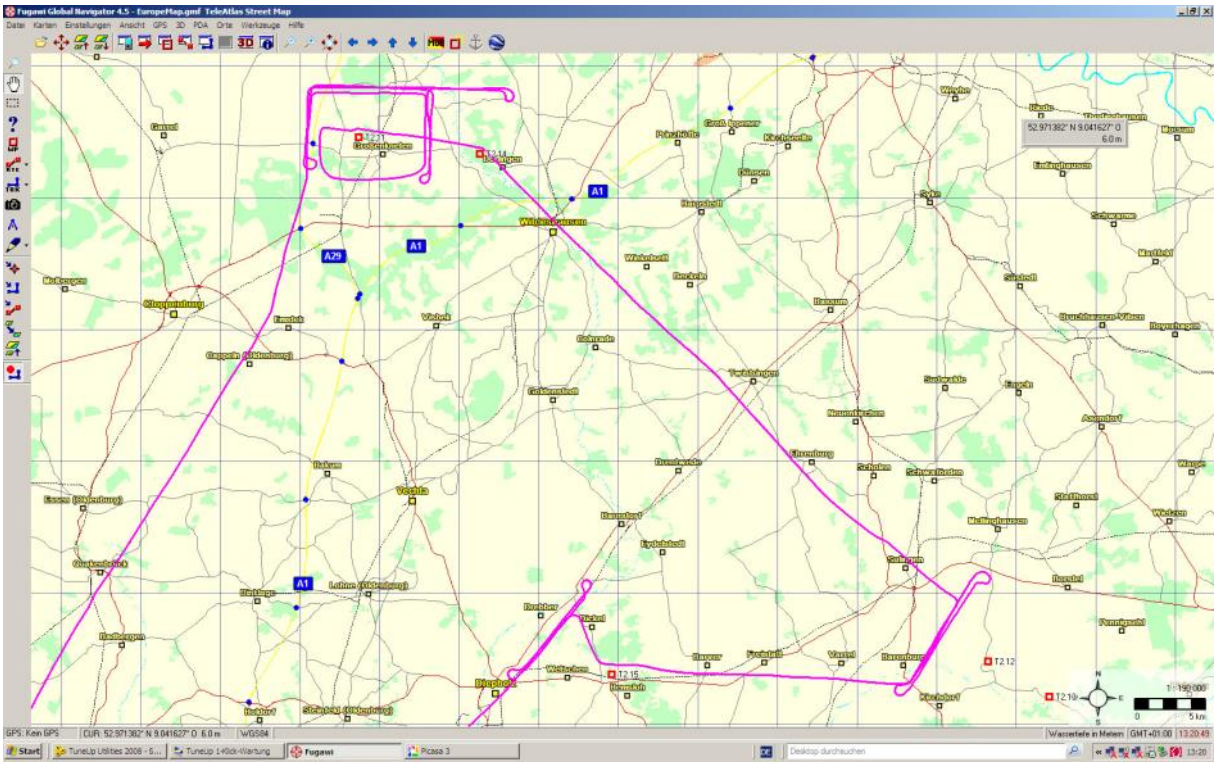

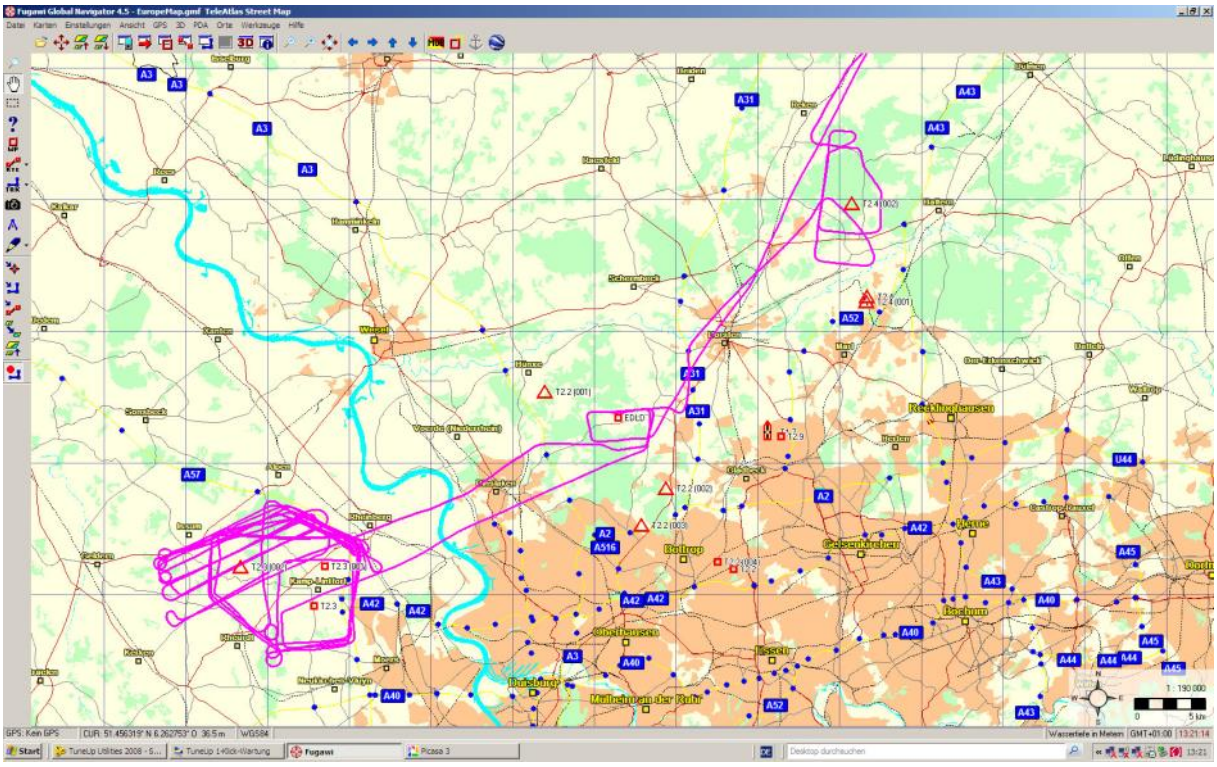

Flight Day 15.08.2012

MAMAP

Target(s): Scholven (PG), Niederaussem (PG), Neurath (PG), Fimmersdorf (PG), Prosper-Haniel (CM)

Flight ID : 2012_08_15_1

Start of Measurement: 10:53 UTC (Prosper-Haniel, Scholven, Ruhr-Oil Gelsenkirchen)

End of Measurement: 11:40 UTC (Prosper-Haniel, Scholven, Ruhr-Oil Gelsenkirchen)

Start of Measurement: 11:53 UTC (Niederaussem, Neurath, Fimmersdorf)

End of Measurement: 13:41 UTC (Niederaussem, Neurath, Fimmersdorf)

Start of Measurement: 13:50 UTC (Prosper-Haniel, Scholven, Ruhr-Oil Gelsenkirchen)

End of Measurement: 14:23 UTC (Prosper-Haniel, Scholven, Ruhr-Oil Gelsenkirchen)

Spectrometer Temperature: 32°C

Weather description: in the area of Scholven stronger Cirrus, no consecutive measurements over shaft Hünxe und Förderberg due to clouds, wind from SW, ca. 6-7 m/sec. At Neurath, Fimmersdorf, Niederaussem area slight broken cirrus at the center of the flight legs (less as compared to Scholven area) and stronger Cirrus at the beginning and end of the flight legs. During the flight, Cumulus developement in direction from East to West. Last legs flown between the Cirrus trying to avoid measurements in the cloud shadows. BL ca. 1200 m (visually estimated). In BW-West area stronger Cirrus.

Figure 7: Cloud situation Scholven area.

Figure 8: left: Neurath, Fimmersdorf, Niederaussem. right: cloud free situation at the centers of the flight legs.

Figure 9: Cloud situation at both ends of the flight tracks/legs.

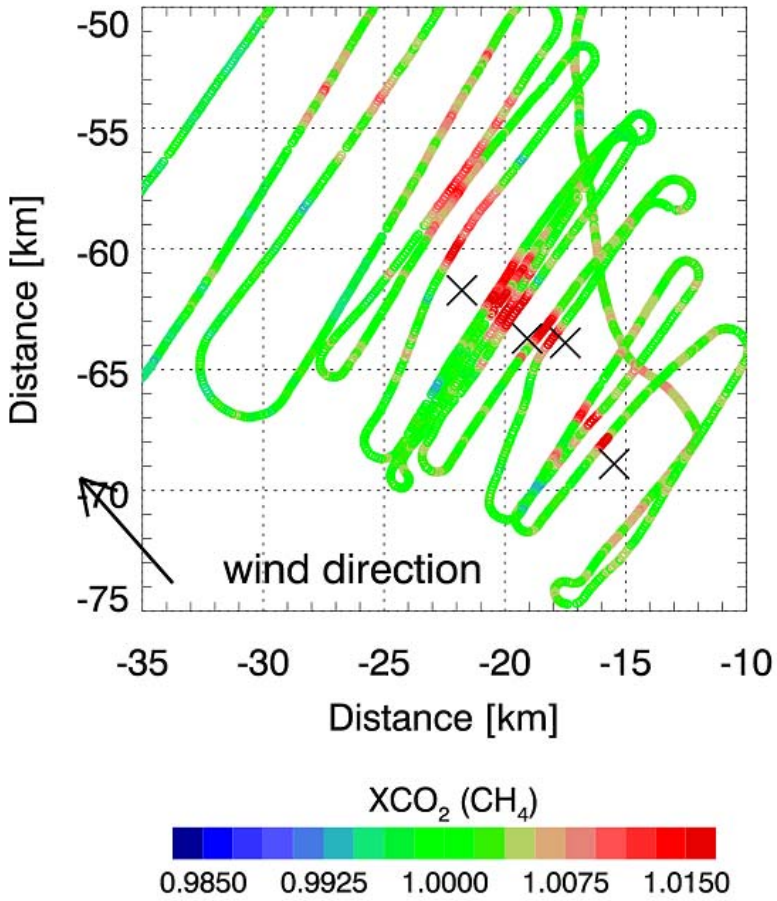

Figure 10: MAMAP flight pattern and quick-look analysis power plants Niederaussem, Neurath and Fimmersdorf 15.8.2012.

METAIR

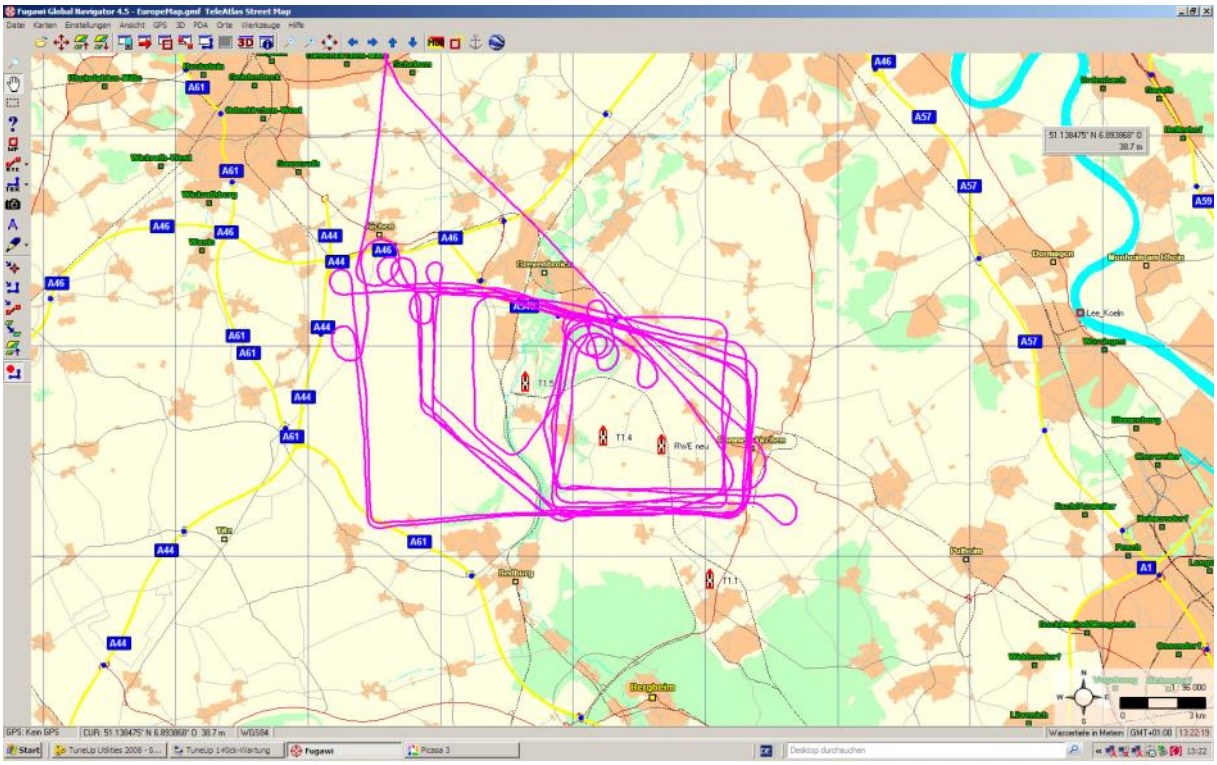

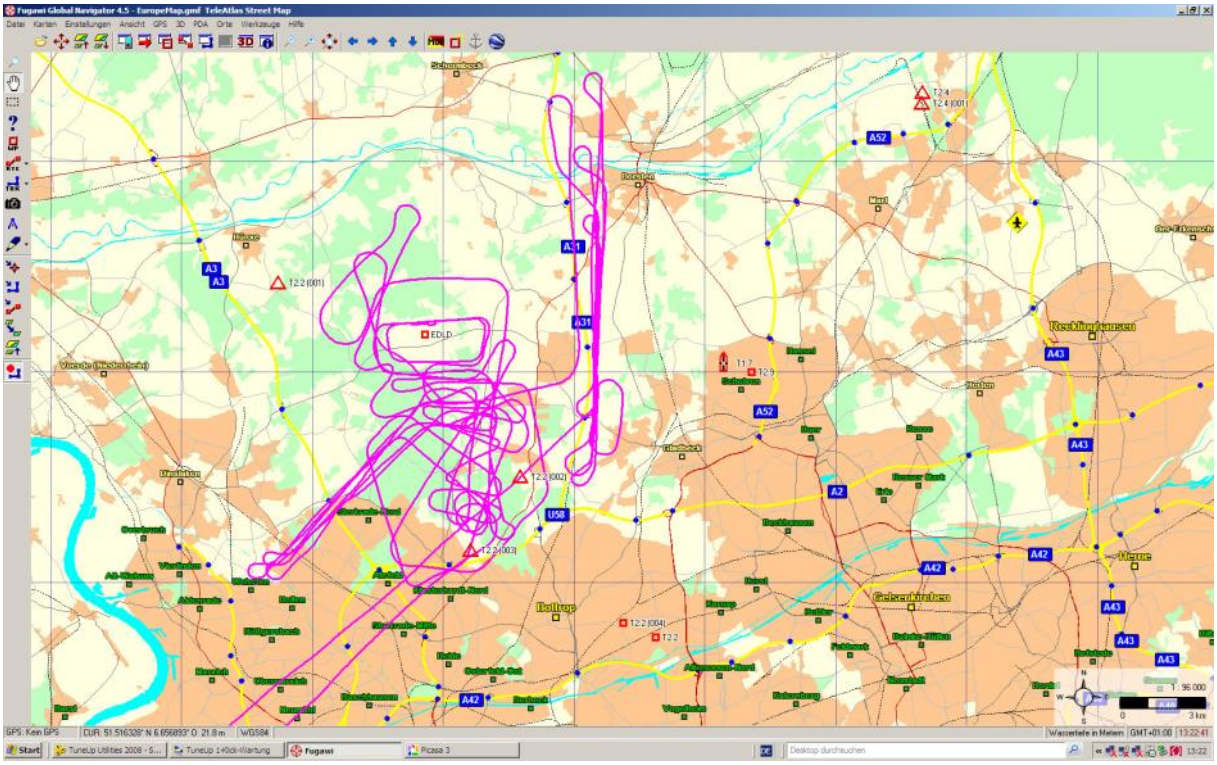

Flight Day 16.08.2012

MAMAP

Target(s): Niederaussem (PG), Neurath (PG), Fimmersdorf (PG), Bergwerk-West (CM)

Flight ID : 2012_08_16_1

Start of Measurement: 08:57 UTC (Neurath, Niederaussem, Fimmersdorf)

End of Measurement: 09:29 UTC (Neurath, Niederaussem, Fimmersdorf)

Start of Measurement: 09:34 UTC (Bergwerk-West)

End of Measurement: 10:12 UTC (Bergwerk-West)

Spectrometer Temperature: 32°C

Weather description: measurements over Niederaussem, Neurath, Fimmersdorf aborted due to Cumulus development. Measurements taken only over BW-West, shaft FH-4 due to Cumulus over the Rossenray shaft. Further measurements abborted due to further Cumulus development. BL ca. 1600 m (visual estimate), wind ca. 8 m/sec.

Figure 11: Cumulus situation over the power plants.

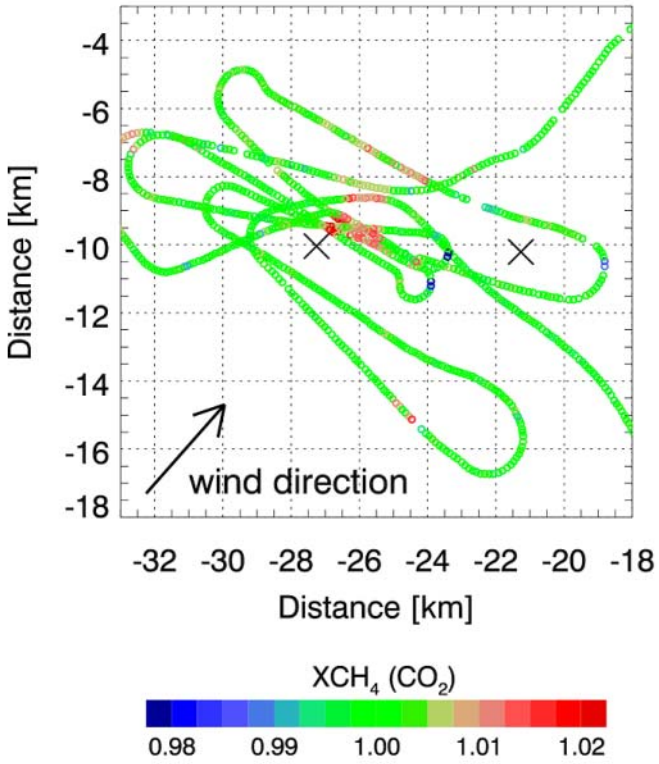

Figure 12: MAMAP flight pattern and quick-look analysis Bergwerk West 16.8.2012.

METAIR

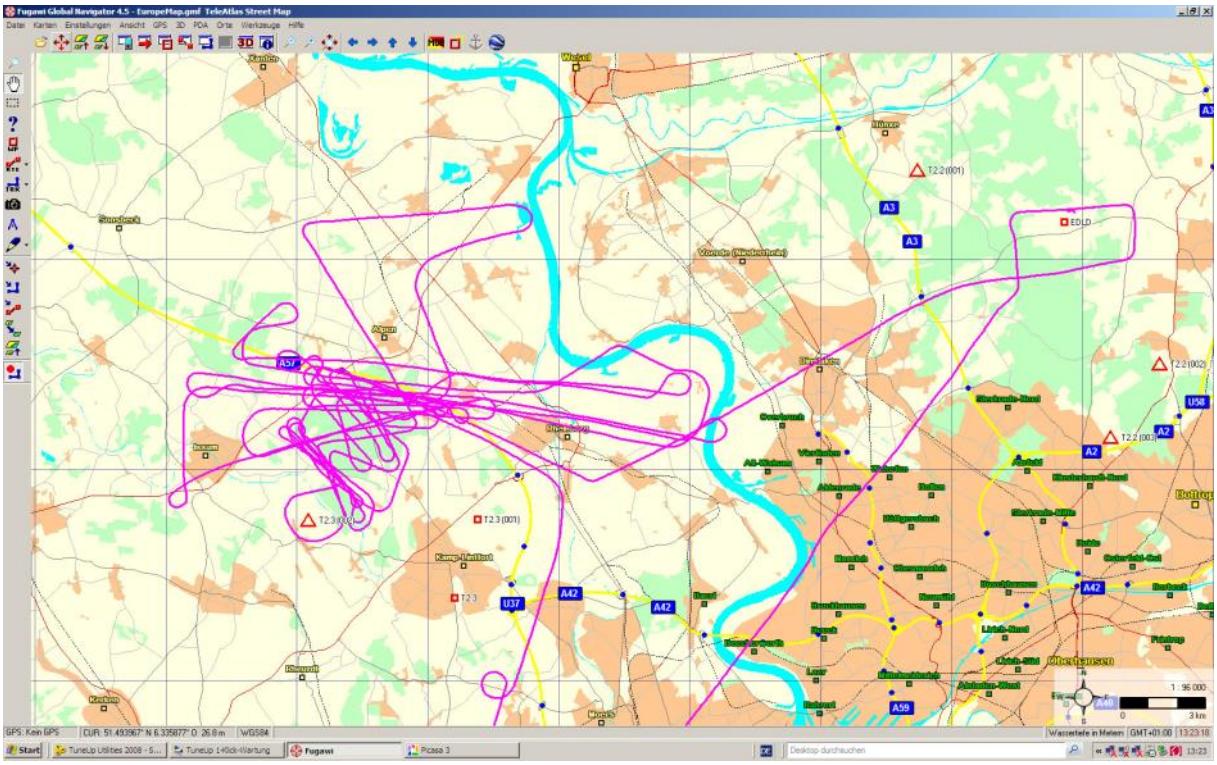

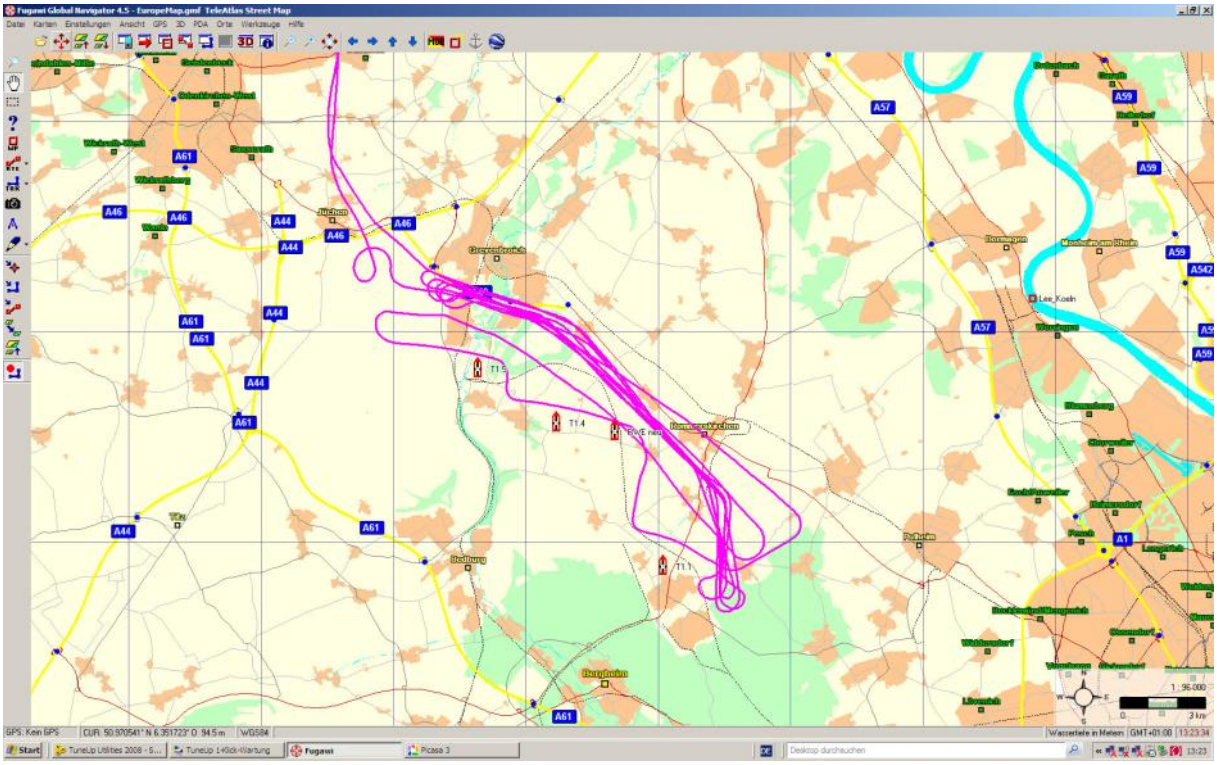

Flight Day 17.08.2012

MAMAP

Target(s): (Scholven (PG)), Niederaussem (PG), Neurath (PG), Fimmersdorf (PG), Bergwerk-West (CM)

Flight ID : 2012_08_17_1

Start of Measurement: 09:25 UTC (Niederaussem, Neurath, Fimmersdorf)

End of Measurement: 10:47 UTC (Niederaussem, Neurath, Fimmersdorf)

Start of Measurement: 10:56 UTC (Bergwerk-West)

End of Measurement: 12:13 UTC (Bergwerk-West)

Spectrometer Temperature: 32°C

Weather description: no measurements performed in the Scholven area due to string Cirrus. Slight to medium inhomogeneous Cirrus at Niederaussem, Neurath, Fimmersdorf area. Later development of Cumulus from Luv to Lee-ward. Aircraft flown always in-front of Cumuli outside the cloud-shadows. Last track/leg potentially affected by Cumulus shadows.

Measurements performed at larger distance to the plant-stacks due to strong steam cloud development over the cooling towers. In the BW-West slight to medium/stronger Cirrus. Later Cumulus development. Wind from SSW.

Figure 13: Situation at the beginning of the measurements at Niederaussem, Neurath and Fimmersdorf area.

Figure 14: Development of Cumulus from Luv to Lee-ward

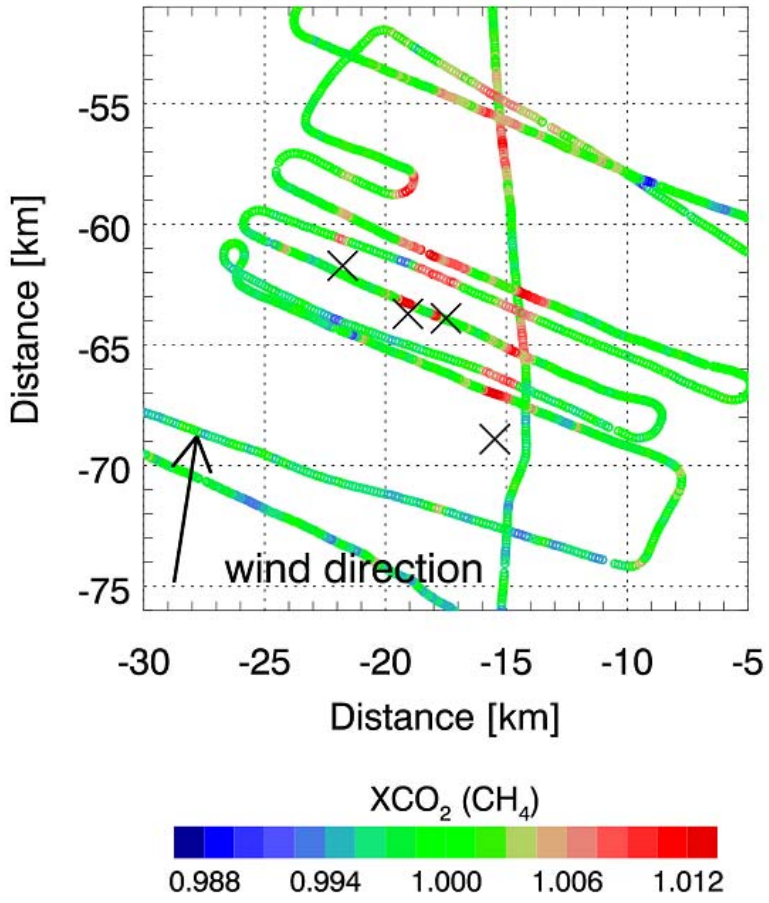

Figure 15: MAMAP flight pattern and quick-look analysis power plants Niederaussem, Neurath and Fimmersdorf 17.8.2012.

METAIR

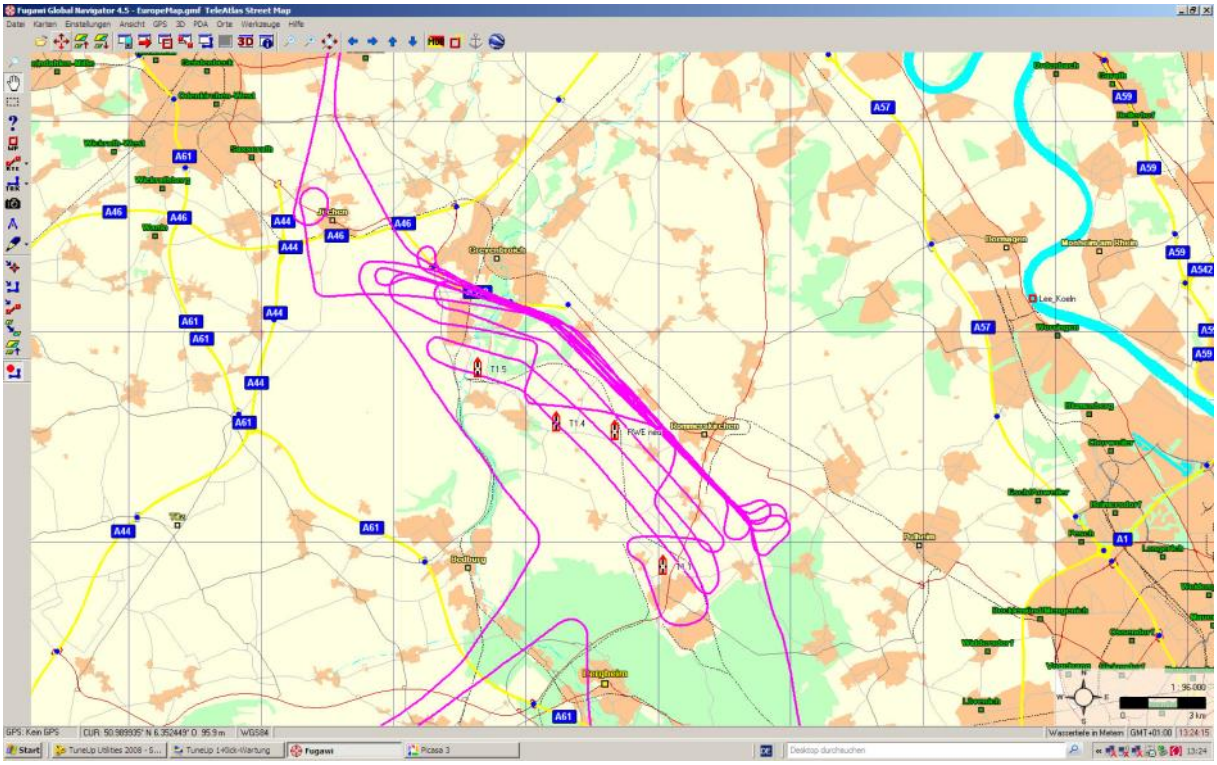

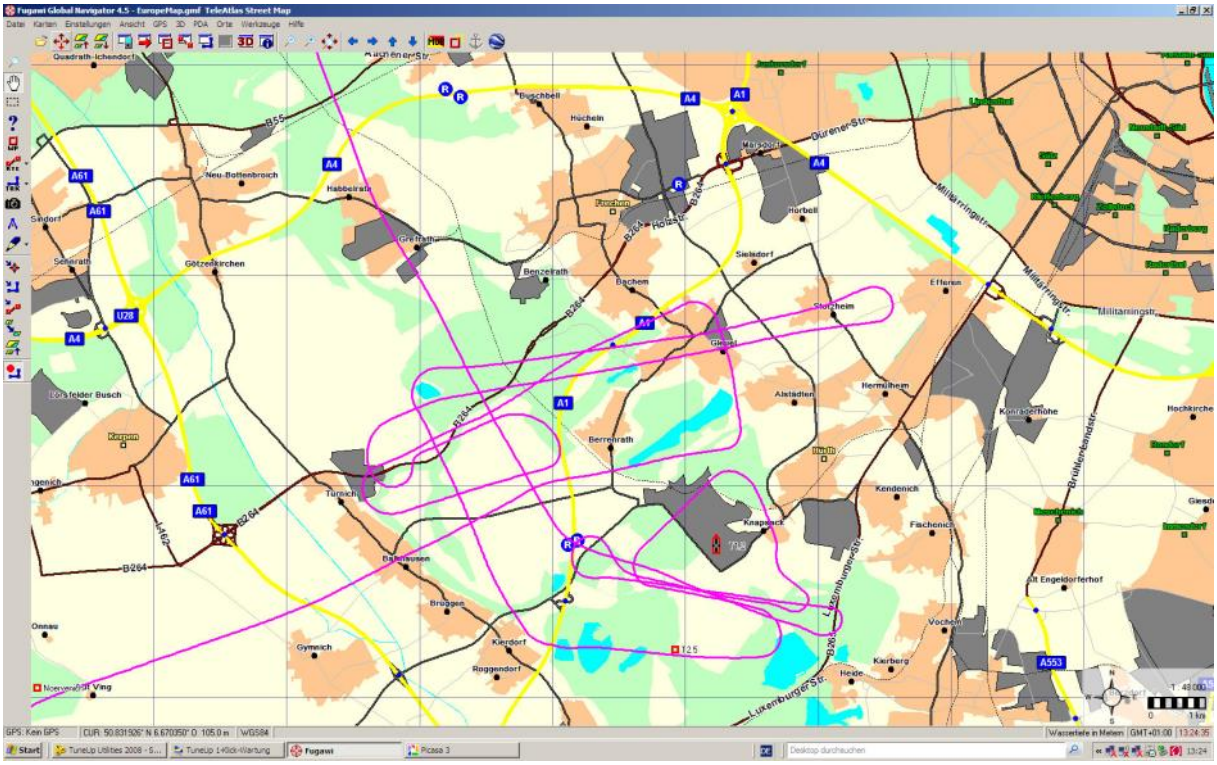

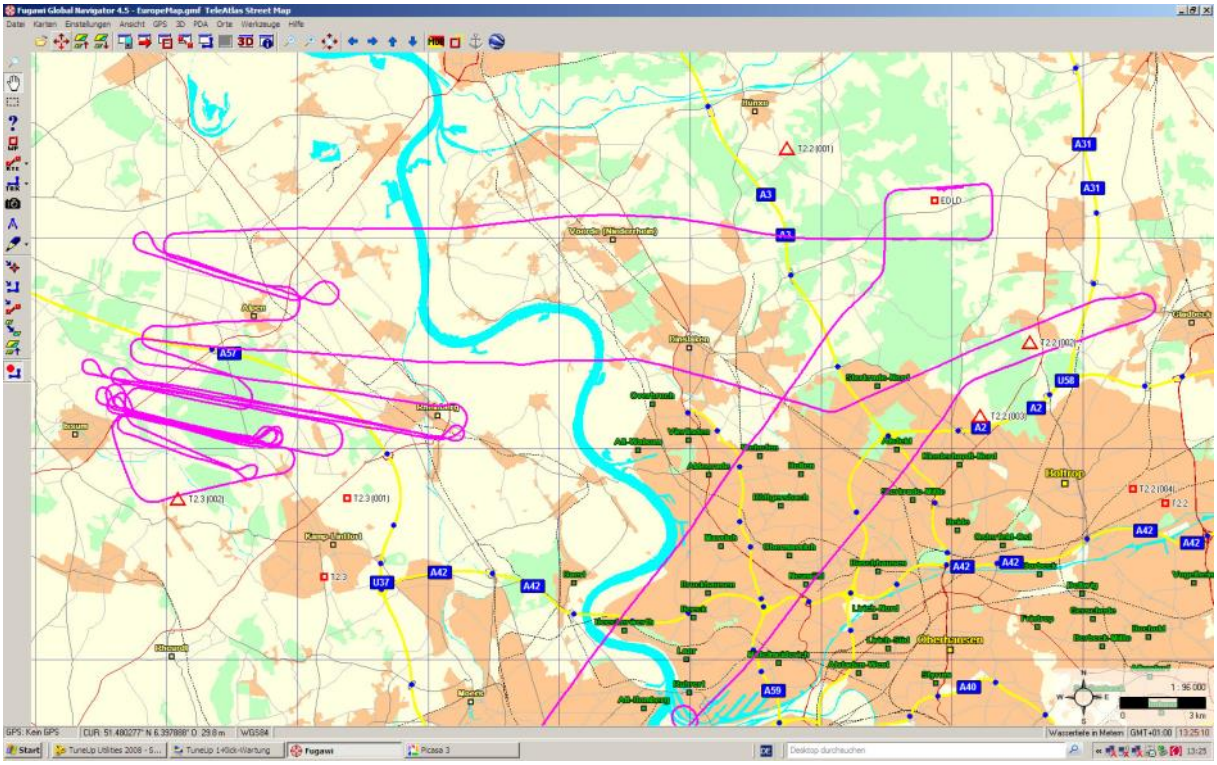
A31
A3
A57
A2
A42
A59
A40
U58
U37

Flight Day 18.08.2012

MAMAP Morning

Target(s): Niederaussem (PG), Neurath (PG), Fimmersdorf (PG), Vereinigte-Ville (LF), (Goldenberg (PG))

Flight ID : 2012_08_18_1

Start of Measurement: 07:54 UTC (Niederaussem, Neurath, Fimmersdorf)

End of Measurement: 10:27 UTC (Niederaussem, Neurath, Fimmersdorf)

Start of Measurement: 10:38 UTC (Vereinigte Ville, Goldenberg)

End of Measurement: 11:04 UTC (Vereinigte Ville, Goldenberg)

Spectrometer Temperature: 32°C

Weather description: in the Niederaussem, Neurath, Fimmersdorf area slight to medium Cirrus. In the area around Ville, clear sky with slight Cirrus, decreasing over time. Only few measurements performed over Vereinigte Ville due to lack of fuel. Wind from SSE, ca. 6 m/sec.

Figure 16: Situation at the Niederaussem, Neurath and Fimmersdorf (PG) area.

Figure 17: Situation over the Vereinigte Ville landfill.

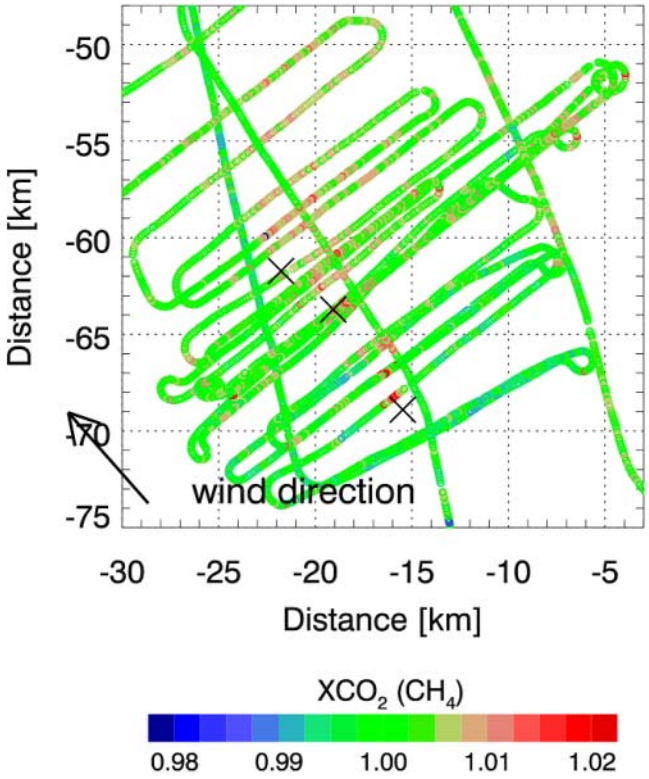

Figure 18: MAMAP flight pattern and quick-look analysis power plants Niederaussem, Neurath and Fimmersdorf 18.8.2012.

MAMAP Afternoon

Target(s): Eschweiler (PG), Vereinigte-Ville (LF), (Goldenberg (PG)), Rheinland Raffinerie Godorf (RF)

Flight ID : 2012_08_18_2

Start of Measurement: 13:34 UTC (Eschweiler)

End of Measurement: 14:35 UTC (Eschweiler)

Start of Measurement: 14:38 UTC (Vereinigte-Ville, Goldenberg, Rheinland Raffinerie Godorf)

End of Measurement: 16:24 UTC (Vereinigte-Ville, Goldenberg, Rheinland Raffinerie Godorf)

Spectrometer Temperature: 36°C

Weather description: in the Eschweiler and Vereinigte-Ville area, clear sky. In the Godorf area: initially clear sky, later on slight medium height clouds and development of Cumulus.

Figure 19: Cloud situation in the Eschweiler area.

Figure 20: Cloud situation in the Vereinigte Ville area.

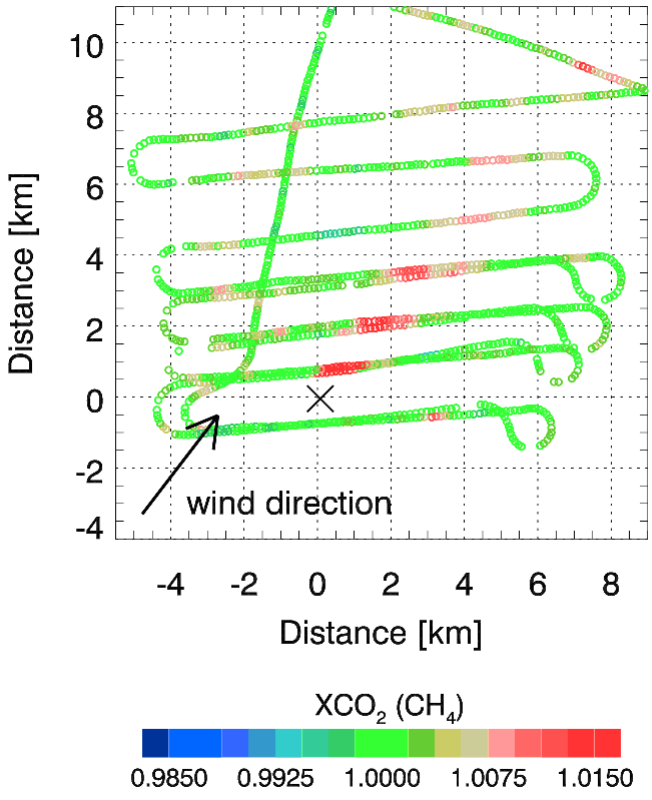

Figure 21: MAMAP flight pattern and quick-look analysis power plant Eschweiler 18.8.2012.

METAIR

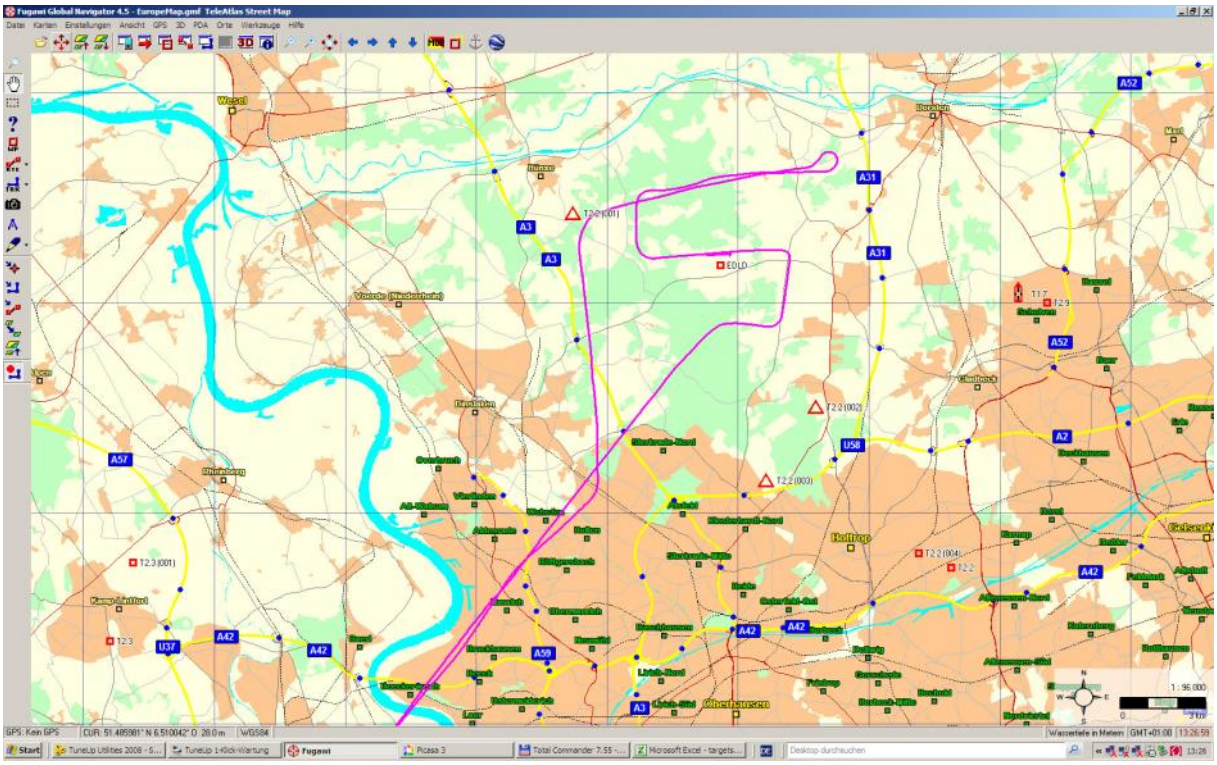

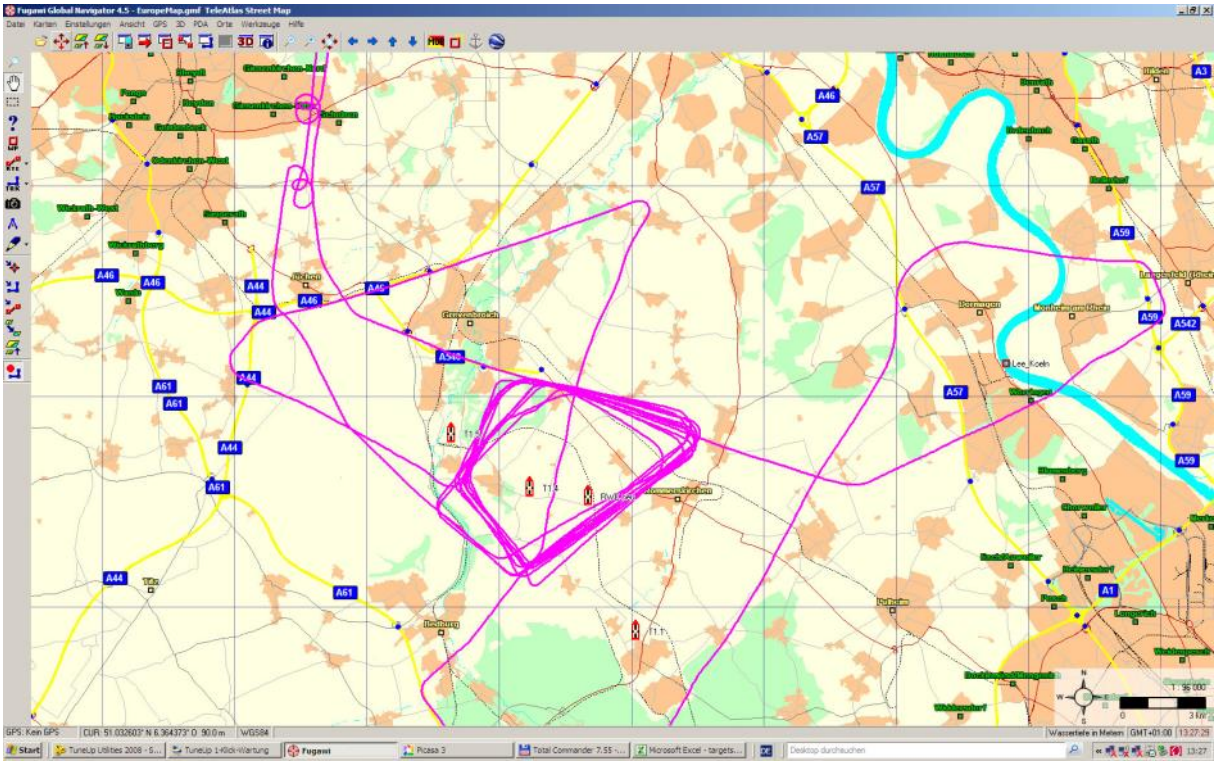

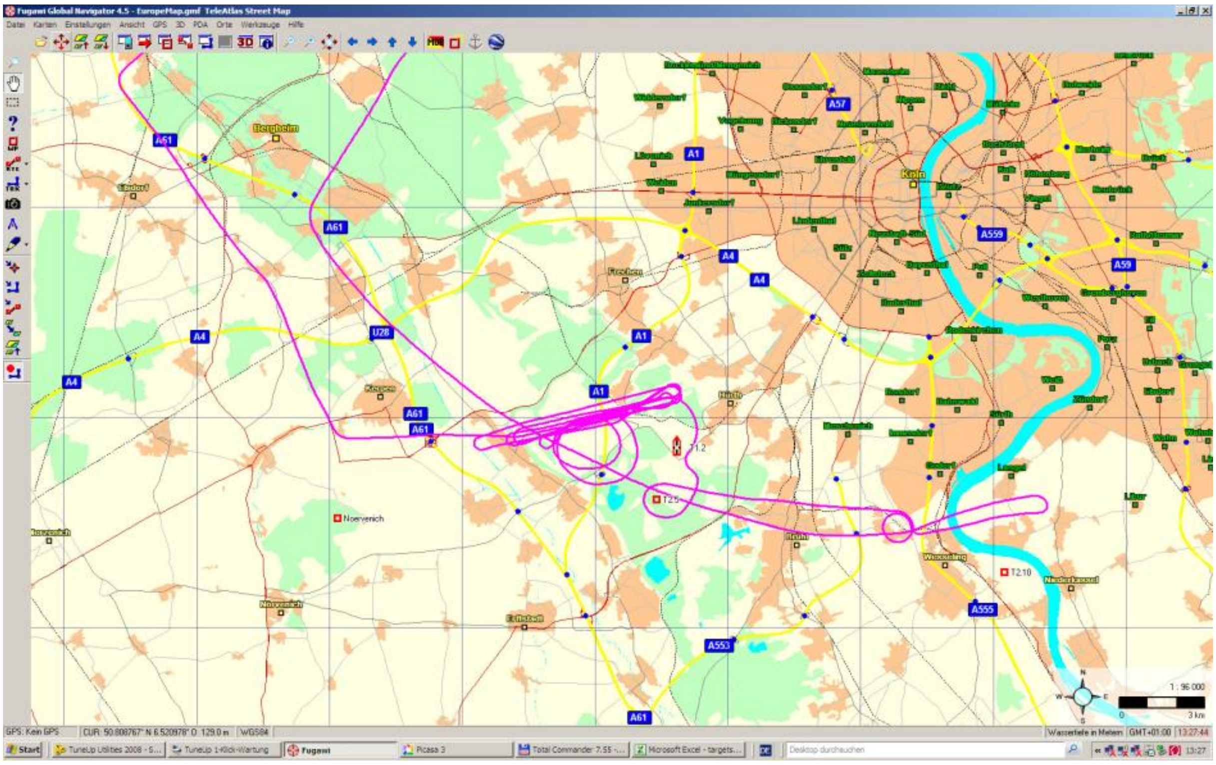

Fugawi Global Navigator 4.5 - EuropeMap.gmf TeleAtlas Street Map
A61
A4
A1
A57
A559
A59
A555
A553
U28
Bergheim
Noervenich
T2.5
T2.10
1 : 96 000

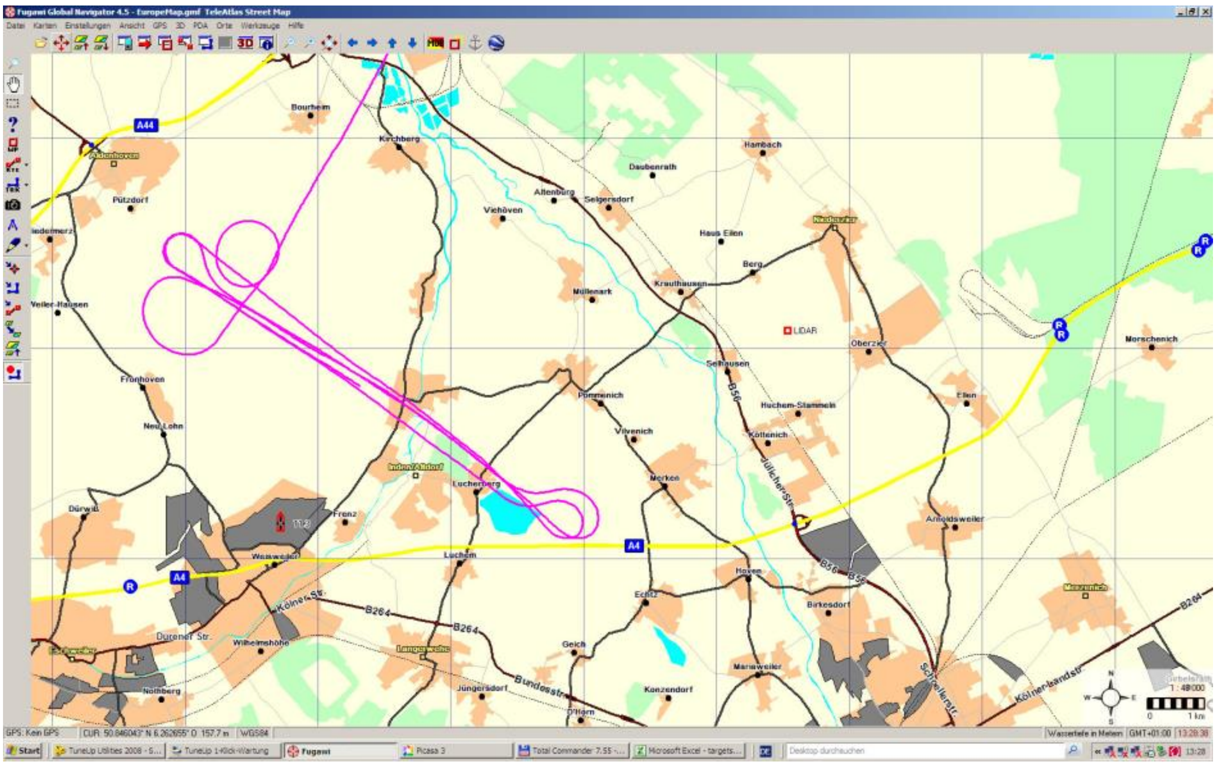

Fugawi Global Navigator 4.5 - EuropeMap.gmf TeleAtlas Street Map
A44
A4
B264
B56
LIDAR
1 : 48 000

Flight Day 19.08.2012

MAMAP Morning

Target(s): Ibbenbüren (CM)

Flight ID : 2012_08_19_1

Start of Measurement: 08:25 UTC

End of Measurement: 10:49 UTC

Spectrometer Temperature: 36°C

Weather description: in the Ibbenbüren area, clear sky. At the End of the flight, march through of medium height clouds in some areas with visible shadows.

Figure 22: Cloud situation over Ibbenbüren

Figure 23: Situation at the End of the flight, march through of medium height clouds in some areas with visible shadows.

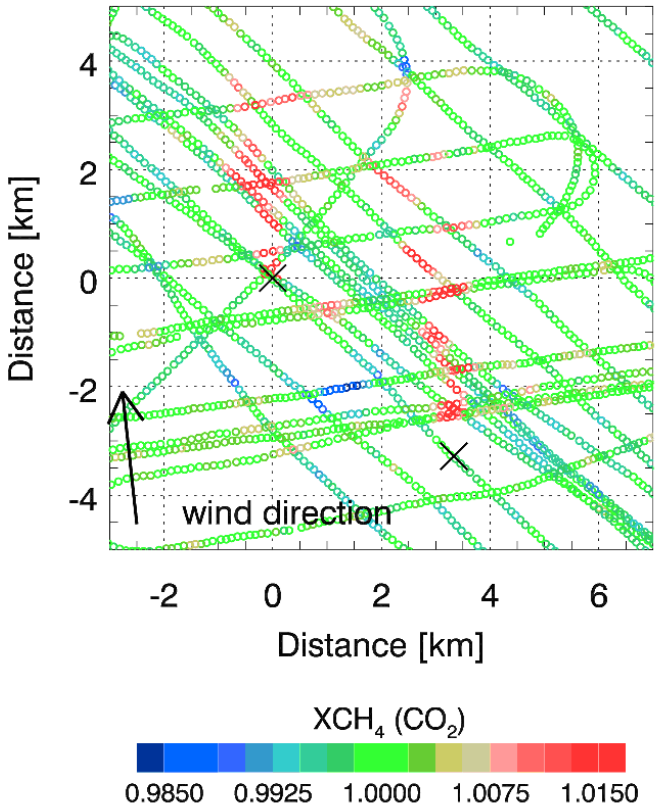

Figure 24: MAMAP flight pattern and quick-look analysis Ibbenbühren (exhaust shafts Bockradener-Schacht and Theodor-Schacht) 19.8.2012.

MAMAP Afternoon

Target(s): Prosper-Haniel (CM), Scholven (PG), Ruhr Öl Gelsenkirchen (RF), Auguste-Viktoria (CM)

Flight ID : 2012_08_19_2

Start of Measurement: 12:12 UTC (Prosper-Haniel, Scholven, Ruhr Öl Gelsenkirchen)

End of Measurement: 15:13 UTC (Prosper-Haniel, Scholven, Ruhr Öl Gelsenkirchen)

Start of Measurement: 15:13 UTC (Auguste Viktoria AV7)

End of Measurement: 15:30 UTC (Auguste Viktoria AV7)

Spectrometer Temperature: 36°C

Weather description: in the Prosper-Haniel area clear sky at the beginning, later on development of medium height clouds over Scholven and the rafinery. At the End of the flight stronger medium height clouds. Last both legs/tracks taken over the refinery should not be used for data processing because of strong clouds.

Figure 25: Cloud situation at the End of the flight over the refinery.

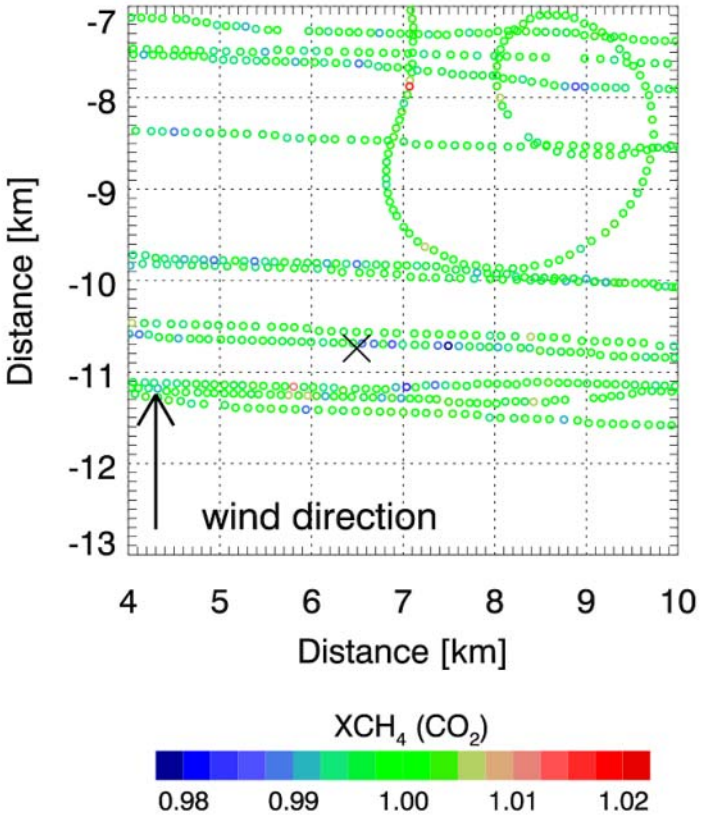

Figure 26: MAMAP flight pattern and quick-look analysis Prosper-Haniel (exhaust shaft Förderberg) 19.8.2012.

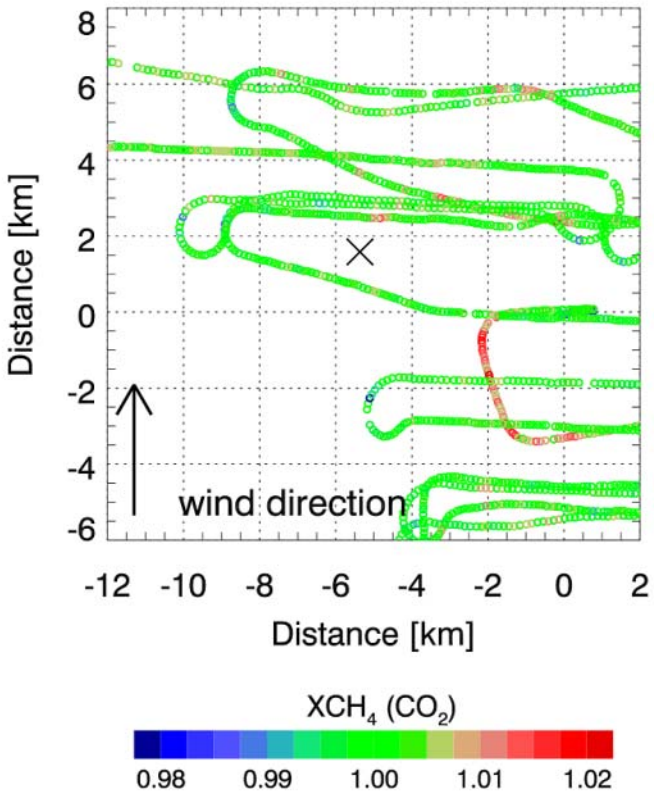

Figure 27: MAMAP flight pattern and quick-look analysis Prosper-Haniel (exhaust shaft Hünxe) 19.8.2012.

METAIR

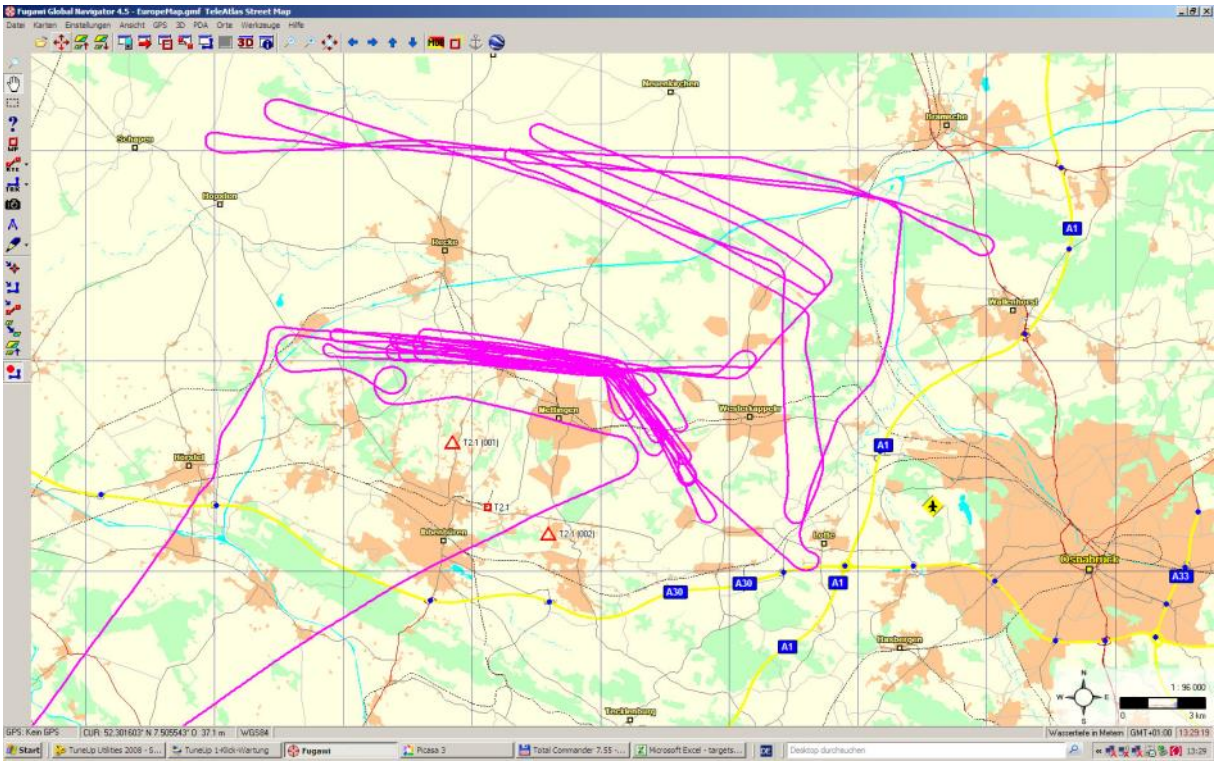

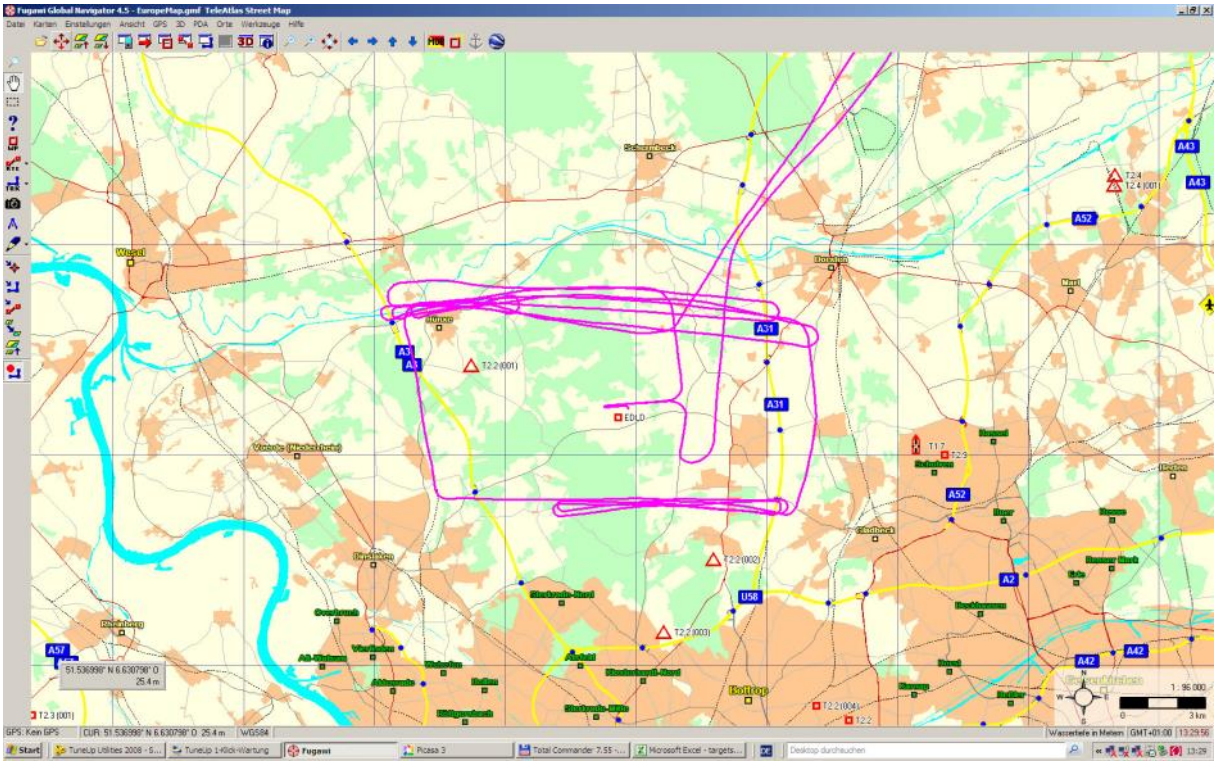

Flight Day 23.08.2012

MAMAP

Target(s): Eschweiler (PG), Selhausen (FLEX), Altendorf (FLEX), Eschweiler (PG), Selhausen (FLEX)

Flight ID : 2012_08_23_1

Start of Measurement: 09:59 UTC (Eschweiler, Selhausen)

End of Measurement: 11:12 UTC (Eschweiler, Selhausen)

Start of Measurement: 11:18 UTC Altendorf

End of Measurement: 11:47 UTC Altendorf

Start of Measurement: 11:54 UTC (Eschweiler, Selhausen)

End of Measurement: 13:02 UTC (Eschweiler, Selhausen)

Spectrometer Temperature: 36°C

Weather description:

Eschweiler : before Noon Cirrus, Afternoon clear sky.

Selhausen: before Noon Cirrus, Afternoon clear sky.

Altendorf: closed cloud cover or broken Cumulus at Noon.

Figure 28: Situation at Eschweiler/ Selhausen before noon.

Figure 29: Situation at Altendorf around noon.

Figure 30: Situation at Eschweiler/ Selhausen in the afternoon.

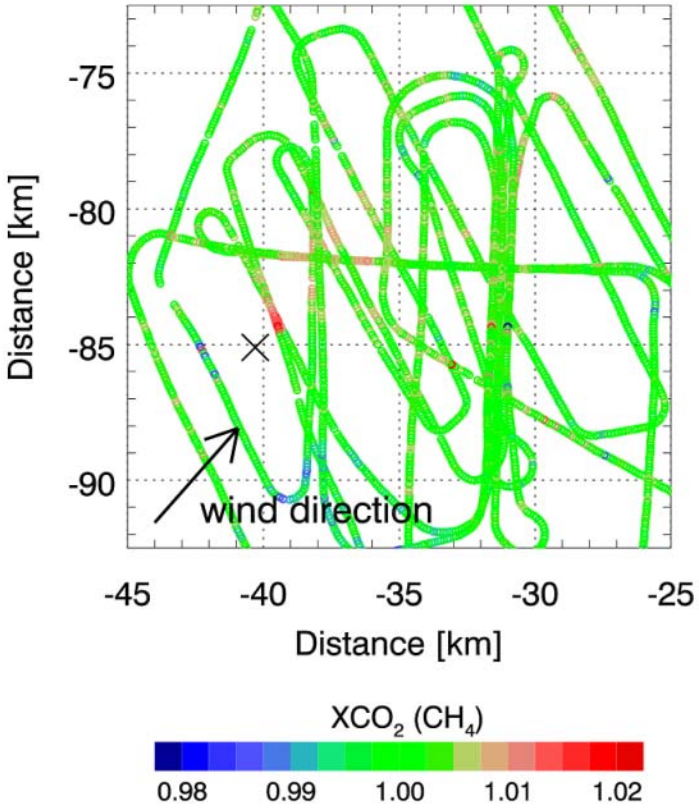

Figure 31: MAMAP flight pattern and quick-look analysis power plant Eschweiler and area around Selhausen 23.8.2012.

METAIR

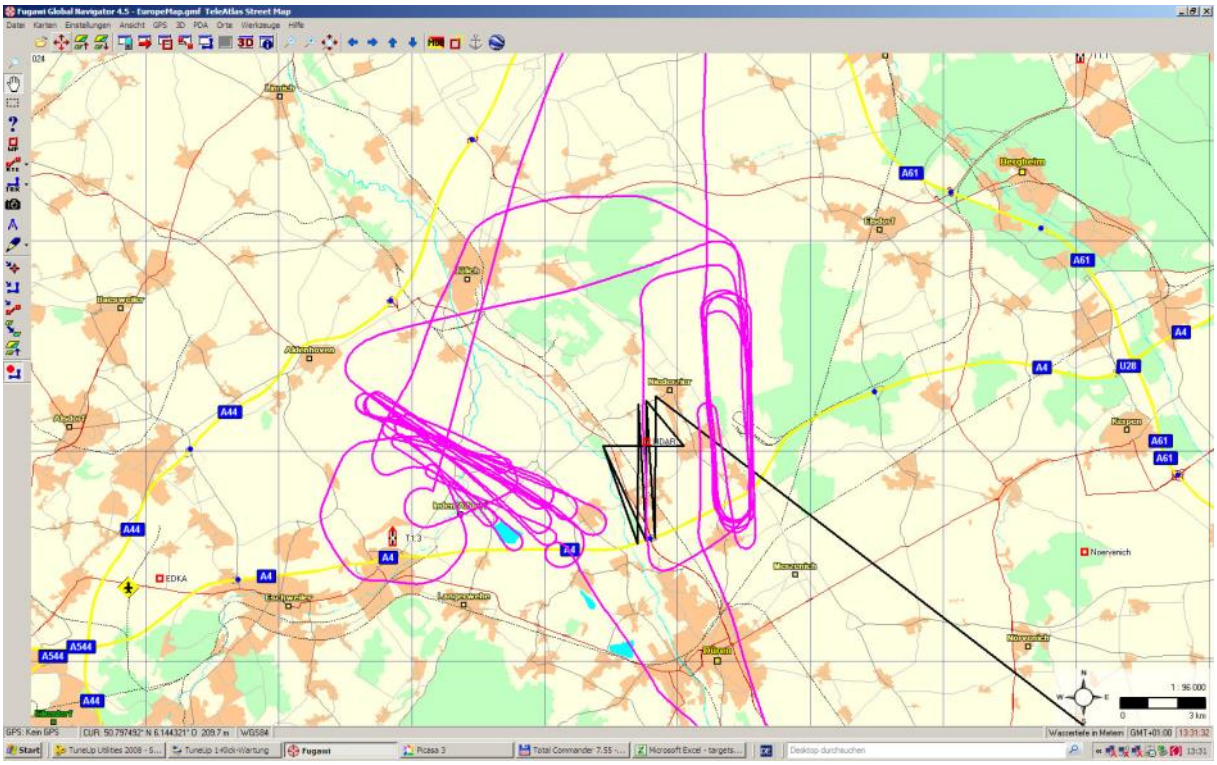

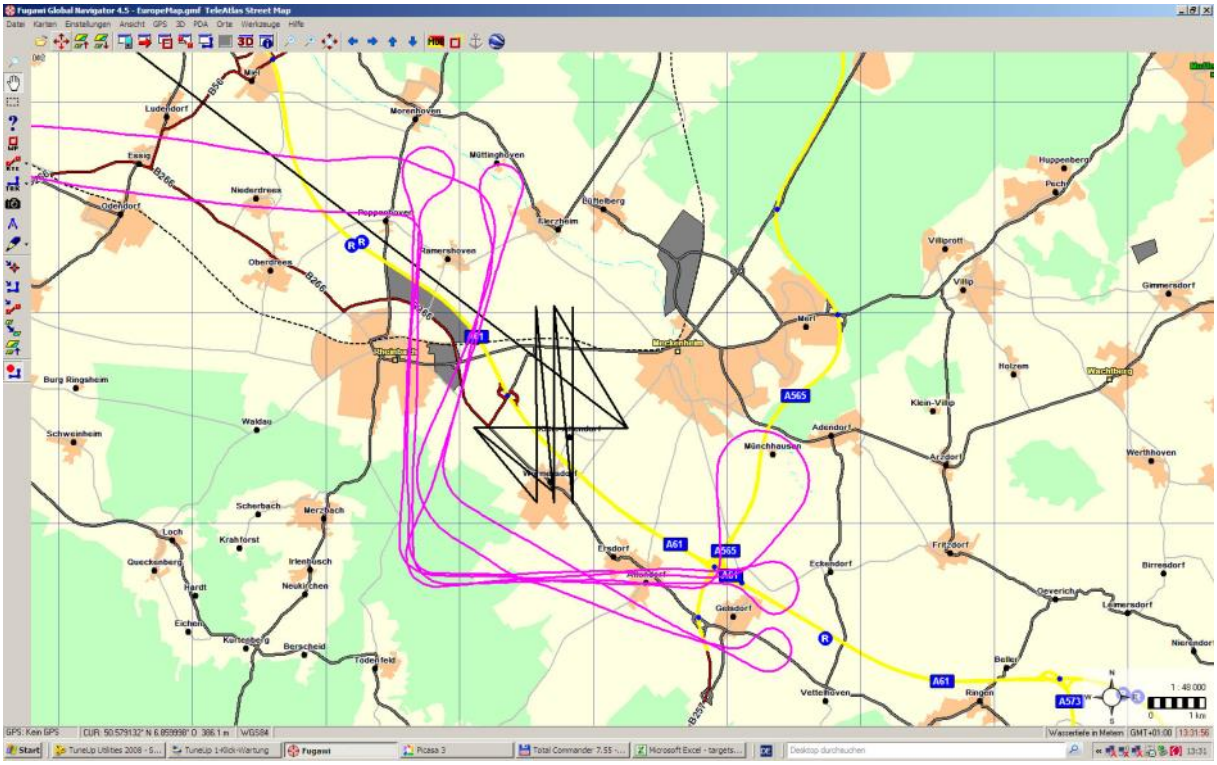

Annex 3: Content of the in-situ result files (METAIR)

The title is identifying the case and some parameters like the extrapolation scheme ("SE1" means extrapolation to the digital terrain) and the horizontal and vertical resolution (50 m each):

```
23_Weisw_CrossSect CO2_T1_3  SE1   50   50
```

Then, the total column mass concentration of CO_2 exceeding the background is given:

```
ME  236.869 kg     18.763 kg      0.000 kg   (92.1 % measured)
```

The 237 kg are the total, and the 19 kg are the extrapolated mass between the lowest flight track and the surface. No extrapolation was necessary on top. 92.1 % of the mass was measured, and only 7.9 % was extrapolated.

```
FE  671.191 kg/s    9.073 kg/s    0.000 kg/s (98.6 % measured)
```

The horizontal flux of CO_2 from the point source (exceeding the background concentration) was 671 kg/s, from which only 9 kg/s was extrapolated to the surface, i.e. 98.6 % was explicitly measured.

```
estimated emission of 21.17 Mt/a and an inverted average wind speed of 2.83
m/s
```

The 9 kg/s are equal to 21 Mt/a. When the flux is divided by total mass in the cross section, an average wind speed of 2.8 m/s is resulting. This can be compared with the wind speed used for the inversion of MAMAP.
The average cross wind component is to check the proper alignement (fig. 4 shows that this is not important).

```
average crosswind component = 0.1 m/s
```

In cases with relevant convection, the vertical flux of CO_2 or CH_4 above the source was calculated based on flight-tracks above the sources. However, this was not the case in this example:

```
estimated vertical flux of 0.000..0.000 kg/s or 0.00..0.00 Mt/a
```

The average concentration of CO_2 in the cross section:

```
CT average concentration was 389.72 ppm
```

The average concentration of CO_2 above the background concentration in the cross section:

```
CE average concentration above background was 8.69 ppm
```

Obviously, the background concentration was 381 ppm.

The following table is summarising the average positions of the flight track, i.e. the "centre of gravity" of the measurements:
ih is the index of the column (comparable with "A" to "N" in **Fehler! Verweisquelle konnte nicht gefunden werden.**); n is the number of measurements; xr and yr are the coordinates relative to the source [m], xa and ya are the UTM-coordinates [km] of the column

"ih"	"n"	"xr"	"yr"	"xa"	"ya"	"xrl"	"yrl"	"xal"	"yal"	"terr"
-80	20	982	5571	335	5101	6.3378	50.8890	6.3286	50.8848	114
-79	33	1011	5530	339	5058	6.3382	50.8886	6.3287	50.8844	115
-78	36	1040	5489	374	5023	6.3386	50.8883	6.3292	50.8841	116
-77	36	1068	5448	355	4948	6.3391	50.8879	6.3289	50.8834	117
-76	35	1097	5407	445	4949	6.3395	50.8875	6.3302	50.8834	117
-75	35	1126	5366	471	4908	6.3399	50.8872	6.3306	50.8830	116
...										
-5	105	3133	2499	2945	2368	6.3684	50.8614	6.3658	50.8602	115

-4	102	3162	2458	2969	2323	6.3688	50.8610	6.3661	50.8598	114
-3	104	3191	2417	3027	2303	6.3692	50.8607	6.3669	50.8596	111
-2	101	3219	2376	3090	2286	6.3697	50.8603	6.3678	50.8595	110
-1	101	3248	2335	3115	2242	6.3701	50.8599	6.3682	50.8591	109
0	101	3277	2294	3139	2198	6.3705	50.8596	6.3685	50.8587	109
1	99	3305	2253	3204	2184	6.3709	50.8592	6.3694	50.8586	110
2	104	3334	2212	3250	2153	6.3713	50.8588	6.3701	50.8583	111
3	98	3363	2171	3285	2116	6.3717	50.8585	6.3706	50.8580	111
4	101	3391	2130	3343	2096	6.3721	50.8581	6.3714	50.8578	111
5	98	3420	2090	3389	2068	6.3725	50.8577	6.3721	50.8575	111

...

75	13	5428	-778	7122	409	6.4011	50.8320	6.4252	50.8426	118
76	13	5456	-818	7157	371	6.4015	50.8316	6.4257	50.8423	118
77	13	5485	-859	7190	334	6.4019	50.8312	6.4262	50.8420	118
78	15	5514	-900	7227	301	6.4023	50.8309	6.4267	50.8417	119
79	19	5542	-941	7266	266	6.4027	50.8305	6.4272	50.8413	120
80	11	5571	-982	7288	235	6.4031	50.8301	6.4275	50.8411	120

With this print-plot, the column mass concentrations along the cross section are shown:

```
ME EXCESSIVE COLUMN MASS CONCENTRATIONS IN g/m2
-4000  m         8.998     g/m2   >>>>>>
-3950  m        11.136     g/m2   >>>>>>>
-3900  m        10.951     g/m2   >>>>>>>
-3850  m        10.673     g/m2   >>>>>>>
...
-3600  m        13.591     g/m2   >>>>>>>>
-3550  m        14.354     g/m2   >>>>>>>>>
-3500  m        19.298     g/m2   >>>>>>>>>>>>
-3450  m        16.846     g/m2   >>>>>>>>>>
-3400  m        19.789     g/m2   >>>>>>>>>>>>
-3350  m        20.279     g/m2   >>>>>>>>>>>>
-3300  m        27.076     g/m2   >>>>>>>>>>>>>>>>>
-3250  m        28.867     g/m2   >>>>>>>>>>>>>>>>>>
-3200  m        27.035     g/m2   >>>>>>>>>>>>>>>>>
-3150  m        25.235     g/m2   >>>>>>>>>>>>>>>
-3100  m        25.436     g/m2   >>>>>>>>>>>>>>>>
-3050  m        27.769     g/m2   >>>>>>>>>>>>>>>>>
-3000  m        40.314     g/m2   >>>>>>>>>>>>>>>>>>>>>>>>>
-2950  m        44.692     g/m2   >>>>>>>>>>>>>>>>>>>>>>>>>>>
-2900  m        50.548     g/m2   >>>>>>>>>>>>>>>>>>>>>>>>>>>>>>>
-2850  m        33.450     g/m2   >>>>>>>>>>>>>>>>>>>>
-2800  m        32.964     g/m2   >>>>>>>>>>>>>>>>>>>>
-2750  m        31.501     g/m2   >>>>>>>>>>>>>>>>>>>
-2700  m        42.387     g/m2   >>>>>>>>>>>>>>>>>>>>>>>>>>
-2650  m        41.576     g/m2   >>>>>>>>>>>>>>>>>>>>>>>>>
-2600  m        36.932     g/m2   >>>>>>>>>>>>>>>>>>>>>>>
-2550  m        30.547     g/m2   >>>>>>>>>>>>>>>>>>>
-2500  m        27.519     g/m2   >>>>>>>>>>>>>>>>>
-2450  m        30.024     g/m2   >>>>>>>>>>>>>>>>>>
-2400  m        28.516     g/m2   >>>>>>>>>>>>>>>>>
-2350  m        29.510     g/m2   >>>>>>>>>>>>>>>>>>
-2300  m        35.762     g/m2   >>>>>>>>>>>>>>>>>>>>>>
-2250  m        32.228     g/m2   >>>>>>>>>>>>>>>>>>>>
-2200  m        36.204     g/m2   >>>>>>>>>>>>>>>>>>>>>>
-2150  m        36.715     g/m2   >>>>>>>>>>>>>>>>>>>>>>
-2100  m        32.612     g/m2   >>>>>>>>>>>>>>>>>>>>
-2050  m        36.707     g/m2   >>>>>>>>>>>>>>>>>>>>>>
-2000  m        39.739     g/m2   >>>>>>>>>>>>>>>>>>>>>>>>
-1950  m        38.796     g/m2   >>>>>>>>>>>>>>>>>>>>>>>>
-1900  m        38.567     g/m2   >>>>>>>>>>>>>>>>>>>>>>>>
-1850  m        39.533     g/m2   >>>>>>>>>>>>>>>>>>>>>>>>
-1800  m        40.138     g/m2   >>>>>>>>>>>>>>>>>>>>>>>>>
-1750  m        41.945     g/m2   >>>>>>>>>>>>>>>>>>>>>>>>>>
-1700  m        44.440     g/m2   >>>>>>>>>>>>>>>>>>>>>>>>>>>
-1650  m        54.661     g/m2   >>>>>>>>>>>>>>>>>>>>>>>>>>>>>>>>>
-1600  m        47.676     g/m2   >>>>>>>>>>>>>>>>>>>>>>>>>>>>>
-1550  m        47.496     g/m2   >>>>>>>>>>>>>>>>>>>>>>>>>>>>>
-1500  m        46.693     g/m2   >>>>>>>>>>>>>>>>>>>>>>>>>>>>>
-1450  m        49.551     g/m2   >>>>>>>>>>>>>>>>>>>>>>>>>>>>>>
-1400  m        62.119     g/m2   >>>>>>>>>>>>>>>>>>>>>>>>>>>>>>>>>>>>>>
-1350  m        73.738     g/m2   >>>>>>>>>>>>>>>>>>>>>>>>>>>>>>>>>>>>>>>>>>>>>
-1300  m        62.606     g/m2   >>>>>>>>>>>>>>>>>>>>>>>>>>>>>>>>>>>>>>
-1250  m        78.848     g/m2   >>>>>>>>>>>>>>>>>>>>>>>>>>>>>>>>>>>>>>>>>>>>>>>>
-1200  m        81.650     g/m2   >>>>>>>>>>>>>>>>>>>>>>>>>>>>>>>>>>>>>>>>>>>>>>>>>>
-1150  m        76.180     g/m2   >>>>>>>>>>>>>>>>>>>>>>>>>>>>>>>>>>>>>>>>>>>>>>>
-1100  m        71.108     g/m2   >>>>>>>>>>>>>>>>>>>>>>>>>>>>>>>>>>>>>>>>>>>>
-1050  m        59.146     g/m2   >>>>>>>>>>>>>>>>>>>>>>>>>>>>>>>>>>>>
-1000  m        46.360     g/m2   >>>>>>>>>>>>>>>>>>>>>>>>>>>>
-950   m        35.417     g/m2   >>>>>>>>>>>>>>>>>>>>>>
-900   m        37.857     g/m2   >>>>>>>>>>>>>>>>>>>>>>>
```

```
-850   m        44.857     g/m2   >>>>>>>>>>>>>>>>>>>>>>>>>>>
-800   m        49.395     g/m2   >>>>>>>>>>>>>>>>>>>>>>>>>>>>>>>>
-750   m        47.957     g/m2   >>>>>>>>>>>>>>>>>>>>>>>>>>>>>>>
-700   m        47.958     g/m2   >>>>>>>>>>>>>>>>>>>>>>>>>>>>>>>
-650   m        45.766     g/m2   >>>>>>>>>>>>>>>>>>>>>>>>>>>>>
-600   m        48.960     g/m2   >>>>>>>>>>>>>>>>>>>>>>>>>>>>>>>>
-550   m        42.133     g/m2   >>>>>>>>>>>>>>>>>>>>>>>>>>>
-500   m        38.337     g/m2   >>>>>>>>>>>>>>>>>>>>>>>>
-450   m        37.129     g/m2   >>>>>>>>>>>>>>>>>>>>>>>>
-400   m        36.950     g/m2   >>>>>>>>>>>>>>>>>>>>>>>>
-350   m        40.602     g/m2   >>>>>>>>>>>>>>>>>>>>>>>>>>>
-300   m        40.546     g/m2   >>>>>>>>>>>>>>>>>>>>>>>>>>>
-250   m        41.038     g/m2   >>>>>>>>>>>>>>>>>>>>>>>>>>>
-200   m        45.763     g/m2   >>>>>>>>>>>>>>>>>>>>>>>>>>>>>>
-150   m        51.228     g/m2   >>>>>>>>>>>>>>>>>>>>>>>>>>>>>>>>>
-100   m        51.647     g/m2   >>>>>>>>>>>>>>>>>>>>>>>>>>>>>>>>>>
 -50   m        48.488     g/m2   >>>>>>>>>>>>>>>>>>>>>>>>>>>>>>>>
   0   m        39.765     g/m2   >>>>>>>>>>>>>>>>>>>>>>>>>
  50   m        42.038     g/m2   >>>>>>>>>>>>>>>>>>>>>>>>>>>
 100   m        41.096     g/m2   >>>>>>>>>>>>>>>>>>>>>>>>>>
 150   m        41.257     g/m2   >>>>>>>>>>>>>>>>>>>>>>>>>>
 200   m        45.449     g/m2   >>>>>>>>>>>>>>>>>>>>>>>>>>>>>
 250   m        51.257     g/m2   >>>>>>>>>>>>>>>>>>>>>>>>>>>>>>>>>
 300   m        45.618     g/m2   >>>>>>>>>>>>>>>>>>>>>>>>>>>>>
 350   m        37.607     g/m2   >>>>>>>>>>>>>>>>>>>>>>>>>
 400   m        42.782     g/m2   >>>>>>>>>>>>>>>>>>>>>>>>>>>>
 450   m        47.879     g/m2   >>>>>>>>>>>>>>>>>>>>>>>>>>>>>>>
 500   m        43.229     g/m2   >>>>>>>>>>>>>>>>>>>>>>>>>>>>
 550   m        47.029     g/m2   >>>>>>>>>>>>>>>>>>>>>>>>>>>>>>>
 600   m        49.669     g/m2   >>>>>>>>>>>>>>>>>>>>>>>>>>>>>>>>
 650   m        50.406     g/m2   >>>>>>>>>>>>>>>>>>>>>>>>>>>>>>>>
 700   m        43.246     g/m2   >>>>>>>>>>>>>>>>>>>>>>>>>>>
 750   m        47.976     g/m2   >>>>>>>>>>>>>>>>>>>>>>>>>>>>>>
 800   m        55.275     g/m2   >>>>>>>>>>>>>>>>>>>>>>>>>>>>>>>>>>>>>>>>>>>
 850   m        40.104     g/m2   >>>>>>>>>>>>>>>>>>>>>>>>>>
 900   m        47.941     g/m2   >>>>>>>>>>>>>>>>>>>>>>>>>>>>>
 950   m        43.169     g/m2   >>>>>>>>>>>>>>>>>>>>>>>>>>>
1000   m        41.161     g/m2   >>>>>>>>>>>>>>>>>>>>>>>>>>
1050   m        42.215     g/m2   >>>>>>>>>>>>>>>>>>>>>>>>>>>
1100   m        39.352     g/m2   >>>>>>>>>>>>>>>>>>>>>>>>>
1150   m        29.660     g/m2   >>>>>>>>>>>>>>>>>>
1200   m        27.565     g/m2   >>>>>>>>>>>>>>>>>>
1250   m        22.462     g/m2   >>>>>>>>>>>>>>>
1300   m        24.403     g/m2   >>>>>>>>>>>>>>>>
1350   m        25.119     g/m2   >>>>>>>>>>>>>>>>
1400   m        22.265     g/m2   >>>>>>>>>>>>>>>
1450   m        20.661     g/m2   >>>>>>>>>>>>>>
1500   m        21.556     g/m2   >>>>>>>>>>>>>>
1550   m        20.887     g/m2   >>>>>>>>>>>>>>
1600   m        16.775     g/m2   >>>>>>>>>>
1650   m        18.299     g/m2   >>>>>>>>>>>
1700   m        16.244     g/m2   >>>>>>>>>>
1750   m        16.468     g/m2   >>>>>>>>>>
1800   m        16.628     g/m2   >>>>>>>>>>
1850   m        16.365     g/m2   >>>>>>>>>>
1900   m        17.444     g/m2   >>>>>>>>>>>
1950   m        17.817     g/m2   >>>>>>>>>>>
2000   m        16.049     g/m2   >>>>>>>>>>
2050   m        13.436     g/m2   >>>>>>>>
2100   m        13.368     g/m2   >>>>>>>>
2150   m        14.259     g/m2   >>>>>>>>>
2200   m        16.784     g/m2   >>>>>>>>>>
2250   m        17.038     g/m2   >>>>>>>>>>
2300   m        16.030     g/m2   >>>>>>>>>>
```

```
2350   m        15.532     g/m2   >>>>>>>>>>
2400   m        13.937     g/m2   >>>>>>>>>
2450   m        16.055     g/m2   >>>>>>>>>>
2500   m        15.709     g/m2   >>>>>>>>>>
2550   m        14.958     g/m2   >>>>>>>>>
2600   m        14.013     g/m2   >>>>>>>>>
2650   m        13.040     g/m2   >>>>>>>>
2700   m        13.001     g/m2   >>>>>>>>
2750   m        10.576     g/m2   >>>>>>
2800   m         9.264     g/m2   >>>>>>
2850   m        11.050     g/m2   >>>>>>>
2900   m         3.712     g/m2   >>
2950   m         4.210     g/m2   >>>
3000   m         3.788     g/m2   >>
3050   m         3.349     g/m2   >>
3100   m         2.989     g/m2   >>
3150   m         1.857     g/m2   >
...
3650   m         2.227     g/m2   >
3700   m         2.940     g/m2   >>
3750   m         2.610     g/m2   >>
3800   m         2.169     g/m2   >
3850   m         2.432     g/m2   >
3900   m         1.461     g/m2   >
3950   m         1.590     g/m2   >
4000   m         7.250     g/m2   >>>>
```

With this print-plot, the background column mass concentrations along the cross section are shown.

```
MB BACKGROUND COLUMN MASS CONCENTRATIONS IN g/m2
-4000  m      1007.980     g/m2   <<<<<<<<<<<<<<<<<<<<<<<<<<<<<<<<<<<<<<<<<<<<<<<<<<
-3950  m      1007.980     g/m2   <<<<<<<<<<<<<<<<<<<<<<<<<<<<<<<<<<<<<<<<<<<<<<<<<<
-3900  m      1007.980     g/m2   <<<<<<<<<<<<<<<<<<<<<<<<<<<<<<<<<<<<<<<<<<<<<<<<<<
-3850  m      1007.980     g/m2   <<<<<<<<<<<<<<<<<<<<<<<<<<<<<<<<<<<<<<<<<<<<<<<<<<
-3800  m      1007.980     g/m2   <<<<<<<<<<<<<<<<<<<<<<<<<<<<<<<<<<<<<<<<<<<<<<<<<<
-3750  m      1007.980     g/m2   <<<<<<<<<<<<<<<<<<<<<<<<<<<<<<<<<<<<<<<<<<<<<<<<<<
-3700  m      1007.980     g/m2   <<<<<<<<<<<<<<<<<<<<<<<<<<<<<<<<<<<<<<<<<<<<<<<<<<
-3650  m      1007.980     g/m2   <<<<<<<<<<<<<<<<<<<<<<<<<<<<<<<<<<<<<<<<<<<<<<<<<<
-3600  m      1007.980     g/m2   <<<<<<<<<<<<<<<<<<<<<<<<<<<<<<<<<<<<<<<<<<<<<<<<<<
-3550  m      1007.980     g/m2   <<<<<<<<<<<<<<<<<<<<<<<<<<<<<<<<<<<<<<<<<<<<<<<<<<
-3500  m      1007.980     g/m2   <<<<<<<<<<<<<<<<<<<<<<<<<<<<<<<<<<<<<<<<<<<<<<<<<<
...
-1000  m      1007.980     g/m2   <<<<<<<<<<<<<<<<<<<<<<<<<<<<<<<<<<<<<<<<<<<<<<<<<<
-950   m      1007.980     g/m2   <<<<<<<<<<<<<<<<<<<<<<<<<<<<<<<<<<<<<<<<<<<<<<<<<<
-900   m      1007.980     g/m2   <<<<<<<<<<<<<<<<<<<<<<<<<<<<<<<<<<<<<<<<<<<<<<<<<<
-850   m      1007.980     g/m2   <<<<<<<<<<<<<<<<<<<<<<<<<<<<<<<<<<<<<<<<<<<<<<<<<<
-800   m      1007.980     g/m2   <<<<<<<<<<<<<<<<<<<<<<<<<<<<<<<<<<<<<<<<<<<<<<<<<<
-750   m      1007.980     g/m2   <<<<<<<<<<<<<<<<<<<<<<<<<<<<<<<<<<<<<<<<<<<<<<<<<<
-700   m      1007.980     g/m2   <<<<<<<<<<<<<<<<<<<<<<<<<<<<<<<<<<<<<<<<<<<<<<<<<<
-650   m      1007.980     g/m2   <<<<<<<<<<<<<<<<<<<<<<<<<<<<<<<<<<<<<<<<<<<<<<<<<<
-600   m      1007.980     g/m2   <<<<<<<<<<<<<<<<<<<<<<<<<<<<<<<<<<<<<<<<<<<<<<<<<<
-550   m      1007.980     g/m2   <<<<<<<<<<<<<<<<<<<<<<<<<<<<<<<<<<<<<<<<<<<<<<<<<<
-500   m      1007.980     g/m2   <<<<<<<<<<<<<<<<<<<<<<<<<<<<<<<<<<<<<<<<<<<<<<<<<<
-450   m      1007.980     g/m2   <<<<<<<<<<<<<<<<<<<<<<<<<<<<<<<<<<<<<<<<<<<<<<<<<<
-400   m      1007.980     g/m2   <<<<<<<<<<<<<<<<<<<<<<<<<<<<<<<<<<<<<<<<<<<<<<<<<<
-350   m      1007.980     g/m2   <<<<<<<<<<<<<<<<<<<<<<<<<<<<<<<<<<<<<<<<<<<<<<<<<<
-300   m      1007.980     g/m2   <<<<<<<<<<<<<<<<<<<<<<<<<<<<<<<<<<<<<<<<<<<<<<<<<<
-250   m      1007.980     g/m2   <<<<<<<<<<<<<<<<<<<<<<<<<<<<<<<<<<<<<<<<<<<<<<<<<<
-200   m      1007.980     g/m2   <<<<<<<<<<<<<<<<<<<<<<<<<<<<<<<<<<<<<<<<<<<<<<<<<<
-150   m      1007.980     g/m2   <<<<<<<<<<<<<<<<<<<<<<<<<<<<<<<<<<<<<<<<<<<<<<<<<<
-100   m      1007.980     g/m2   <<<<<<<<<<<<<<<<<<<<<<<<<<<<<<<<<<<<<<<<<<<<<<<<<<
 -50   m      1007.980     g/m2   <<<<<<<<<<<<<<<<<<<<<<<<<<<<<<<<<<<<<<<<<<<<<<<<<<
```

```
   0   m      1007.980      g/m2   <<<<<<<<<<<<<<<<<<<<<<<<<<<<<<<<<<<<<<<<<<<<<<<<<<<<<<<<
  50   m      1007.980      g/m2   <<<<<<<<<<<<<<<<<<<<<<<<<<<<<<<<<<<<<<<<<<<<<<<<<<<<<<<<
 100   m      1007.980      g/m2   <<<<<<<<<<<<<<<<<<<<<<<<<<<<<<<<<<<<<<<<<<<<<<<<<<<<<<<<
 150   m      1007.980      g/m2   <<<<<<<<<<<<<<<<<<<<<<<<<<<<<<<<<<<<<<<<<<<<<<<<<<<<<<<<
 200   m      1007.980      g/m2   <<<<<<<<<<<<<<<<<<<<<<<<<<<<<<<<<<<<<<<<<<<<<<<<<<<<<<<<
 250   m      1007.980      g/m2   <<<<<<<<<<<<<<<<<<<<<<<<<<<<<<<<<<<<<<<<<<<<<<<<<<<<<<<<
 300   m      1007.980      g/m2   <<<<<<<<<<<<<<<<<<<<<<<<<<<<<<<<<<<<<<<<<<<<<<<<<<<<<<<<
 350   m      1007.980      g/m2   <<<<<<<<<<<<<<<<<<<<<<<<<<<<<<<<<<<<<<<<<<<<<<<<<<<<<<<<
 400   m      1007.980      g/m2   <<<<<<<<<<<<<<<<<<<<<<<<<<<<<<<<<<<<<<<<<<<<<<<<<<<<<<<<
 450   m      1007.980      g/m2   <<<<<<<<<<<<<<<<<<<<<<<<<<<<<<<<<<<<<<<<<<<<<<<<<<<<<<<<
 500   m      1007.980      g/m2   <<<<<<<<<<<<<<<<<<<<<<<<<<<<<<<<<<<<<<<<<<<<<<<<<<<<<<<<
 550   m      1007.980      g/m2   <<<<<<<<<<<<<<<<<<<<<<<<<<<<<<<<<<<<<<<<<<<<<<<<<<<<<<<<
 600   m      1007.980      g/m2   <<<<<<<<<<<<<<<<<<<<<<<<<<<<<<<<<<<<<<<<<<<<<<<<<<<<<<<<
 650   m      1007.980      g/m2   <<<<<<<<<<<<<<<<<<<<<<<<<<<<<<<<<<<<<<<<<<<<<<<<<<<<<<<<
 700   m      1007.980      g/m2   <<<<<<<<<<<<<<<<<<<<<<<<<<<<<<<<<<<<<<<<<<<<<<<<<<<<<<<<
 750   m      1007.980      g/m2   <<<<<<<<<<<<<<<<<<<<<<<<<<<<<<<<<<<<<<<<<<<<<<<<<<<<<<<<
 800   m      1007.980      g/m2   <<<<<<<<<<<<<<<<<<<<<<<<<<<<<<<<<<<<<<<<<<<<<<<<<<<<<<<<
 850   m      1007.980      g/m2   <<<<<<<<<<<<<<<<<<<<<<<<<<<<<<<<<<<<<<<<<<<<<<<<<<<<<<<<
 900   m      1007.980      g/m2   <<<<<<<<<<<<<<<<<<<<<<<<<<<<<<<<<<<<<<<<<<<<<<<<<<<<<<<<
 950   m      1007.980      g/m2   <<<<<<<<<<<<<<<<<<<<<<<<<<<<<<<<<<<<<<<<<<<<<<<<<<<<<<<<
1000   m      1007.980      g/m2   <<<<<<<<<<<<<<<<<<<<<<<<<<<<<<<<<<<<<<<<<<<<<<<<<<<<<<<<
...
3500   m      1007.980      g/m2   <<<<<<<<<<<<<<<<<<<<<<<<<<<<<<<<<<<<<<<<<<<<<<<<<<<<<<<<
3550   m      1007.980      g/m2   <<<<<<<<<<<<<<<<<<<<<<<<<<<<<<<<<<<<<<<<<<<<<<<<<<<<<<<<
3600   m      1007.980      g/m2   <<<<<<<<<<<<<<<<<<<<<<<<<<<<<<<<<<<<<<<<<<<<<<<<<<<<<<<<
3650   m      1007.980      g/m2   <<<<<<<<<<<<<<<<<<<<<<<<<<<<<<<<<<<<<<<<<<<<<<<<<<<<<<<<
3700   m      1007.980      g/m2   <<<<<<<<<<<<<<<<<<<<<<<<<<<<<<<<<<<<<<<<<<<<<<<<<<<<<<<<
3750   m      1007.980      g/m2   <<<<<<<<<<<<<<<<<<<<<<<<<<<<<<<<<<<<<<<<<<<<<<<<<<<<<<<<
3800   m      1007.980      g/m2   <<<<<<<<<<<<<<<<<<<<<<<<<<<<<<<<<<<<<<<<<<<<<<<<<<<<<<<<
3850   m      1007.980      g/m2   <<<<<<<<<<<<<<<<<<<<<<<<<<<<<<<<<<<<<<<<<<<<<<<<<<<<<<<<
3900   m      1007.980      g/m2   <<<<<<<<<<<<<<<<<<<<<<<<<<<<<<<<<<<<<<<<<<<<<<<<<<<<<<<<
3950   m      1007.980      g/m2   <<<<<<<<<<<<<<<<<<<<<<<<<<<<<<<<<<<<<<<<<<<<<<<<<<<<<<<<
4000   m      1007.980      g/m2   <<<<<<<<<<<<<<<<<<<<<<<<<<<<<<<<<<<<<<<<<<<<<<<<<<<<<<<<
```

Since the background along the cross section is constant, the background as a function of altitude is not. However, also this profile is quite robust, with little variation:

```
MB LAYERED BACKGROUND MASS CONCENTRATIONS IN g/m2
1850   m        29.254     g/m2   <<<<<<<<<<<<<<<<<<<<<<<<<<<<<<<<<<<<<<<<<<<<
1800   m        29.324     g/m2   <<<<<<<<<<<<<<<<<<<<<<<<<<<<<<<<<<<<<<<<<<<<
1750   m        29.506     g/m2   <<<<<<<<<<<<<<<<<<<<<<<<<<<<<<<<<<<<<<<<<<<<
1700   m        29.667     g/m2   <<<<<<<<<<<<<<<<<<<<<<<<<<<<<<<<<<<<<<<<<<<<<
1650   m        29.798     g/m2   <<<<<<<<<<<<<<<<<<<<<<<<<<<<<<<<<<<<<<<<<<<<<
1600   m        29.935     g/m2   <<<<<<<<<<<<<<<<<<<<<<<<<<<<<<<<<<<<<<<<<<<<<
1550   m        30.171     g/m2   <<<<<<<<<<<<<<<<<<<<<<<<<<<<<<<<<<<<<<<<<<<<<
1500   m        30.249     g/m2   <<<<<<<<<<<<<<<<<<<<<<<<<<<<<<<<<<<<<<<<<<<<<<
1450   m        30.407     g/m2   <<<<<<<<<<<<<<<<<<<<<<<<<<<<<<<<<<<<<<<<<<<<<<
1400   m        30.564     g/m2   <<<<<<<<<<<<<<<<<<<<<<<<<<<<<<<<<<<<<<<<<<<<<<
1350   m        30.721     g/m2   <<<<<<<<<<<<<<<<<<<<<<<<<<<<<<<<<<<<<<<<<<<<<<
1300   m        30.878     g/m2   <<<<<<<<<<<<<<<<<<<<<<<<<<<<<<<<<<<<<<<<<<<<<<<
1250   m        31.035     g/m2   <<<<<<<<<<<<<<<<<<<<<<<<<<<<<<<<<<<<<<<<<<<<<<<
1200   m        31.192     g/m2   <<<<<<<<<<<<<<<<<<<<<<<<<<<<<<<<<<<<<<<<<<<<<<<
1150   m        31.349     g/m2   <<<<<<<<<<<<<<<<<<<<<<<<<<<<<<<<<<<<<<<<<<<<<<<
1100   m        31.505     g/m2   <<<<<<<<<<<<<<<<<<<<<<<<<<<<<<<<<<<<<<<<<<<<<<<
1050   m        31.662     g/m2   <<<<<<<<<<<<<<<<<<<<<<<<<<<<<<<<<<<<<<<<<<<<<<<<
1000   m        31.818     g/m2   <<<<<<<<<<<<<<<<<<<<<<<<<<<<<<<<<<<<<<<<<<<<<<<<
 950   m        31.962     g/m2   <<<<<<<<<<<<<<<<<<<<<<<<<<<<<<<<<<<<<<<<<<<<<<<<
 900   m        32.105     g/m2   <<<<<<<<<<<<<<<<<<<<<<<<<<<<<<<<<<<<<<<<<<<<<<<<
 850   m        32.249     g/m2   <<<<<<<<<<<<<<<<<<<<<<<<<<<<<<<<<<<<<<<<<<<<<<<<<
 800   m        32.392     g/m2   <<<<<<<<<<<<<<<<<<<<<<<<<<<<<<<<<<<<<<<<<<<<<<<<<
 750   m        32.595     g/m2   <<<<<<<<<<<<<<<<<<<<<<<<<<<<<<<<<<<<<<<<<<<<<<<<<
 700   m        32.756     g/m2   <<<<<<<<<<<<<<<<<<<<<<<<<<<<<<<<<<<<<<<<<<<<<<<<<
 650   m        32.905     g/m2   <<<<<<<<<<<<<<<<<<<<<<<<<<<<<<<<<<<<<<<<<<<<<<<<<<
 600   m        33.051     g/m2   <<<<<<<<<<<<<<<<<<<<<<<<<<<<<<<<<<<<<<<<<<<<<<<<<<
 550   m        33.127     g/m2   <<<<<<<<<<<<<<<<<<<<<<<<<<<<<<<<<<<<<<<<<<<<<<<<<<
 500   m        33.200     g/m2   <<<<<<<<<<<<<<<<<<<<<<<<<<<<<<<<<<<<<<<<<<<<<<<<<<
 450   m        33.151     g/m2   <<<<<<<<<<<<<<<<<<<<<<<<<<<<<<<<<<<<<<<<<<<<<<<<<<
 400   m        33.151     g/m2   <<<<<<<<<<<<<<<<<<<<<<<<<<<<<<<<<<<<<<<<<<<<<<<<<<
 350   m        33.151     g/m2   <<<<<<<<<<<<<<<<<<<<<<<<<<<<<<<<<<<<<<<<<<<<<<<<<<
 300   m        33.151     g/m2   <<<<<<<<<<<<<<<<<<<<<<<<<<<<<<<<<<<<<<<<<<<<<<<<<<
```

The next print plot is depicting a horizontal cross section through the fluxes:

```
FE HORIZONTAL FLUXES PER COLUMN IN  kg/s
-4000  m         0.051      kg/s  >
...
-3500  m         0.117      kg/s  >>
-3450  m         0.106      kg/s  >
-3400  m         0.157      kg/s  >>
-3350  m         0.295      kg/s  >>>>
-3300  m         0.633      kg/s  >>>>>>>>>
-3250  m         0.630      kg/s  >>>>>>>>>
-3200  m         0.497      kg/s  >>>>>>>
-3150  m         0.570      kg/s  >>>>>>>>
-3100  m         0.688      kg/s  >>>>>>>>>
-3050  m         0.594      kg/s  >>>>>>>>
-3000  m         0.977      kg/s  >>>>>>>>>>>>>
-2950  m         1.061      kg/s  >>>>>>>>>>>>>>
-2900  m         1.061      kg/s  >>>>>>>>>>>>>>
-2850  m         0.766      kg/s  >>>>>>>>>>
-2800  m         0.925      kg/s  >>>>>>>>>>>>>
-2750  m         0.960      kg/s  >>>>>>>>>>>>>
-2700  m         1.682      kg/s  >>>>>>>>>>>>>>>>>>>>>>>
-2650  m         1.528      kg/s  >>>>>>>>>>>>>>>>>>>>>
-2600  m         1.248      kg/s  >>>>>>>>>>>>>>>>>
-2550  m         1.112      kg/s  >>>>>>>>>>>>>>>
-2500  m         1.075      kg/s  >>>>>>>>>>>>>>>
-2450  m         1.453      kg/s  >>>>>>>>>>>>>>>>>>>>
-2400  m         1.397      kg/s  >>>>>>>>>>>>>>>>>>>
-2350  m         1.448      kg/s  >>>>>>>>>>>>>>>>>>>>
-2300  m         1.594      kg/s  >>>>>>>>>>>>>>>>>>>>>>
-2250  m         1.582      kg/s  >>>>>>>>>>>>>>>>>>>>>
-2200  m         1.442      kg/s  >>>>>>>>>>>>>>>>>>>>
-2150  m         1.395      kg/s  >>>>>>>>>>>>>>>>>>>
-2100  m         1.329      kg/s  >>>>>>>>>>>>>>>>>>
-2050  m         1.691      kg/s  >>>>>>>>>>>>>>>>>>>>>>>
-2000  m         1.715      kg/s  >>>>>>>>>>>>>>>>>>>>>>>
-1950  m         1.171      kg/s  >>>>>>>>>>>>>>>>
-1900  m         0.654      kg/s  >>>>>>>>>
-1850  m         0.490      kg/s  >>>>>>>
-1800  m         0.516      kg/s  >>>>>>>
-1750  m         0.813      kg/s  >>>>>>>>>>>
-1700  m         1.066      kg/s  >>>>>>>>>>>>>>
-1650  m         0.956      kg/s  >>>>>>>>>>>>>
-1600  m         0.682      kg/s  >>>>>>>>>
-1550  m         0.877      kg/s  >>>>>>>>>>>>
-1500  m         1.079      kg/s  >>>>>>>>>>>>>>>
-1450  m         0.934      kg/s  >>>>>>>>>>>>>
-1400  m         0.798      kg/s  >>>>>>>>>>>
-1350  m         3.601      kg/s  >>>>>>>>>>>>>>>>>>>>>>>>>>>>>>>>>>>>>>>>>>>>>>>>>
-1300  m         3.164      kg/s  >>>>>>>>>>>>>>>>>>>>>>>>>>>>>>>>>>>>>>>>>>>
-1250  m         3.682      kg/s  >>>>>>>>>>>>>>>>>>>>>>>>>>>>>>>>>>>>>>>>>>>>>>>>>>
-1200  m         3.227      kg/s  >>>>>>>>>>>>>>>>>>>>>>>>>>>>>>>>>>>>>>>>>>>>
-1150  m         3.218      kg/s  >>>>>>>>>>>>>>>>>>>>>>>>>>>>>>>>>>>>>>>>>>>>
-1100  m         3.526      kg/s  >>>>>>>>>>>>>>>>>>>>>>>>>>>>>>>>>>>>>>>>>>>>>>>>
-1050  m         3.069      kg/s  >>>>>>>>>>>>>>>>>>>>>>>>>>>>>>>>>>>>>>>>>>
-1000  m         2.227      kg/s  >>>>>>>>>>>>>>>>>>>>>>>>>>>>>>
-950   m         1.785      kg/s  >>>>>>>>>>>>>>>>>>>>>>>>
-900   m         2.219      kg/s  >>>>>>>>>>>>>>>>>>>>>>>>>>>>>>
-850   m         2.175      kg/s  >>>>>>>>>>>>>>>>>>>>>>>>>>>>>>
-800   m         2.055      kg/s  >>>>>>>>>>>>>>>>>>>>>>>>>>>>
-750   m         1.912      kg/s  >>>>>>>>>>>>>>>>>>>>>>>>>>
-700   m         2.277      kg/s  >>>>>>>>>>>>>>>>>>>>>>>>>>>>>>>
-650   m         2.340      kg/s  >>>>>>>>>>>>>>>>>>>>>>>>>>>>>>>>
```

```
-600   m         1.840       kg/s  >>>>>>>>>>>>>>>>>>>>>>>>>
-550   m         1.386       kg/s  >>>>>>>>>>>>>>>>>>>
-500   m         1.547       kg/s  >>>>>>>>>>>>>>>>>>>>>>
-450   m         1.244       kg/s  >>>>>>>>>>>>>>>>>
-400   m         1.174       kg/s  >>>>>>>>>>>>>>>>
-350   m         0.952       kg/s  >>>>>>>>>>>>>
-300   m         1.051       kg/s  >>>>>>>>>>>>>>
-250   m         1.143       kg/s  >>>>>>>>>>>>>>>>
-200   m         0.880       kg/s  >>>>>>>>>>>>
-150   m         1.004       kg/s  >>>>>>>>>>>>>>
-100   m         1.101       kg/s  >>>>>>>>>>>>>>>
 -50   m         1.277       kg/s  >>>>>>>>>>>>>>>>>
   0   m         1.094       kg/s  >>>>>>>>>>>>>>>
  50   m         0.923       kg/s  >>>>>>>>>>>>>
 100   m         0.781       kg/s  >>>>>>>>>>>
 150   m         0.775       kg/s  >>>>>>>>>>>
 200   m         0.829       kg/s  >>>>>>>>>>>
 250   m         0.935       kg/s  >>>>>>>>>>>>
 300   m         0.786       kg/s  >>>>>>>>>>>
 350   m         0.765       kg/s  >>>>>>>>>>
 400   m         0.868       kg/s  >>>>>>>>>>>>
 450   m         1.005       kg/s  >>>>>>>>>>>>>>
 500   m         0.967       kg/s  >>>>>>>>>>>>>
 550   m         1.176       kg/s  >>>>>>>>>>>>>>>>
 600   m         1.082       kg/s  >>>>>>>>>>>>>>>
 650   m         1.068       kg/s  >>>>>>>>>>>>>>>
 700   m         1.385       kg/s  >>>>>>>>>>>>>>>>>>>
 750   m         1.300       kg/s  >>>>>>>>>>>>>>>>>>
 800   m         1.513       kg/s  >>>>>>>>>>>>>>>>>>>>>
 850   m         1.579       kg/s  >>>>>>>>>>>>>>>>>>>>>
 900   m         1.403       kg/s  >>>>>>>>>>>>>>>>>>>
 950   m         1.412       kg/s  >>>>>>>>>>>>>>>>>>>
1000   m         1.194       kg/s  >>>>>>>>>>>>>>>>>
1050   m         1.232       kg/s  >>>>>>>>>>>>>>>>>>
1100   m         1.021       kg/s  >>>>>>>>>>>>>>>
1150   m         0.916       kg/s  >>>>>>>>>>>>
1200   m         0.561       kg/s  >>>>>>>>
1250   m         0.638       kg/s  >>>>>>>>>
1300   m         0.547       kg/s  >>>>>>>
1350   m         0.601       kg/s  >>>>>>>>
1400   m         0.509       kg/s  >>>>>>>
1450   m         0.392       kg/s  >>>>>
1500   m         0.477       kg/s  >>>>>>
1550   m         0.420       kg/s  >>>>>>
1600   m         0.379       kg/s  >>>>>
1650   m         0.496       kg/s  >>>>>>>
1700   m         0.463       kg/s  >>>>>>
1750   m         0.513       kg/s  >>>>>>>
1800   m         0.312       kg/s  >>>>
1850   m         0.333       kg/s  >>>>>
1900   m         0.354       kg/s  >>>>>
1950   m         0.427       kg/s  >>>>>>
2000   m         0.336       kg/s  >>>>>
2050   m         0.075       kg/s  >
...
2350   m         0.078       kg/s  >
2400   m         0.105       kg/s  >
2450   m         0.177       kg/s  >>
2500   m         0.154       kg/s  >>
2550   m         0.085       kg/s  >
2600   m         0.073       kg/s  >
2650   m         0.065       kg/s  >
2700   m         0.047       kg/s  >
2750   m         0.047       kg/s  >
```

```
2800   m         0.047      kg/s  >
2850   m         0.047      kg/s  >
2900   m         0.047      kg/s  >
2950   m         0.047      kg/s  >
3000   m         0.047      kg/s  >
3050   m         0.047      kg/s  >
3100   m         0.047      kg/s  >
3150   m         0.047      kg/s  >
3200   m         0.047      kg/s  >
3250   m         0.001      kg/s
3300   m         0.006      kg/s
3350   m         0.001      kg/s
3400   m         0.002      kg/s
3450   m         0.001      kg/s
3500   m         0.001      kg/s
3550   m         0.001      kg/s
3600   m         0.000      kg/s
3650   m         0.000      kg/s
3700   m         0.000      kg/s
3750   m         0.000      kg/s
3800   m         0.000      kg/s
3850   m         0.000      kg/s
3900   m         0.000      kg/s
3950   m         0.000      kg/s
4000   m         0.051      kg/s  >
```

The same fluxes per layer, showing that the maximum was at 1100 to 1150 mAMSL:

```
FE HORIZONTAL FLUXES PER LAYER IN  kg/s
1850   m         0.021      kg/s
1800   m         0.014      kg/s
1750   m         0.294      kg/s  >>>>
1700   m         0.438      kg/s  >>>>>>
1650   m         0.582      kg/s  >>>>>>>>
1600   m         0.727      kg/s  >>>>>>>>>>
1550   m         0.871      kg/s  >>>>>>>>>>>>
1500   m         1.015      kg/s  >>>>>>>>>>>>>>
1450   m         1.160      kg/s  >>>>>>>>>>>>>>>>
1400   m         1.304      kg/s  >>>>>>>>>>>>>>>>>>
1350   m         1.448      kg/s  >>>>>>>>>>>>>>>>>>>>
1300   m         1.593      kg/s  >>>>>>>>>>>>>>>>>>>>>>
1250   m         1.737      kg/s  >>>>>>>>>>>>>>>>>>>>>>>>
1200   m         1.498      kg/s  >>>>>>>>>>>>>>>>>>>>
1150   m         3.526      kg/s  >>>>>>>>>>>>>>>>>>>>>>>>>>>>>>>>>>>>>>>>>>>>>>>>
1100   m         3.682      kg/s  >>>>>>>>>>>>>>>>>>>>>>>>>>>>>>>>>>>>>>>>>>>>>>>>>>
1050   m         1.691      kg/s  >>>>>>>>>>>>>>>>>>>>>>>
1000   m         1.715      kg/s  >>>>>>>>>>>>>>>>>>>>>>>
 950   m         0.902      kg/s  >>>>>>>>>>>>
 900   m         1.042      kg/s  >>>>>>>>>>>>>>
 850   m         0.840      kg/s  >>>>>>>>>>>
 800   m         1.579      kg/s  >>>>>>>>>>>>>>>>>>>>>
 750   m         1.065      kg/s  >>>>>>>>>>>>>>
 700   m         1.079      kg/s  >>>>>>>>>>>>>>>
 650   m         0.549      kg/s  >>>>>>>
 600   m         0.960      kg/s  >>>>>>>>>>>>>
 550   m         0.145      kg/s  >>
 500   m         0.601      kg/s  >>>>>>>>
 450   m         0.073      kg/s  >
 400   m         0.333      kg/s  >>>>>
 350   m         0.080      kg/s  >
 300   m         0.140      kg/s  >>
 250   m         0.140      kg/s  >>
 200   m         0.140      kg/s  >>
 150   m         0.095      kg/s  >
 100   m         0.023      kg/s
  50   m         0.000      kg/s
   0   m         0.000      kg/s
```

The maximum absolute concentration per column
(not very interesting – see rather the excessive concentrations = net concentrations below):

```
CT MAXIMUM CONCENTRATION PER COLUMN in ppm
-4000  m       395.550      ppm    >>>>>>>>>>>>>>>>>>>>>>>>>>>>>>>>>>>>>
...
-3350  m       413.392      ppm    >>>>>>>>>>>>>>>>>>>>>>>>>>>>>>>>>>>>>>
-3300  m       439.917      ppm    >>>>>>>>>>>>>>>>>>>>>>>>>>>>>>>>>>>>>>>>>
...
-3150  m       432.968      ppm    >>>>>>>>>>>>>>>>>>>>>>>>>>>>>>>>>>>>>>>>
-3100  m       424.650      ppm    >>>>>>>>>>>>>>>>>>>>>>>>>>>>>>>>>>>>>>>
-3050  m       418.578      ppm    >>>>>>>>>>>>>>>>>>>>>>>>>>>>>>>>>>>>>>>
-3000  m       449.988      ppm    >>>>>>>>>>>>>>>>>>>>>>>>>>>>>>>>>>>>>>>>>>
-2950  m       463.148      ppm    >>>>>>>>>>>>>>>>>>>>>>>>>>>>>>>>>>>>>>>>>>>
-2900  m       476.044      ppm    >>>>>>>>>>>>>>>>>>>>>>>>>>>>>>>>>>>>>>>>>>>>
-2850  m       455.558      ppm    >>>>>>>>>>>>>>>>>>>>>>>>>>>>>>>>>>>>>>>>>>
...
-2700  m       529.132      ppm    >>>>>>>>>>>>>>>>>>>>>>>>>>>>>>>>>>>>>>>>>>>>>>>>>
-2650  m       508.572      ppm    >>>>>>>>>>>>>>>>>>>>>>>>>>>>>>>>>>>>>>>>>>>>>>>
-2600  m       478.788      ppm    >>>>>>>>>>>>>>>>>>>>>>>>>>>>>>>>>>>>>>>>>>>>
...
-2050  m       490.970      ppm    >>>>>>>>>>>>>>>>>>>>>>>>>>>>>>>>>>>>>>>>>>>>>>
-2000  m       498.340      ppm    >>>>>>>>>>>>>>>>>>>>>>>>>>>>>>>>>>>>>>>>>>>>>>
-1950  m       462.350      ppm    >>>>>>>>>>>>>>>>>>>>>>>>>>>>>>>>>>>>>>>>>>>
...
  -50  m       438.545      ppm    >>>>>>>>>>>>>>>>>>>>>>>>>>>>>>>>>>>>>>>>>
    0  m       429.287      ppm    >>>>>>>>>>>>>>>>>>>>>>>>>>>>>>>>>>>>>>>>
   50  m       433.304      ppm    >>>>>>>>>>>>>>>>>>>>>>>>>>>>>>>>>>>>>>>>
...
  700  m       471.642      ppm    >>>>>>>>>>>>>>>>>>>>>>>>>>>>>>>>>>>>>>>>>>>>
  750  m       473.004      ppm    >>>>>>>>>>>>>>>>>>>>>>>>>>>>>>>>>>>>>>>>>>>>
  800  m       483.469      ppm    >>>>>>>>>>>>>>>>>>>>>>>>>>>>>>>>>>>>>>>>>>>>>
  850  m       486.291      ppm    >>>>>>>>>>>>>>>>>>>>>>>>>>>>>>>>>>>>>>>>>>>>>
  900  m       480.055      ppm    >>>>>>>>>>>>>>>>>>>>>>>>>>>>>>>>>>>>>>>>>>>>
  950  m       469.067      ppm    >>>>>>>>>>>>>>>>>>>>>>>>>>>>>>>>>>>>>>>>>>>
 1000  m       457.191      ppm    >>>>>>>>>>>>>>>>>>>>>>>>>>>>>>>>>>>>>>>>>>
 1050  m       455.332      ppm    >>>>>>>>>>>>>>>>>>>>>>>>>>>>>>>>>>>>>>>>>>
 1100  m       442.296      ppm    >>>>>>>>>>>>>>>>>>>>>>>>>>>>>>>>>>>>>>>>>
 1150  m       434.717      ppm    >>>>>>>>>>>>>>>>>>>>>>>>>>>>>>>>>>>>>>>>
 1200  m       417.828      ppm    >>>>>>>>>>>>>>>>>>>>>>>>>>>>>>>>>>>>>>>
 1250  m       417.243      ppm    >>>>>>>>>>>>>>>>>>>>>>>>>>>>>>>>>>>>>>>
 1300  m       413.923      ppm    >>>>>>>>>>>>>>>>>>>>>>>>>>>>>>>>>>>>>>
 1350  m       428.552      ppm    >>>>>>>>>>>>>>>>>>>>>>>>>>>>>>>>>>>>>>>>
 1400  m       434.312      ppm    >>>>>>>>>>>>>>>>>>>>>>>>>>>>>>>>>>>>>>>>
 1450  m       425.898      ppm    >>>>>>>>>>>>>>>>>>>>>>>>>>>>>>>>>>>>>>>
 1500  m       423.172      ppm    >>>>>>>>>>>>>>>>>>>>>>>>>>>>>>>>>>>>>>>
 1550  m       418.286      ppm    >>>>>>>>>>>>>>>>>>>>>>>>>>>>>>>>>>>>>>>
 1600  m       410.713      ppm    >>>>>>>>>>>>>>>>>>>>>>>>>>>>>>>>>>>>>>
 1650  m       415.528      ppm    >>>>>>>>>>>>>>>>>>>>>>>>>>>>>>>>>>>>>>>
 1700  m       412.790      ppm    >>>>>>>>>>>>>>>>>>>>>>>>>>>>>>>>>>>>>>
 1750  m       413.834      ppm    >>>>>>>>>>>>>>>>>>>>>>>>>>>>>>>>>>>>>>
 1800  m       404.915      ppm    >>>>>>>>>>>>>>>>>>>>>>>>>>>>>>>>>>>>>>
 1850  m       401.236      ppm    >>>>>>>>>>>>>>>>>>>>>>>>>>>>>>>>>>>>>
 1900  m       400.926      ppm    >>>>>>>>>>>>>>>>>>>>>>>>>>>>>>>>>>>>>
...
 2350  m       397.838      ppm    >>>>>>>>>>>>>>>>>>>>>>>>>>>>>>>>>>>>>
...
 2700  m       395.550      ppm    >>>>>>>>>>>>>>>>>>>>>>>>>>>>>>>>>>>>>
...
 4000  m       395.550      ppm    >>>>>>>>>>>>>>>>>>>>>>>>>>>>>>>>>>>>>
```

The maximum absolute concentration per layer
(not very interesting – see rather the excessive concentrations = net concentrations below):

```
CT MAXIMUM CONCENTRATION PER LAYER in ppm
1850   m       382.545      ppm    >>>>>>>>>>>>>>>>>>>>>>>>>>>>>>>>>>>>>>
1800   m       382.272      ppm    >>>>>>>>>>>>>>>>>>>>>>>>>>>>>>>>>>>>>>
1750   m       383.899      ppm    >>>>>>>>>>>>>>>>>>>>>>>>>>>>>>>>>>>>>>>>
1700   m       384.835      ppm    >>>>>>>>>>>>>>>>>>>>>>>>>>>>>>>>>>>>>>>>
1650   m       392.433      ppm    >>>>>>>>>>>>>>>>>>>>>>>>>>>>>>>>>>>>>>>>
1600   m       397.689      ppm    >>>>>>>>>>>>>>>>>>>>>>>>>>>>>>>>>>>>>>>>>
1550   m       402.945      ppm    >>>>>>>>>>>>>>>>>>>>>>>>>>>>>>>>>>>>>>>>>
1500   m       406.140      ppm    >>>>>>>>>>>>>>>>>>>>>>>>>>>>>>>>>>>>>>>>>
1450   m       391.825      ppm    >>>>>>>>>>>>>>>>>>>>>>>>>>>>>>>>>>>>>>>>
1400   m       431.056      ppm    >>>>>>>>>>>>>>>>>>>>>>>>>>>>>>>>>>>>>>>>>>
1350   m       454.708      ppm    >>>>>>>>>>>>>>>>>>>>>>>>>>>>>>>>>>>>>>>>>>
1300   m       456.059      ppm    >>>>>>>>>>>>>>>>>>>>>>>>>>>>>>>>>>>>>>>>>>
1250   m       493.107      ppm    >>>>>>>>>>>>>>>>>>>>>>>>>>>>>>>>>>>>>>>>>>>>
1200   m       489.257      ppm    >>>>>>>>>>>>>>>>>>>>>>>>>>>>>>>>>>>>>>>>>>>
1150   m       529.700      ppm    >>>>>>>>>>>>>>>>>>>>>>>>>>>>>>>>>>>>>>>>>>>>>>>
1100   m       539.410      ppm    >>>>>>>>>>>>>>>>>>>>>>>>>>>>>>>>>>>>>>>>>>>>>>>>
1050   m       529.132      ppm    >>>>>>>>>>>>>>>>>>>>>>>>>>>>>>>>>>>>>>>>>>>>>>>
1000   m       498.340      ppm    >>>>>>>>>>>>>>>>>>>>>>>>>>>>>>>>>>>>>>>>>>>>>
 950   m       448.865      ppm    >>>>>>>>>>>>>>>>>>>>>>>>>>>>>>>>>>>>>>>>>>
 900   m       463.185      ppm    >>>>>>>>>>>>>>>>>>>>>>>>>>>>>>>>>>>>>>>>>>>
 850   m       442.110      ppm    >>>>>>>>>>>>>>>>>>>>>>>>>>>>>>>>>>>>>>>>>
 800   m       486.291      ppm    >>>>>>>>>>>>>>>>>>>>>>>>>>>>>>>>>>>>>>>>>>>>
 750   m       384.231      ppm    >>>>>>>>>>>>>>>>>>>>>>>>>>>>>>>>>>>>>>>
 700   m       464.465      ppm    >>>>>>>>>>>>>>>>>>>>>>>>>>>>>>>>>>>>>>>>>>>
 650   m       434.312      ppm    >>>>>>>>>>>>>>>>>>>>>>>>>>>>>>>>>>>>>>>>
 600   m       441.685      ppm    >>>>>>>>>>>>>>>>>>>>>>>>>>>>>>>>>>>>>>>>>
 550   m       387.138      ppm    >>>>>>>>>>>>>>>>>>>>>>>>>>>>>>>>>>>>>>
 500   m       410.802      ppm    >>>>>>>>>>>>>>>>>>>>>>>>>>>>>>>>>>>>>>>
 450   m       385.440      ppm    >>>>>>>>>>>>>>>>>>>>>>>>>>>>>>>>>>>>>
 400   m       411.752      ppm    >>>>>>>>>>>>>>>>>>>>>>>>>>>>>>>>>>>>>>>
 350   m       390.795      ppm    >>>>>>>>>>>>>>>>>>>>>>>>>>>>>>>>>>>>>
 300   m       393.381      ppm    >>>>>>>>>>>>>>>>>>>>>>>>>>>>>>>>>>>>>
 250   m       393.381      ppm    >>>>>>>>>>>>>>>>>>>>>>>>>>>>>>>>>>>>>
 200   m       393.381      ppm    >>>>>>>>>>>>>>>>>>>>>>>>>>>>>>>>>>>>>
 150   m       393.381      ppm    >>>>>>>>>>>>>>>>>>>>>>>>>>>>>>>>>>>>>
 100   m       385.440      ppm    >>>>>>>>>>>>>>>>>>>>>>>>>>>>>>>>>>>>>
  50   m         0.000      ppm
   0   m         0.000      ppm
```

The maximum excessive concentrations (net concentrations) per column:

```
CE MAXIMUM EXCESSIVE CONCENTRATION PER COLUMN in ppm
-4000  m        13.870      ppm    >>>>
...
-3550  m        13.870      ppm    >>>>
-3500  m        14.320      ppm    >>>>>
-3450  m        13.870      ppm    >>>>
-3400  m        19.742      ppm    >>>>>>
-3350  m        32.722      ppm    >>>>>>>>>>
...
-3000  m        69.318      ppm    >>>>>>>>>>>>>>>>>>>>>>
-2950  m        82.478      ppm    >>>>>>>>>>>>>>>>>>>>>>>>>>
-2900  m        95.374      ppm    >>>>>>>>>>>>>>>>>>>>>>>>>>>>>>
-2850  m        74.888      ppm    >>>>>>>>>>>>>>>>>>>>>>>>
-2800  m        82.504      ppm    >>>>>>>>>>>>>>>>>>>>>>>>>>
-2750  m        84.020      ppm    >>>>>>>>>>>>>>>>>>>>>>>>>>>
-2700  m       148.462      ppm    >>>>>>>>>>>>>>>>>>>>>>>>>>>>>>>>>>>>>>>>>>>>>>>
-2650  m       127.902      ppm    >>>>>>>>>>>>>>>>>>>>>>>>>>>>>>>>>>>>>>>>
-2600  m        98.118      ppm    >>>>>>>>>>>>>>>>>>>>>>>>>>>>>>>
-2550  m        81.980      ppm    >>>>>>>>>>>>>>>>>>>>>>>>>>
-2500  m        83.807      ppm    >>>>>>>>>>>>>>>>>>>>>>>>>>
-2450  m       105.596      ppm    >>>>>>>>>>>>>>>>>>>>>>>>>>>>>>>>>
-2400  m        95.380      ppm    >>>>>>>>>>>>>>>>>>>>>>>>>>>>>>
-2350  m        92.067      ppm    >>>>>>>>>>>>>>>>>>>>>>>>>>>>>
-2300  m       103.084      ppm    >>>>>>>>>>>>>>>>>>>>>>>>>>>>>>>>>
-2250  m       104.362      ppm    >>>>>>>>>>>>>>>>>>>>>>>>>>>>>>>>>
-2200  m        96.027      ppm    >>>>>>>>>>>>>>>>>>>>>>>>>>>>>>
-2150  m       101.168      ppm    >>>>>>>>>>>>>>>>>>>>>>>>>>>>>>>>
-2100  m        86.212      ppm    >>>>>>>>>>>>>>>>>>>>>>>>>>>
-2050  m       110.300      ppm    >>>>>>>>>>>>>>>>>>>>>>>>>>>>>>>>>>>
-2000  m       117.378      ppm    >>>>>>>>>>>>>>>>>>>>>>>>>>>>>>>>>>>>>
-1950  m        81.388      ppm    >>>>>>>>>>>>>>>>>>>>>>>>>>
-1900  m        55.631      ppm    >>>>>>>>>>>>>>>>>>
-1850  m        69.162      ppm    >>>>>>>>>>>>>>>>>>>>>>
-1800  m        79.795      ppm    >>>>>>>>>>>>>>>>>>>>>>>>>
-1750  m        98.769      ppm    >>>>>>>>>>>>>>>>>>>>>>>>>>>>>>>
-1700  m        99.699      ppm    >>>>>>>>>>>>>>>>>>>>>>>>>>>>>>>
-1650  m       132.340      ppm    >>>>>>>>>>>>>>>>>>>>>>>>>>>>>>>>>>>>>>>>>>
-1600  m        68.661      ppm    >>>>>>>>>>>>>>>>>>>>>>
-1550  m        71.564      ppm    >>>>>>>>>>>>>>>>>>>>>>>
-1500  m        82.593      ppm    >>>>>>>>>>>>>>>>>>>>>>>>>>
-1450  m        82.104      ppm    >>>>>>>>>>>>>>>>>>>>>>>>>>
-1400  m       111.793      ppm    >>>>>>>>>>>>>>>>>>>>>>>>>>>>>>>>>>>
-1350  m       158.419      ppm    >>>>>>>>>>>>>>>>>>>>>>>>>>>>>>>>>>>>>>>>>>>>>>>>>>
...
-1000  m       108.543      ppm    >>>>>>>>>>>>>>>>>>>>>>>>>>>>>>>>>>
-950   m        90.047      ppm    >>>>>>>>>>>>>>>>>>>>>>>>>>>>
-900   m       110.645      ppm    >>>>>>>>>>>>>>>>>>>>>>>>>>>>>>>>>>>
-850   m       116.275      ppm    >>>>>>>>>>>>>>>>>>>>>>>>>>>>>>>>>>>>>
-800   m       110.867      ppm    >>>>>>>>>>>>>>>>>>>>>>>>>>>>>>>>>>>
-750   m       103.346      ppm    >>>>>>>>>>>>>>>>>>>>>>>>>>>>>>>>>
-700   m       117.802      ppm    >>>>>>>>>>>>>>>>>>>>>>>>>>>>>>>>>>>>>
-650   m       110.623      ppm    >>>>>>>>>>>>>>>>>>>>>>>>>>>>>>>>>>>
-600   m       103.827      ppm    >>>>>>>>>>>>>>>>>>>>>>>>>>>>>>>>>
-550   m        74.252      ppm    >>>>>>>>>>>>>>>>>>>>>>>
-500   m        82.185      ppm    >>>>>>>>>>>>>>>>>>>>>>>>>>
-450   m        59.742      ppm    >>>>>>>>>>>>>>>>>>>
-400   m        61.620      ppm    >>>>>>>>>>>>>>>>>>>
-350   m        66.449      ppm    >>>>>>>>>>>>>>>>>>>>>
-300   m        70.000      ppm    >>>>>>>>>>>>>>>>>>>>>>
-250   m        57.636      ppm    >>>>>>>>>>>>>>>>>>
-200   m        57.451      ppm    >>>>>>>>>>>>>>>>>>
-150   m        63.449      ppm    >>>>>>>>>>>>>>>>>>>>
-100   m        61.250      ppm    >>>>>>>>>>>>>>>>>>>
```

```
 -50   m        56.879     ppm    >>>>>>>>>>>>>>>>>>
   0   m        48.107     ppm    >>>>>>>>>>>>>>>>
  50   m        51.708     ppm    >>>>>>>>>>>>>>>>>
 100   m        45.659     ppm    >>>>>>>>>>>>>>>
 150   m        49.784     ppm    >>>>>>>>>>>>>>>>>
 200   m        53.136     ppm    >>>>>>>>>>>>>>>>>>
 250   m        63.829     ppm    >>>>>>>>>>>>>>>>>>>>>
 300   m        60.542     ppm    >>>>>>>>>>>>>>>>>>>>
 350   m        58.973     ppm    >>>>>>>>>>>>>>>>>>>>
 400   m        62.257     ppm    >>>>>>>>>>>>>>>>>>>>>
 450   m        68.423     ppm    >>>>>>>>>>>>>>>>>>>>>>>
 500   m        67.656     ppm    >>>>>>>>>>>>>>>>>>>>>>
 550   m        90.026     ppm    >>>>>>>>>>>>>>>>>>>>>>>>>>>>>>
 600   m        84.125     ppm    >>>>>>>>>>>>>>>>>>>>>>>>>>>
 650   m        84.644     ppm    >>>>>>>>>>>>>>>>>>>>>>>>>>>
 700   m        91.242     ppm    >>>>>>>>>>>>>>>>>>>>>>>>>>>>>
 750   m        92.604     ppm    >>>>>>>>>>>>>>>>>>>>>>>>>>>>>
 800   m       103.069     ppm    >>>>>>>>>>>>>>>>>>>>>>>>>>>>>>>>>
 850   m       105.891     ppm    >>>>>>>>>>>>>>>>>>>>>>>>>>>>>>>>>
 900   m        99.655     ppm    >>>>>>>>>>>>>>>>>>>>>>>>>>>>>>>
 950   m        88.667     ppm    >>>>>>>>>>>>>>>>>>>>>>>>>>>>
1000   m        76.791     ppm    >>>>>>>>>>>>>>>>>>>>>>>>>
1050   m        74.933     ppm    >>>>>>>>>>>>>>>>>>>>>>>>>
1100   m        61.896     ppm    >>>>>>>>>>>>>>>>>>>>>>
1150   m        54.317     ppm    >>>>>>>>>>>>>>>>>>>
1200   m        37.428     ppm    >>>>>>>>>>>>
1250   m        35.577     ppm    >>>>>>>>>>>
1300   m        32.244     ppm    >>>>>>>>>>
1350   m        46.872     ppm    >>>>>>>>>>>>>>>>
1400   m        52.632     ppm    >>>>>>>>>>>>>>>>>>
1450   m        44.219     ppm    >>>>>>>>>>>>>>>
1500   m        41.506     ppm    >>>>>>>>>>>>>>
1550   m        36.620     ppm    >>>>>>>>>>>>
1600   m        29.047     ppm    >>>>>>>>>
1650   m        33.862     ppm    >>>>>>>>>>>
1700   m        31.124     ppm    >>>>>>>>>>
1750   m        32.168     ppm    >>>>>>>>>>
1800   m        23.249     ppm    >>>>>>>
1850   m        20.439     ppm    >>>>>>
1900   m        19.975     ppm    >>>>>>
1950   m        26.600     ppm    >>>>>>>>
2000   m        24.573     ppm    >>>>>>>>
2050   m        27.729     ppm    >>>>>>>>>
2100   m        14.435     ppm    >>>>>
2150   m        22.655     ppm    >>>>>>>
2200   m        30.955     ppm    >>>>>>>>>>
2250   m        26.267     ppm    >>>>>>>>
2300   m        23.153     ppm    >>>>>>>
2350   m        17.041     ppm    >>>>>
2400   m        13.870     ppm    >>>>
...
2850   m        13.870     ppm    >>>>
2900   m         3.084     ppm    >
...
3950   m         1.617     ppm    >
```

The maximum excessive concentrations (net concentrations) per layer, showing that also the fluxes (not only the concentrations) are maximum in the altitude interval between 1050 and 1150 mAMSL:

```
CE MAXIMUM EXCESSIVE  CONCENTRATION PER LAYER in ppm
1850   m         0.900     ppm
1800   m         0.645     ppm
1750   m         2.564     ppm    >
1700   m         3.700     ppm    >
1650   m        11.223     ppm    >>>>
1600   m        16.194     ppm    >>>>>
1550   m        21.364     ppm    >>>>>>>
1500   m        24.597     ppm    >>>>>>>>
1450   m        10.258     ppm    >>>
1400   m        49.499     ppm    >>>>>>>>>>>>>>>>
1350   m        73.112     ppm    >>>>>>>>>>>>>>>>>>>>>>>
1300   m        74.448     ppm    >>>>>>>>>>>>>>>>>>>>>>>
1250   m       111.863     ppm    >>>>>>>>>>>>>>>>>>>>>>>>>>>>>>>>>>>
1200   m       107.933     ppm    >>>>>>>>>>>>>>>>>>>>>>>>>>>>>>>>>>
1150   m       148.520     ppm    >>>>>>>>>>>>>>>>>>>>>>>>>>>>>>>>>>>>>>>>>>>>>>>
1100   m       158.419     ppm    >>>>>>>>>>>>>>>>>>>>>>>>>>>>>>>>>>>>>>>>>>>>>>>>>>
1050   m       148.462     ppm    >>>>>>>>>>>>>>>>>>>>>>>>>>>>>>>>>>>>>>>>>>>>>>>
1000   m       117.378     ppm    >>>>>>>>>>>>>>>>>>>>>>>>>>>>>>>>>>>>>
 950   m        68.043     ppm    >>>>>>>>>>>>>>>>>>>>>
 900   m        82.504     ppm    >>>>>>>>>>>>>>>>>>>>>>>>>>
 850   m        61.570     ppm    >>>>>>>>>>>>>>>>>>>
 800   m       105.891     ppm    >>>>>>>>>>>>>>>>>>>>>>>>>>>>>>>>>
 750   m         2.760     ppm    >
 700   m        82.593     ppm    >>>>>>>>>>>>>>>>>>>>>>>>>>
 650   m        52.632     ppm    >>>>>>>>>>>>>>>>>
 600   m        60.019     ppm    >>>>>>>>>>>>>>>>>>>
 550   m         6.322     ppm    >>
 500   m        30.005     ppm    >>>>>>>>>
 450   m         4.624     ppm    >
 400   m        30.955     ppm    >>>>>>>>>>
 350   m         9.998     ppm    >>>
 300   m        12.585     ppm    >>>>
 250   m        12.585     ppm    >>>>
 200   m        12.585     ppm    >>>>
 150   m        12.585     ppm    >>>>
 100   m         4.643     ppm    >
  50   m         0.000     ppm
   0   m         0.000     ppm
```